Aspects of string model building and heterotic/F-theory duality

Callum Ryan Brodie

Brasenose College
University of Oxford

A thesis submitted for the degree of
Doctor of Philosophy

Trinity Term 2019

Aspects of string model building and heterotic/F-theory duality

Callum Ryan Brodie

Brasenose College
University of Oxford

A thesis submitted for the degree of
Doctor of Philosophy

Trinity Term 2019

In this thesis, we develop tools for model building in heterotic string theory and F-theory. We focus in particular on heterotic line bundle models and their F-theory duals. The first reason for this is that line bundle models are particularly fruitful models for phenomenology, and the second reason is that they provide a convenient background in which to make progress in studying heterotic/F-theory duality for more general features.

In the first two parts of this thesis, we focus on transferring unique model building advantages between the heterotic and F-theory descriptions, via heterotic/F-theory duality. In the first part, we lay groundwork by analysing the interplay between phenomenological constraints and the requirement of an F-theory dual, for heterotic line bundle models. We describe the required geometries in detail and construct many examples. We also describe the constraints on the line bundle sums, and perform a systematic search for phenomenologically interesting models, finding several hundred.

In the second part, we first develop in detail the F-theory dual picture of heterotic line bundle models. The spectral cover description is inappropriate, so we first conjecture the details of the duality. We then verify various aspects, including gauge groups, spectra, supersymmetry conditions, and anomaly conditions, and we treat some interesting subtleties. Using knowledge of this duality, we then develop the F-theory perspective on a well-known but little-utilised aspect of heterotic model building: heterotic NS5-branes, including stacks and intersections. We describe the dual geometry to various NS5-brane configurations, including singular transitions between configurations. We make heavy use of toric geometry and find many pleasing correspondences between the toric data and the NS5-brane configuration.

In the third part, we develop methods to determine closed-form expressions for line bundle cohomology. We focus on the simpler case of complex surfaces as a step towards understanding the case of Calabi-Yau manifolds. These surfaces can also be used as bases for elliptic three-folds, and their cohomology lifted via the Leray spectral sequence. We derive index expressions

for all line bundle cohomology on del Pezzo and Hirzebruch surfaces, and give methods to derive similar formulae on any compact tori surface, using a form of Zariski decomposition. We also discuss general methods to determine formulae on generic spaces, and in a companion paper we construct machine learning networks for this purpose.

Acknowledgements

First and foremost, I would like to acknowledge the enormity of the part that my parents have played in anything that I have achieved. I owe them infinite gratitude, for a lifetime of their unconditional love and tireless support. Every opportunity I have had has been possible only because of their actions, and their part in my life has underpinned everything positive that I have done. I also want to thank my older brother, for a lifetime of support, love, and friendship.

On the road to my graduate studies, I have been indebted also to many others. I would like to acknowledge in particular Paul Baily, without whose enthusiasm, encouragement, and example I would have never pursued physics. I also especially thank Jonathan Jones, for his years of dedicated support and passionate teaching.

In the pursuit of my DPhil, I am deeply indebted to my supervisor, Andre Lukas, for his passion and excitement, for his knowledge and ability, and for his generosity and forbearance. I would also like to offer my heartfelt thanks to my collaborators, for their generosity and their patience, and for their encouragement and their friendship. These thanks go to Andreas Braun, Andrei Constantin, Rehan Deen, and Fabian Rühle.

Finally, these years have been perhaps my happiest, and it would not be so without the friendship of remarkable individuals. I would like to single out two in particular, George Johnson and Hannah Tillim, to whom I owe very much, for their friendship, love, and support. I am also deeply indebted to innumerable others, in particular many members of my college, for their friendship and their delightful company.

My graduate studies would not have been possible without the financial support of a studentship grant from the Science and Technology Facilities Council. I also thank Brasenose College for financial support.

Contents

1 Introduction

1.1 Motivation

In this thesis we will be concerned with aspects of string phenomenology, and specifically there will be a focus on aspects of model building in heterotic string theory and F-theory. Hence we begin with some motivation of these directions. We will begin first with some motivation of string phenomenology in general, before justifying an emphasis on particular kinds of constructions in heterotic string theory and F-theory.

String phenomenology

To work on string phenomenology is to take string theory seriously as a candidate to describe our four-dimensional universe. The programme is to connect the ten-dimensional physics to four-dimensional physics, by developing the conceptual understanding and technical tools to construct, control, and derive the consequences of varied compactification spaces, field backgrounds, and brane content.

Naively, it might go without saying that string phenomenology is well-motivated, since string theory remains the strongest candidate to provide a significantly more unified, fundamental theory of particle physics. There are however several reasonable arguments against studying string phenomenology, and here we argue that it is worthwhile to pursue this direction even in the face of these difficulties.

First let us outline perhaps two of the most reasonable arguments against doing string phenomenology. The first is that we do not understand vacuum selection: we do not know whether or how string theory picks out specific solutions in preference over others. If a vacuum selection principle is understood in future, then all but a tiny fraction of the vast number of hard-earned constructions will be cast aside. Worse, if there is no such mechanism, string theory may not be predictive at all.

The second argument is as follows. Forgetting vacuum selection, we do not even have a complete understanding of how to check whether a given model is indeed a solution, that is, we lack a full understanding of stabilisation[1]. If the present understanding of stabilisation is significantly overturned, then many constructions will be consigned to the waste basket. Worse, we may discover it is not possible to stabilise a universe like ours in string theory.

[1]There continues to be controversy surrounding even the best-understood constructions, most notably the KKLT construction, and the issue has been even more prominent in recent times, in the debate surrounding the de Sitter conjecture.

Some reasons why it is sensible to pursue string phenomenology in the face of these problems are as follows. First, if a vacuum selection is discovered, or if our understanding of stabilisation shifts[2], we must still in both cases understand in detail the path from string compactification data to four-dimensional physics. We must in particular develop the requisite understanding and mathematical tools. These tasks fall in the domain of string phenomenology.

Second, consider the worst case scenario that string theory fails totally as a realistic theory. Certainly some work on string phenomenology would be unceremoniously consigned to irrelevance[3]. However, the study of string phenomenology has at least two compensating virtues. First, many of the mathematical results in the domain of string phenomenology are also of interest irrespective of whether string theory is realistic. In this thesis for example, this is hopefully true of the programme we embark on in Chapter 5. A more classic example is the discovery of Mirror Symmetry. Second, while string model building may fail to give rise to complete models which are controlled and realistic, in the attempt we may discover novel features for Beyond the Standard Model physics, or sharpen our understanding of existing ones, and these theoretical ideas may be experimentally testable on their own merits.

The challenges in string phenomenology fall roughly into two categories. The first challenge is to construct more models, either (a) constructing large classes in the hope of being exhaustive or at least representative, or (b) directly constructing models that are expected to be promising. Of a different flavour is the second challenge, to develop the conceptual understanding and mathematical tools to control and compute the four-dimensional physics resulting in a given model. In this thesis we will be concerned primarily with the second challenge, but we will use the construction of models as a stepping stone.

Heterotic and F-theory phenomenology and their duality

Heterotic string theory continues to provide an attractive avenue in which to pursue questions in string phenomenology. Heterotic $E_8 \times E_8$ string theory was one of the earliest approaches to string phenomenology, and many of the reasons this was an attractive approach then remain valid today. Most obviously, it comes naturally with a large gauge group into which the Standard Model fits, and one consequence is that gauge unification is automatic. Indeed, further, all GUT

[2]We also note that the work in this thesis is to a good degree independent of our precise understanding of stabilisation, since when constructing or studying compactification spaces and gauge backgrounds, the questions we concern ourselves with are essentially at the level of the topology and not the geometry, eschewing in particular the legitimate worries of moduli stabilisation.

[3]Of course, working on any as yet unproven theory runs a similar risk, but it is likely that more effort has been put into string theory than any other similarly unproven theory.

groups are contained, including the exceptional ones, allowing for example SU(5), SO(10), or E_6 GUT groups. Another important feature is that compactifications of the heterotic string give chiral low-energy theories.

There are however other attractive options for string phenomenology, and a particularly appealing one is F-theory. While string theories that come bearing gauge fields are clearly attractive, it was realised with the discovery of D-branes [1] that other string theories too could provide gauge sectors capable of containing the Standard Model. Arguably, the option with the most advantages is the Type IIB description[4]. Some important advantages are that more is known about moduli stabilisation, spacetime-filling D-branes wrap holomorphic cycles and so can be described with the tools of complex geometry, and it is possible to create desirable scale hierarchies through warping [2]. However, there is a prominent drawback in pursuing phenomenology with Type IIB constructions: in D-brane constructions, one cannot realise certain desirable GUT groups and representations. Importantly however, this has been made possible by the advent of F-theory, because it allows the description of non-perturbative features of Type IIB string theory. In particular, in F-theory it is possible to have the spinor representation of SO(10), and to naturally generate the $\mathbf{10\,10\,5}$ Yukawa coupling in SU(5) GUT models, both of which are not present in perturbative Type IIB models. This is a justification from a phenomenological perspective to study F-theory over Type IIB string theory. Additionally there is the practical reason, that by geometrising much of the data, F-theory provides a powerful framework in which we can deploy a well-developed mathematical toolkit.

Given the scope of options, it is particularly interesting to compare across different string theories the possibilities and characteristics for model building in different descriptions. There are several conceivable desirable outcomes. For example, one may learn that a particular attractive feature for model building is most readily implemented in, or even unique to, one description. In another direction, one may be able to gain understanding or technical control of some feature by rephrasing its description with string dualities.

Heterotic line bundle models

The particular corner of string theory that we will focus on is that of heterotic line bundle models, and their dual picture in F-theory.

The reason one might want to specialise to a sub-class of vector bundles is that it is very

[4]Type IIA and Type IIB on Calabi-Yaus are dual through mirror symmetry. But this is not understood to the degree that a specific stable compactification in IIB can be translated to another in IIA. So the virtues of the description of important quantities in IIB do not dualise to virtues in IIA.

difficult to construct and control generic examples. In heterotic string theory the background values of the gauge fields in the internal space are described by vector bundles. For the gauge field values to obey the equations of motion and satisfy any desired phenomenological requirements, such as four-dimensional supersymmetry, the vector bundle in turn must satisfy various constraints. However it is in general very difficult to construct examples of vector bundles that can be shown to satisfy those constraints, even when one has explicit expressions, for example using algebraic geometry, for the bundle and for the compactification manifold. Indeed, historically the construction of appropriate vector bundles has been one of the largest roadblocks to constructing heterotic models.

Line bundle sums are a sub-class of vector bundles which are flexible enough to accommodate very many phenomenologically interesting scenarios but are at the same time simple enough to work with. Line bundles are first of all easy to describe, as they are in one-to-one correspondence with lists of integers of a certain length; this ease is in contrast to the situation for all but the simplest vector bundles. Secondly, it is much easier to prove that a given line bundle sum satisfies the various required mathematical conditions to represent a consistent and desirable heterotic gauge field background. For example, the (poly-)stability condition for supersymmetry is very difficult to prove for a general vector bundle, but is much easier for a line bundle sum. Additionally it is also much easier to compute the four-dimensional massless spectrum of a given line bundle model, because the required cohomology calculations are much more tractable. Because of these two facts, one can systematically construct large sets of examples and scan for phenomenologically interesting models.

Another reason to study line bundle models is that they are a starting point or building block for several purposes. One specific way they can be used as building blocks is to build more general non-Abelian models, for example through the monad construction. Relatedly, line bundle sums are points inside a moduli space for non-Abelian bundles, so one can explore general models by deformations. Additionally since line bundle models are not only global models but are also in some sense rather 'clean', they provide an environment in which other aspects of heterotic string theory can be studied. An example is in the study of NS5-branes in heterotic/F-theory duality which we complete in Chapter 4.

1.2 Outline

In this section we outline the work that will be presented in the later chapters, to give a map of what is to come.

In Chapter 3 we treat the construction of heterotic line bundle models whose F-theory duals are of interest, as a first step towards understanding heterotic/F-theory duality in this scheme, before we turn in Chapter 4 to aspects of the duality.

For heterotic line bundle models to both be phenomenologically interesting and potentially have an F-theory dual, the compactification manifold must be of a certain type, and we first determine and describe this class of manifolds and their relevant properties. In order for there to potentially be an F-theory dual, the heterotic manifold must first of all be elliptically fibered. But additionally a phenomenological requirement, specifically the existence[5] of a Wilson line, requires the compactification manifold to admit a freely-acting involution, with the implication that the elliptic fibration has two sections. Hence we describe in detail manifolds with an elliptic fibration with two sections, satisfying also some additional constraints to ensure the presence of the involution. We derive or collect the relevant geometric properties of these manifolds for model building purposes, such as divisor and curve bases, the second Chern class, and the Mori and Kähler cones. The smoothness of the elliptic fibration together with the existence of a freely-acting involution also constrains the base: in particular the base must admit an involution with at most fixed points, i.e. there must be no fixed curves. Together with the later discussion of the line bundle sums, this represents a construction and collection of knowledge and model building tools tailored to this class of models.

Next we turn to describing the general conditions on the line bundle sum, for the model to be phenomenologically viable and to potentially have an F-theory dual, and we collect and explain the tools required to deduce properties of these models. There are interesting interplays and tensions between the requirements for an F-theory dual to exist and the conditions for the model to be phenomenologically viable, which we discuss explicitly. Much of our time is spent collecting and explaining the specifically tailored tools that are required to compute the properties of these line bundle models. One interesting aspect of this is in cohomology computations, where we must use a tailored version of the Leray spectral sequence to relate cohomologies to those on the base.

Finally, we construct examples of suitable manifolds[6], and we then systematically construct hundreds of line bundle models on these manifolds, to both illustrate the application of our model building tools and to provide a vast concrete testing ground for future studies of F-

[5]We will discuss Wilson lines in more detail below. They are a part of the gauge background, having zero field strength but able to break the GUT group to the Standard Model gauge group.

[6]In particular, we are exhaustive within the class of weak Fano toric bases. These are toric surfaces with nef and big anti-canonical bundle. This includes for example several Hirzebruch and del Pezzo surfaces.

theory duals. For each of these constructed models we compute the massless spectrum, and an important point is that we find the unexpected result that heterotic line bundle models with F-theory duals tend to have atypical features: in particular, they have an unusually large number of vector-like states. We collect the statistics of the spectra for comparison with generic models without potential F-theory duals.

In Chapter 4 we turn to describing some key aspects of the F-theory duals of heterotic line bundle models. We conjecture the F-theory duals and perform many non-trivial checks of the duality, and we complete an in-depth study of the duality for NS5-branes. The work in this chapter is complementary to that in the previous chapter, treating other parts of the problem.

A central result of this work is that we conjecture the dual F-theory models to heterotic line bundle compactifications, and we verify the conjecture by checking many aspects of the duality in detail. While for phenomenology we are in the end interested in chiral heterotic models, for the purpose of checking many aspects of the duality we are able to work with non-chiral heterotic models. This is useful because for these models heterotic/F-theory duality is better understood. These duality checks are then one part of the story of completing the full duality study for non-chiral models. Following our conjecture we explicitly construct the global dual F-theory four-fold geometry and flux, in particular making ample use of the tools of toric geometry to give an efficient description. With the explicit heterotic models and the explicit F-theory models, we then are able to concretely match many features, including anomaly conditions, supersymmetry conditions, and counts of chiral multiplets, vector multiplets, and massless U(1)s. In the process of matching the chiral multiplets, we also expose an interesting subtlety: in a particular sub-class of examples, the standard heterotic and F-theory multiplet counts are in contradiction. We discuss in detail the mechanisms lying behind the multiplet mismatch and we explain a likely resolution.

Another central result is the completion of an extensive study of the global F-theory duals of consistent heterotic models containing NS5-branes. This is in part opportunistic: following our conjecture, one finds that heterotic line bundle models have especially 'clean' F-theory duals. This means the situation is especially convenient for studying in general the F-theory dual picture of heterotic NS5-branes. Additionally, heterotic line bundle models themselves generically contain NS5-branes, so for the purpose of understanding these models it is crucial to develop knowledge of this duality, and in particular of the interplay with the features dual to line bundle sums. It is known that the heterotic NS5-branes are in F-theory encoded entirely in

the geometry of the F-theory four-fold[7]. Our description of the F-theory geometry in terms of toric data is particularly useful here: many properties of the NS5-brane configuration are neatly mirrored in the toric description. We discuss these connections in detail. We note that literature on the subject of NS5-branes in heterotic/F-theory duality has been essentially 'local' [4–6], and our study in this direction advances that understanding to global models.

Having done the work of constructing the global F-theory models dual to arbitrary NS5-brane configurations, we take the opportunity to develop understanding of a poorly-understood aspect of heterotic string theory, intersecting and coincident NS5-branes, by studying in detail the F-theory dual picture of the transitions between different possible NS5-brane configurations. Intersections and stacks of NS5-branes are a little-utilised corner of model building in heterotic string theory, and by constructing and controlling the global dual F-theory picture we may gain further understanding. Since NS5-branes are a generic feature of heterotic models, this is one aspect of the understanding of heterotic line bundle models, but it is also more general. Again the toric description that we utilise makes for several very pleasing correspondences. Aspects of brane transitions can be seen to nicely correspond to operations on the toric description of the F-theory four-fold, for example coincident branes and brane orderings are seen as the removal of toric rays or as changes in the triangulation of the toric polytope.

In Chapter 5 we turn to addressing a technical aspect of heterotic line bundle model building. Specifically, we make substantial progress on the problem of analytically understanding line bundle cohomologies. As we will see, this gives us control over a key aspect of model building in the context of heterotic/F-theory duality, and also has a broad range of other applications.

In general, having closed-form expressions for line bundle cohomologies would be hugely significant for our understanding of phenomenology. The computation of line bundle cohomologies is crucial because these give the spectrum of a given model. However cohomologies usually have to be computed on a case-by-case method, using methods of computational algebraic geometry implemented in software packages. There are two reasons why this is an undesirable situation. Firstly, these computations are often intensive in the use of both computational power and time. Secondly, this does not provide any understanding of the general features of line bundle cohomologies, since these computations are essentially 'black boxes'. Having closed-form expressions drastically reduces the required computational power and time, but secondly and more importantly this would allow for bottom-up model building, since we would be able to

[7]We do not discuss NS5-branes wrapping the heterotic fiber, since it is well-understood how these map into D3 branes [3].

directly construct the models with a desired spectrum.

In this chapter, we focus on determining closed-form expressions for line bundle cohomologies on complex surfaces that are commonly used in string theory applications. Partly this is a step towards understanding cohomology on higher-dimensional complex manifolds in general, but importantly it also will immediately lead to closed-form expressions on elliptic Calabi-Yau three-folds, which are the spaces of interest for heterotic/F-theory duality. The reason for the implication on the three-fold is that, through the Leray spectral sequence, closed-form expressions for line bundle cohomology on the base can be lifted to cohomology on the elliptic three-fold. The complex surfaces for which we derive closed-form expressions are some of the most commonly used base spaces for elliptic three-folds. They also often appear in other string theory contexts, for example as loci for D7-branes in Type IIB string theory or F-theory. The piecewise (almost) polynomial formulae we derive are also an important step towards understanding recently observed phenomena in line bundle cohomology on Calabi-Yau three-folds [7–11].

In particular, we determine closed-form index expressions for line bundle cohomology on all Hirzebruch and del Pezzo surfaces, and additionally outline more general methods and in many cases an algorithm to determine the expressions for any complex surface. For this purpose we implement a form of Zariski decomposition, a powerful piece of mathematics that is relatively under-utilised in string theory. We also illustrate general methods to determine from raw cohomology data the underlying piecewise (almost) polynomial formulae, including machine learning methods which we pursue at length in a companion paper [12].

The below chapters are based on work that has been published elsewhere. Chapter 3 is based on Ref. [13], Chapter 4 is based on Ref. [14], and Chapter 5 is based on Ref. [15], while having connections also with Ref. [12].

2 Background

2.1 Superstring theories in ten dimensions

In this section we give a very brief overview of some key basic facts about the five superstring theories, M-theory, and branes.

Superstring theory

The classical theory, whose quantisation corresponds to the basic idea for a string theory, is that of a relativistic string. A string is a one-dimensional object, which can be either open or closed, having the topology of either a line or a circle. The action S for a relativistic string is

proportional to the area of the 'worldsheet', which is the locus traced out in spacetime under time evolution of the string. That is,

$$S = -T \int \mathrm{d}A \,, \tag{2.1}$$

where $\mathrm{d}A$ is the area element, and T is an overall constant which we call the 'string tension', having units of energy per unit length. An open and closed string trace out a sheet and a cylinder respectively, but in both cases we refer to the 'worldsheet'.

An important viewpoint is that of the 'worldsheet theory'. Crucially, the action for the dynamics of the string's evolution in spacetime can alternatively be treated as an action for a field theory on the worldsheet. Here, the fields are scalar fields whose values correspond to the values of the spacetime coordinates of the points of the worldsheet in its embedding into spacetime.

To upgrade the classical theory of a relativistic string to a quantum-mechanical theory, one can enhance the worldsheet field theory to a quantum field theory. In the field theory description, excitations of the scalar fields correspond to oscillations on the string.

One can also upgrade this theory to be supersymmetric. The scalar fields corresponding to coordinate values are of course bosonic, and one can add their supersymmetric partners to complete the action into that of a supersymmetric two-dimensional field theory. The resulting theory is called a 'superstring theory'.

Supersymmetry on the worldsheet theory often gives rise to supersymmetry in the 'target space', i.e. the spacetime of the propagating string. This is the case in the commonly considered superstring theories, and we will focus on these theories below. However there are also string theories without target space supersymmetry, for example Type 0 string theory.

There are several remarkable features of the superstring theories. The most obvious is that superstring theory is a theory of quantum gravity. This occurs because one of the excitations of the quantum-mechanical relativistic string can be seen to give rise to a massless spin-2 particle, which one can identify as the graviton.

Second, unusually for theories in physics, the consistency of the relativistic, supersymmetric two-dimensional field theory requires that the number of spacetime dimensions for the string embedding be fixed[8]: this number must be 10. We also note that when the field theory is not enhanced to be supersymmetric, giving what is called 'bosonic string theory', the critical dimension is instead 26.

[8]It is possible to define string theories in other dimensions, but one tends to lose important properties, like spacetime Lorentz invariance or stability. The theories in 26 or 10 dimensions are called 'critical' string theories.

Third, the superstring theories have only a single parameter: the string tension T mentioned above. Equivalently, one can define the 'string length' l_s or the 'Regge slope parameter' α', by

$$\alpha' \equiv \frac{1}{2\pi T}\,, \quad l_s^2 = \alpha'\,. \tag{2.2}$$

The chosen parameter is in principle a quantity to be determined by experiment. Usually these are estimated to be around the Planck scale, since string theory is a theory of quantum gravity.

There are also many other remarkable features, some of which we will discuss below.

The consistent superstring theories

There are five known superstring theories with spacetime supersymmetry, each of which lives in ten dimensions. These are called Type I, Type IIA, Type IIB, heterotic SO(32), and heterotic $\mathrm{E}_8 \times \mathrm{E}_8$.

These theories contain different combinations of open and closed strings: the heterotic string theories contain only closed strings, while Type I and the Type II theories contain both closed and open strings. Relatedly, they contain different brane content, which we discuss below.

These theories also have different amounts of spacetime supersymmetry: the Type I theory and the two heterotic theories have $\mathcal{N} = 1$ supersymmetry, and the Type II theories have $\mathcal{N} = 2$ supersymmetry. The minimal spinor in ten dimensions, which is Majorana-Weyl, has 16 components, so these theories have 16 and 32 supercharges respectively. Additionally, while the two Type II string theories have the same amount of supersymmetry, they have different kinds: in the case of Type IIA supergravity, the two spinor generators of the supersymmetry have opposite chirality, while for IIB supergravity the generators have the same chirality. These types of supersymmetry are respectively referred to as '(1,1)' and '(2,0)' supersymmetry.

The Type I and the two heterotic string theories, unlike the Type II theories, have gauge symmetries: Type I string theory has an SO(32) gauge symmetry, while the two heterotic theories have their eponymous gauge symmetries. In the low-energy supergravity description, which we discuss in Section 2.2 below, there are vector fields corresponding to these gauge groups.

M-theory

The five superstring theories are theories of quantum gravity. In addition to these, there is also a related, hypothesised 11-dimensional theory of quantum gravity, which has been named 'M-theory'. The fundamental objects in M-theory are not strings but higher-dimensional branes, and since these do not have a microscopic description, we lack even a partial microscopic description of M-theory, in contrast to the situation in the superstring theories.

M-theory is conjectured to be the theory whose low-energy description is given by 11-dimensional supergravity. We will discuss 11-dimensional supergravity in Section 2.2 below, but we note here that from this low-energy description, one can deduce partial information about M-theory. Two key observations are as follows. First, this theory has $\mathcal{N} = 1$ supersymmetry, and so has 32 supercharges, corresponding to the minimal (Majorana) spinor in eleven dimensions. Second, one can deduce that the fundamental objects in M-theory are 3-dimensional and 6-dimensional branes, which we call 'M2-branes' and 'M5-branes'.

One reason to conjecture the existence of M-theory is the presumption that 11-dimensional supergravity can be UV completed into a quantum gravity, as the 10-dimensional supergravities are UV completed into the five superstring theories. Another reason is that the assumption of the existence of M-theory helps to connect various string dualities into a single framework.

Open strings and branes

The five superstring theories discussed above, while formulated in terms of strings, also imply the existence of higher-dimensional objects, called 'branes'. One class of these are the 'D-branes', which are intimately related to and understood via open strings. Below we will also discuss the NS5-brane, which is not related to open strings.

The existence of D-branes is implied by the dynamics of strings with Dirichlet boundary conditions: they are objects on which open strings can end. The D-brane itself is a higher-dimensional object; one often writes Dp-brane where p is the number of space dimensions, so that the D-brane is $(p+1)$-dimensional.

In perturbative string theory, a D-brane is a non-perturbative object, i.e. its dynamics cannot be directly seen in the string spectrum. As far as perturbative string theory is concerned, a D-brane is a feature of a consistent background state about which perturbation theory can be performed.

In perturbation theory about a D-brane solution, open strings can attach (at one end or both) to the D-brane, giving localised states. By having computational understanding and control over the dynamics of open strings attached to D-branes, one indirectly gains computational control over the dynamics of the D-brane. Hence while D-branes are non-perturbative objects, their dynamics can be understood in perturbation theory.

Additionally, closed strings can be absorbed and emitted in the presence of a D-brane solution, which gives the D-brane long-range influence. We briefly discuss the appearance of D-branes in the low-energy field theory description of supergravity in Section 2.2.2 below.

In the heterotic string theories, there are no open strings and no D-branes. In Type I string theory, there are D1-, D5-, and D9- branes, and additionally open strings exist as perturbative states about an empty vacuum background. In the Type II string theories, one can have D-brane vacuum solutions, and open strings appear as perturbations around (only) these solutions. In Type IIA string theory there are D0-, D2-, D4-, D6-, and D8-branes, while in Type IIB string theory there are[9] D(-1)-, D1-, D3-, D5-, D7-, and D9-branes.

There is also the NS5-brane, which is a non-perturbative (5+1)-dimensional object, present in heterotic and the Type II string theories. In contrast to D-branes, open strings do not attach to the NS5-brane, and so there is no similar (indirect) microscopic understanding of the dynamics of an NS5-brane. We will discuss NS5-branes from a field theory point of view in Section 2.2.2 below.

2.2 Effective supergravities

At low energies compared to the string scale, the superstring theories are well-approximated by supergravity theories, which capture the dynamics of the massless states. Supergravity theories are quantum field theories. They are also supersymmetric: in particular, these are the theories where supersymmetry has been upgraded to a local symmetry (this means the supersymmetry generator is upgraded to a field, and in particular this can be identified with a gravitino, the superpartner of the graviton).

In this section we will focus on the heterotic and Type II supergravities, and more briefly 11-dimensional supergravity, as these will be the relevant supergravities for our discussions of heterotic and F-theory compactifications in later chapters.

2.2.1 Field content and action

Heterotic supergravity

Heterotic supergravity has $\mathcal{N} = 1$ supersymmetry. Both types of heterotic supergravity contain as their massless field content a single gravity multiplet and 496 vector multiplets. In $E_8 \times E_8$ heterotic supergravity, these vector multiplets transform in the adjoint representation of $E_8 \times E_8$. Similarly, in SO(32) heterotic supergravity they transform in the adjoint representation of SO(32).

[9] Recall a Dp-brane is $(p+1)$-dimensional, so a D(-1)-brane is 0-dimensional. Hence it is an example of an instanton.

In the gravity multiplet of heterotic supergravity, the bosonic fields are the scalar dilaton ϕ^{H}, the graviton G_{MN}, and the 2-form Kalb-Ramond field B_{MN}. In a vector multiplet, the bosonic field is the gauge vector field A.

The bosonic sector action, which takes the same form for either heterotic supergravity, is

$$S^{\text{het.}} = \frac{1}{2\kappa_{10}^2}\int \mathrm{d}^{10}X\sqrt{-G}\,e^{-2\phi^{\mathrm{H}}}\left(R + 4\partial_M\phi^{\mathrm{H}}\partial^M\phi^{\mathrm{H}} - \frac{1}{2}|H_3|^2 - \frac{\alpha'}{4}\mathrm{tr}|F_2|^2\right) . \tag{2.3}$$

The overall constant is given by $2\kappa_{10} \equiv (2\pi)^7\alpha'^4$. The fields in the action correspond to the fields in the above multiplets as follows. R is the Ricci scalar constructed from the metric G. In the expression, an instance of G without any indices is the determinant. The two-form F_2 is a field strength for the non-Abelian vector field A,

$$F_2 = \mathrm{d}A + A\wedge A\,, \tag{2.4}$$

and the three-form H_3 is shorthand for the following useful combination of quantities, which we see appears in the action like a corrected field strength for B_2,

$$H_3 := \mathrm{d}B_2 - \tfrac{1}{4}\alpha'\left(\omega_3^{\text{gauge}} - \omega_3^{\text{grav.}}\right) . \tag{2.5}$$

Here ω_3^{gauge} and $\omega_3^{\text{grav.}}$ are Chern-Simons terms, defined as

$$\begin{aligned}\omega_3^{\text{gauge}} &:= \frac{1}{30}\mathrm{tr}\left(A\wedge\mathrm{d}A - \frac{i}{3}A\wedge A\wedge A\right) ,\\ \omega_3^{\text{grav.}} &:= \mathrm{tr}\left(\xi\wedge\mathrm{d}\xi - \frac{i}{3}\xi\wedge\xi\wedge\xi\right) ,\end{aligned} \tag{2.6}$$

where ξ is the spin connection. The traces are taken in the adjoint representations.

Type IIB supergravity

As discussed in Section 2.1 above, both Type II string theories have $\mathcal{N} = 2$ supersymmetry, but they are distinguished in that the two supersymmetry generators have opposite chirality in Type IIA and the same chirality in Type IIB. The same is true of the Type II supergravities. In both Type II supergravities, the massless field content consists of a single gravity multiplet, but the fields in the multiplet differ in the two cases because of the difference in the chiralities of the supersymmetry generators.

We will be primarily interested in Type IIB supergravity, so we skip the Type IIA description. In Type IIB supergravity the bosonic fields in the gravity multiplet are the scalar dilaton ϕ^{IIB}, the graviton G_{MN}, and the 2-form Kalb-Ramond field B_{MN}, as well as a scalar a, a 2-form C_{MN}, and a 4-form C_{MNPQ}.

The bosonic sector action is

$$S^{\text{IIB}} = \frac{1}{2\kappa_{10}^2}\int \mathrm{d}^{10}X\sqrt{-G}\left[e^{-2\phi^{\text{IIB}}}\left(R + 4\partial_M\phi^{\text{IIB}}\partial^M\phi^{\text{IIB}} - \frac{1}{2}|H_3|^2\right) - \frac{1}{2}|F_1|^2 - \frac{1}{2}|\tilde{F}_3|^2 - \frac{1}{2}|\tilde{F}_5|^2\right] - \frac{1}{2}\int C_4 \wedge H_3 \wedge F_3\,. \tag{2.7}$$

Here H_3 is as in Equation (2.5), and $\tilde{F}_3$ and $\tilde{F}_5$, which appear in the action as corrected fields strengths, are given by

$$\tilde{F}_3 := F_3 - aH_3\,, \quad \tilde{F}_5 := F_5 - \frac{1}{2}C_2 \wedge H_3 + \frac{1}{2}B_2 \wedge F_3\,, \tag{2.8}$$

and where F_1, F_3, and F_5 are ordinary fields strengths for the zero-form a, the 2-form C_2, and the 4-form C_4.

Additionally this action should be supplemented by a self-duality condition for the 5-form field strength,

$$F_5 = *F_5\,, \tag{2.9}$$

where $*$ denotes the Hodge dual.

11-dimensional supergravity

In 11 dimensions, there is precisely one theory of supergravity, which we may then refer to as '11-dimensional supergravity'. This supergravity theory is the low-energy limit of the hypothesised M-theory.

11-dimensional supergravity is considerably simpler than the supergravities in ten dimensions. It has $\mathcal{N} = 1$ supersymmetry, and the massless field content consists of just a single gravity multiplet. The bosonic fields in the 11d gravity multiplet are the graviton $\mathcal{G}_{MN}$ and a 3-form $\mathcal{C}_3$. The bosonic sector action is

$$S^{\text{11d}} = \frac{1}{2\kappa_{11}^2}\int \mathrm{d}^{11}\mathcal{X}\sqrt{-\mathcal{G}}\left(R - \frac{1}{2}|F_4|^2\right) - \frac{1}{6}\int \mathcal{C}_3 \wedge F_4 \wedge F_4\,, \tag{2.10}$$

where $F_4 := \mathrm{d}\mathcal{C}_3$. Here $\mathcal{G}$ is the determinant of the metric.

2.2.2 Brane solutions

In string theory, branes appear as non-perturbative background states around which perturbative string theory can be performed, as discussed above in Section 2.1. In the low-energy regime where supergravity is a good description, these brane backgrounds are seen as background values for fields. In particular, the brane backgrounds are seen in the following fields. The NS5-brane is a background solution in the metric, the dilaton, and the Kalb-Ramond two-form. A D-brane in

Type IIA (IIB) is a background solution in the metric, the dilaton, and the odd (even) differential forms.

The localised degrees of freedom which are supported on the brane also find a field theory description. That is, the branes can be seen to support localised field theories.

An important example is the case of gauge fields localised on D-branes, which are fields in a localised super Yang-Mills theory with unitary gauge group. This theory corresponds to the localised degrees of freedom of attached open strings, discussed in Section 2.1 above.

Additionally, we recall that at the intersection between D-branes there are localised degrees of freedom corresponding to open strings stretching between the branes. These give rise to localised matter multiplets[10]. These are particularly important for phenomenology, as we discuss in Section 2.3.3 below.

2.3 Compactification

One can consider 'compactifying' a theory, by putting it on a background spacetime that has compact dimensions. The simplest situation is to take the topology of the spacetime S_D to be a product, $S_D = \mathcal{S}_d \times X_{D-d}$, between a compact 'internal' space X_{D-d} and an 'external' non-compact spacetime $\mathcal{S}_d$.

Compactification is crucial in string phenomenology for the following reason. When the size of the compactified dimensions is very small compared to length scales accessible in experiment, to an observer physics is captured by an effective theory of d spacetime dimensions. This allows superstring theory to be a candidate to describe our observed four-dimensional physics.

Here we will only discuss the case of a product topology, since it is the simplest case and a common choice. However we note that one can also consider more complicated topologies. For example, one can consider a fibration.

Note that even if the topology is a product, the geometry might not be: the background metric may not separate into a product metric. Again we will focus on the simplest and most common choice, of a product metric. In particular, the external space will be taken to be Minkowski spacetime. However there are other possibilities. Perhaps the simplest deviation from a product metric is to allow the external dimensions to be rescaled on movement through the internal dimensions, in what is called a 'warped product' geometry.

[10]There are always massless chiral fermions at the intersection, but whether their superpartners are massless depends on the angles of the brane intersection.

Of course, it is important to note that the background metric cannot be chosen with total freedom: only some metrics will be solutions of the theory. One must check that any assumed background fields indeed satisfy the equations of motion.

2.3.1 Supersymmetry in the external space

Usually, one considers compactifications that preserve some supersymmetry in the external dimensions. Historically, this could be motivated by the explanatory power of observable low-energy supersymmetry, but since supersymmetry has now not been observed at the most desired energy scale this has become a weaker argument.

However, it is nonetheless very useful to study supersymmetric models. The reason is that in these models it is much easier to control and study the resulting effective theory in the uncompactified dimensions. Hence these provide toy models, to help to understand more general compactifications.

We hence focus on the constructing compactification spaces that guarantee $\mathcal{N} = 1$ supersymmetry in the external dimensions. This means considering compactification spaces that are such that one of the 10-dimensional supersymmetry generators descends to a 4-dimensional supersymmetry generator.

For a 10-dimensional spinor field to give rise to a 4-dimensional one, there must be 10-dimensional spinor solutions ξ that vary only in the uncompactified dimensions, being covariantly constant in the internal space,

$$\nabla_6 \, \xi_{10} = 0 \,, \tag{2.11}$$

where ∇_6 is the covariant derivative in the internal directions. This is called a 'Killing spinor' on the internal space.

Holonomy

The existence of a Killing spinor has a very important implication. Since a covariantly constant spinor is invariant under parallel transport around loops, the spinor must form a singlet under the holonomy group of the manifold, and the existence of singlet representations constrains the holonomy. In particular, singlet representations exist when the holonomy group is SU(3), and hence we are interested in compact Riemannian manifolds with SU(3) holonomy.

It can be shown that a manifold with SU(3) holonomy is a complex manifold, and in fact further that it is a Kähler manifold. Hence we are interested in the subset of compact Kähler manifolds that have SU(3) holonomy. Generically, the holonomy group of a compact Kähler

manifold is U(3), but when the manifold admits a Ricci-flat metric, the holonomy group is SU(3). Hence we are interested in searching for those compact Kähler manifolds that admit Ricci-flat metrics.

Calabi-Yau manifolds

It is in general very hard to construct explicit metrics on all but the simplest manifolds. Hence if checking that a manifold admitted a Ricci-flat metric required constructing the metric, it would be very difficult to find the desired compact Kähler manifolds.

Luckily, however, there is a simple topological condition that guarantees the existence of a Ricci-flat metric. This is due to the Calabi conjecture, which was conjectured by Eugenio Calabi and proved by Shing-Tung Yau. The relevant consequence is that when a compact Kähler manifold has vanishing first Chern class, then it admits a (unique) Ricci-flat metric, and hence has SU(3) holonomy. These manifolds are called 'Calabi-Yau manifolds', and they are ubiquitous in string theory applications.

2.3.2 Features in the internal space

In the following, we will use a supergravity description for many aspects. This is a good description whenever the curvature scale of the internal space is large compared to the string length.

Algebraic geometry

It is common to represent the internal space as an algebraic variety, i.e. as the zero locus of a polynomial, inside a simple embedding space. One common example is the Complete Intersection Calabi-Yaus (CICYs), where the ambient space consists of a product of complex projective spaces. In another of the most common examples, the ambient space is a toric variety.

The reason to use an algebraic representation of the manifold is that it allows useful explicit control over certain properties. For example, to control the appearance of a singularity one would typically need to write down an explicit metric, but with the algebraic representation the appearance of the singularity can be implemented by constraining the allowed monomials in the defining polynomial. With the algebraic representation in hand one can use powerful methods of algebraic geometry.

Wrapped branes

Branes are higher-dimensional objects and so extend in several directions. They can wrap internal directions or extend across external directions, in various combinations. The combination

we will typically be concerned with is the 'spacetime-filling' case, where the brane wraps all four of the external directions, while possibly also wrapping internal directions. These are common ingredients in string model building because they do not break the Poincaré symmetry of the external spacetime.

Alternatively, branes can wrap some some smaller number (< 4) of the external dimensions, as well as possibly some internal dimensions. For example, a wrapped brane could extend into two dimensions of the external spacetime, and in this case it appears in the external space as a string. Finally, branes can also be entirely internal, existing only at a point in the external spacetime.

In addition to preserving Poincaré symmetry, typically one is interested in brane configurations that preserve supersymmetry of the effective theory in the external spacetime. When a brane wraps a submanifold, or 'cycle', of the internal space in a way that preserves some external supersymmetry, the cycle is called a 'supersymmetric cycle'.

When a brane wraps an even-dimensional cycle, the supersymmetric cycles are simply the holomorphic submanifolds. When it wraps an odd-dimensional cycle, the supersymmetric cycles are what are called 'special Lagrangian' cycles. When restricting to spacetime-filling branes, these cases correspond respectively to the wrapping of an even-dimensional or odd-dimensional brane.

Internal field backgrounds

In the supergravity description, there are gauge fields present in the heterotic and Type II string theories, and these gauge fields can take on non-trivial background expectation values. Note that, while turning on vector field backgrounds in the external spacetime would be a detectable violation of Lorentz invariance, this is not so for internal vector field backgrounds.

In heterotic supergravity, there are gauge fields already in the 10-dimensional theory, and these can take on background values throughout the internal space. In the Type II supergravities, as mentioned in Section 2.2.2 above, the gauge fields are localised on D-branes.

In order to preserve supersymmetry in the external dimensions, the expectation values must satisfy certain conditions.

In the heterotic case, the equations of motion for the background gauge fields are called the 'Hermitian Yang-Mills' equations. These are

$$F_{2,0} = 0\,, \quad F_{0,2} = 0\,, \quad F \wedge J \wedge J = 0\,, \tag{2.12}$$

where $F_{2,0}$ is the holomorphic-antiholomorphic part of the field strength F, with respect to the complex structure on the internal manifold, and similarly for $F_{0,2}$, and J is the Kähler form.

In the case of gauge fields on D-branes, the situation depends on whether the D-brane is even- or odd-dimensional. In the case of even-dimensional D-branes (which appear in Type IIB string theory and wrap holomorphic cycles), the background gauge fields satisfy a Hermitian Yang-Mills equation. In the case of odd-dimensional D-branes (which appear in Type IIA string theory and wrap special Lagrangian cycles), the background gauge fields vanish[11].

Mathematically, the internal gauge field backgrounds can be represented by vector bundles[12]. For example, line bundle sums correspond to turning on backgrounds in U(1) subgroups of the gauge group.

The conditions in Equation (2.12) on the gauge field background, for external supersymmetry to be preserved, translate into natural conditions on the vector bundle. This translation is due to the Donaldson-Uhlenbeck-Yau theorem [16, 17]. The result is that the first two conditions correspond to the bundle being holomorphic, and the final condition is satisfied when the bundle is poly-stable. Note that, while holomorphicity is relatively easy to impose, poly-stability is more difficult, and this is a significant obstacle in determining viable bundles.

2.3.3 Physics in the external space

For phenomenology, one is interested in the effective theory in the external spacetime. Here we discuss how some important aspects of the external physics are determined by properties of the internal space and features within it.

Algebraic topology

A given aspect of the external physics is determined by particular properties of the internal space and its features. In many cases this mapping from internal properties to external physics is well-known. However, it may still be very difficult to perform the requisite mathematical computation to determine those relevant internal features. This is perhaps the most common difficulty faced in string phenomenology.

Some internal properties are significantly easier to compute, because they are topological. In particular, very often one requires only the computation of some algebraic object, and often only

[11] Note that on a D-brane, the natural background field is not quite the gauge field strength, but rather the difference between it and the Kalb-Ramond field. This is the field whose dynamics we are discussing.

[12] Actually, more complicated examples require more complicated mathematical descriptions, for example in cases of singular geometries one requires sheaves.

their coarse properties. For example, the computation of dimensions of homology or cohomology groups often suffices to determine the number of particles with given spin, charge, etc, in the external effective theory. For these computations, one can use the powerful tools in algebraic topology.

Some properties of the external physics, on the other hand, require computations in differential geometry. These are in general much more difficult, because they require one to work with explicit realisations of the geometry of the internal space, bundles, etc, which are very complicated. For example, in order to compute the physical Yukawa couplings of the external effective theory, one requires an explicit metric.

Gauge symmetries

The observable gauge fields in the external spacetime, which are an important aspect of 4-dimensional physics, are determined by an interplay between the string theory and the compactification space. This works differently in the heterotic and Type II theories.

In the heterotic theories, gauge fields are already present throughout the external dimensions, and the internal gauge field backgrounds determine how the initial $E_8 \times E_8$ or $SO(32)$ gauge group is broken in the external dimensions. Hence in the heterotic theories the gauge symmetry is carved out from an initial gauge group. In the Type II theories, on the other hand, since the gauge fields are localised on D-branes, it is spacetime-filling D-branes that can give rise to gauge groups in the external dimensions. Hence in Type II theories the gauge symmetry is built up using branes. One can also turn on background fields on the branes to break to a smaller gauge group.

Recall from Section 2.3.2 above that gauge field backgrounds are represented mathematically by vector bundles. The choice of vector bundle corresponds to a choice for the kind of gauge field background. For example, line bundle sums turn on $U(1)$ subgroup backgrounds, and hence tend to leave $U(1)$ factors in the unbroken gauge group[13]. As a more specific example, using a rank-five line bundle sum with vanishing first Chern class corresponds to turning on a background in a $S(U(1)^5))$ subgroup, and this breaks an E_8 symmetry as follows,

$$E_8 \to SU(5) \times S(U(1)^5)\,. \tag{2.13}$$

This is a commonly-used breaking pattern in heterotic $E_8 \times E_8$ string theory since $SU(5)$ is a desirable GUT group.

Matter

[13]These tend to be made massive by the Green-Schwarz mechanism. See e.g. Refs. [18, 19].

Crucial for model building is the appearance of appropriate matter charged under the unbroken gauge symmetries. The appearance of charged matter works differently in the heterotic and Type II string theories.

First we discuss the heterotic case. Note that the effective theory in the external dimensions has Lorentz symmetry, which comes from restricting the symmetry of the 10-dimensional spacetime. Hence a 10-dimensional vector can restrict upon compactification to a vector plus several scalars, which are however still charged under the gauge symmetry. In this way gauge fields can give rise to charged matter in the uncompactified dimensions. In the heterotic theories, charged matter descends from the 10-dimensional $\mathrm{E}_8 \times \mathrm{E}_8$ or SO(32) gauge field multiplets. We discuss a specific example of an SU(5) GUT theory in Section 3.3.2.

Next we discuss D-brane constructions. There are two sources of matter: 'bulk matter' and 'localised matter'. Bulk matter descends from the gauge fields that propagate on the bulk of the brane, to the external spacetime filled by the D-brane, much as in the heterotic case. But additionally, extra matter states can arise at brane intersections from localised degrees of freedom. Importantly, this localised fermionic matter can be chiral. In particular, the chirality can be counted by the intersection number between the wrapped cycles. In the duality checks in Section 4.4 we compute the matter spectrum in some particular IIB/F-theory models.

Moduli

Moduli are massless scalar fields appearing in the external spacetime. Here we discuss several sources of moduli. Note that, for phenomenology, massless scalar fields are undesirable[14], since they are not present in our observable universe. Hence these should ultimately be 'lifted' to have masses.

One constant source are moduli arising from the metric of the compactification manifold. For a Calabi-Yau, these can be separated into the complex structure and Kähler parameters. The numbers of these two types of moduli are counted by the Hodge numbers of the compactification space X,

$$\#\text{ Kähler mod.} = h^{1,1}(X)\,, \quad \#\text{ com. str. mod.} = h^{2,1}(X)\,. \tag{2.14}$$

Second, there may be deformations of the gauge vector bundle background that continue to satisfy the equations of motion. These deformations appear in the effective external theory as massless moduli, and these are called 'bundle moduli'. For example, in line bundle models such moduli will deform the bundle into a more general, non-Abelian one.

[14]Some massless scalars may be acceptable, depending on their interaction with other fields. Axions are an example of acceptable massless scalars.

Third, possible deformations of branes give rise to moduli. Recall from Section 2.3.2 above that branes preserving external supersymmetry must wrap supersymmetric cycles. When there is a continuous set of supersymmetric submanifolds, then there are certain directions in which it costs no energy for a brane to move and deform. These possibilities appear as 'deformation moduli' in the massless spectrum in the effective theory in the external dimensions (conversely, deformations to a non-supersymmetric cycle are obstructed). These deformation moduli appear as scalar fields in the worldvolume theory of the brane.

3 Heterotic Line Bundle Models on Elliptically Fibered Calabi-Yau Three-folds

In this chapter we analyze heterotic line bundle models on elliptically fibered Calabi-Yau (CY) three-folds over weak Fano bases. In order to facilitate Wilson line breaking to the Standard Model group, we focus on elliptically fibered three-folds with a second section and a freely-acting involution. Specifically, we consider toric weak Fano surfaces as base manifolds and identify six such manifolds with the required properties. The requisite mathematical tools for the construction of line bundle models on these spaces, including the calculation of line bundle cohomology, are developed. A computer scan leads to more than 400 line bundle models with the right number of families and an $SU(5)$ GUT group which could descend to Standard-like Models after taking the $\mathbb{Z}_2$ quotient. A common and surprising feature of these models is the presence of a large number of vector-like states.

The work presented in this chapter in based on Ref. [13], and was completed in collaboration with Andreas P. Braun and Andre Lukas. We thank Evgeny Buchbinder for collaboration at an early stage of this work, and Fabian Ruehle for helpful discussions during preparation.

3.1 Introduction

Heterotic string model building on CY manifolds requires an understanding of the gauge bundle on the compactification space and this constitutes one of the main technical challenges in constructing realistic models, particularly for gauge bundles with a non-Abelian structure group. Indeed, only a relatively small number of quasi-realistic models based on such gauge bundles are known in the literature [20–23].

However, it has been realised [19,24] that quasi-realistic models can also be constructed using gauge bundles with Abelian structure groups which are considerably easier to handle than their non-Abelian counterparts. For these models, the vector bundle is a direct sum of line bundles

which are classified and can be analyzed systematically. By scanning this space of heterotic line bundle models, a large number of examples which lead to the Standard Model spectrum has been found [19, 24]. For technical reasons, these models have been obtained using the arguably simplest type of CY manifolds - complete intersections in product of projective spaces - and, to a lesser extent, CY hypersurfaces in toric four-folds. The main purpose of the present work is to study heterotic line bundle models for another class of CY manifolds, namely elliptically fibered CY three-folds.

There are a number of motivations for addressing this problem. Firstly, we would like to develop the necessary tools for constructing line bundle models on elliptically fibered CY three-folds, including the calculation of line bundle cohomology on these manifolds. Secondly, by studying line bundle models on another class of CY manifolds, we would like to gain some insight into which of their properties are generic and which are related to the particular type of underlying CY manifold. Finally, we are motivated by heterotic/F-theory duality which is formulated for elliptically fibered CY manifolds. More specifically, this duality normally relies on spectral cover bundles [3], usually with a non-Abelian structure group, on elliptically fibered CY manifolds. It would be interesting to understand in detail how the duality works for line bundle models. In the present work we focus on the construction of models on the heterotic side as a first step in this direction while the discussion of heterotic/F-theory duality for these models will be the subject of future work.

There are strong indications [25] that the construction of phenomenologically interesting heterotic CY models requires a CY manifold with a non-trivial first fundamental group which facilitates the presence of a Wilson line. In such constructions, the part of the bundle with a non-flat connection is used to break to a GUT group, such as $SU(5)$, while the Wilson line breaks further to the Standard Model group. The correct chiral asymmetry is easily engineered at the GUT level by imposing a single condition on the index of the bundle. The Wilson line, while breaking the GUT multiplets up into Standard Model multiplets, does not change this chiral asymmetry. In this way three chiral families are easily obtained by imposing one condition on the bundle. On the other hand, the direct breaking to the Standard Model group without the presence of a Wilson line requires imposing one index condition per Standard Model multiplet. It can be shown [25] that the combination of these conditions leads to serious phenomenological problems.

For this reason we would like to follow the standard two-step construction with an intermediate GUT group, which we choose to be $SU(5)$, and subsequent Wilson line breaking. The required CY manifolds with a non-trivial first fundamental group are usually constructed by start-

ing with a simply-connected "upstairs" CY manifold X with a freely-acting discrete symmetry Γ and then taking the quotient X/Γ. We would like to follow this approach and should, therefore, construct elliptically fibered CY three-folds with freely-acting symmetries. For our purpose, we consider the simplest case where $\Gamma = \mathbb{Z}_2$, that is, we consider freely-acting involutions. The construction and analysis of such elliptically fibered CY three-folds with a freely-acting involution constitutes another technical complication, partly addressed in earlier work [26, 27], which we review and further develop for our purposes. For the vector bundle to descend under the quotient map, it must be 'equivariant' under the symmetry action. In this work, we restrict ourselves to a necessary check for equivariance, as this is better suited to a systematic model scan.

The main idea for constructing such freely-acting involutions is as follows. Consider an elliptically fibered CY three-fold X with projection $\pi : X \to B$, two-fold base B and with a section $\sigma : B \to X$. We can describe the typical elliptic fiber, $E_b = \pi^{-1}(b)$ where $b \in B$, by its Jacobian, that is, by a complex w plane with identifications $w \sim w + 1$ and $w \sim w + \tau_b$, where τ_b is the complex structure of E_b. An obvious starting point is to consider an involution ι_X of X which acts on the fiber as a half-shift, that is, as $\iota_E : w \to w + 1/2$. This looks promising since this action of ι_E is already fixed point free. However, there are two complications which can be inferred from the following argument. The presence of the half-shift on the fibers means that the elliptic fibration has to have a second section, $\zeta = \iota_E \circ \sigma$, in addition to σ. Such elliptic fibrations with two sections are known to have a special structure and, in particular, the discriminant locus (the locus on the base B over which the torus fiber degenerates) splits into two components. It turns out that on one of these components the fiber degenerates such that the entire CY manifold becomes singular. To produce a smooth manifold, the singular loci need to be blown-up and this leads to an additional (second and fourth) cohomology class. The other component of the discriminant locus does not lead to singularities of X but the action of ι_E on the corresponding degenerate fibers is not fixed point free. To remedy this problem we construct ι_X by combining the half-shift, ι_E, on the fiber with a simultaneous action ι_B on the base. The latter does not have to be fixed point free on B. In order to ensure that ι_X is fixed point free it is sufficient to require that the fixed point locus of ι_B should not intersect the above mentioned second component of the discriminant locus where ι_E has fixed points on the fiber. This is generically the case if ι_B has at most fixed points (rather than fixed curves) on B and this is what we will require.

This construction has implications for the possible choices of base spaces B. Smoothness of a generic Weierstrass model over B implies that B should be weak Fano [28, 29], which are spaces

with nef and big anti-canonical bundle. Further, finding a freely-acting involution ι_X along the lines described above requires the existence of an involution ι_B with at most fixed points. We will focus on two-dimensional toric Fano base spaces B and find that there are six such spaces which lead to smooth CY three-folds and have a suitable involution ι_B.

For such elliptically fibered three-folds X with a freely-acting involution and two sections we systematically develop the required model building tools. This includes the construction of a suitable integral basis of the second and fourth homology, calculation of the intersection ring, the construction of Kähler and Mori cones and the analysis of line bundles $L \to X$ and their properties. In particular, we show how to calculate the cohomology of line bundles by combining the Leray spectral sequence with known methods for calculating line bundle cohomology on toric manifolds [30, 31].

Based on these results, we scan rank five line bundle models for the six suitable base spaces and find more than 400 $SU(5)$ GUT models with the correct chiral asymmetry. Upon taking the quotient by the involution and introducing a $\mathbb{Z}_2$ Wilson line in the hypercharge direction these will lead to models with the Standard Model gauge group and three chiral families. A common feature of all models is the presence of a large number of vector-like states. In $SU(5)$ language all models have at least one $\mathbf{10}$–$\overline{\mathbf{10}}$ vector-like pair and at least 20 (!) $\mathbf{5}$–$\bar{\mathbf{5}}$ vector-like pairs. Particularly the latter number is surprising compared with the results obtained for heterotic line bundle models on complete intersection CY manifolds [19, 24, 32]. For complete intersection CY manifolds, imposing the right chiral asymmetry frequently meant the absence of $\mathbf{10}$–$\overline{\mathbf{10}}$ vector-like pairs and a small number of $\mathbf{5}$–$\bar{\mathbf{5}}$ vector-like pairs.

The plan of the chapter is as follows. In the next section, we will introduce elliptically fibered CY manifolds and discuss their properties including line bundles on these spaces. In Section 3.3, heterotic line bundle models are reviewed and in Section 3.4 we present the results of our model scan. We conclude in Section 3.5. In the main part of the chapter, we will keep the discussion informal and as non-technical as the subject allows; technical details can be found in the Appendices.

3.2 Elliptically fibered CY three-folds with involutions

In this section, we discuss the required background on elliptically fibered CY three-folds, specifically when such a space admits a freely-acting involution. Much of the following can be inferred by combining results in the literature [26, 27], but we would like to collect and organise the material to facilitate systematic model building. We will here focus on the key ideas while technical details can be found in Appendices A and B.

3.2.1 Elliptically fibered CY three-folds with two sections

Single-section case

As a warm-up, we consider elliptically fibered CY three-folds X over a two-fold base B with projection $\pi : X \to B$ and a single section $\sigma : B \to X$. Points on the base are denoted by $b \in B$ and K_B is the canonical bundle of the base. A Weierstrass model for X is given by the equation

$$zy^2 = x^3 + f(b)xz^2 + g(b)z^3\,, \tag{3.1}$$

which, for each base point $b \in B$, describes an elliptic curve, $E_b = \pi^{-1}(b)$, embedded in $\mathbb{P}^2$ with homogeneous coordinates x, y, z. Here, f and g are sections of the line bundles K_B^{-4} and K_B^{-6}, respectively, which encode the variation of the elliptic curve over the base. In these $\mathbb{P}^2$ coordinates the section can be explicitly written as $\sigma(b) = (b, (0, 1, 0))$, that is, it is "located" at the point $(x, y, z) = (0, 1, 0) \in E_b$ in each fiber.

A typical torus fiber E_b can also be described by its Jacobian, that is, by a complex w plane with identifications $w \sim w + 1$ and $w \sim w + \tau_b$, where τ_b is the complex structure of E_b. For each point $b \in B$, this complex structure is related to the sections f and g by the equation

$$j(\tau_b) = \frac{4(24f(b))^3}{4f(b)^3 + 27g(b)^2}\,. \tag{3.2}$$

The denominator on the right-hand side of this expression, that is,

$$\Delta(b) = 4f(b)^3 + 27g(b)^2 \tag{3.3}$$

is a section of K_B^{-12} and is called the discriminant. The discriminant locus, defined by $\{b \in B \mid \Delta(b) = 0\}$, is a curve in the base over which the fiber E_b degenerates. This will be discussed in more detail in the next sub-section for the case of two sections.

A basis of curves and divisors of X can be obtained from a basis of curves on B by using the maps π^{-1} and σ. Other relevant properties of X, such as the intersection ring, the Mori cone and the Kähler cone, can also be obtained in terms of properties of the base. Since we are primarily interested in the two-section case, we will defer the details of this to the following sub-sections.

Involutions and the double-section case

As indicated earlier, we would like to construct elliptically fibered CY three-folds X with a freely-acting involution ι_X, starting with an involution ι_E on each fiber which acts as a half-shift $w \to w + 1/2$. The presence of ι_E implies the presence of a second section $\zeta = \iota_E \circ \sigma : B \to X$ of the fibration, located at the "two-torsion point" in each fiber, in addition to the section

$\sigma : B \to X$. We should, therefore, discuss the structure of elliptically fibered CY three-folds with two sections.

Starting from the general Weierstrass model (3.1), a Weierstrass model with a second section can be found by an appropriate tuning of parameters, the general form of which has been found in Ref. [33]. As explained in Appendix A.2, a second section located at the two-torsion point of the elliptic fiber emerges by choosing the specific, factorisable form (see also Ref. [26])

$$zy^2 = (x - \alpha z)(x^2 + \alpha x z + \beta z^2)\,, \tag{3.4}$$

of the Weierstrass model, where α and β are sections of K_B^{-2} and K_B^{-4}, respectively. Comparison with Eq. (3.1) shows that this corresponds to choosing the sections f and g in the general Weierstrass model as

$$f = \beta - \alpha^2\,, \qquad g = -\alpha\beta\,. \tag{3.5}$$

The two sections of such a fibration are given by

$$\sigma(b) = (b, (0, 1, 0))\,, \quad \zeta(b) = (b, (\alpha, 0, 1))\,, \tag{3.6}$$

so they are located at $(x, y, z) = (0, 1, 0)$ and $(x, y, z) = (\alpha, 0, 1)$, respectively.

As can be inferred from the factorised form of the Weierstrass model, this model has singularities which we need to resolve. This can be explicitly seen be working out the discriminant (3.3) which becomes

$$\Delta = \Delta_1 \Delta_2^2\,, \quad \text{where} \quad \Delta_1 := 4\beta - \alpha^2\,, \quad \Delta_2 := 2\alpha^2 + \beta\,. \tag{3.7}$$

Using this notation and (shifted) affine coordinates $X = x/z - \alpha$, $Y = y/z$ on the patch of $\mathbb{P}^2$ where $z \neq 0$, it is shown in Appendix A.2 that the half-shift ι_E on regular fibers can be written as

$$X \to \frac{\Delta_2}{X}\,, \quad Y \to -\frac{\Delta_2 Y}{X^2}\,. \tag{3.8}$$

From the above discriminant, there are singularities, corresponding to fibers of Kodaira type I_2, over the curve $\{b \in B \,|\, \Delta_2(b) = 0\}$ in the base. In order to obtain a smooth CY three-fold, these singularities need to be resolved, after which the fibers over the locus $\Delta_2(b) = 0$ become a pair of $\mathbb{P}^1$'s touching in a point. In addition, the action of ι_E has to be extended to these blown-up fibers. Appendix A.2 provides the details of the blow-up procedure and shows explicitly that ι_E can indeed be extended to the blow-up and has no fixed points on the blown-up fibers. More specifically, it turns out that ι_E exchanges the two $\mathbb{P}^1$ curves of the blown-up fibers. For these reducible fibers, the section σ takes values in one of the $\mathbb{P}^1$ curves and the second section ζ takes values in the other $\mathbb{P}^1$.

From Eq. (3.7), there is another component of the discriminant locus, given by the curve $\{b \in B \,|\, \Delta_1(b) = 0\}$ in the base. The degenerate fibers over this locus do not lead to singularities of the entire three-fold so that there is no need for a further blow-up. However, as discussed in Appendix A.2 , the map ι_E does have fixed points on the fibers over this locus, while it is fixed point free on all other fibers. This means that the involution ι_X, if it is to be fixed point free, cannot simply be taken to be ι_E with a trivial action on the base. However, we can obtain a fixed point free involution ι_X by combining ι_E with an involution ι_B on the base whose fixed point locus does not intersect the curve $\{b \in B \,|\, \Delta_1(b) = 0\}$. This is generically the case if ι_B has at most fixed points (rather than fixed curves) on B and this is what we will require. The presence of such an involution ι_B places constraints on the allowed base manifolds which we will discuss below.

Alternatively, one may realise elliptic CY three-folds with a second section at the two-torsion point by embedding the elliptic fiber into the Hirzebruch surface $\mathbb{F}_2$, see [33–35]. We will review this approach in Appendix A.3. This approach has the advantage that, for a toric base space B, the corresponding elliptic CY three-fold can be presented as a hypersurface in a toric variety. We will use this alternative method to realise the relevant CY manifolds to check some of our results, particularly in relation to line bundle cohomology.

Double-section case: curves and divisors

We would now like to construct a number of objects, as required for our model building purposes, including a basis of curve and divisor classes, on elliptically fibered three-folds X with a freely-acting involution and two sections, in terms of the corresponding objects on the base B. Technical details can be found in Appendix A.4.

We begin by introducing an integral basis $\{\mathcal{C}^i\}$ of the second homology of the base B, as well as a dual basis, $\{\mathcal{C}_i\}$, of curve classes such that

$$\mathcal{C}^i \cdot \mathcal{C}_j = \delta^i_j \,. \tag{3.9}$$

Here and in the following we use indices $i, j, \ldots$ to indicate the index range $1, \ldots, h^{1,1}(B)$. The intersection forms for these basis curves are denoted by

$$g_{ij} := \mathcal{C}_i \cdot \mathcal{C}_j \,, \qquad g^{ij} := \mathcal{C}^i \cdot \mathcal{C}^j \,, \tag{3.10}$$

and it is easy to see that g^{ij} is the inverse of g_{ij}. Further, these "metrics" can be used to raise and lower indices, that is, $\mathcal{C}^i = g^{ij}\mathcal{C}_j$ and $\mathcal{C}_i = g_{ij}\mathcal{C}^j$. For later purposes, it is also useful to introduce the quantities

$$\lambda_i := K_B \cdot \mathcal{C}_i \,, \quad \lambda := K_B^2 = c_1(B)^2 = \lambda^i \lambda_i \,, \tag{3.11}$$

where $K_B = -c_1(B)$ is the canonical bundle of the base and $\lambda^i = g^{ij}\lambda_j$.

We can use either one of the two sections σ and ζ to raise these curve classes on the base to curve classes on the entire three-fold. The three-fold has two more classes which cannot be obtained in this way. These are the class F of a generic fiber and the new class N introduced by the blow-up, the latter chosen such that the component of the reducible fibers over $\{b \in B \,|\, \Delta_2(b) = 0\}$ which is met by the zero section σ has class $F - N$. For a general curve class, $\mathcal{C}$, on the base we have the relation

$$\zeta(\mathcal{C}) = \sigma(\mathcal{C}) + (\mathcal{C} \cdot c_1(B))\,[F - 2N] \ , \tag{3.12}$$

which shows that lifts of base curves with the two sections σ and ζ are linearly related. It is, therefore, sufficient to consider lifts by one of the sections and we will use the zero section σ for this purpose. Accordingly, we introduce a basis $\{C^I\}$, where $I = (0, \hat{0}, i)$, of curve classes on X by

$$C^0 = F - N \ , \quad C^{\hat{0}} = N \ , \quad C^i = \sigma(\mathcal{C}^i) - \lambda^i(F - N) \ . \tag{3.13}$$

Divisor classes on X can be obtained from curve classes, $\mathcal{C}$, on the base by the inverse image $\pi^{-1}(\mathcal{C})$. There are two further classes, the images $\sigma(B)$ and $\zeta(B)$ of the base under the two sections, which cannot be obtained in this way. Hence, we introduce a basis $\{D_I\}$ of divisor classes, where $I = (0, \hat{0}, i)$, by

$$D_0 = \sigma(B) \ , \quad D_{\hat{0}} = \zeta(B) \ , \quad D_i = \pi^{-1}(\mathcal{C}_i) \ . \tag{3.14}$$

From the intersections in Table 5 in Appendix A.4 we can see that this basis of divisor classes is dual to the above basis of curve classes, that is

$$D_I \cdot C^J = \delta_I^J \ . \tag{3.15}$$

Combining the information from Table 5 and Table 6 in Appendix A.4 we can work out the intersection numbers

$$d_{IJK} = D_I \cdot D_J \cdot D_K \tag{3.16}$$

which are explicitly given by

$$d_{000} = d_{\hat{0}\hat{0}\hat{0}} = \lambda \ , \quad d_{00i} = d_{\hat{0}\hat{0}i} = \lambda_i \ , \quad d_{0ij} = d_{\hat{0}ij} = g_{ij} \ , \tag{3.17}$$

with all other components either fixed by symmetry from the above or else vanishing.

For our model building purposes we also require the Mori and Kähler cones of X. We begin with the Mori cone, $\mathcal{M}_X$ of X which, following Appendix A.4, can be written as

$$\mathcal{M}_X = \left\{ n_0(F - N) + n_{\hat{0}} N + \sigma(\mathcal{C}) + \zeta(\mathcal{C}') \,|\, n_0, n_{\hat{0}} \in \mathbb{Z}^{\geq 0} \ , \ \mathcal{C}, \mathcal{C}' \in \mathcal{M}_B \right\} \ , \tag{3.18}$$

where $\mathcal{M}_B$ is the Mori cone of the base. If we write Kähler forms as $J = t^I D_I$ with the Kähler moduli $\mathbf{t} = (t^I)$ relative to the divisor basis $\{D_I\}$, the Kähler cone is the dual of the Mori cone, that is,

$$\begin{aligned} \mathcal{K}_X &= \left\{ J = t^I D_I \,|\, J \cdot C \geq 0 \text{ for all } C \in \mathcal{M}_X \right\} && (3.19) \\ &\cong \left\{ \mathbf{t} \,|\, \mathbf{t} \cdot \mathbf{n} \geq 0 \text{ for all } n^I C_I \in \mathcal{M}_X \right\} . && (3.20) \end{aligned}$$

and can, hence, be explicitly worked out once the Mori cone is known.

We should also discuss how the above basis of curve and divisor classes relates to the involution ι_X on X and its action ι_B on the base. We find

$$\iota_X(F - N) = N \,, \quad \iota_X(\sigma(\mathcal{C})) = \zeta(\iota_B(\mathcal{C})) \,, \tag{3.21}$$

$$\iota_X(\sigma(B)) = \zeta(B) \,, \quad \iota_X(\pi^{-1}(\mathcal{C})) = \pi^{-1}(\iota_B(\mathcal{C})) \,, \tag{3.22}$$

where $\mathcal{C}$ is a curve class on the base. In particular, as is evident from the second line, ι_X exchanges $D_0 = \sigma(B)$ with $D_{\hat{0}} = \zeta(B)$.

Finally, the second Chern class and Euler number of X are given by (see Refs. [26, 27])

$$\begin{aligned} c_2(X) &= 12\sigma(c_1(B)) + (c_2(B) + 11c_1(B)^2)(F - N) + (c_2(B) - c_1(B)^2)N && (3.23) \\ &= (c_2(B) - \lambda)(C^0 + C^{\hat{0}}) - 12\lambda_i C^i \,, && (3.24) \\ \chi(X) &= -36 \int_B c_1(B)^2 = -36\lambda \,. && (3.25) \end{aligned}$$

We have thus succeeded in expressing all basic properties of elliptically fibered CY three-folds with two sections in terms of corresponding properties of the base.

3.2.2 Invariant line bundles and their cohomology

Line bundles and involutions

We now collect properties of line bundles $L \to X$ on elliptically fibered CY three-folds with a freely-acting involution and two sections. As usual, we denote by $\mathcal{O}_X(D)$ a line bundle with first Chern class or character

$$\mathrm{ch}_1(\mathcal{O}_X(D)) = c_1(\mathcal{O}_X(D)) = D \,. \tag{3.26}$$

To write down explicit expressions for the second Chern character and the index of a line bundle it is convenient to represent the corresponding divisor as a linear combination $D = k^I D_I$, where $k^I \in \mathbb{Z}$, relative to the basis $\{D_I\}$. Then we find

$$\begin{aligned} \mathrm{ch}_2(\mathcal{O}_X(k^I D_I)) &= \frac{1}{2} d_{IJK} k^I k^J C^K && (3.27) \\ \mathrm{ind}(\mathcal{O}_X(k^I D_I)) &= \frac{1}{6} d_{IJK} k^I k^J k^K + \frac{1}{12} k^I c_{2I}(X) \,, && (3.28) \end{aligned}$$

where $c_{2I}(X)$ are the components of the second Chern class of X, defined by $c_2(X) = c_{2I}(X)C^I$, given in Eq. (3.24). We also require an expression for the slope of a line bundle. With the Kähler form written as $J = t^I D_I$ the slope of a line bundle $L = \mathcal{O}_X(k^I D_I)$ is defined by

$$\mu_X(L) := \int_X J \wedge J \wedge c_1(L) = d_{IJK} t^I t^J k^K \ . \tag{3.29}$$

Later, we will be interested in line bundles L whose slope vanishes somewhere in the (interior, $\mathring{\mathcal{K}}_X$, of the) Kähler cone (3.19), so we have to solve the quadratic equation $d_{IJK} t^I t^J k^K = 0$ for $\mathbf{t} \in \mathring{\mathcal{K}}_X$.

To build heterotic line bundle models, we also need to know which line bundles L admit an equivariant structure under the involution ι_X. In fact, in this work, we will be content checking invariance of L, a necessary but not sufficient condition for equivariance which is better suited for a systematic model search. A line bundle $L = \mathcal{O}_X(D)$ is invariant under ι_X iff $\iota_X^* L \cong L$ or, equivalently, iff $\iota_X(D) = D$. From Eqs. (3.22), the last condition can be worked out more explicitly as

$$\iota_X(k^I D_I) = k^I D_I \quad \Longleftrightarrow \quad k^0 = k^{\hat{0}} \text{ and } I^i_{Bj} k^j = k^i \ , \tag{3.30}$$

where I_B is a matrix which describes the action of the involution ι_B on the basis $\{\mathcal{C}_i\}$ of curve classes on the base such that

$$\iota_B(\mathcal{C}_j) = I^i_{Bj} \mathcal{C}_i \ . \tag{3.31}$$

Stated differently, invariant line bundles must be of the form

$$L = \mathcal{O}_X(n\Sigma) \otimes \pi^*(\mathcal{L}) \ , \quad \Sigma = \sigma(B) + \zeta(B) \ , \tag{3.32}$$

where $n \in \mathbb{Z}$ and $\mathcal{L} = \mathcal{O}_B(k^i \mathcal{C}_i)$ is a line bundle on the base which satisfies $I^i_{Bj} k^j = k^i$.

Line bundle cohomology on elliptically fibered CYs with two sections

To determine the full spectrum of line bundle models we need to compute line bundle cohomology, rather than merely line bundle indices. Later on, we will be interested in line bundles $L \to X$ whose slope $\mu_X(L)$ vanishes somewhere in the interior of Kähler cone. It is useful to note that, from a general vanishing theorem [36], such line bundles satisfy

$$h^0(X, L) = h^3(X, L) = 0 \quad \Longrightarrow \quad \text{ind}(L) = h^2(X, L) - h^1(X, L) \ , \tag{3.33}$$

with the exception of the trivial line bundle. Even for such line bundles, the index does not provide the full information and at least one more cohomology needs to be computed.

The cohomology of line bundles $L \to X$ on an elliptically fibered CY three-fold X can be expressed in terms of line bundle cohomology on the base B, using the direct image $\pi_* L$ and

the associated higher direct images, $R^q\pi_*L$, together with the Leray spectral sequence [3,37,38]. Here we outline the structure of this calculation and its main results. Further details can be found in Appendix C, including details on the Leray spectral sequence and computations of the direct images and higher direct images.

The starting point of the computation is the exact sequence

$$0 \to E_2^{1,0} \to H^1 \to E_2^{0,1} \to E_2^{2,0} \to H^2 \to E_2^{1,1} \to 0\,, \tag{3.34}$$

where

$$H^p := H^p(X,L)\,, \quad E_2^{p,q} := H^p(B, R^q\pi_*L)\,. \tag{3.35}$$

As discussed in Appendix C.1, this exact sequence follows from the Leray spectral sequence. For our model building effort we require invariant line bundles, that is line bundles of the form (3.32), and we will restrict the cohomology calculation to such cases. To work out the higher direct images of such invariant line bundles, we are helped by the projection formula

$$R^i\pi_*(\mathcal{O}_X(n\Sigma)\otimes\pi^*(\mathcal{L})) = R^i\pi_*(\mathcal{O}_X(n\Sigma))\otimes\mathcal{L}\,, \tag{3.36}$$

which shows that all we require is the (higher) direct images of the line bundles $\mathcal{O}_X(n\Sigma)$. As discussed in more detail in Appendix C, these are explicitly given by

$$\pi_*\mathcal{O}_X(n\Sigma) = \begin{cases} 0 & \text{for } n<0 \\ \mathcal{O}_B & \text{for } n=0 \\ \mathcal{O}_B\oplus K_B & \text{for } n=1 \\ \mathcal{O}_B\oplus K_B\oplus\left(K_B^{\otimes 2}\oplus K_B^{\otimes 3}\oplus\ldots\oplus K_B^{\otimes n}\right)^{\oplus 2} & \text{for } n\geq 2 \end{cases}, \tag{3.37}$$

$$R^1\pi_*\mathcal{O}_X(n\Sigma) = \begin{cases} 0 & \text{for } n>0 \\ K_B & \text{for } n=0 \\ \mathcal{O}_B\oplus K_B & \text{for } n=-1 \\ \mathcal{O}_B\oplus K_B\oplus\left(K_B^{\otimes(-1)}\oplus K_B^{\otimes(-2)}\oplus\ldots\oplus K_B^{\otimes(-n+1)}\right)^{\oplus 2} & \text{for } n\leq -2 \end{cases}, \tag{3.38}$$

where 0 is the rank-zero bundle. The above results imply that $E_2^{2,0}=0$ for $n<0$ and $E_2^{0,1}=0$ for $n>0$ and, hence, that the sequence (3.34) splits for all $n\neq 0$. For $n=0$ this cannot be inferred in general. However, it turns out that, for our choices of base spaces and line bundles with $n=0$, one of $E_2^{2,0}$ and $E_2^{0,1}$ is always zero. This means that the sequence (3.34) splits for all cases of interest. In conclusion, for line bundles invariant under the involution ι_X, that is

line bundles of the form $L = \mathcal{O}_X(n\Sigma) \otimes \pi^*(\mathcal{L})$ (with $\mathcal{L}$ a line bundle on the base), we have

$$H^q(X,L) = \begin{cases} E_2^{q-1,1} & \text{for} \quad n < 0 \\ E_2^{q-1,1} \oplus E_2^{q,0} & \text{for} \quad n = 0 \\ E_2^{q,0} & \text{for} \quad n > 0 \end{cases} , \tag{3.39}$$

for $q = 1, 2$, where

$$E_2^{i,j} = H^i(B, R^j\pi_*(\mathcal{O}_X(n\Sigma)) \otimes \mathcal{L}) \, . \tag{3.40}$$

Hence, we can compute the relevant line bundle cohomologies on the CY three-fold X from line bundle cohomologies on the base B.

In practice, as our two-fold base spaces are toric, to compute line bundle cohomology on the base we use the cohomCalg code, developed in Ref. [30, 31].

Alternative cohomology computation

The CY manifolds used in this chapter can also be realised as hypersurfaces in toric four-folds, as described in Appendix A.3 and this provides us with an alternative method to calculate line bundle cohomology. More specifically, a line bundle $\mathcal{L}$ on the toric ambient four-fold $\mathcal{A}$ and its restriction L to the CY three-fold X are related by the Koszul sequence

$$0 \to K_{\mathcal{A}} \otimes \mathcal{L} \to \mathcal{L} \to L \to 0 \, , \tag{3.41}$$

where[15] $K_{\mathcal{A}}$ is the canonical bundle of $\mathcal{A}$. The cohomologies of $\mathcal{L}$ and $K_{\mathcal{A}} \otimes \mathcal{L}$ can again be computed using the cohomCalg code [30, 31], this time applied to the ambient toric four-fold $\mathcal{A}$. The cohomology of L can then be inferred from the long exact sequence associated to the above Koszul sequence. We have carried this out for ι_X invariant line bundles and we find that the cohomology of L can be determined easily from the long exact sequence without the need to compute ranks of maps (that is, the sequence always splits). Moreover, the results always agree with the previous method, based on the Leray spectral sequence.

3.2.3 Base space choices and involutions

We have now expressed all relevant properties of elliptically fibered CY three-folds X with two sections in terms of properties of the base manifold B. The final step in our model building set-up is to find a suitable explicit class of base manifolds and to develop all their required characteristics. Here we will present the main results with details relegated to Appendix B.

[15] More generally, the bundle here is N^*, where N is the line bundle whose restriction to the hypersurface is the normal bundle. In the case of a CY hypersurface, this is the anti-canonical bundle $K_{\mathcal{A}}^*$.

We begin by discussing the general constraints imposed on the base manifolds. Recall from Section 3.2.1 that we require the existence of a freely-acting involution ι_X of X which is constructed by combining a half-shift ι_E on the elliptic fibers with an involution ι_B on the base. The presence of this involution implies the existence of two sections, σ and ζ, of the fibration, as well as the factorisation of the discriminant, that is, $\Delta = \Delta_1\Delta_2^2$. This leads to two requirements on the base manifold B. Firstly, the three-folds $X \to B$ described by Eq. (3.4) should be smooth after resolving the singularity over the locus $\Delta_2 = 0$. Secondly, in order for ι_X to be fixed point free, the fixed point locus of ι_B should not intersect the locus $\Delta_1 = 0$, where ι_E is not freely-acting on the fibers. To ensure this we require that ι_B has at most fixed points on B.

The first requirement means in particular that a generic Weierstrass model (3.1) over B should be smooth, which happens only when the base space B is a weak Fano two-fold [28, 29]. If the base space B is not weak Fano, it is still possible to construct a corresponding smooth elliptic CY three-fold X by resolving the singular Weierstrass model. After such a resolution, X will have additional divisors beyond the two sections and divisors inherited from the base, which need to be taken into account when constructing and analysing models. The properties of such additional divisors depend on the choice of the base space which complicates the model building significantly. For this reason, we focus on the case of weak Fano base spaces in the present work. More specifically, we will only consider toric weak Fano two-folds. From the 61,359 toric base spaces giving rise to flat elliptic CY three-folds [28], 16 are weak Fano and lead to generically smooth fibrations [28, 29]. These correspond to the 16 inequivalent reflexive polygons in two dimensions. We depict these polygons in Figure 27 in Appendix B.[16]

To implement the second requirement – the existence of an involution ι_B with at most fixed points – we have searched these 16 surfaces for involutions which can be realised linearly on the homogeneous coordinates. We find that 6 out of these 16 manifolds allow for an involution of this kind which has at most fixed points. The polygons for these 6 possible base manifolds B, on which we will focus for the construction of line bundle models, are shown in Figure 1. Some basic properties of these six base spaces are listed in Table 1 with more details available in Appendix B.

From Eq. (3.17), the intersection numbers of the CY three-fold X can be expressed in terms of intersections on the base, that is, in terms of the quantities λ_i and λ given in Table 1 and in terms of the intersection forms $g_{ij} = \mathcal{C}_i \cdot \mathcal{C}_j$ given in Appendix B. The second Chern class of the CY three-fold X, which will be important to check that models are anomaly-free, can be

[16] There are sensible ways to group these 16 polygons according to their properties. One example is the grouping in Figure 1 of Ref. [39].

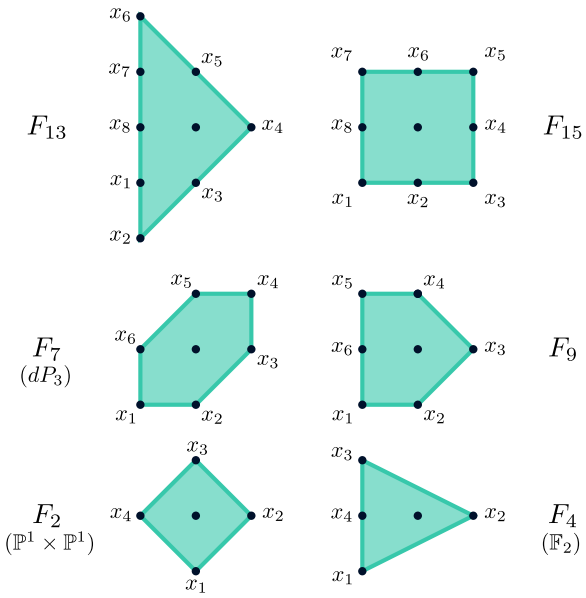

Figure 1: *The 6 reflexive polytopes corresponding to toric base spaces B which lead to smooth elliptically fibered CY three-folds and allow for an involution with at most fixed points. The notation F_i follows Ref. [40]. The homogeneous coordinates x_i associated to the rays are indicated and will be used throughout the chapter.*

computed from the data in Table 1 inserted into Eq. (3.23). This leads to

$$c_2(X) = \begin{cases} -4(C^0 + C^{\hat{0}}) + 24(C^1 + C^2) & B = F_2 \\ -4(C^0 + C^{\hat{0}}) + 24C^1 & B = F_4 \\ 12(3C^1 - C^2 - C^3 - C^4) & B = F_7 \\ 12(C^1 + 2C^2 + C^3) & B = F_9 \\ 4(C^0 + C^{\hat{0}}) + 12(C^2 + 2C^3 + C^4) & B = F_{13} \\ 4(C^0 + C^{\hat{0}}) + 12(C^2 + 2C^3 + 2C^4 + 2C^5 + C^6) & B = F_{15} \end{cases} \tag{3.42}$$

The Mori cone of X can be obtained from the Mori cone $\mathcal{M}_B$ of the base B via Eq. (3.18) and the generators of $\mathcal{M}_B$ for the six base spaces are given in Appendix B.

We will also need to know the explicit action of the involution ι_B on the homogeneous coordinates x_i. For each of the base space choices B, there are multiple distinct actions on the homogeneous coordinates that give involutions with only fixed points. Most of these differ only by signs, and many of these result in the same action, I_B, on the curve classes in B (see Eq. (3.31)). For the purpose of this work, it is only the action I_B on the curve classes which enters the discussion, while the action on the coordinates is not explicitly used. For this reason,

B	F_2	F_4	F_7	F_9	F_{13}	F_{15}
name	$\mathbb{P}^1 \times \mathbb{P}^1$	$\mathbb{F}_2$	dP_3	–	–	–
$h^{1,1}(B)$	2	2	4	4	6	6
$h^{1,1}_{\mathrm{inv}}(B)$	2	2	3	3	4	4
$c_2(B)$	4	4	6	6	8	8
$\{\mathcal{C}^i\}$	$l_1 = x_1$ $l_2 = x_2$	x_2, x_3	$l = x_4 + x_5 + x_6$ $e_1 = x_6$ $e_2 = x_2$ $e_3 = x_4$	$x_2, \ldots, x_5$	$x_2, \ldots, x_7$	$x_2, \ldots, x_7$
$(-\lambda_i)$	$(2, 2)$	$(2, 0)$	$(3, -1, -1, -1)$	$(1, 2, 1, 0)$	$(0, 1, 2, 1, 0, 0)$	$(0, 1, 2, 2, 2, 1)$
λ	8	8	6	6	4	4
K_B	$-2(l_1 + l_2)$	$-2x_2$	$-3l + e_1$ $+e_2 + e_3$	$-x_2 - x_4$ $-2x_3$	$-x_3 - x_5$ $-2x_4$	$-x_3 - x_7 - 2x_4$ $-2x_5 - 2x_6$

Table 1: *Some basic properties of the six toric bases spaces B which lead to smooth elliptically fibered CY three-folds and allow for an involution with at most fixed points. The coordinates x_i have been defined in Figure 1 and are also used to denote the curve classes defined by $x_i = 0$. The row denoted $h^{1,1}_{\mathrm{inv}}(B)$ gives the dimension of the second homology invariant under the involution ι_B. The first Chern class of B is obtained from $c_1(B) = -K_B$ and the dual basis, $\{\mathcal{C}_i\}$, of curve classes can be obtained from the intersection forms g_{ij} given in Appendix B, via the relation $\mathcal{C}_i = g_{ij}\mathcal{C}^j$. Also recall the definitions $\lambda_i = K_B \cdot \mathcal{C}_i$ and $\lambda = \lambda^i \lambda_i$.*

it is sufficient to consider one representative action ι_X for each I_B. These are explicitly given by

$$\iota_B(x_1, \ldots, x_{h^{1,1}(B)+2}) = \begin{cases} (x_1, x_2, -x_3, -x_4) & B = F_2 \\ (x_1, x_2, -x_3, -x_4) & B = F_4 \\ (x_4, x_5, x_6, x_1, x_2, x_3) & B = F_7 \\ (x_5, x_4, x_3, x_2, x_1, -x_6) & B = F_9 \\ (x_7, x_6, x_5, x_4, x_3, x_2, x_1, -x_8) & B = F_{13} \\ (x_5, x_6, x_7, x_8, x_1, x_2, x_3, x_4) & B = F_{15}^{(a)} \\ (x_7, x_6, x_5, x_4, x_3, x_2, x_1, -x_8) & B = F_{15}^{(b)} \end{cases} \tag{3.43}$$

Note that there are two inequivalent choices, referred to as cases (a) and (b), for the base space F_{15}. These two cases do indeed lead to different actions I_B on the curve classes of B and should, hence, both be taken into account. The explicit matrices I_B in each case are provided in Appendix B.

We recall from Eq. (3.30) that line bundles on the CY three-fold which are invariant under the involution ι_X involve curve classes on B which are ι_B invariant. It is, therefore, important

to have explicit expressions for all such ι_B invariant curve classes $k^i\mathcal{C}_i$, that is, classes which satisfy $I^i_{Bj}k^j = k^i$. Using the explicit matrices I_B given in Appendix B these invariant curves can be characterised as follows.

$$\iota_B(k^i\mathcal{C}_i) = k^i\mathcal{C}_i \quad \Longleftrightarrow \quad \begin{cases} \text{no constraint} & B = F_2 \\ \text{no constraint} & B = F_4 \\ k^1 = k^2 + k^3 + k^4 & B = F_7 \\ k^1 = k^3 & B = F_9 \\ \begin{cases} k^1 = k^5 \\ k^2 = k^4 \end{cases} & B = F_{13} \\ \begin{cases} k^1 = k^5 \\ k^2 = k^6 \end{cases} & B = F_{15}^{(a)} \\ \begin{cases} k^1 = k^3 \\ k^2 = k^6 + 2k^5 - 2k^3 \end{cases} & B = F_{15}^{(b)} \end{cases} \tag{3.44}$$

Finally, we need to be able to compute the cohomology for line bundles on B. Methods to compute line bundle cohomology on toric spaces have been developed in Ref. [30,31] and we will use the accompanying code cohomCalg for our calculations.

3.3 Line bundle models

All mathematical ingredients for the construction of heterotic line bundle models on elliptically fibered CY three-folds with two sections are now in place. In this section, we review the general construction of line bundle models and the structure of their low-energy spectrum (see Refs. [19] for a comprehensive account) as well as some particular features of line bundle models for elliptically fibered CY three-folds with two sections. A systematic line bundle model search on these CY manifolds will be presented in the next section.

3.3.1 Construction

General construction

A heterotic $E_8 \times E_8$ line bundle model is defined by two ingredients: a CY three-fold X and a line bundle sum

$$V = \bigoplus_{a=1}^{r} L_a \,, \tag{3.45}$$

with rank $r = \mathrm{rk}(V)$, where L_a are line bundles on X. We think of V as the bundle in the "observable" E_8 sector and will comment on the fate of the hidden sector below. In practice, it is useful to represent line bundles relative to an integral basis $\{D_I\}$ of divisor classes on X

and we write $L = \mathcal{O}_X(\mathbf{k})$ for a line bundle L with first Chern class $c_1(L) = k^I D_I$. Using this notation, the line bundles

$$L_a = \mathcal{O}_X(\mathbf{k}_a) \,, \tag{3.46}$$

can each be represented by an integer vector $\mathbf{k}_a$ and the entire line bundle sum V by a $h^{1,1}(X) \times r$ integer matrix $K = (k^I{}_a)$.

The data (X, V) is subject to three conditions which are required for the consistency of the model. Firstly, we need to be able to embed the structure group of the bundle V into E_8. Apart from the obvious rank constraint , $r \leq 8$, this requires the vanishing for the first Chern class of V, that is,

$$c_1(V) = \sum_{a=1}^{r} c_1(L_a) \stackrel{!}{=} 0 \qquad \Longleftrightarrow \qquad \sum_{a=1}^{r} \mathbf{k}_a \stackrel{!}{=} 0 \,. \tag{3.47}$$

Provided this is satisfied the structure group of V is generically $S(U(1)^r)$ which allows for an embedding into E_8 via the sub-group chain $S(U(1)^r) \subset SU(r) \subset E_8$.

The second constraint originates from the requirement that the bundle V preserve supersymmetry. It can be formulated in terms of the slope of a line bundle $L = \mathcal{O}_X(\mathbf{k})$ which is defined as

$$\mu_X(L) = \int_X J \wedge J \wedge c_1(L) = d_{IJK} t^I t^J k^K \,, \tag{3.48}$$

where $d_{IJK} = D_I \cdot D_J \cdot D_K$ are the triple intersection numbers of X. Supersymmetry of V requires that the slope of all line bundles L_a vanishes simultaneously somewhere in the interior, $\mathring{\mathcal{K}}_X$, of the Kähler cone of X. This means that the equations

$$\mu_X(L_a) = d_{IJK} t^I t^J k_a^K \stackrel{!}{=} 0 \,, \tag{3.49}$$

for $a = 1, \ldots, r$ should have a common solution $\mathbf{t} \in \mathring{\mathcal{K}}_X$.

The third requirement is anomaly cancellation which demands the existence of a hidden bundle $\tilde{V}$ (which should also be supersymmetric) and a holomorphic curve $W \subset X$ (around which a five-brane wraps) such that

$$\mathrm{ch}_2(V) + \mathrm{ch}_2(\tilde{V}) - \mathrm{ch}_2(TX) = [W] \,. \tag{3.50}$$

A practical way to ensure that this condition can be satisfied is to demand that

$$c_2(TX) - c_2(V) \in \mathcal{M}_X \,, \tag{3.51}$$

where $\mathcal{M}_X$ is the Mori cone (that is, the cone of effective curve classes) on X. Indeed, provided Eq. (3.51) holds, we can always choose a holomorphic curve W with $[W] = c_2(TX) - c_2(V)$, so that the anomaly condition (3.50) is satisfied for a trivial hidden bundle (although different

choices for $[W]$ combined with a non-trivial hidden bundle $\tilde{V}$ are usually possible as well). To check the condition (3.51) explicitly, we introduce a basis $\{C^I\}$ of curve classes on X, dual to our basis $\{D_I\}$ of divisor classes such that $C^I \cdot D_J = \delta^I_J$. Then, the second Chern class of V can be written as

$$c_2(V) = -\frac{1}{2} d_{IJK} \left(\sum_{a=1}^{r} k_a^I k_a^J \right) C^K \ , \tag{3.52}$$

and can be compared with the second Chern class of the tangent bundle expressed in the same basis as $c_2(TX) = c_{2I}(TX) C^I$.

Invariance

Provided the above three conditions are satisfied we have a consistent line bundle model with defining data (X, V). For phenomenological purposes, we would like to quotient this model by a freely-acting symmetry, Γ, of the CY three-fold X and obtain a model on the quotient CY manifold $\hat{X} = X/\Gamma$. The symmetry Γ should lift to the bundle V (in mathematical terminology, the bundle V should have a Γ-equivariant structure) so that it descends to a bundle $\hat{V} \to \hat{X}$ on the quotient. The final step is to add a Wilson line bundle $\mathcal{W}$ so that the complete "downstairs" bundle is $\hat{V} \oplus \mathcal{W}$.

For the purpose of this work, we would like to carry out a necessary (but not quite sufficient) check, adapted to our algorithmic model search, for equivariance. We will check that the line bundle sum V in Eq. (3.45) is Γ-invariant, which is the case iff $\gamma^*(V) \cong V$ for all $\gamma \in \Gamma$. A line bundle sum is Γ-invariant iff $\gamma^*(V)$ amounts to a permutations of the various line bundles. As a further simplification, we focus on cases where these permutations are trivial, so that every line bundle L_a is invariant by itself. Given that the symmetry group we consider is $\Gamma = \mathbb{Z}_2$, generated by an involution ι_X, we therefore demand that

$$\iota_X^*(c_1(L_a)) = c_1(L_a) \ , \tag{3.53}$$

for all $a = 1, \ldots, r$.

Models on elliptically fibered spaces

Recall that on elliptically fibered CY three-folds, line bundles L_a can be written as $L_a = \mathcal{O}_X(k_a^I D_I)$, where the basis $\{D_I\} = \{D_0 = \sigma(B), D_{\hat{0}} = \zeta(B), D_i = \pi^{-1}(\mathcal{C}_i)\}$ of divisor classes has been defined in Eq. (3.14). Hence, every line bundle can be represented by an integer vector

$$\mathbf{k}_a = (k^I{}_a) = (k^0{}_a, k^{\hat{0}}{}_a, k^i{}_a)^T \ . \tag{3.54}$$

From Eq. (3.32), ι_X invariance of the line bundles means that

$$k^0{}_a = k^{\hat{0}}{}_a \quad \text{and} \quad k^i{}_a \text{ of the form (3.44), for all } a = 1, \ldots, 5 \ . \tag{3.55}$$

Alternatively, we will also represent the entire line bundle sum V by an $h^{1,1}(X) \times 5$ integer matrix

$$K = (k^I{}_a) \tag{3.56}$$

with the columns corresponding to the line bundles. In view of the condition $c_1(V) \sim \sum_a \mathbf{k}_a \stackrel{!}{=} 0$ and Eq. (3.55), the number of independent integers in K is given by $4(h^{1,1}_{\text{inv}}(B) + 1)$, where the numbers $h^{1,1}_{\text{inv}}(B)$ have been listed in Table 1.

3.3.2 Spectrum

The (observable) low-energy gauge group is the commutant of $S(U(1)^r)$, the structure group of the line bundle sum V, within E_8. From a phenomenological point of view, the most attractive choice is $r = 5$ and in this case the low-energy gauge group is given by

$$G = SU(5) \times S(U(1)^5) \,. \tag{3.57}$$

Under the maximal sub-group $SU(5) \times SU(5) \subset E_8$ the adjoint representation of E_8 branches as

$$\mathbf{248}_{E_8} \to (\mathbf{24},\mathbf{1}) \oplus (\mathbf{1},\mathbf{24}) \oplus (\mathbf{10},\mathbf{5}) \oplus (\overline{\mathbf{10}},\overline{\mathbf{5}}) \oplus (\overline{\mathbf{5}},\mathbf{10}) \oplus (\mathbf{5},\overline{\mathbf{10}}) \,. \tag{3.58}$$

Embedding $G \subset SU(5) \times SU(5)$ the representations on the right-hand side branch further into the G-representations

$$\begin{array}{rclcrcl} (\mathbf{24},\mathbf{1}) & \to & \mathbf{24_0} & , & (\mathbf{1},\mathbf{24}) & \to & \bigoplus_{a,b} \mathbf{1}_{\mathbf{e}_a - \mathbf{e}_b} \\ (\mathbf{10},\mathbf{5}) & \to & \bigoplus_a \mathbf{10}_{\mathbf{e}_a} & , & (\overline{\mathbf{10}},\overline{\mathbf{5}}) & \to & \bigoplus_a \overline{\mathbf{10}}_{-\mathbf{e}_a} \\ (\overline{\mathbf{5}},\mathbf{10}) & \to & \bigoplus_{a<b} \overline{\mathbf{5}}_{\mathbf{e}_a + \mathbf{e}_b} & , & (\mathbf{5},\overline{\mathbf{10}}) & \to & \bigoplus_{a<b} \mathbf{5}_{-\mathbf{e}_a - \mathbf{e}_b} \,. \end{array} \tag{3.59}$$

Here, $\mathbf{r_q}$ denotes an $SU(5)$ representation $\mathbf{r}$ with $S(U(1)^5)$ charge $\mathbf{q}$, a five-dimensional integer vector, defined up to multiples of $(1,1,1,1,1)$. Further, $\mathbf{e}_a$, where $a = 1,\ldots,5$, denote the five-dimensional standard unit vector. This means that, for example, the multiplet $\mathbf{10}_{\mathbf{e}_a}$ carries charge $+1$ under the a^{th} $U(1)$ symmetry in $S(U(1)^5)$ and is uncharged under the others. For simplicity, we will frequently replace the sub-scipt $\mathbf{e}_a$ by a, so that, for example, $\mathbf{10}_{\mathbf{e}_a}$ is written as $\mathbf{10}_a$.

The G-representations on the right-hand sides of Eq. (3.59) provide a list of possible multiplets which can arise in the effective theory. If we formally assign the charge $\mathbf{e}_a$ to the line bundle L_a then every tensor product of these line bundles and their duals acquires an induced charge, in the obvious way. For example, the line bundles $L_a \otimes L_b$ then carry charges $\mathbf{e}_a + \mathbf{e}_b$. Then, every multiplet $\mathbf{r_q}$ in (3.59) can be associated to the line bundle, $L \in \{L_a, L_a \otimes L_b, L_a \otimes L_b^*, L_a^* \otimes L_b^*\}$, with the same $S(U(1)^5)$ charge $\mathbf{q}$. The first cohomology, $h^1(X,L)$, of this associated line bundle

counts the multiplicity of a multiplet. The details of this correspondence are provided in Table 2. We recall that all line bundles L_a (and, hence, their duals and all their tensor products) need to

multiplet	$S(U(1)^5)$ charge	associated L	contained in
$\mathbf{10}_a$	$\mathbf{e}_a$	L_a	V
$\overline{\mathbf{10}}_a$	$-\mathbf{e}_a$	L_a^*	V^*
$\bar{\mathbf{5}}_{a,b}$	$\mathbf{e}_a + \mathbf{e}_b$	$L_a \otimes L_b$	$\wedge^2 V$
$\mathbf{5}_{a,b}$	$-\mathbf{e}_a - \mathbf{e}_b$	$L_a^* \otimes L_b^*$	$\wedge^2 V^*$
$\mathbf{1}_{a,b}$	$\mathbf{e}_a - \mathbf{e}_b$	$L_a \otimes L_b^*$	$V \otimes V^*$

Table 2: *A list of $SU(5) \times S(U(1)^5)$ multiplets in the low-energy theory and their associated line bundles. The multiplicity of each multiplet is computed by the cohomology $h^1(X, L)$ of the associated line bundle L.*

have a vanishing slope which implies that $h^0(X, L) = h^3(X, L) = 0$ for all line bundles L which appear in Table 2 (with the exception of $L_a \otimes L_a^* = \mathcal{O}_X$). This means that the chiral asymmetry of multiplets is computed by the index, that is,

$$\#\mathbf{10}_a - \#\overline{\mathbf{10}}_a = h^1(X, L_a) - h^1(X, L_a^*) = -\text{ind}(L_a) \tag{3.60}$$

$$\#\bar{\mathbf{5}}_{a,b} - \#\mathbf{5}_{a,b} = h^1(X, L_a \otimes L_b) - h^1(X, L_a^* \otimes L_b^*) = -\text{ind}(L_a \otimes L_b) \, . \tag{3.61}$$

What should be required of this spectrum for a physically promising model? First, we remark that the additional gauge bosons associated to the $S(U(1)^5)$ symmetry do not constitute a phenomenological problem. They are either heavy due to the Green-Schwarz effect or can acquire mass due to spontaneous symmetry breaking induced by the $SU(5)$ singlet fields in the last row of Table 2. For the correct total chiral asymmetry in the $\mathbf{10}$–$\overline{\mathbf{10}}$ sector we should require that

$$\text{ind}(V) = \sum_a \text{ind}(L_a) \stackrel{!}{=} -3|\Gamma| \, . \tag{3.62}$$

This condition guarantees three chiral $\mathbf{10}$ families after dividing by the symmetry Γ with order $|\Gamma|$. Fortunately, for $SU(5)$ bundles V, we have $\text{ind}(V) = \text{ind}(\wedge^2 V)$ so that the above condition also guarantees the correct chiral asymmetry in the $\bar{\mathbf{5}}$–$\mathbf{5}$ sector.

For models where each line bundle L_a is equivariant by itself we should also ensure that the chiral asymmetry in every $S(U(1)^5)$ charge sector has the "correct" sign, that is, that there is no excess of $\overline{\mathbf{10}}_a$ over $\mathbf{10}_a$ multiplets for any a and no excess of $\mathbf{5}_{a,b}$ over $\bar{\mathbf{5}}_{a,b}$ multiplets for any a, b. To avoid such "wrong" chiral asymmetries we impose that

$$\text{ind}(L_a) \leq 0 \, , \qquad \text{ind}(L_a \otimes L_b) \leq 0 \tag{3.63}$$

for all $a, b = 1, \ldots, 5$ with $a < b$.

Further, for a "clean" spectrum we should demand the absence of $\mathbf{10}$–$\overline{\mathbf{10}}$ vector-like pairs and the presence of precisely one $\bar{\mathbf{5}}$–$\mathbf{5}$ vector-like pair to account for the Higgs doublets. These requirements can be expressed as

$$h^1(X, V^*) = \sum_a h^1(X, L_a^*) \stackrel{!}{=} 0 \,, \qquad h^1(X, \wedge^2 V^*) = \sum_{a<b} h^1(X, L_a^* \otimes L_b^*) \stackrel{!}{=} 1 \,. \tag{3.64}$$

If all these conditions are satisfied, a model with the precise MSSM spectrum can usually be obtained after dividing by the symmetry Γ. The only exotic states left in the upstairs theory are the Higgs triplets contained in the $\bar{\mathbf{5}}$–$\mathbf{5}$ vector-like pair. They can normally be projected out for a suitable choice of equivariant structure and Wilson line, while the Higgs doublets can be kept.

While the conditions (3.64) give rise to a clean Standard Model spectrum in this way they are by no means necessary. Additional vector-like states as they arise when the conditions (3.64) are violated can receive a mass from superpotential terms of the form $\mathbf{1}\,\mathbf{10}\,\overline{\mathbf{10}}$ and $\mathbf{1}\,\mathbf{5}\,\bar{\mathbf{5}}$ (or even higher-dimensional operators with multiple singlet insertions), when the $SU(5)$ singlet fields acquire a vacuum expectation value. It is worth noting that these singlet fields, which appear in the last row of Table 2, carry a $S(U(1)^5)$ charge so that the presence of such terms is constrained by the $S(U(1)^5)$ symmetry. Switching on singlet vacuum expectation values (which, in the language of the effective theory, has to be done preserving D- and F-flatness) corresponds to moving in the bundle moduli space and deforming the line bundle sum V to a bundle with non-Abelian structure group. It is perfectly possible and likely to happen in many cases, that unwanted vector-like states can be removed in this way, but checking this is a matter of detailed analysis within each model.

Chiral asymmetry and F-theory dual models

One of the motivations for considering line bundle models on elliptically fibered CY three-folds with involutions, which are a class of phenomenologically promising heterotic models, is to begin a programme to understand their F-theory duals, as discussed briefly in the introduction to this chapter. However, interestingly, one can immediately see from the preceding discussion on the spectrum computation that it remains to understand a gap in heterotic/F-theory duality, as we now explain.

Specifically, it is interesting to consider the total chiral asymmetry of the required invariant line bundle models. From Equations (3.28) and (3.47), this is given by

$$\mathrm{ind}(V) = \sum_a \mathrm{ind}(L_a) = -\frac{1}{6} d_{IJK} \sum_a k_a^I k_a^J k_a^K \,. \tag{3.65}$$

Since the pure base intersection numbers d_{ijk} vanish from Eq. (3.17), if this quantity is to be non-zero, to achieve a chiral model, then at least some of the integers k_a^0 and $k_a^{\hat{0}}$ along the zeroth direction must be non-zero. In other words, some of the line bundles L_a need to have a first Chern class with a non-zero coefficient in the direction of $\sigma(B)$ or $\zeta(B)$. But this would lead to a non-trivial bundle upon restriction to the fibers, and heterotic/F-theory duality, in its current formulation, requires bundles which are flat on the fibers [3]. Hence, at present, there is no obvious F-theory dual for chiral line bundle models. It would be interesting to study in the future precisely how heterotic/F-theory duality must be extended in order to account for such cases.

3.4 Systematic model search

We have now collected all ingredients required for the construction of heterotic line bundle models on elliptically fibered CY three-folds with a freely-acting involution. In this section, we describe the results of a systematic scan, searching for physically promising models, which covers the six possible base manifolds in Table 1 and rank five line bundles sums. We also illustrate our results by explicitly presenting a specific model found in this scan.

3.4.1 Scan results

Our search has been carried out for all six base spaces in Table 1. For each base space, we have scanned over all line bundle sums $K = ({k^I}_a)$ which satisfy Eq. (3.55) (so that each constituent line bundle is ι_X invariant) and whose entries are bounded by $|{k^I}_a| \leq k_{\text{max}}$. The quantity k_{max} has been maximised in view of computational limitations on a desktop machine and its values are listed in Table 3.

From the line bundle sums generated in this way, we have selected the physically promising ones by the following set of criteria.

- Eq. (3.47), $c_1(V) = 0$, is satisfied so that the structure group is $S(U(1)^5)$.
- There is a locus in Kähler moduli space where the slopes of all line bundles L_a vanish, that is, Eq. (3.49) is satisfied for all L_a. This means the line bundle sum V preserves supersymmetry.
- The anomaly condition (3.51) is satisfied.
- Following Eq. (3.62), the index of the line bundle sum satisfies $\text{ind}(V) = -6$. This guarantees three chiral families of quarks and leptons after taking the quotient by the involution

ι_X.

- The indices of L_a and $L_a \otimes L_b$ are constrained by Eqs. (3.63) to avoid a chiral asymmetry with the wrong sign in any $S(U(1)^5)$ charge sector.

The number of models satisfying these conditions is given in the last column in Table 3. The

base B	k_{max}	k_{mod}	#models
F_2	10	–	0
F_4	10	–	0
F_7	10	4	54
F_9	7	6	22
F_{13}	3	3	≥ 46
$F_{15}^{(a)}$	3	3	≥ 236
$F_{15}^{(b)}$	3	3	≥ 84
total	–	–	≥ 442

Table 3: *The number of phenomenologically interesting models found for each of the six base manifolds. The scan was carried out over all line bundle models with* $|k^I{}_a| \leq k_{\text{max}}$ *and* k_{mod} *gives the largest value of* $|k^I{}_a|$ *which arises in a physically interesting model. The* $\geq$ *signs indicate where* k_{max} *was not large enough to ensure all models were found.*

list of all integer matrices K for those physically promising models can be downloaded from Ref. [41].

The number of models found for each base manifold B can be qualitatively understood by considering the number $h^{1,1}_{\text{inv}}(B)+1$ (see Table 1 for the values of $h^{1,1}_{\text{inv}}(B)$) of independent integers which specify a ι_X invariant line bundle. For $B = F_2, F_4$ we have $h^{1,1}_{\text{inv}}(B) = 2$ and this does evidently not provide enough freedom to allow for interesting models. For $B = F_7, F_9$ we have $h^{1,1}_{\text{inv}}(B) = 3$ and in these case we are able to find all physically promising models by extending the scan to a sufficiently large k_{max}. For the last two base spaces, $B = F_{13}, F_{15}$, with $h^{1,1}_{\text{inv}}(B) = 4$ the space of line bundle sums becomes quite large and we have only carried out a partial scan for $k_{\text{max}} = 3$. For those cases, the number of interesting models exceeds the numbers given in Table (3). In total, we find 442 models for all six base manifolds.

For those 442 models, we have also determined the complete spectrum by computing all relevant line bundle cohomologies, as explained in Section 3.3.2. The results of these computations are summarised in Figs. 2, 3 and 4 which provide frequency plots for the number of $\overline{\mathbf{10}}$

multiplets, **5** multiplets and singlets, respectively. As these plots show, there is unfortunately

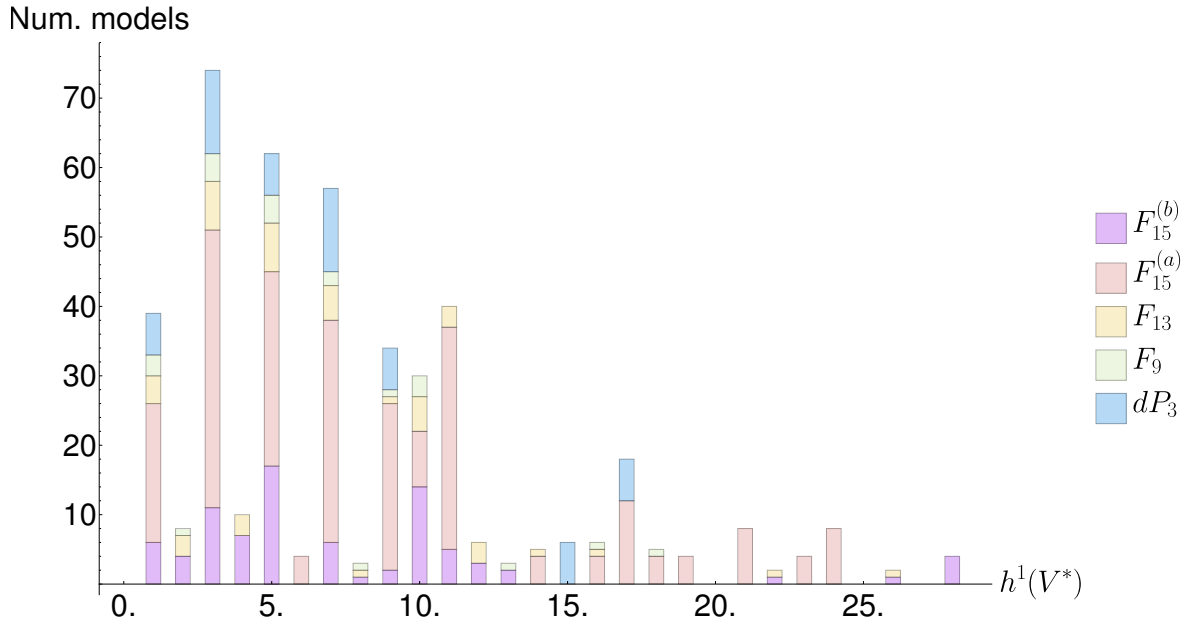

Figure 2: *Frequency plot of* $h^1(V^*)$ *which gives the number of* $\overline{\mathbf{10}}$ *multiplets, combined for all base spaces.*

no model without additional vector-like pairs. From Figure 2, there exists always at least one $\mathbf{10}$–$\overline{\mathbf{10}}$ vector-like pair and frequently many more. Figure 3 shows that the situation is worse for $\mathbf{5}$–$\bar{\mathbf{5}}$ vector-like pairs, where the minimal number is 20. This large number of vector-like pairs comes as a surprise, given the experience with line bundle models on complete intersection CY three-folds [19, 24, 32] where imposing the correct chiral asymmetry frequently resulted in the absence of additional vector-like states.

As we have argued above, these vector-like states do not necessarily render the models unphysical since they can be given a mass via couplings to singlet fields with non-vanishing vacuum expectation values. Figure 4 shows that our models do indeed have a significant number of such singlet fields and it is likely that they can be used to remove unwanted vector-like pairs in many cases. Analysing this is a matter of more detailed model building which is beyond the scope of the present work.

3.4.2 An example model

As an illustration, we will now present one of the physically interesting models from the previous sub-section in detail. Our example is for the base space $B = F_7 = \mathrm{dP}_3$ which, following Appendix B, has a basis of curve classes $\{\mathcal{C}^i\} = \{l, e_1, e_2, e_3\}$ with dual basis $\{\mathcal{C}_i\} = \{l, -e_1, -e_2, -e_3\}$. Line bundles will be represented relative to the basis $\{D_I\} = \{D_0, D_{\hat{0}}, D_i\}$,

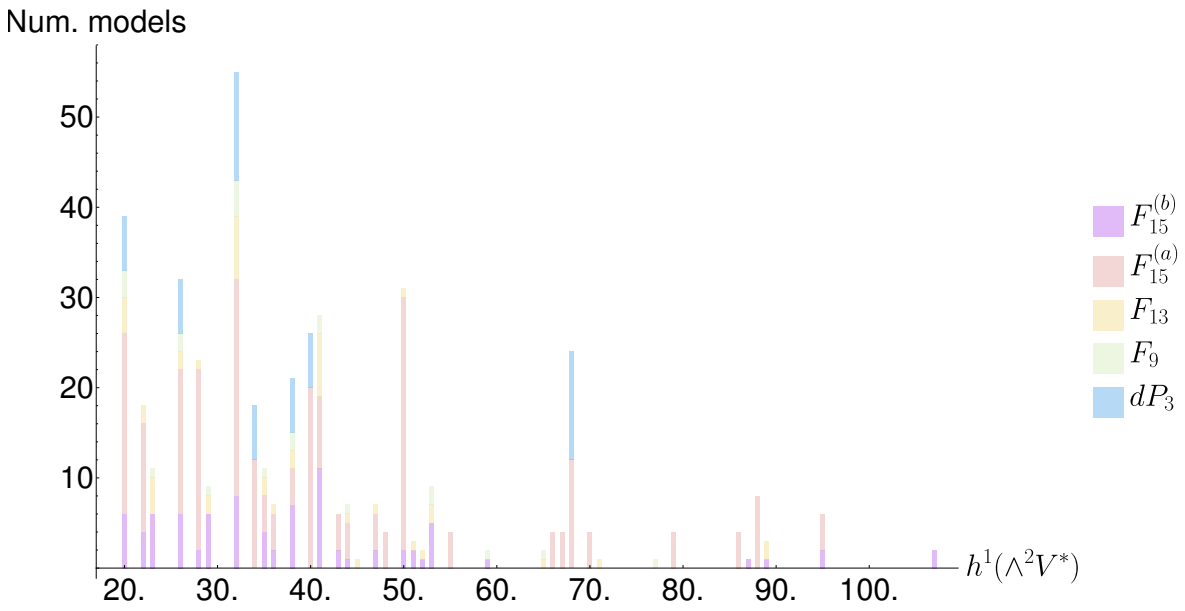

Figure 3: *Frequency plot of* $h^1(\wedge^2 V^*)$ *which gives the number of* **5** *multiplets, combined all base space spaces.*

where

$$D_0 = \sigma(B)\ , \quad D_{\hat{0}} = \zeta(B)\ , \quad D_i = \pi^{-1}(\mathcal{C}_i)\ , \quad i = 1, \ldots, 4\ . \tag{3.66}$$

Writing $L_a = \mathcal{O}_X(k^I{}_a D_I)$ as before, the integer matrix $K = (k^I{}_a)$ which defines our example is given by

$$K = \begin{pmatrix} -1 & 0 & 0 & 0 & 1 \\ -1 & 0 & 0 & 0 & 1 \\ 1 & 0 & 0 & 0 & -1 \\ -1 & 1 & 1 & 1 & -2 \\ 1 & -1 & -1 & -1 & 2 \\ 1 & 0 & 0 & 0 & -1 \end{pmatrix}\ , \tag{3.67}$$

with every column representing one of the line bundles L_a. First, we note that the columns sum up to zero so that the constraint (3.47), $c_1(V) \sim \sum_a \mathbf{k}_a = 0$, is indeed satisfied. Further, we see that the matrix is consistent with ι_X invariance of each line bundle. Specifically, the first and second rows are identical, so that $k^0{}_a = k^{\hat{0}}{}_a$, and the last four rows satisfy $k^1{}_a = k^2{}_a + k^3{}_a + k^4{}_a$, in accordance with Eq. (3.55).

Following the list of required properties in Section 3.4.1, we should next check that the slope of all line bundles vanishes somewhere in the Kähler cone. Given the structure of the matrix (3.67) it is sufficient to do this for the line bundles L_1 and L_2 whose slopes are explicitly

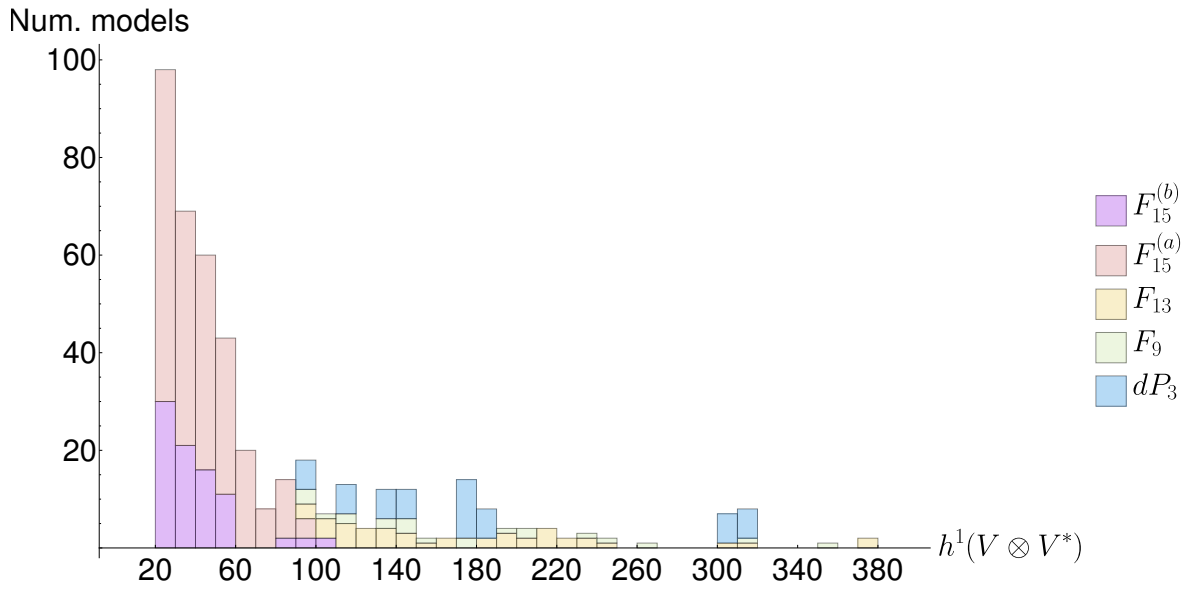

Figure 4: *Frequency plot of $h^1(V \otimes V^*)$ which gives the number of singlet fields, combined for all base spaces.*

given by

$$\begin{aligned} \mu_X(L_1) &= -8t_0^2 + 8t_0t_1 - 2t_1^2 + 2t_2^2 - 4t_0t_3 + 2t_3^2 \\ &\quad -4t_0t_4 + 2t_4^2 + 8t_1t_{\hat{0}} - 4t_3t_{\hat{0}} - 4t_4t_{\hat{0}} - 8t_{\hat{0}}^2 \,, \qquad (3.68) \\ \mu_X(L_2) &= -2t_0t_2 + 2t_0t_3 - 2t_2t_{\hat{0}} + 2t_3t_{\hat{0}} \,. \qquad (3.69) \end{aligned}$$

It can be verified that $\mu_X(L_1) = \mu_X(L_2) = 0$ for

$$t_0 = \frac{5}{8} \,, \quad t_{\hat{0}} = \frac{5}{8} \,, \quad t_1 = \frac{43}{12} \,, \quad t_2 = 1 \,, \quad t_3 = 1 \,, \quad t_4 = \frac{19}{12} \,. \qquad (3.70)$$

Comparison with Eq. (B.29) shows that this point it indeed in the interior of the Kähler cone of X.

Next, we should verify the anomaly condition for this model. The second Chern class of the bundle V is given by

$$c_2(V) = 18(F - N) - 2N + 10\,\sigma(l) - 4\,\sigma(e_1) - 6\,\sigma(e_3) \qquad (3.71)$$

and comparing this with the second Chern class of the tangent bundle (3.42) gives

$$c_2(X) - c_2(V) = 54(F - N) + 2N + 8\sigma(l - e_1) + 12\sigma(l - e_2) + 6\sigma(l - e_3) \,. \qquad (3.72)$$

Since $F - N$ and N are effective curves and, from Appendix B, $l - e_a$ are effective curves in dP_3 this class is indeed effective. Hence, the anomaly can be cancelled by wrapping a five-brane on a holomorphic curve in this class. Finally, using Eqs. (3.28) and (3.65) we can verify that indeed $\mathrm{ind}(V) = -6$, $\mathrm{ind}(L_a) \leq 0$ and $\mathrm{ind}(L_a \otimes L_b) \leq 0$ for all $a, b = 1, \ldots, 5$.

In summary, we have seen that this line bundle sum is invariant under the involution and provides a consistent model with the correct chiral asymmetry.

To determine the spectrum in more detail we consider line bundle cohomologies. For the line bundle sum V we find

$$h^\bullet(X,V) = (0,7,1,0)\ . \tag{3.73}$$

This overall result originates from the individual line bundle cohomologies

$$h^\bullet(X,L_1) = (0,1,1,0)\ , \quad h^\bullet(X,L_5) = (0,6,0,0)\ , \tag{3.74}$$

with the cohomologies of all other L_a vanishing. For $\wedge^2 V$ we have

$$h^\bullet(X,\wedge^2 V) = (0,26,20,0)\ , \tag{3.75}$$

obtained as a sum of the cohomologies

$$h^\bullet(X,L_1\otimes L_2) = h^\bullet(X,L_1\otimes L_3) = h^\bullet(X,L_1\otimes L_4) = (0,2,0,0) \tag{3.76}$$

$$h^\bullet(X,L_2\otimes L_3) = h^\bullet(X,L_2\otimes L_4) = h^\bullet(X,L_3\otimes L_4) = (0,3,3,0) \tag{3.77}$$

$$h^\bullet(X,L_2\otimes L_5) = h^\bullet(X,L_3\otimes L_5) = h^\bullet(X,L_4\otimes L_5) = (0,1,1,0) \tag{3.78}$$

$$h^\bullet(X,L_1\otimes L_5) = (0,8,8,0)\ . \tag{3.79}$$

Combining these results the chiral spectrum of the model is

$$6\,\mathbf{10}_5\ ,\ 2\,\bar{\mathbf{5}}_{1,2}\ ,\ 2\,\bar{\mathbf{5}}_{1,3}\ ,\ 2\,\bar{\mathbf{5}}_{1,4}\ , \tag{3.80}$$

and we have the additional vector-like pairs

$$(\mathbf{10}_1\oplus\overline{\mathbf{10}}_1)\ ,\ 3\,(\mathbf{5}_{2,3}\oplus\bar{\mathbf{5}}_{2,3})\ ,\ 3\,(\mathbf{5}_{2,4}\oplus\bar{\mathbf{5}}_{2,4})\ ,\ 3\,(\mathbf{5}_{3,4}\oplus\bar{\mathbf{5}}_{3,4}) \tag{3.81}$$

$$8\,(\mathbf{5}_{1,5}\oplus\bar{\mathbf{5}}_{1,5})\ ,\ (\mathbf{5}_{2,5}\oplus\bar{\mathbf{5}}_{2,5})\ ,\ (\mathbf{5}_{3,5}\oplus\bar{\mathbf{5}}_{3,5})\ ,\ (\mathbf{5}_{4,5}\oplus\bar{\mathbf{5}}_{4,5})\ . \tag{3.82}$$

This illustrates the aforementioned proliferation of vector-like pairs. In addition, across all $S(U(1)^5)$ charge sectors, the model has $h^1(V\otimes V^*) = 94$ singlet fields whose $S(U(1)^5)$ charges we do not list explicitly.

3.5 Conclusions

In this chapter, we have studied heterotic line bundle models on elliptically fibered CY three-folds. Standard heterotic model building requires a non-trivial first fundamental group of the CY three-fold which is normally realised by starting with a simply-connected CY three-fold X with a freely-acting symmetry Γ and then taking the quotient X/Γ. This has led us to study

elliptically fibered CY three-folds with the simplest type of symmetry, a freely-acting involution ι_X. We have realised this involution by combining a half-shift ι_E on the elliptic fibers with an involution ι_B on the base B of the fibration. Such elliptic fibrations necessarily have two sections which are exchanged by ι_E.

We have systematically developed the tools required for heterotic line bundle model building on such manifolds, including the calculation of line bundle cohomology, by expressing all relevant properties in terms of properties of the base B.

The choice of base spaces is restricted by requiring a generically smooth Weierstrass elliptic CY three-fold X and a fixed point free involution ι_X. The latter can be realised if the involution ι_B on the base has at most fixed points. In this chapter, we have focused on toric two-fold base spaces B and, from this class, the above requirements single out six spaces, represented by the reflexive polygons shown in Figure 1.

For those six base spaces, we have systematically searched for physically promising models, that is models based on rank five line bundles sums V, with each constituent line bundle being ι_X invariant, and a total chiral asymmetry of six. After taking the quotient by ι_X and including a Wilson line these give rise to theories with the Standard Model group and three chiral families. Over the six possible base manifolds, we have found a total of 442 models of this kind and we have computed the complete spectrum for all these models.

A generic feature is the presence of vector-like states, specifically at least one $\mathbf{10}$–$\overline{\mathbf{10}}$ pair and at least 20 $\mathbf{5}$–$\bar{\mathbf{5}}$ pairs in each case. In this respect, the results are very different from the ones obtained for line bundle models on complete intersection CY three-folds [19, 24, 32], where vector-like pairs were absent for most models with the correct chiral asymmetry. The underlying reason for this difference seems to be the different structure of line bundle cohomology for the two constructions. Complete intersection CY three-folds are defined in ambient spaces consisting of products of projective spaces. They inherit to some degree the relatively simply structure of line bundle cohomology on projective spaces, where at most one cohomology of a line bundle can be non-vanishing. On the other hand, for the elliptically fibered CY three-folds considered in this chapter, line bundle cohomology is determined from line bundle cohomology on the toric two-fold base (or, alternatively, from line bundle cohomology on the ambient toric four-fold), which tends to be more complicated as compared to projective spaces.

The presence of vector-like states does not mean that our models are phenomenologically ruled out. All models contain Standard Model singlet fields (which should be interpreted as bundle moduli) and, depending on details, may allow for superpotential couplings of the form $\mathbf{1}\,\mathbf{10}\,\overline{\mathbf{10}}$ or $\mathbf{1}\,\mathbf{5}\,\bar{\mathbf{5}}$ (or similar, higher-dimensional operators with multiple singlet insertions). Non-

trivial singlet vacuum expectation values which correspond to deformations of the bundle away from a line bundle sum and to a bundle with non-Abelian structure group can then generate masses for the vector-like pairs and remove these states from the low-energy spectrum. A detailed study of this is beyond the scope of the present work and a subject of future work. Specifically, it would be interesting to check if all unwanted vector-like states can be removed in this way while the desired pair of Higgs doublets can be kept light at the same time.

We have also seen that chiral line bundle models on elliptically fibered CY three-folds necessarily have a bundle V which restricts non-trivially to the fibers. Since heterotic/F-theory duality is formulated in terms of spectral cover bundles which, by construction, are flat on the fibers it is not clear whether the models found in this chapter have an F-theory dual. It would be interesting to investigate the possible relation to F-theory further and work along these lines is in progress.

It is likely that our model building strategy can be generalised to base spaces which are not weak Fano. Besides finding appropriate involutions on those base spaces, this would require us to find an extension of the half-shift involution ι_X to the reducible fibers present in such models. As such models have more divisors than those associated with sections and divisors of the base, the set of possible line bundles and the Mori cone are larger and more complicated. In practice, the realisation of elliptically fibered CY three-folds as hypersurfaces in toric four-folds, as described in Appendix A.3, may provide the appropriate framework for such a generalisation to base spaces which are not weak Fano. Pursuing this is an interesting direction for future work.

4 NS5-Branes and Line Bundles in Heterotic/F-theory Duality

In this chapter we study F-theory duals of heterotic line bundle models on elliptically fibered CY three-folds. These models necessarily contain NS5-branes which are geometrised in the dual F-theory compactifications. We initiate a systematic study of the correspondence between various configurations of NS5-branes and the dual geometries in F-theory and perform several checks of the duality. Furthermore, we discuss the singular transitions between different configurations of NS5-branes.

The work presented in this chapter was is based on Ref. [14], and completed in collaboration with Andreas P. Braun, Andre Lukas, and Fabian Ruehle. We thank Lara Anderson, Evgeny Buchbinder, Thomas Grimm, Hans Jockers, Dave Morrison, and Wati Taylor for useful discussions while preparing this work.

4.1 Introduction

Over the years, F-theory and heterotic string theory have proven particularly promising candidates for providing a UV completion to the (supersymmetric extension of the) Standard Model (MSSM). The duality between these theories has been extensively studied (see e.g. Refs. [3, 42–52]) since the discovery of F-theory [4, 53, 54] more than 20 years ago. Despite this wealth of publications, the duality has been mostly studied within the context of the rather complicated set of heterotic vector bundle models using the spectral cover construction. For the class of heterotic line bundle models [19, 24, 32, 55–57], where most physical examples are known and whose heterotic description is more tractable, the duality has so far not been worked out in detail.

In this chapter, we initiate a study of this duality. We consider line bundles sums in $E_8 \times E_8$, together with NS5-branes, on the heterotic side. In order to apply the standard heterotic/F-theory duality fiberwise in the stable degeneration limit, we need to restrict the heterotic model we start with. First, we have to assume that the CY on the heterotic side is elliptically fibered. We will also assume that this fibration has a holomorphic section, so we can mostly focus on a Weierstrass description. For the duality to hold we furthermore construct a heterotic vector bundle, given in terms of a sum of line bundles, that is flat on the fiber. As we shall discuss, this necessitates the inclusion of heterotic NS5-branes wrapping cycles in the base, or their M5-brane analogues in the Hořava-Witten M-theory description [58, 59]. NS5-branes typically feature prominently in heterotic constructions [60, 61] and the detailed study of their duality will be the main focus of this chapter. Albeit discussed in the context of line bundle models, we expect many of the results of the 5-brane duality to carry over to other bundle constructions as well, since the majority of the discussion applies to M5-branes in the bulk and thus away from the E_8 branes. For simplicity, we will focus on the case where the line bundles are embedded into the first E_8 only; a generalisation to an embedding into both E_8 factors should be straightforward.

A crucial difference between the F-theory duals of bona fide heterotic vector bundles described by a spectral cover and heterotic line bundle models is that the latter have a trivial spectral sheet and the entire information of the bundle is captured by the spectral sheaf[17]. In the former description, the vector bundle, which breaks the primordial heterotic gauge group, is mapped onto geometry in such a way that the dual F-theory ADE singularity corresponds to the commutant of the original heterotic $E_8 \times E_8$ gauge group with the structure group of

[17] Line bundle sums actually have no spectral cover description in the original construction of Ref. [3, 62], as they are not 'regular' on the elliptic fiber. A slightly more general construction should allow a spectral cover description, though this is not important for our purposes, as we will not use this description.

the bundle. For the latter case of line bundle models, however, the bundle is not mapped onto geometry, and the F-theory dual still comes with the full $E_8 \times E_8$ singularity. Since the structure group of each line bundle on the heterotic side is U(1) and hence commutes, the heterotic gauge group is broken to a non-Abelian (in general) subgroup times a collection of U(1) factors, which are, however, generically Green-Schwarz massive. On the F-theory side, breaking of the $E_8 \times E_8$ symmetry is purely accounted for by a non-trivial G_4 flux on the E_8 branes, onto which the heterotic line bundle data is mapped.

The aforementioned NS5- or M5-branes also exhibit an interesting behaviour under the duality. Depending on the cycle that is wrapped by the 5-brane, they are either mapped onto D3-branes or onto geometry on the F-theory side [45, 63, 64]. However, on the heterotic side these different branes are on equal footing. Since the duality with and the physics of D3-branes is very well understood, we focus in this work on the duality between NS5-branes and geometry. As the F-theory geometry dual to heterotic line bundle models is in some respects quite clean, it provides a useful arena in which to study this duality. The world-volume theories of NS5-branes are notoriously hard to study and they exhibit interesting behaviour, such as the appearance of superconformal field theories from tensionless strings [65–70].

The rest of the chapter is organised as follows: in Section 4.2 we introduce our notation and review the basics of heterotic line bundle models and heterotic/F-theory duality. We then describe how to construct F-theory duals of heterotic line bundle models. We demonstrate two crucial consequences of the condition to choose a flat bundle in the fiber direction on the heterotic side in order to construct the F-theory dual: first, we necessarily need NS5-branes and second, the resulting models cannot be chiral. In Section 4.3 we discuss various aspects of the duality in compactifications to six dimensions. This serves to illustrate key concepts of the duality in a simpler and cleaner setup first. Our analysis heavily relies on toric geometry. After this, we move on to the discussion of compactifications to four dimensions in Section 4.4. On top of our discussion of 5-branes, we discuss the duality map for anomaly conditions, bundle stability, and the spectrum (i.e. the gauge group and matter representations) on the heterotic and F-theory side. We end the section with a discussion of a subtle case where an NS5-brane wraps a curve in the heterotic base that does not intersect the anti-canonical divisor of the base. In Section 4.5 we discuss the duality of multiple coincident and intersecting NS5-branes. We first describe in detail the relationship between the NS5-brane configuration and the F-theory geometry. When the NS5-branes intersect or coincide, there are singularities in the F-theory base. As the description of the four-dimensional theory resulting from compactifying F-theory on the resulting singular CY four-fold is challenging and subtle, we restrict to describing the

three-dimensional theory which arises upon compactification of M-theory on the four-fold, which lifts to the four-dimensional theory. We summarise our results in Section 4.6. Appendices D.1 and D.2 contain details of toric resolutions in the six-dimensional and four-dimensional models of Sections 4.3 and 4.4, respectively.

4.2 F-theory duals of heterotic line bundle models

4.2.1 Heterotic line bundle models on elliptically fibered CYs

In this section we collect pertinent information first on heterotic line bundle models and second on elliptically fibered CY manifolds. Note that we also discussed heterotic line bundle models in some detail in Chapter 3 above.

Heterotic line bundle models

For the heterotic compactification space we choose a CY n-fold X_n. We need to further specify a vector bundle $V = V_1 \oplus V_2$ with the structure group of V_i contained in E_8. For line bundle models, the vector bundle V is taken to simply be a sum of line bundles,

$$V = V_1 \oplus V_2 = \bigoplus_{a=1}^{\mathfrak{r}} L_a \,. \tag{4.1}$$

Each line bundle is associated to a particular $\mathrm{U}(1)$ factor in the Cartan subgroup of $\mathrm{E}_8 \times \mathrm{E}_8$. The first Chern classes of V_1 and V_2 need to be trivial,

$$c_1(V_1) = c_1(V_2) = 0 \,, \tag{4.2}$$

in order to ensure that the structure group of V can be embedded into $\mathrm{E}_8 \times \mathrm{E}_8$, which is traceless. For the sake of brevity, we will often take V_2 to be trivial. We will write $\mathcal{O}_{X_n}(D)$ for a line bundle with first Chern class or Chern character (Poincaré dual to) D,

$$\mathrm{ch}_1(\mathcal{O}_{X_n}(D)) = c_1(\mathcal{O}_{X_n}(D)) = D \,. \tag{4.3}$$

A divisor D can be expanded in a basis $\{D_I\}$ of $H_{2n-2}(X_n, \mathbb{Z})$, so we can write $D = k^I D_I$ where $k^I \in \mathbb{Z}$, and this list of integers k^I characterises the line bundle. Thus, line bundle sums (4.1) are characterised by a matrix of integers k_a^I. For later computations involving the anomaly condition in compactifications to four dimensions, we will need the expression for the second Chern character of a line bundle sum on a CY three-fold X_3, which reads

$$\mathrm{ch}_2(L_a) = \frac{1}{2} d_{IJK} k_a^I k_a^J C^K \,, \qquad \mathrm{ch}_2(V) = \frac{1}{2} d_{IJK} \left(\sum_{a=1}^{\mathfrak{r}} k_a^I k_a^J \right) C^K \,. \tag{4.4}$$

In these expressions, $d_{IJK} \equiv D_I \cdot D_J \cdot D_K$ are the triple intersection numbers of X_3, and C^K are a basis of curves satisfying $C^I \cdot D_J = \delta^I_J$. We also note that for a vector bundle E with $c_1(E) = 0$, we simply have $\mathrm{ch}_2(E) = -c_2(E)$.

The gauge and compactification background have to be chosen such that they satisfy the anomaly cancellation and supersymmetry constraints. The former is ensured via the Bianchi identity of the NS three-form field H,

$$\mathrm{d}H = \mathrm{ch}_2(V_1) + \mathrm{ch}_2(V_2) - \mathrm{ch}_2(X_n) - W\,. \tag{4.5}$$

Here, $\mathrm{ch}_2(V_i)$ and $\mathrm{ch}_2(X_n)$ are the second Chern characters of the vector and the tangent bundle, respectively. Furthermore, we have allowed for the presence of NS5-branes that span the d non-compact dimensions and wrap an internal $(6-d)$ cycle with homology class $[W]$.

Unbroken supersymmetry requires that the vector bundle satisfies the Hermitian Yang-Mills equations, which can be achieved if the flux is a $(1,1)$-form and it is poly-stable with slope zero [16,17]. As line bundles are slope-stable, this reduces to a slope zero condition for each line bundle. The slope $\mu_{X_3}(L_a)$ of a line bundle L_a on a CY three-fold X_3 is defined as

$$\mu_{X_3}(L_a) := \int_{X_3} J \wedge J \wedge c_1(L) = d_{IJK} t^I t^J k_a^K\,, \tag{4.6}$$

where $J = t^I D_I$ is the Kähler form expanded in a basis of divisors D_I with Kähler parameters t^I.

Data of the elliptically fibered CY

As we shall discuss in the next subsection, the CY manifold X_n needs to be elliptically fibered over a base B_{n-1},[18]

$$\begin{array}{ccc} T^2 \hookrightarrow & X_n & \\ & \downarrow \pi_H & \\ & B_{n-1} & \end{array} \tag{4.7}$$

We will write $\sigma : B_{n-1} \to X_n$ for the section of the elliptic fibration, and F for the generic fiber. We will be discussing the duality in compactifications to six dimensions ($n = 2$) and four dimensions ($n = 3$).

We now collect some general details and notation on this heterotic geometry in the case of compactification to four dimensions, which we will make use of throughout. In this case we have a CY three-fold X_3 with an elliptic fibration $\pi_H : X_3 \to B_2$. We write $\{\mathcal{C}^i\}$ for an integral basis

[18] While the existence of a section is not required, we will focus on Weierstrass models that have a holomorphic section, the so-called zero section.

of curves on B_2, and $\{\mathcal{C}_i\}$ for a dual basis satisfying $\mathcal{C}_i \cdot \mathcal{C}^j = \delta_i^j$. We also define $\mathfrak{g}_{ij} := \mathcal{C}_i \cdot \mathcal{C}_j$. For an integral basis of curves $\{C^I\}$ and divisors $\{D_I\}$ on X_3, where $I = (0, i)$, we can then take

$$\begin{aligned} C^0 = F\,, \quad C^i = \sigma(\mathcal{C}^i)\,, \\ D_0 = \sigma(B_2) - \xi^i D_i\,, \quad D_i = \pi_H^*(\mathcal{C}_i)\,, \end{aligned} \tag{4.8}$$

where $\xi^i = K_{B_2} \cdot \mathcal{C}^i$ and $\sigma(B_2) \cong B_2$. Here K_{B_2} is the canonical divisor on B_2. Note we will freely use the same symbol for the canonical divisor and the canonical bundle. We will also use the same symbol for Poincaré dual forms and divisors. This divisor basis is chosen to be orthonormal to the curve basis, $C^I \cdot D_J = \delta_I^J$, as seen from the following intersection properties.

$\cdot$	$\sigma(B_2)$	$\pi_H^*(\mathcal{C}')$
F	1	0
$\sigma(\mathcal{C})$	$\mathcal{C} \cdot K_{B_2}$	$\mathcal{C} \cdot \mathcal{C}'$

$\cdot$	$\sigma(B_2)$	$\pi_H^*(\mathcal{C}')$
$\sigma(B_2)$	$\sigma(K_{B_2})$	$\sigma(\mathcal{C}')$
$\pi_H^*(\mathcal{C})$	$\sigma(\mathcal{C})$	$(\mathcal{C} \cdot \mathcal{C}')F$

In particular, we can identify t^0 as the volume of the fiber in the Kähler form $J = t^I D_I$. The triple intersection numbers in this basis are

$$d_{000} = \xi_i \xi^i\,, \quad d_{00i} = -\xi_i\,, \quad d_{0ij} = \mathfrak{g}_{ij}\,, \quad d_{ijk} = 0\,. \tag{4.9}$$

Additionally, the second Chern class of the tangent bundle is (see e.g. Ref. [3])

$$\begin{aligned} c_2(X_3) = -\mathrm{ch}_2(X_3) &= \pi_H^*\left(c_2(B_2)\right) + 11\pi_H^*\left(c_1(B_2)^2\right) + 12\sigma(c_1(B_2)) \\ &= \left[\int_{B_2} \left(c_2(B_2) + 11 c_1(B_2)^2\right)\right] F - 12\sigma(K_{B_2})\,, \end{aligned} \tag{4.10}$$

and we will need this expression in computations involving the anomaly condition.

In compactifications to four dimensions on an elliptically fibered CY manifold X_3, the heterotic NS5-branes can wrap either (i) the fiber, or (ii) a curve in the base[19], or (iii) some combination. We refer to the first kind as 'vertical' NS5-branes, and to the second as 'horizontal' NS5-branes. In a Hořava-Witten picture, heterotic NS5-branes are M5-branes with positions in the bulk of the 11d interval $S^1/\mathbb{Z}_2$, and we will often make use of this picture. At the two ends of the interval, M5-branes transition into small instantons on the respective E_8 brane. We will occasionally refer to 'horizontal' or 'vertical' instantons, depending on the type of M5-brane they originate from under the small instanton transition.

4.2.2 F-theory models and fiberwise duality

Let us now turn to F-theory duals of heterotic models. Similarly to the heterotic case, we need to specify the compactification data, which means choosing a CY $(n+1)$-fold Y_{n+1} and a

[19] This characterisation is slightly crude. We will be more precise in Section 4.4.

four-form flux G_4. We will discuss the $n = 2$ and the $n = 3$ case, the first in order to develop understanding, and the second as compactifications to four dimensions will be our primary interest. In the $n = 3$ case, the F-theory analogue of the heterotic Bianchi identity is D3-brane tadpole cancellation [5, 6], which reads [71]

$$N_3 - \frac{\chi(Y_4)}{24} + \frac{1}{2}\int_{Y_4} G_4 \wedge G_4 = 0\,, \tag{4.11}$$

where N_3 is the number of D3-branes and $\chi(Y_4)$ is the Euler number of Y_4.

The compactification background Y_{n+1} needs to be elliptically fibered and – in case of duality to the heterotic string – the base of the elliptic fibration needs to furthermore be $\mathbb{P}^1$ fibered (so that Y_{n+1} is fibered by K3 surfaces with an elliptic fibration),

$$\begin{array}{ccc} T^2 \hookrightarrow & Y_{n+1} & \\ & \downarrow \pi_F & \\ \mathbb{P}^1 \hookrightarrow & \mathcal{B}_n & \\ & \downarrow \tilde{\pi}_F & \\ & B_{n-1} & \end{array} \quad , \qquad \begin{array}{ccc} K3 \hookrightarrow & Y_{n+1} & \\ & \downarrow p_F & \\ & B_{n-1} & \end{array} \quad . \tag{4.12}$$

Note that the base B_{n-1} in (4.12) is identified with the base B_{n-1} in (4.7), which is why we use the same symbol. We will refer to the extra $\mathbb{P}^1$ which appears in F-theory, i.e. the base of the elliptic fibration on the K3 surface, as the 'F-theory $\mathbb{P}^1$'.

This duality can be understood by fiberwise application of heterotic/F-theory duality in 8d. Here, heterotic strings on a T^2 with Wilson line moduli was proposed to be dual to F-theory on a K3 surface [53],

$$\text{Heterotic on } T^2 \overset{\text{dual}}{\longleftrightarrow} \text{ F-theory on K3}\,,$$

due to the equivalence of their moduli spaces.

In order to capture compactifications of heterotic string theory in the supergravity limit, the K3 fiber of the F-theory background must be in the stable degeneration limit, in which the K3 fiber degenerates to a union of two rational elliptic surfaces [3, 42, 43]. The extension of the duality to compactification to fewer dimensions consists of fibering both sides over a common space, giving an elliptically fibered and a K3 fibered CY manifold respectively. Besides guaranteeing that the elliptic fiber on the heterotic side is large compared to the string scale, the stable degeneration limit is also crucial to ensure that the heterotic background is described by conventional geometry, i.e. not patched together by maps involving T-dualities, see Refs. [72, 73] for a discussion of the relevant geometry.

The limit in which the heterotic string becomes weakly coupled corresponds to the adiabatic limit of the K3 fibration on the F-theory side, that is the limit in which the volume of the 'F-theory $\mathbb{P}^1$' (the base of the elliptic fibration on the K3 surface) becomes small compared to the (properly normalised) volumes of B_{n-1} (the base of the K3 fibration). This is in line with thinking about the F-theory $\mathbb{P}^1$ as a fibration of S^1 over an interval, which is identified with the interval of the M-theory lift of heterotic strings.

Similarly, we will assume that the elliptic fibration on the heterotic side is adiabatic in the sense that the volume of the fiber $T^2_{\text{Het.}}$ is small compared to volumes of the base B_{n-1}. Note that in the conventional application of duality between heterotic string theory and F-theory employing vector bundles constructed by means of spectral covers, this condition ensures stability of the bundles [3, 62]. The required hierarchies of volumes can then be summarised as,

$$\text{vols}(B_{n-1}) \gg \text{vol}(T^2_{\text{Het.}}) \to \infty\,, \quad \text{vols}(B_{n-1}) \gg \text{vol}(\mathbb{P}^1_{\text{F}-\text{th.}}) \to 0\,. \tag{4.13}$$

We now collect some general details and notation on this F-theory geometry in the case of compactification to four dimensions. In this case we have a CY four-fold Y_4 with a K3 fibration $p_F : Y_4 \to B_2$ and an elliptic fibration $\pi_F : Y_4 \to \mathcal{B}_3$. We will often represent the generic fiber of the elliptic fibration in a $\mathbb{P}_{123}$ ambient space[20] whose coordinates we denote $\{x, y, w\}$. The F-theory elliptic fibration, as on the heterotic side, is characterised by a Weierstrass equation, which describes the fiber in its ambient space over each point in the base,

$$y^2 = x^3 + fxw^4 + gw^6\,, \tag{4.14}$$

where the functions appearing are sections, $f = \Gamma(K_{\mathcal{B}_3}^{-4})$ and $g = \Gamma(K_{\mathcal{B}_3}^{-6})$. The elliptic curve degenerates over the locus defined by the vanishing of the discriminant

$$\Delta = 4f^3 + 27g^2\,, \tag{4.15}$$

and the vanishing orders of (f, g, Δ) reflect the severity of the degeneration.

If the vanishing orders of (f, g, Δ) are $(4, 6, 12)$ or higher in codimension ≥ 2, as in the cases we discuss, resolving with a blow-up which does not change the base of the elliptic fibration results in a 'non-flat fibration', in which the fiber dimension can jump. On this four-fold, tensionless strings appear in the F-theory limit, and the resulting theory is expected to have no standard supergravity description. Alternatively, for such singularities, one can find crepant resolutions which change the base of the elliptic fibration, resulting in a flat fibration with an $\mathcal{N} = 1$ supergravity description in the F-theory limit [4]. We will be interested in resolutions of the latter type.

[20]The weighted projective space $\mathbb{P}_{123}$ satisfies the equivalence relation $(x, y, z) \sim (\lambda x, \lambda^2 y, \lambda^3 z)$ for $\lambda \in \mathbb{C}^*$.

4.2.3 F-theory duals of heterotic line bundle models

Above we have discussed the heterotic and F-theory compactifications and the basic idea behind the duality between them, and this completes the general review. Now we turn to analysing the F-theory duals of heterotic line bundle models. In this section we will give a basic description of many aspects of the duality which we will cover in more detail in the remainder of the chapter.

As mentioned above, historically the spectral cover construction has been particularly useful for constructing F-theory duals of heterotic vector bundle models. In the original 8d duality, the heterotic bundle on the elliptic fiber has only Wilson line moduli. If we consider lower-dimensional dualities obtained by fibering the 8d duality, the vector bundles restricted to the generic elliptic curve should retain this property. Consequently, on each elliptic fiber of the heterotic three-fold, each of the E_8 vector bundles is determined by a set of points [3]. This provides a branched covering of the heterotic base called the 'spectral sheet' which describes the deformations of the E_8 singularities on the F-theory side. In addition to the spectral sheet, the description of the heterotic vector bundles requires also a 'spectral sheaf' on the spectral sheet, together giving the spectral cover. This information can then be translated into F-theory geometry and flux.

However, for duals of heterotic line bundle models the spectral cover construction becomes essentially trivial. The condition that a bundle restricts on the generic elliptic fiber to give only Wilson line moduli means that it restricts to a sum of degree zero line bundles. For a global line bundle sum V, each of the line bundles in V has to be trivial on the fiber, and hence is a pullback bundle from the base,

$$V = \bigoplus_{a}^{\mathfrak{r}} \pi_H^* \left(N_a \right) , \tag{4.16}$$

where N_a are line bundles on the base B_{n-1}. Recalling the divisor basis defined in Equation (4.8), this condition is equivalent to requiring that the matrix of integers k_a^I determining the line bundle sums satisfies

$$k_a^0 = 0 \quad \forall a \, . \tag{4.17}$$

Since the restriction of a pullback bundle to the elliptic fiber is trivial, the spectral sheet is trivial – it is $\mathfrak{r}$ copies of the zero section – and the information about the bundle is encoded entirely in the spectral sheaf. Trivial spectral sheets correspond to two undeformed surfaces of E_8 singularities in the F-theory dual, each of which is diffeomorphic to the heterotic base B_{n-1}. We will frequently refer to these as the E_8 branes. As the two heterotic bundles are pullbacks from B_{n-1}, we naturally expect the fluxes on the two E_8 stacks to be equal to the fluxes pulled back from B_{n-1}, or equivalently that the two spectral sheaves correspond to the two bundles

on B_{n-1}. This constitutes a main difference to the situations usually studied in pure F-theory constructions or in heterotic/F-theory duality with bona fide vector bundles: the E_8 symmetries on the F-theory side are broken *purely by flux*, rather than by geometry.

In order to link the flux F in the heterotic theory and the flux G_4 in F-theory, we can use the M-theory description. In this description, we resolve the singular F-theory space Y_{n+1} to a smooth space $\hat{Y}_{n+1}$. Next, we can expand G_4 in terms of two-forms $\mathrm{w}_a^{(1)}$, $\mathrm{w}_b^{(2)}$ $(a, b = 1, \ldots, \mathrm{rk}(E_8))$ dual to the exceptional divisors of the blow-up of the two E_8 singularities,

$$G_4 = \tilde{F}^{(1)\,a} \wedge \mathrm{w}_a^{(1)} + \tilde{F}^{(2)\,a} \wedge \mathrm{w}_a^{(2)}\,, \tag{4.18}$$

where $\tilde{F}^{(1)\,a}$ and $\tilde{F}^{(2)\,a}$ are pullbacks of flux two-forms from the E_8 branes. In the duality for heterotic line bundle models, from Equation (4.16) the identification of flux is rather clear: the fluxes $\tilde{F}^{(1)\,a}$ and $\tilde{F}^{(2)\,a}$ correspond to the two E_8 fluxes on the heterotic base B_{n-1} that are pulled back to the CY manifold X_n. One could also phrase this in a local picture of the E_8 branes, in which again the flux identification is clear. In Section 4.4 we will discuss this duality of fluxes in much greater detail.

The restriction (4.16) on the heterotic gauge flux has far-reaching consequences for compactifications to four dimensions, which will be analysed in the rest of the chapter. First, in order to satisfy the Bianchi identities (4.5), we necessarily have to include horizontal NS5-branes, wrapping curves in the base B_2. The class of these NS5-branes is easily seen to be $-12K_{B_2}$, as we discuss in Section 4.4.1 below. The F-theory duals of NS5-branes are well-known: while vertical NS5-branes are mapped to D3-branes [3], horizontal branes are mapped to geometry, or more precisely to blow-ups [4–6],

$$\begin{array}{lcl} \text{vertical heterotic NS5/M5-branes} & \overset{\text{dual}}{\longleftrightarrow} & \text{D3-branes} \\ \text{horizontal heterotic NS5/M5-branes} & \overset{\text{dual}}{\longleftrightarrow} & \text{blow-ups in } \mathcal{B}_3 \end{array}\,.$$

In particular, the blow-ups are of the following kind. On the F-theory side, the base of the elliptic fibration is in simple cases a $\mathbb{P}^1$ times the heterotic base B_2. The blow-ups dual to the NS5-branes are then over curves in the base $\mathcal{B}_3$ that sit at either end of the F-theory $\mathbb{P}^1$. Each of these ends is diffeomorphic to the heterotic base B_2, and the contained curves over which blow-ups are performed correspond to the curves wrapped by the NS5-branes. These blow-ups precisely resolve the singularities of the F-theory four-fold Y_4 where the vanishing orders of (f, g, Δ) are (4,6,12) or higher, as discussed in detail in Section 4.3. The Kähler moduli of these blow-ups correspond to the positions of the corresponding M5-branes in the Hořava-Witten interval. In Section 4.3 we will give a detailed description of this aspect of the duality in the

simpler case of compactification to six dimensions. This aspect will then form a key ingredient in the global models we construct in Section 4.4.

We will freely switch between referring to the branes as NS5- or M5-branes in this chapter. The picture of heterotic M-theory, where NS5-branes become M5-branes, gives the right geometric intuition in that two NS5-branes which wrap coincident or intersecting curves in the CY manifold are not truly intersecting branes unless their positions in the interval $S^1/\mathbb{Z}_2$ of the Hořava-Witten M-theory description coincide.

Second, in compactifications to four dimensions, line bundle sums subjected to (4.16) are, unfortunately, necessarily non-chiral, i.e.

$$\text{ind}(V) = \int_{X_3} \text{ch}(V)\text{td}(X_3) = 0\,, \tag{4.19}$$

where $\text{td}(X_3)$ is the Todd class,

$$\text{td}(X_3) = 1 + \tfrac{1}{2}c_1 + \tfrac{1}{12}(c_1^2 + c_2) + \tfrac{1}{24}c_1c_2 + \dots\,, \tag{4.20}$$

in which we have written $c_i(X_3) \equiv c_i$ on the right. This can be seen by expanding $\text{ch}(V)$ and $\text{td}(X_3)$ in terms of a divisor basis D_I. Using $c_1(V) = c_1(X_3) = 0$, $k_a^0 = 0$ due to flatness of the flux along the fiber (4.16), and the intersection ring properties (4.9) (in particular that $d_{ijk} = 0$), we find that (4.19) vanishes identically. This means that pure heterotic line bundle sums that are flat on the fiber are not immediately useful for model building purposes. It is an interesting question whether the duality could be extended to more general line bundle sums, see e.g. Ref. [74] for some progress in this direction. In this work, however, we restrict ourselves to this class of line bundle sums[21].

The duality between the heterotic line bundle flux in the two E_8 gauge groups and the F-theory G_4 flux on the two E_8 branes is rather simple. It is hence rather plausible that checks of this aspect of the duality, for example of the duality of stability conditions and of the spectrum in this sector, will work out. We will perform these checks in Section 4.4.4. These are essentially independent of the duality between NS5-branes and blow-ups. However, we choose to first deal with this latter aspect of the duality, in order to have the full F-theory geometry at hand.

4.3 Blow-ups and branes: review and global 6d models

We would like to build global F-theory models dual to heterotic line bundle models, in compactifications to four dimensions. As discussed in Section 4.2, the duality between horizontal NS5-branes and F-theory geometry is the most non-trivial aspect of this duality. In this section

[21] Much of what we will discuss below will apply not just to such line bundle sums but to any pullback bundle.

we will discuss this in detail, in the simpler case of compactification to six dimensions. This is intended to be a pedagogical discussion, to build intuition for our later construction of global models in four dimensions. We first review what is known in the literature, and flesh out ideas in toy examples. We will be particularly interested in the relevant aspects of toric descriptions. In Section 4.3.3, we build global models for compactification to six dimensions. When we then turn to the description of global models for compactification to four dimensions in Section 4.4, we will freely use the intuition developed here.

4.3.1 Singularities and small instantons in 6d

First we discuss the duality between singularities of the F-theory three-fold and heterotic small instantons. We first briefly recall aspects of the six-dimensional duality. The heterotic compactification space is a K3 surface X_2. We will choose to have no heterotic flux, since the purpose of our discussion of compactification to six dimensions is to develop an understanding of the duality between heterotic NS5-branes and F-theory geometry. (When we discuss the four-dimensional case we will include flux, in the form of line bundles, since four-dimensional line bundle models are our primary interest.) Since we have no heterotic flux, there must be NS5-branes: as the second Chern class of a K3 surface integrates to 24, the anomaly cancellation condition (4.5) implies that there are 24 NS5-branes or, before their movement into the bulk of the Hořava-Witten interval, 24 small instantons. These span the 6 non-compact dimensions and are point-like in the compact space.

The dual F-theory space is a K3 fibration over a $\mathbb{P}^1$ and an elliptic fibration over a two-fold base $\mathcal{B}_2$. Hence $\mathcal{B}_2$ is a fibration of $\mathbb{P}^1$ over $\mathbb{P}^1$, and hence is a Hirzebruch surface $\mathbb{F}_m$. The type m of this Hirzebruch surface is matched on the heterotic side by the distribution $(12-m, 12+m)$ of the 24 instantons on the two E_8 branes. There are E_8 singularities at either end of the F-theory $\mathbb{P}^1$, since on the heterotic side there is no flux. At higher codimension there will be singularities worse than E_8, whose resolution requires blow-ups in the base. In particular as we will see there are 24 such points. This is the same number as of NS5-branes, as expected since in six dimensions all NS5-branes are dual to blow-ups, as we will review.

We first recall the geometry of singularities in F-theory arising where the remaining discriminant locus intersects the E_8 singularities. We assume a trivial fibration $\mathcal{B}_2 = \mathbb{P}^1 \times \mathbb{P}^1$ for the F-theory base. The result after blow-ups will be independent of this choice; this is clear since on the heterotic side, whatever the initial instanton distribution the end result will be the same, with all M5-branes pulled into the bulk. We write the F-theory $\mathbb{P}^1$ as $\mathbb{P}_z$ with coordinates

$\{z_1, z_2\}$, and the heterotic base, which is the other $\mathbb{P}^1$ in $\mathcal{B}_2$, as $\mathbb{P}^1_u$ with coordinates $\{u_1, u_2\}$. The canonical divisor of $\mathcal{B}_2$ is the sum

$$K_{\mathcal{B}_2} = K_{\mathbb{P}^1_z} + K_{\mathbb{P}^1_u}\,, \tag{4.21}$$

where for simplicity we do not write the obvious pullback maps. We recall that in the Weierstrass polynomial in Equation (4.14), we have $f \in \Gamma(K_{\mathcal{B}_2}^{-4})$, $g \in \Gamma(K_{\mathcal{B}_2}^{-6})$, and

$$\Delta = \left(4f^3 + 27g^2\right) \in \Gamma(K_{\mathcal{B}_2}^{-12})\,. \tag{4.22}$$

Since $K_{\mathbb{P}^1} = \mathcal{O}_{\mathbb{P}^1}(-2)$, f and g are respectively of bidegree (8,8) and (12,12) in the coordinates of $\mathbb{P}^1_z$ and $\mathbb{P}^1_u$. Hence they can be written as

$$f = \sum_{i=0}^{8} z_1^i z_2^{8-i} f_i\,, \quad g = \sum_{i=0}^{12} z_1^i z_2^{12-i} g_i\,, \tag{4.23}$$

where $f_i \in \Gamma(K_{\mathbb{P}^1_u}^{-4})$ and $g_i \in \Gamma(K_{\mathbb{P}^1_u}^{-6})$. To enforce the presence of the two E_8s at $z_1 = 0$ and $z_2 = 0$ requires vanishing orders $(f, g, \Delta) \sim (\geq 4, 5, 10)$, so that in the above expansion very few terms can be present. This constrains f, g, and Δ to

$$f = z_1^4 z_2^4 f_4\,, \quad g = z_1^5 z_2^5 \left(z_1^2 g_7 + z_1 z_2 g_6 + z_2^2 g_5\right)\,, \quad \Delta = z_1^{10} z_2^{10} \Delta_r\,, \tag{4.24}$$

$$\Delta_r \equiv 4 z_1^2 z_2^2 f_4^3 + 27 \left(z_1^2 g_7 + z_1 z_2 g_6 + z_2^2 g_5\right)^2\,, \tag{4.25}$$

where we have defined the 'remaining discriminant' Δ_r. We also note that f_4 and g_6 are identified in the duality with the f and g polynomials in the Weierstrass equation for the heterotic K3 surface [4],

$$\text{Heterotic K3:} \quad y^2 = x^3 + f_4 x w^4 + g_6 w^6\,, \tag{4.26}$$

where for simplicity we have used the same coordinate names for the $\mathbb{P}_{123}$ ambient space of the heterotic elliptic curve as we did on the F-theory side.

The degeneration of the fiber worsens at the intersection of the E_8 brane stacks with the rest of the D7-brane locus $\{\Delta_r = 0\}$. Setting $z_1 = 0$ or $z_2 = 0$ in Δ_r, and fixing the other coordinate to 1, we have respectively

$$\Delta_r|_{z_1=0} = 27 g_5^2\,, \quad \Delta_r|_{z_2=0} = 27 g_7^2\,. \tag{4.27}$$

Each of these intersections consists of 12 double points, for generic g_7 and g_5. At these points, the vanishing orders of (f, g, Δ) are $(4, 6, 12)$, so the fiber degenerations are so severe that resolutions not changing the base lead to a non-flat fibration.

As we now explain, the singularity at these points is characterised in affine coordinates by an equation of form

$$0 = y^2 + x^3 + z^6 + u^6\,, \tag{4.28}$$

and we will refer to this singularity as an $\tilde{\mathrm{E}}_8$. As a weighted homogeneous singularity, its type depends only on the weights of the coordinates: using the scalings $y \sim \lambda^{1/2}, x \sim \lambda^{1/3}, \ldots$, additional terms that scale as λ are 'marginal deformations'. The Weierstrass equation for the above models is of this form in the vicinity of an $\tilde{\mathrm{E}}_8$ singularity: if a zero of g_5 is at $u_1 = 0$, then close to the singularity and in affine coordinates we have up to numerical factors

$$0 = y^2 + x^3 + (z_1^4 + \ldots)x + (z_1^5 u_1 + \ldots)\,, \tag{4.29}$$

which expresses the $\tilde{\mathrm{E}}_8$ singularity, sitting in a locus of E_8 singularities. Crucially this singularity admits a crepant resolution, in which an extra coordinate ε is introduced, with a new scaling relation

$$\begin{array}{ccccc} y & x & z_1 & u_1 & \varepsilon \\ \hline 3 & 2 & 1 & 1 & -1 \end{array}\,, \tag{4.30}$$

and the singular point is excised. The proper transform corresponds to dividing out 6 powers of ε from the equation defining the hypersurface, so that this is a crepant resolution. Conversely, f and g have to be divisible by ε^4 and ε^6 respectively for such a blow-up to be crepant, reflecting the requirement of vanishing orders (4,6,12). These are the resolutions which are dual to the introduction of NS5-branes and the Kähler moduli associated to the blow-ups correspond to positions of the M5-branes in the Hořava-Witten interval. We will discuss this in some depth in Section 4.3.2. However first we must review the explicit duality between the $\tilde{\mathrm{E}}_8$ singularities and small instantons.

The presence of (4,6,12) singularities is dual to the presence of heterotic small instantons. Beyond the match of their numbers, the explicit duality between singularities and small instantons has been discussed in Ref. [42], and we briefly review this discussion. Before stable degeneration, the F-theory base is a Hirzebruch surface. In the stable degeneration limit, the F-theory $\mathbb{P}^1$ splits into two $\mathbb{P}^1 s$ which meet at a point. Figure 5, which is a rendition of Figure 3 in Ref. [42], shows a schematic depiction of the base of the F-theory fibration after stable degeneration. This base consists of two Hirzebruch surfaces that meet along a curve C_* that we identify with the $\mathbb{P}^1$ base of the heterotic K3, and the elliptic fibration over C_* is identified with the heterotic K3. We can note that the II^* fibers are away from this intersection.

The remaining I_1 locus intersects the II^* fibers at a set of points. Each point sits in a particular copy of a component of the F-theory $\mathbb{P}^1_z$ fiber over a point in the heterotic $\mathbb{P}^1_u$. This

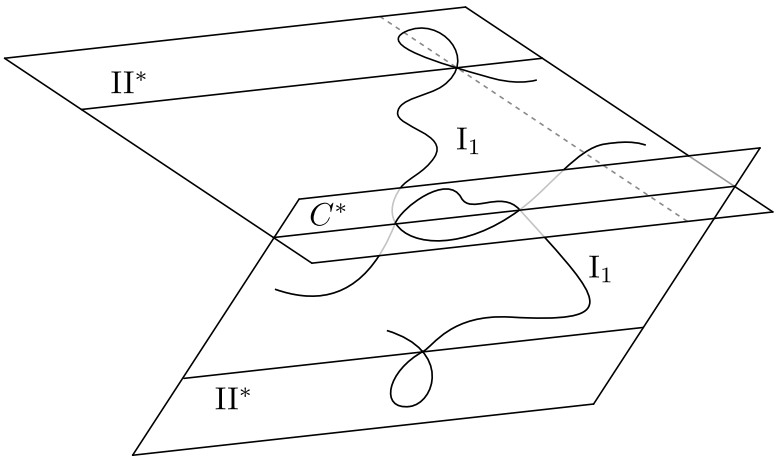

Figure 5: *Schematic depiction of the F-theory base after stable degeneration of a Hirzebruch base. Note this is a rendition of Figure 3 in Ref. [42]. In this picture there are no five-branes in the heterotic dual, only small instantons. Note C_* is identified with the heterotic base.*

F-theory $\mathbb{P}^1_z$, represented by the dotted line in Figure 5, intersects C_* at one point. Since C_* is identified with the heterotic base, it is natural to identify this point with the position of the corresponding heterotic small instanton in the heterotic base. Additionally, the small instanton has a position in the heterotic fiber, which corresponds in the duality to Ramond-Ramond moduli (in the IIB picture) on the F-theory side. This aspect will mainly not concern us, since in four dimensions the horizontal NS5-branes/small instantons usually cannot move in the heterotic fiber, however it will be important in the discussion of Section 4.4.5.

This moduli match for small instantons also holds for NS5-branes. The transition from a small instanton to an NS5-brane corresponds to a position in the 11d bulk: a position at either endpoint of the interval gives a small instanton and positions in between give an NS5-brane[22]. Moving an instanton into the bulk corresponds on the F-theory side to resolving the singularities discussed above, where Kähler moduli are dual to the positions in the bulk. Throughout this transition, the position of the instanton/NS5-brane in the heterotic space and the position of the singularity/blown-up locus in the F-theory space remain unchanged, so the matching between positions of the heterotic small instantons and the positions of $(4, 6, 12)$ singularities in F-theory carries over to a match of NS5-branes and the loci of blow-ups. In the K3 fibration of the resolved three-fold $\hat{Y}_3$ on the F-theory side, these become the loci of reducible K3 fibers. In perfect agreement with the spirit of fiberwise duality, the monodromy in the K3 fibration corresponds to a shift in the B-field on the heterotic side, as appropriate for an NS5-brane. A general discussion of reducible K3 fibers, their monodromies, and the relation to NS5-branes

[22]We will mostly not discuss the physics of the transition from a small instanton to an NS5-brane, which has been discussed elsewhere [4, 69, 75–81].

can be found in Ref. [82].

4.3.2 Toric descriptions of required resolutions

In Section 4.3.1 we discussed the duality between (4,6,12) singularities in F-theory and small instantons in heterotic string theory. We now discuss the blow-ups of these singularities. We would like to later give a toric description for the resulting global F-theory models dual to heterotic line bundle models, as many computations are thus simplified. Hence we develop toric descriptions of the required blow-ups dual to NS5-branes. See e.g. Refs. [83, 84] for an introduction to toric geometry, Refs. [85, 86] for an introduction to its applications in F-theory, and Ref. [87] for a recent base-independent discussion of toric transitions.

We can understand the F-theory geometry dual to the presence of an NS5-brane in multiple ways. One way is to note that different heterotic instanton distributions correspond to different Hirzebruch surface bases in F-theory, so that the presence of an NS5-brane is an intermediate situation between different distributions. From this perspective, it is clear that the intermediate geometry should allow blow-downs to both geometries dual to the two instanton distributions. More precisely, these blow-downs will require flops; we discuss this below. There should also be an elliptic fibration over some intermediate base, and this base should admit blow-downs to the two Hirzebruch surfaces. An obvious candidate for an intermediate space, which we call $\mathbb{F}_{n,n+1}$, is shown in Figure 6 along with the two Hirzebruch spaces.

Another way to understand this is through the duality between singularities and small instantons. A small instanton is dual to an $\tilde{\mathrm{E}}_8$ singularity, which has a crepant resolution, and this resolution is dual to the transition to an NS5-brane. Letting the small instanton first sit at $u_1 = 0$, from Equation (4.30) the resolution clearly demands the introduction of the following ray $\vec{\varepsilon}$ in the polytope of the ambient toric four-fold,

$$\vec{\varepsilon} = 2\vec{x} + 3\vec{y} + \vec{z_1} + \vec{u_1}\,, \tag{4.31}$$

where the coordinate ε describes the exceptional divisor of the blow-up. This resolution corresponds to moving to the intermediate space in Figure 6, after starting from the $\mathbb{F}_n$ base. This is the toric implementation of the weighted blow-up

$$y = \hat{y}\varepsilon^3\,, \quad x = \hat{x}\varepsilon^2\,, \quad z_1 = \hat{z}_1\varepsilon\,, \quad u_1 = \hat{u}_1\varepsilon\,, \tag{4.32}$$

where hats temporarily indicate coordinates after the blow-up. The proper transform of the Weierstrass equation consists of dividing by ε^6 to give a new Weierstrass equation

$$\hat{y}^2 = \hat{x}^3 + \hat{f}\hat{x}w^4 + \hat{g}w^6\,, \tag{4.33}$$

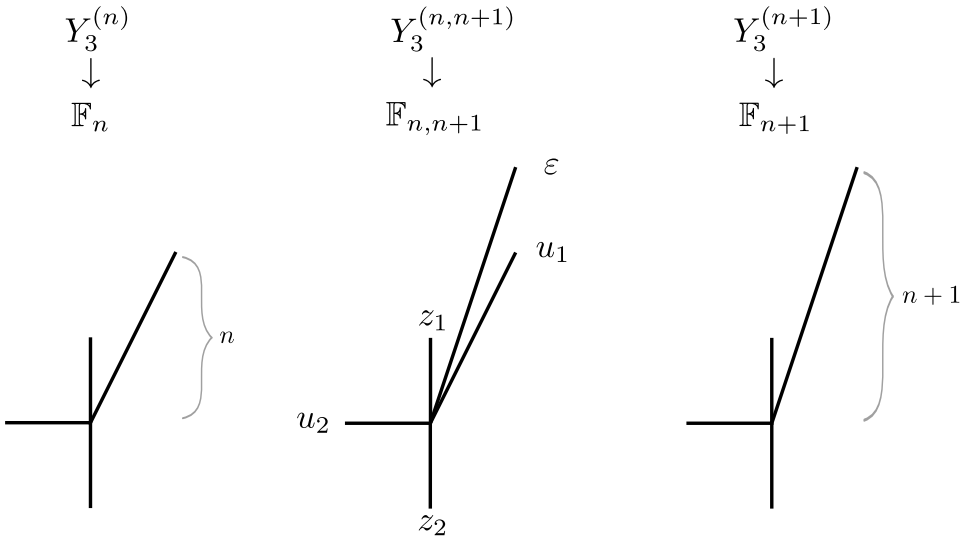

Figure 6: *Toric fans for the Hirzebruch surfaces $\mathbb{F}_n$ and $\mathbb{F}_{n+1}$, as well as the fan for the intermediate space, which we call $\mathbb{F}_{n,n+1}$, in which we have blown up $\mathbb{F}_n$ but have not yet blown down to $\mathbb{F}_{n+1}$. We have also indicated that we wish to consider elliptic fibrations $Y_3^{(\cdot)}$ over these bases.*

where we have defined $\hat{f} = \varepsilon^{-4} f$ and $\hat{g} = \varepsilon^{-6} g$. This also corresponds to having $\hat{f}$, $\hat{g}$ be sections of $K^{-4}_{\mathbb{F}_{n,n+1}}$ and $K^{-6}_{\mathbb{F}_{n,n+1}}$ respectively, as we know must be the case. It is easy to see that the resulting space is CY. As in the previous perspective, we have maintained a toric description by placing the instanton/brane at the vanishing locus of homogeneous coordinates. More general instanton/brane configurations will be considered in detail below.

The weight system of the resulting ambient toric four-fold can be written as

y	x	w	z_1	z_2	u_1	u_2	ε
3	2	1	0	0	0	0	0
6	4	0	1	1	0	0	0
$3n+6$	$2n+4$	0	0	n	1	1	0
3	2	0	1	0	1	0	-1

. (4.34)

Here we have written the final line in a form allowing us to read off the structure of the blow-up of the three-fold with $\mathbb{F}_n$ base. These weights reflect the resolution of a $\tilde{\text{E}}_8$ singularity as described in Equation (4.30). Equivalently, we can rewrite the weight system as

y	x	w	z_1	z_2	u_1	u_2	ε
3	2	1	0	0	0	0	0
3	2	0	0	1	-1	0	1
$3(n+1)+6$	$2(n+1)+4$	0	0	n+1	0	1	1
6	4	0	1	1	0	0	0

. (4.35)

The third row of this form reflects that one can reach this situation also by blowing up the

three-fold with $\mathbb{F}_{n+1}$ base. This corresponds to the fact we can pull an M5-brane off either E_8 brane in the 11d interval, or inversely, absorb the brane back into either E_8 brane. The weight system above describes the 4d polytope of the intermediate situation, but not the 4d fan: a triangulation is also required. We might start with either Hirzebruch base case, which each have given fans, and include the necessary blow-up ray, giving a new specific fan. However as we now discuss, these blow-ups destroy the elliptic fibration structure, and flops are required to retrieve it.

In the two Hirzebruch base space cases and the intermediate case, there exists a polytope of the ambient four-fold which may admit many triangulations. In each case, for an F-theory interpretation we are interested in those triangulations that describe an elliptic fibration for the CY hypersurface. In fact this condition uniquely determines the fan, as follows. Writing down a Weierstrass model anticipates that the fibration descends from the toric ambient space in a particular way, namely from a fibration of $\mathbb{P}_{123}$ over the base. This projection is a particular instance of a toric morphism. Toric morphisms are induced from maps, in our case a projection, of the fan. In order to be a toric morphism it must not happen that cones are mapped one-to-many, but each cone must be mapped onto a unique cone (of course many cones can be mapped to the same cone). Fans of this type can be built from the 'product' of cones in the base and cones in the fiber, so for example in the case of a fibration of $\mathbb{P}_{123}$ over the base $\mathbb{F}_n$ shown in the left of Figure 6, the top-dimensional cones are given by all pairings

$$\{(u_2, z_1), (z_1, u_1), (u_1, z_2), (z_2, u_2)\} \times \{(x, y), (y, w), (w, x)\}\,, \tag{4.36}$$

where $\times$ is the Cartesian product and each pairing, e.g. (u_2, z_1, x, y), is the cone spanned by the given four rays.

Including blow-up rays simply refines the cone in which such a ray sits, and for this reason destroys the fibration structure. Blowing up by inserting the ray $\vec{\varepsilon} = 2\vec{x} + 3\vec{y} + \vec{u}_1 + \vec{z}_1$, the resulting cones are as before except one of the old cones is replaced by four,

$$(x, y, u_1, z_1) \to \{(\varepsilon, y, u_1, z_1), (x, \varepsilon, u_1, z_1), (x, y, \varepsilon, z_1), (x, y, u_1, \varepsilon)\}\,. \tag{4.37}$$

The fibration of the original three-fold over the base is inherited from one on the ambient space, specifically the map that collapses the directions of the $\mathbb{P}_{123}$, and after introducing the blow-up ray, this map is no longer a toric morphism. We can see this by the fact that under the projection map, the map of cones includes for example

$$(\varepsilon, y, u_1, z_1) \to (u_1, \varepsilon) \cup (\varepsilon, z_1)\,, \tag{4.38}$$

so that this cone is split in half by the projection and the map between cones is one-to-many. This means that there is no toric morphism, and hence no projection of the ambient space for the three-fold to inherit, so that the fibration has been destroyed.

However, we would like to preserve the fibration structure of the three-fold in order to have an F-theory interpretation. The blown-up space has a flop[23] from this 'naively' blown-up fan to that with the product cone structure. We will henceforth assume the required flops have been performed, giving an elliptic fibration in situations with NS5-branes. Practically speaking, this means we should imagine blowing up the base, and then adding the elliptic fibration, and we will often speak in this way.

4.3.3 Toric global models in 6d

We have discussed the explicit duality between heterotic NS5-branes and F-theory blow-ups in compactification to six dimensions, and we can use this knowledge to build global F-theory models dual to six-dimensional heterotic models with only NS5-branes. This will be useful to study their generalisation to duals of four-dimensional line bundle sum models.

We have discussed the toric description of a blow-up dual to a single NS5-brane, however anomaly cancellation requires 24 heterotic NS5-branes, dual to the blow-ups of all 24 $\tilde{\mathrm{E}}_8$ singularities in the F-theory three-fold. We would like to give a toric description of the geometry in F-theory after all of these blow-ups. We first note that before the transition of instantons into NS5-branes, the precise Hirzebruch surface occurring as the F-theory base reflects the initial distribution of heterotic instantons. One can take as a starting point a $\mathbb{P}^1 \times \mathbb{P}^1$ base, since all instantons will be pulled into M5-branes in the bulk, washing out dependence on initial distribution. Then 12 blow-ups will be associated to each E_8 stack. From the discussion in Section 4.3.2, the base spaces shown in Figure 7 are obvious proposals for the resulting geometry. The different distributions of blow-up rays correspond to different configurations of small instantons/NS5-branes: blow-up rays associated to u_1 (u_2) are dual to NS5-branes at $u_1 = 0$ ($u_2 = 0$). These bases are those with simple toric descriptions, and this corresponds to these restricted positions for NS5-branes in the heterotic space. More general brane configurations require more involved descriptions, but as these are only general configurations of points they are not very interesting. We will discuss arbitrary brane configurations in the more interesting four-dimensional context in Section 4.4.3.

We take the left possibility in Figure 7 as a concrete example in the following. This base

[23] Before the flops, there does not appear to be an obvious F-theory interpretation and it appears F-theory does not see the intermediate process [4].

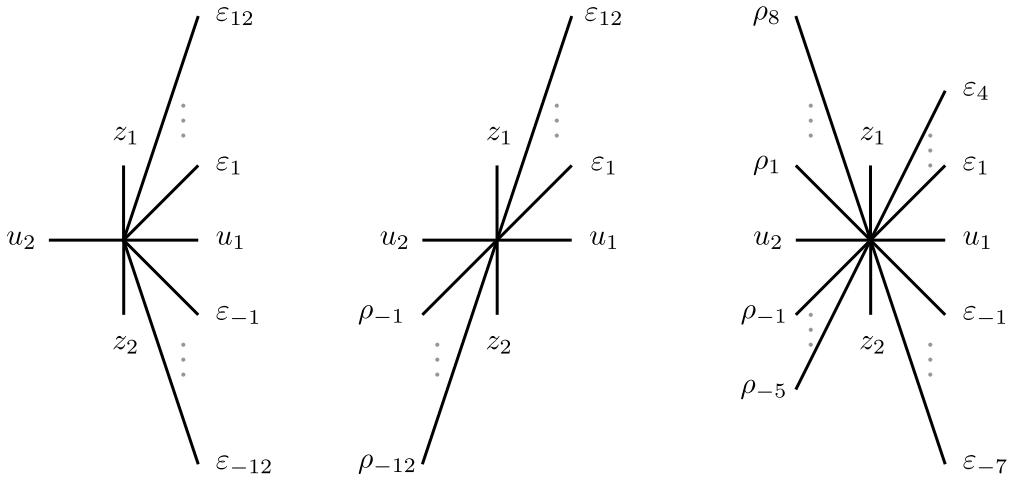

Figure 7: *Possible toric bases of the F-theory three-fold after blowing up all intersections of the* E_8 *stacks with the remaining brane locus.*

space is a $\mathbb{P}^1 \times \mathbb{P}^1$ with two series of blow-ups. In order for these blow-up rays to reduce all singularities to mere E_8s, the intersection of the remaining brane locus with the E_8 stacks must be tuned to sit at the vanishing of toric coordinates. After this tuning, in each series of blow-ups at each stage a $\mathbb{P}^1$ is blown-up on a point of the previous exceptional $\mathbb{P}^1$. In Appendix D.1 we verify explicitly that this toric prescription indeed appropriately reduces the severity of the singularities, leaving only two curves of E_8 singularities which do not worsen further over points in the base. These can then be resolved using standard techniques preserving the flatness of the elliptic fibration. In particular, these crepant resolutions are achieved torically by including new rays at

$$\begin{aligned} &(0,\pm i,2,3) \text{ for } i=1,2,3,4,5,6\,, \qquad (0,\pm i,1,2) \text{ for } i=1,2,3,4\,, \qquad (0,\pm i,1,1) \text{ for } i=1,2,3\,,\\ &(0,\pm i,0,1) \text{ for } i=1,2\,, \qquad\qquad (0,\pm i,0,0) \text{ for } i=1 \end{aligned} \tag{4.39}$$

where $+$ and $-$ are for the E_8 branes at $z_1=0$ and $z_2=0$ respectively, and the first two values are coordinates in the ray diagrams in Figure 7, while the final two coordinates are in the $\mathbb{P}_{123}$ in which $x=(-1,0)$, $y=(0,-1)$, $w=(2,3)$. Note that working with a description of X in terms of reflexive polytopes, the requirement of convexity of the N-lattice polytope Δ^* already forces the introduction of the rays (4.39).

In order to perform the blow-ups in the base using toric methods, we had to tune the intersections of the remaining brane locus with each E_8 stack to be at the zeroes of toric coordinates. Deformations of these intersection positions, or correspondingly of the positions of the NS5-branes in the heterotic base, cannot be seen directly in this toric description. We hence expect these to appear as non-polynomial deformations, as we now verify. We recall Batyrev's for-

mula [88] for complex structure moduli: for a CY hypersurface X defined by an m-dimensional reflexive M-lattice polytope Δ, we have

$$h^{m-2,1}(X) = l(\Delta) - m - 1 - \sum_{\text{codim } \Theta=1} l^*(\Theta) + \sum_{\text{codim } \Theta=2} l^*(\Theta) l^*(\Theta^*)\,, \tag{4.40}$$

where Θ is a face of Δ, and Θ^* the dual face in the dual reflexive polyhedron, and where $l(\cdot)$ denotes the number of integral points while $l^*(\cdot)$ denotes the number of integral points in the interior. The various terms can be identified with the number of polynomial deformations minus the number of automorphisms of the ambient space together with the number of non-polynomial deformations, which correspond to the last term. Such non-polynomial deformation are complex structure deformations of the CY hypersurface which are frozen in the embedding into a toric variety under consideration. In the example under discussion, one can easily verify that the number of complex non-polynomial deformations is 23. These clearly correspond to the moduli used up in stacking 24 NS5-branes in the heterotic base. The middle and right diagrams of Figure 7 both have 22 complex non-polynomial deformations, as expected since on the heterotic side there are now two stacks of NS5-branes.

Finally, before turning to the construction of global four-dimensional models, we perform a multiplet match in the simple above example of the six-dimensional duality, as the four-dimensional multiplet matches will be more involved but somewhat similar. We recall that in compactification to six dimensions we have chosen to have no flux on the heterotic side, so there is no corresponding flux on the E_8 brane stacks. In the following we write $\hat{Y}_3$ for the F-theory three-fold and $\hat{\mathcal{B}}_2$ for the base, where both are the result upon performing all required resolutions, including of the E_8 singularities.

On the F-theory side, we have the following expressions for the number of tensor multiplets $n_{\text{ten.}}$ and the number of hypermultiplets[24] $n_{\text{hyp.}}$ [4]

$$n_{\text{ten.}} = h^{1,1}(\hat{\mathcal{B}}_2) - 1\,, \quad n_{\text{hyp.}} = h^{2,1}(\hat{Y}_3) + 1\,, \tag{4.41}$$

For our specific three-fold in F-theory, we find that $h^{2,1}(\hat{Y}_3) = 43$, $h^{1,1}(\hat{Y}_3) = 43$, and $h^{1,1}(\hat{\mathcal{B}}_2) = 26$, so that $n_{\text{ten.}} = 25$ and $n_{\text{hyp.}} = 44$. We recall that a hypermultiplet contains four real scalars, so that altogether we have 201 real scalars.

On the heterotic side, we have first 24 real parameters for the positions of the NS5-branes in the interval of the 11d Hořava-Witten picture, and these 24 real scalars sit in tensor multiplets.

[24] We also have $\text{rk}(V) = h^{1,1}(\hat{Y}_3) - h^{1,1}(\hat{\mathcal{B}}_2) - 1$ for the rank $\text{rk}(V)$ of the gauge group. From this we can conclude that $\text{rk}(V) = 16$, but since we have an unbroken $\mathrm{E}_8 \times \mathrm{E}_8$ we already know the number of vectors is $n_{\text{vec.}} = 496$.

Together with the tensor multiplet containing the dilaton, we have $n_{\text{ten.}} = 25$ as on the F-theory side. We also have $24 \cdot 4 = 96$ real scalars from the positions in the K3 of the 24 five-branes. Additionally K3 has $b_2 = 22$, giving rise to 22 real scalars. Finally the moduli space of Ricci-flat metrics on K3 has 58 real moduli, and so together we get $96 + 22 + 58 = 176$ real scalars. Since these all sit in hypermultiplets this gives $n_{\text{hyp.}} = 44$ as on the F-theory side. It is clear the anomaly condition $29n_{\text{ten.}} + n_{\text{hyp.}} - n_{\text{vec.}} = 273$ is satisfied.

4.4 Global 4d models

We now turn to a description of global F-theory models dual to heterotic line bundle models in compactifications to four dimensions. After briefly determining the required branes and blow-ups, we will build our first global models in analogy with the toric six-dimensional constructions of Section 4.3.3. We then give a construction that allows for more general NS5-brane configurations. Afterwards, we verify various aspects of the proposed duality between these models and heterotic line bundle models. Note we will freely use the ideas reviewed and developed above in the six-dimensional case, as many ideas required in the four-dimensional case are analogous.

We briefly remind ourselves of some notation in the four-dimensional case. On the heterotic side we have a CY three-fold X_3 which is an elliptic fibration $\pi_H : X_3 \to B_2$. Since the heterotic space is now a three-fold, there are multiple choices for the two-fold base B_2, rather than just $\mathbb{P}^1$ as was the case in compactification to six dimensions. We will mainly treat toric bases, for which there are already many possibilities. On the F-theory side, there is a CY four-fold Y_4 which is a K3 fibration $p_F : Y_4 \to B_2$ and an elliptic fibration $\pi_F : Y_4 \to \mathcal{B}_3$. We write $\hat{Y}_4$ and $\hat{\mathcal{B}}_3$ for the spaces after any required blow-ups have been performed.

4.4.1 Required branes and blow-ups

We first determine the required number of heterotic NS5-branes and F-theory blow-ups, for heterotic line bundle sums. We recall that in compactification to four dimensions, NS5-branes in X_3 can wrap the fiber or curves in the base; these are 'vertical' and 'horizontal' branes respectively. The number and type of NS5-branes required for line bundle sum models with F-theory duals follows from anomaly cancellation. From the triple intersection numbers of X_3 and the fact that $k_a^0 = 0$ for each line bundle L_a in one of the line bundle sums $V_{1,2}$ (as reviewed in Section 4.2), we have that

$$\text{ch}_2(V_{1,2}) = \sum_{a=1}^{\mathfrak{r}} \frac{1}{2} d_{IJK} k_a^I k_a^J C^K = \left(\sum_{a=1}^{\mathfrak{r}} \frac{1}{2} k_a^i k_a^j \mathfrak{g}_{ij} \right) F \,, \tag{4.42}$$

where F is the heterotic fiber. Then recalling the expression for $\mathrm{ch}_2(X_3)$ in Equation (4.10), we see from the anomaly cancellation condition in Equation (4.5) that we require NS5-branes wrapping curves in the base B_2 with total class $[W] = 12\sigma(-K_{B_2})$. This is the required horizontal NS5-brane content. We also have a choice in how to cancel the part of $\mathrm{ch}_2(X_3)$ proportional to F: we can use vertical NS5-branes or the line bundle sums. We will choose to have no vertical NS5-branes, so line bundle sums make up the remainder of the anomaly condition. Summarising,

$$[W]_{\text{hor.}} = 12\sigma(-K_{B_2})\,, \quad [W]_{\text{ver.}} = 0\,. \tag{4.43}$$

Note that as vertical NS5-branes are dual to D3-branes, there are no D3-branes on the F-theory side.

The F-theory dual of a horizontal NS5-brane is a blow-up in the F-theory base $\mathcal{B}_3$, and these blow-ups are the obvious generalisations of the six-dimensional case discussed in Sections 4.3.1 and 4.3.2. The F-theory E_8 symmetries are broken purely by flux, not geometry. The loci of E_8 singularities, which are now two-folds, intersect the remaining brane locus to give curves of $\tilde{\mathrm{E}}_8$ singularities, which are (4,6,12) curves, whose resolution is dual to the introduction of NS5-branes. For simplicity we can take the initial instanton distribution to be symmetric, so that $\mathcal{B}_3 = B_2 \times \mathbb{P}^1$. Then the two intersection curves have classes

$$[z_1]\cdot[\Delta_r] = [g_5] = -6K_{B_2}|_{z_1=0}\,, \quad [z_2]\cdot[\Delta_r] = [g_7] = -6K_{B_2}|_{z_2=0}\,, \tag{4.44}$$

together determining a point locus in the class $-12K_{B_2}$ that is dual to the NS5-brane locus. The precise correspondence between positions of blow-ups and branes is the generalisation of the six-dimensional case in Figure 5.

The characterisation of horizontal branes as sitting in the base is slightly too crude, so let us take a moment to be more precise. A curve $\mathcal{C}$ in the heterotic base B_2 can always be embedded holomorphically into the heterotic three-fold X_3 by the zero section, $C = \sigma(\mathcal{C})$. However in addition, over a given curve $\mathcal{C}$ in B_2 there is an elliptic surface $S_{\mathcal{C}}$ in X_3 which may have more than one section. In particular, if the elliptic surface $S_{\mathcal{C}}$ is a dP_9 there will be (countably) infinitely many sections, and if the elliptic fibration on $S_{\mathcal{C}}$ is trivial there is a continuous family of sections. A nice discussion on such situations is found in Ref. [89]. For simplicity, we will tend to consider all horizontal branes to be embedded by the zero section, unless explicitly stated otherwise. As in the case of compactification to six dimensions, the positions of NS5-branes in the fiber are expected to be dual to Ramond-Ramond moduli (in the IIB picture) on the F-theory side, hence equivalently we assume particular expectation values for these fields. We will

return to a discussion of these extra parameters in Section 4.4.5, where we will be particularly interested in the case of trivially fibered elliptic surfaces.

4.4.2 Toric global models

In Section 4.3.3 above we have built global F-theory models dual to six-dimensional heterotic line bundle sum models, which had particularly simple toric descriptions. Examples of the F-theory base space were shown in Figure 7. It is easy to build global four-dimensional models in direct analogy with those simple constructions, so we will discuss these models first before moving on to more general constructions.

Let us assume the F-theory base space is initially a trivial fibration $\mathcal{B}_3 = \mathbb{P}^1 \times B_2$. The locus of $\tilde{\mathrm{E}}_8$ singularities, whose resolution is dual to the introduction of the required NS5-branes, consists of curves. As in the case of compactification to six dimensions, these loci on the two E_8 surfaces are determined by the vanishing of g_7 and g_5. In order to perform toric blow-ups over these curve loci, we must tune these polynomials to give zeroes only over toric curves, which are those at the vanishing of the toric coordinates. For any such tuning, the natural expectation for how to then build the resolved base space is as follows. We introduce toric blow-up rays into the base ray diagram, in towers above/below the rays of B_2, such that the projection of these onto the B_2 part of the ray diagram gives a set of rays which, when counted with multiplicities, have divisor class $-12K_{B_2}$. That is, the blow-up rays are at

$$\vec{\varepsilon}_{(a),i} = (\vec{u}_a, i) \quad \text{for} \quad i = -m_a, -m_a + 1, \ldots, m_a \,, \tag{4.45}$$

$$\text{with} \quad \sum_a m_a = \sum_a n_a = 6 \cdot c_2(B_2) \,,$$

where $\vec{u}_a$ are the rays of B_2, the third coordinate is along the $\vec{z}_1$ direction, and $c_2(B_2)$ is simply the number of rays in B_2. We show in Figure 8 an example ray diagram for the F-theory base, where the heterotic base is a $\mathbb{P}^1 \times \mathbb{P}^1$ and we have chosen a particular distribution of the blow-up rays. We also show in Figure 9 some possible distributions of blow-ups for the heterotic base choice $B_2 = \mathbb{P}^2$, as this base choice allows reasonably clear diagrams for multiple blow-up distributions.[25]

[25] Note that, unlike in six dimensions, the ray diagram of the base $\hat{\mathcal{B}}_3$ is not enough to specify its fan. While the extra rays are understood to be blow-ups of the original base, this still leaves freedom for the triangulation. For the purposes of this section, the particular triangulation is not important, and we leave a discussion of triangulations to Section 4.5.3.

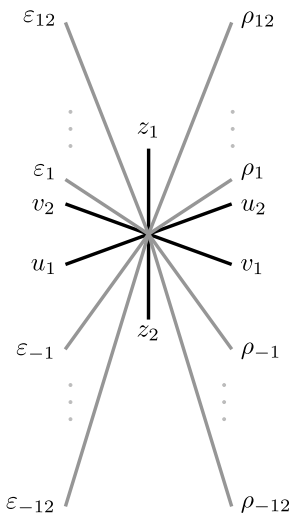

Figure 8: *Ray diagram for the result of blowing up the F-theory base* $\left(\mathbb{P}^1\right)^3$ *to remove intersections of the remaining brane locus with the two* E_8 *stacks. Blow-up rays are a different colour only for clarity. The* ε_i *and* ρ_i *rays are blow-up rays, in the* $u-z$ *and* $v-z$ *planes respectively.*

The distribution of blow-up rays reflects the tuning of g_7 and g_5. In the example of Figure 8, the choice of tuning is

$$g_7 = \alpha u_1^{12} v_1^{12}\,, \quad g_5 = \beta u_1^{12} v_1^{12}\,, \tag{4.46}$$

with α and β arbitrary complex numbers. With this choice, the remaining discriminant locus initially intersects each E_8 stack at $\{u_1 = 0\} \cup \{v_1 = 0\}$. This gives four curves along which blow-ups are required. These blow-ups are performed by the introduction of the rays in Figure 8. In Appendix D.2, we explicitly work through the required tuning and blow-up procedure for the example in Figure 8, showing that this ray diagram is indeed the result of resolving the singularities. We also verify that the loci $\{z_1 = 0\}$, $\{z_2 = 0\}$ in the base, are each diffeomorphic to B_2, so that the GUT surfaces have the same topology as the heterotic base. Similarly we check that the remaining brane locus does not intersect the E_8 stacks, so that the singularities worse than E_8 have all been removed. We also show that the E_8 singularities themselves are now geometrically non-Higgsable.

To retain a simple toric description, g_7 and g_5 are tuned to give zeroes at the vanishing of toric coordinates. This choice of tuning is dual to the choice of NS5-brane configuration on the heterotic side. As in six dimensions, the number of non-polynomial deformations of the toric hypersurface reflects the choice of NS5-brane configuration, analogously to the discussion in Section 4.3.3. For example, in the case of Figure 8, the heterotic dual of this specific F-theory base has two stacks of 24 horizontal NS5-branes, one at $u_1 = 0$ and one at $v_1 = 0$; each brane wraps a $\mathbb{P}^1$. We find from Batyrev's formula that the number of non-polynomial deformations

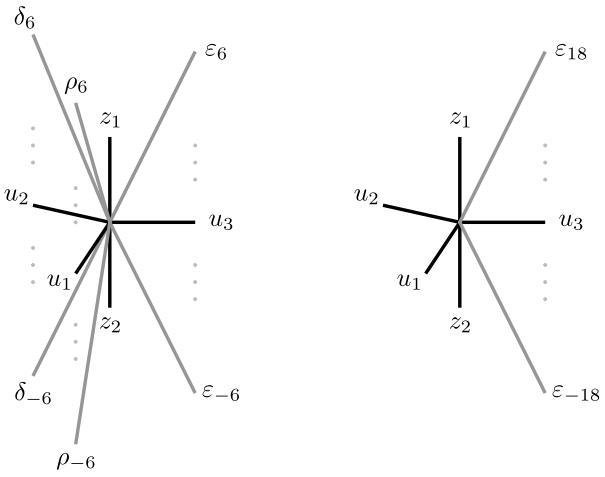

Figure 9: *Examples of blow-up distributions in the case of a heterotic base space* $\mathbb{P}^2$*. Blow-up rays are all above/below one of the rays in the base* (u_1, u_2, u_3)*. In the left diagram the blow-ups are distributed democratically, while on the right they are all associated to one base ray.*

is 46, as expected as this is the number of moduli used up in forcing two stacks of 24 $\mathbb{P}^1$ NS5-branes in $\mathbb{P}^1 \times \mathbb{P}^1$. For different distributions of the blow-ups, the count of non-polynomial deformations will be different, reflecting the number of parameters involved in specifying such a brane configuration.

4.4.3 More general global models

The four-dimensional F-theory models constructed in Section 4.4.2 had particularly simple toric descriptions, but also were rather restrictive. In particular the dual horizontal NS5-branes were forced to wrap $\mathbb{P}^1$s in stacks at loci defined by the vanishing of toric coordinates. Clearly these are not the most general brane configurations; in general on each E_8 brane stack there is an arbitrary curve locus of (4,6,12) singularities with class $-6K_{B_2}$, and these singularities are removed by blowing up over this locus. While the blow-ups in the toric hypersurface models were over toric curves, giving up the hypersurface description allows arbitrary blow-ups. Often the complete intersection CY manifold can be described by a nef partition [90], which allows for straightforward calculation of the Hodge numbers. (However at high codimension, this can become computationally prohibitive.)

A blow-up over a non-toric locus can be achieved torically by increasing the dimension of the toric ambient space by one. First a new coordinate ξ is introduced with the addition of a ray perpendicular to the old fan. An extra equation then expresses that the zero locus of ξ is to be determined by a function F of the other coordinates. Along with any toric constraints, this gives the locus we wish to blow up. Writing c_a for these other coordinates, we have for the

extra ray and the extra equation,

$$\vec{\xi} = (\vec{0}, 1)\,, \quad \text{with} \quad \xi = F(c_a)\,. \tag{4.47}$$

For the extra equation to be well-defined under all scalings, the positions of the rays $\vec{c}_a$ in the new direction must be such that ξ and $F(c_a)$ have the same weights. The blow-up is then performed by adding a ray

$$\vec{\zeta} = \vec{\xi} + \dots\,, \tag{4.48}$$

where the dots represent other rays that correspond to the toric constraints on the blow-up.

We take as an example the case where the heterotic base is $B_2 = \mathbb{P}^2$. We begin with the situation where the blow-ups have all been performed in the simple toric manner in the diagram on the right of Figure 9, except we remove the top n rays in the tower over u_3. The highest ray appearing is then ε_{18-n}. This leaves a singularity on the $z_1 = 0$ surface, which we tune into a more general curve defined by a polynomial of degree n in the $\mathbb{P}^2$ scaling. We will then blow up on this locus by going to a toric complete intersection. This polynomial is represented in the ambient space by a function of coordinates on the pullbacks of curves in B_2 under the $\mathbb{P}^1$ projection. That is, we can use the products of the rays associated to each base ray,

$$u_1\,, \quad u_2\,, \quad U_3 := u_3 \prod_{a=-18}^{18-n} \varepsilon_a\,. \tag{4.49}$$

These 'coordinates' have the same behaviour under all scalings, i.e. they correspond to the same divisor class. We define $\mathcal{F}_n$ to be a degree n polynomial in u_1, u_2, U_3; this is a well-defined function up to an overall scaling. This equation defines a curve on the GUT surface upon intersection with $\{z_1 = 0\}$.

We then perform the blow-up over the curve. In addition to the rays in the original fan,

$$\begin{aligned}
&\vec{u}_1 = (-1,0,0,2,3)\,, && \vec{u}_2 = (0,-1,0,2,3)\,, && \vec{u}_3 = (1,1,0,2,3)\,,\\
&\vec{z}_1 = (0,0,1,2,3)\,, && \vec{z}_2 = (0,0,-1,2,3)\,, && \vec{\varepsilon}_i = (1,1,i,2,3)\,,\\
&\vec{x} = (0,0,0,-1,0)\,, && \vec{y} = (0,0,0,0,-1)\,, && \vec{w} = (0,0,0,2,3)\,,
\end{aligned} \tag{4.50}$$

we then introduce a new coordinate ξ, as well as the additional equation

$$\vec{\xi} = (0,0,0,0,0,1)\,, \quad \xi = \mathcal{F}_n(u_1, u_2, U_3)\,. \tag{4.51}$$

We also give all the old rays the value zero in the new direction, except for u_2 (for example) which we give the value $-n$, i.e.

$$\vec{u}_2 = (0,-1,0,2,3,-n)\,. \tag{4.52}$$

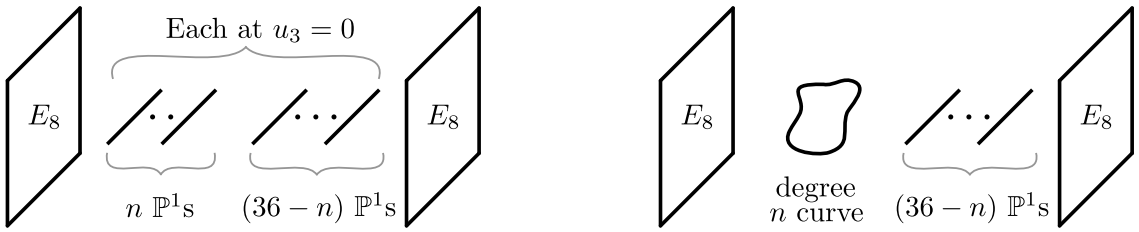

Figure 10: *Horizontal NS5-brane configurations on the heterotic side for a choice of a $\mathbb{P}^2$ heterotic base, in the case of (i) a configuration that has a dual geometry described by a toric hypersurface, and (ii) a configuration whose dual geometrical description requires a codimension two complete intersection.*

This ensures that the equation $\xi = \mathcal{F}_n$ is well-defined under the new scaling relation that has been introduced. Next we perform a blow-up by introducing an extra ray

$$\vec{\zeta} = 2\vec{x} + 3\vec{y} + \vec{\xi} + \vec{z_1} = (0, 0, 1, 0, 0, 1)\,. \tag{4.53}$$

(We then flop to the required fan, as discussed in Section 4.3.2 above.) The coefficients of x and y reflect that we are resolving a $\tilde{\mathrm{E}}_8$ singularity. The F-theory space $\hat{Y}_4$ is then the CY four-fold defined as a complete intersection, in the 6d toric ambient space, by two equations

$$\mathcal{W} = 0\,, \quad \xi\zeta = \mathcal{F}_n(u_1, u_2, U_3)\,, \tag{4.54}$$

where $\mathcal{W}$ is the Weierstrass polynomial. We also have to take the proper transform of $\mathcal{W}$, as discussed above. The base $\hat{\mathcal{B}}_3$ of the F-theory fibration can be described as a hypersurface in a 4d toric ambient space by the second of the above equations.

In this example we have replaced n blow-ups over a $\mathbb{P}^1$ by a single blow-up over a degree n curve on the E_8 surface. In the heterotic dual, we have replaced n $\mathbb{P}^1$ NS5-branes with a single NS5-brane with the topology of a degree n curve in $\mathbb{P}^2$. For example if $n = 3$, the resulting NS5-brane wraps a torus. Figure 10 shows the dual NS5-brane configuration, in the toric hypersurface case and in the complete intersection case we have just discussed[26]. This example was particularly simple. In the slightly more complicated example of a $\mathbb{P}^1 \times \mathbb{P}^1$ base in Figure 8 above, we could for example blow down n of the top rays from the ε tower and m of the top rays from the ρ tower, and then perform a blow-up over a general curve of degrees n, m, analogously to what we have just done for the $\mathbb{P}^2$ case. The new brane will have curve class $n[u_1] + m[v_1]$.

One can note that the procedure we have used replaces the n top or bottom $\mathbb{P}^1$s, and thus creates a general brane configurations 'near' a heterotic E_8 brane, i.e. where there are no branes

[26]Note that we have not discussed the transition between these situations – we will return to this question in Section 4.5 below.

between that M5 and the E_8 brane. This is sufficient for the purposes of this section, as multiplet counting and other checks will not depend on the ordering of branes in the bulk. We will discuss arbitrary configurations of branes with arbitrary orderings in Section 4.5.3 below.

4.4.4 Duality checks independent of NS5-brane configuration

We have now constructed global F-theory models dual to heterotic line bundle sums in four dimensions and spent some time discussing the duality between geometry of the F-theory side and horizontal NS5-brane configurations on the heterotic side. In addition to these ingredients, there is the duality of flux on the two sides: on the heterotic side the two sets of E_8 flux on the base, and on the F-theory side the G_4 flux on the two E_8 surfaces, were naturally proposed to be the same in Section 4.2. With the flux identification as well as the geometry/NS5-brane identification, we are now in a position to check various aspects of this duality.

We begin with those aspects that do not depend on the specific NS5-brane configuration. First we match the heterotic anomaly, which depends only on the class of the NS5-branes and not their configuration, to the D3-charge anomaly. Next we discuss a match of the stability conditions for the flux on the two sides, and then we match the charged matter content as well as the number of massless U(1) vector bosons (these matches only concern the E_8s and not the branes/blow-ups). In the next section we turn to the match of matter content arising from NS5-branes and blow-ups.

Anomalies

We begin with matching anomaly conditions on the two sides. In the process we will also show that the Euler characteristic of the F-theory four-fold is independent of which precise blow-ups are performed, which is dual to independence of the NS5-brane configuration. We recall that on the heterotic side both bundles V_1 and V_2 are taken to be line bundle sums. We use the notation

$$c_1(V_1) = \sum_{a=1}^{\mathfrak{r}_1} c_1(L_a) = k_a^i D_i \,, \quad c_1(V_2) = \sum_{a=1}^{\mathfrak{r}_2} c_1(\tilde{L}_a) = \tilde{k}_a^i D_i \,, \tag{4.55}$$

where we have recalled that $k_a^0 = \tilde{k}_a^0 = 0 \ \forall a$ or equivalently $L_a = \pi_H^* N_a$ and $\tilde{L}_a = \pi_H^* \tilde{N}_a$, as found in Section 4.2. The heterotic anomaly condition is

$$\mathrm{ch}_2(V_1) + \mathrm{ch}_2(V_2) - \mathrm{ch}_2(X_3) = [W] \,, \tag{4.56}$$

where $[W]$ is the NS5-brane class. We recall the expressions for the second Chern characters,

$$-\mathrm{ch}_2(X_3) = \left[\int_{B_2} (c_2(B_2) + 11c_1(B_2)^2)\right] C^0 - 12\xi_i C^i \,, \tag{4.57}$$

$$\mathrm{ch}_2(V_1) = \frac{1}{2} d_{IJK} k_a^I k_a^J C^K = \frac{1}{2} \mathfrak{g}_{ij} k_a^i k_a^j C^0 \,, \tag{4.58}$$

$$\mathrm{ch}_2(V_2) = \frac{1}{2} d_{IJK} \tilde{k}_a^I \tilde{k}_a^J C^K = \frac{1}{2} \mathfrak{g}_{ij} \tilde{k}_a^i \tilde{k}_a^j C^0 \,, \tag{4.59}$$

where we use the notation defined in Section 4.2, and where we recalled the triple intersection numbers from Section 4.2. Hence

$$\mathrm{ch}_2(V_1) + \mathrm{ch}_2(V_2) - \mathrm{ch}_2(X_3) = \left(\int_{B_2} \left(c_2(B_2) + 11c_1(B_2)^2\right) + \frac{1}{2}\mathfrak{g}_{ij} k_a^i k_a^k + \frac{1}{2}\mathfrak{g}_{ij} \tilde{k}_a^i \tilde{k}_a^k\right) C^0 - 12\xi_i C^i \,. \tag{4.60}$$

In our setup, we have chosen the NS5-brane content so that $[W] = -12\xi_i C^i$, i.e. we chose not to include vertical NS5-branes, and hence we have

$$\begin{aligned} 0 &= \int_{B_2} \left(c_2(B_2) + 11c_1(B_2)^2\right) + \frac{1}{2}\mathfrak{g}_{ij} k_a^i k_a^j + \frac{1}{2}\mathfrak{g}_{ij} \tilde{k}_a^i \tilde{k}_a^k \\ &= \int_{B_2} \left(c_2(B_2) + 11c_1(B_2)^2 + \frac{1}{2}\left(\sum_a c_1(N_a)^2 + \sum_a c_1(\tilde{N}_a)^2\right)\right) \,, \end{aligned} \tag{4.61}$$

as the remaining part of the anomaly condition.

On the F-theory side, the corresponding anomaly condition is that of the cancellation of D3-brane charge, which reads [71]

$$N_3 - \frac{\chi(\hat{Y}_4)}{24} + \frac{1}{2}\int_{\hat{Y}_4} G_4 \wedge G_4 = 0 \,, \tag{4.62}$$

where N_3 is the number of D3-branes. In our setup there are no D3-branes, so $N_3 = 0$.[27] For the flux contribution, we can see from the expansion of G_4 in two-forms dual to the blow-ups of the E_8 singularities that

$$\int_{\hat{Y}_4} G_4 \wedge G_4 = -\mathrm{Tr}\int_{S_1} F_1 \wedge F_1 - \mathrm{Tr}\int_{S_2} F_2 \wedge F_2 \,, \tag{4.63}$$

where S_i are the two E_8 surfaces. Since in our identification the D7-brane flux F_i is equal to that of the corresponding heterotic bundle V_i on the heterotic base space, we have

$$\mathrm{Tr}\int_S F_1 \wedge F_1 + \mathrm{Tr}\int_S F_2 \wedge F_2 = \sum_a c_1(N_a)^2 + \sum_a c_1(\tilde{N}_a)^2 \,. \tag{4.64}$$

Hence, the only non-trivial part of the matching of the two anomaly conditions is

$$\int_{B_2} \left(c_2(B_2) + 11c_1(B_2)^2\right) \stackrel{?}{=} \frac{\chi(\hat{Y}_4)}{24} \,. \tag{4.65}$$

[27] Note that the inclusion of D3-branes gives a contribution to the anomaly condition which trivially matches that of the corresponding vertical NS5-branes.

We now show this last match holds. Recall that in addition to the blow-ups of the F-theory four-fold corresponding to horizontal NS5-branes, the geometrically non-Higgsable E_8 singularities must be resolved. These blow-ups enter in the computation of the Euler characteristic. The Euler characteristic for a smooth elliptically fibered CY four-fold that is the result of resolving E_8 singularities over a divisor class S is known to be [5, 91]

$$\chi(\hat{Y}_4) = \int_{\hat{\mathcal{B}}_3} 12(c_1c_2 + 30c_1^3 - 80c_1^2S + 70c_1S^2 - 20S^3)\,, \tag{4.66}$$

where for brevity we write $c_i \equiv c_i(\hat{\mathcal{B}}_3)$ and do not write wedge products. In our case, $S = [z_1] + [z_2]$. Additionally, before the blow-ups dual to horizontal NS5-branes, the first Chern class of $\mathcal{B}_3$ is a sum $c_1(\mathcal{B}_3) = c_1(B_2) + c_1(\mathbb{P}^1)$. Under the blow-ups, the exceptional divisors are added to this expression. Since the class S is equal to $c_1(\mathbb{P}^1)$, we see that we can write $c_1(\hat{\mathcal{B}}_3) = S + \Sigma$ where Σ is a sum over pullbacks from B_2 to $\hat{\mathcal{B}}_3$. To evaluate $\chi(\hat{Y}_4)$, we first note that

$$\begin{aligned}\chi(\hat{Y}_4) &= \int_{\hat{\mathcal{B}}_3} 12\left[c_1c_2 + 30(S^3 + 3S^2\Sigma + 3S\Sigma^2 + \Sigma^3) - 80(S^3 + 2S^2\Sigma + S\Sigma^2) + 70(S^3 + S^2\Sigma) - 20S^3\right] \\ &= \int_{\hat{\mathcal{B}}_3} 12\left[c_1c_2 + 10S\Sigma^2 + 30\Sigma^3\right]\,,\end{aligned} \tag{4.67}$$

where many terms cancelled. The remaining terms are straightforward to evaluate. It is easy to see that the third term vanishes, since three pullbacks will not intersect. For the second, it is straightforward to see that $\int_{\hat{\mathcal{B}}_3} S\cdot\Sigma\cdot\Sigma = \int_{B_2} 2c_1(B_2)^2$: since Σ is a sum of pullbacks, the intersection $\Sigma\cdot[z_{1,2}]$ clearly has curve class $c_1(B_2)$ in $\{z_{1,2} = 0\}$, and hence also clearly $\int_{\hat{\mathcal{B}}_3}[z_{1,2}]\cdot\Sigma\cdot\Sigma = \int_{B_2} c_1(B_2)^2$. In the toric hypersurface cases of Figures 8 and 9, this is the observation that the presence of $[z_1]$ restricts to the cones one sees from 'above', which join $[z_1]$ to the 'highest' ray in each tower, and these cones form a copy of B_2; similarly for the term with $[z_2]$.

It only remains to establish that $\int_{\hat{\mathcal{B}}_3} \frac{1}{2}c_1(\hat{\mathcal{B}}_3)c_2(\hat{\mathcal{B}}_3) = \int_{B_2}\left(c_1(B_2)^2 + c_2(B_2)\right)$. In fact both expressions are equal to 12. This follows from the Hirzebruch-Riemann-Roch theorem, which states that for a holomorphic vector bundle E on a compact complex manifold X,

$$\mathrm{ind}(X,E) = \int_X \mathrm{ch}(E)\mathrm{td}(X)\,, \tag{4.68}$$

where $\mathrm{ind}(X,E)$ is the bundle index, and $\mathrm{ch}(\cdot)$ and $\mathrm{td}(\cdot)$ are the Chern character and Todd class respectively. We apply this to the case of the trivial line bundle, $E = \mathcal{O}_X$, for which we have $\mathrm{ch}(E) = 1$. We also recall the expression for the Todd class in Equation (4.20). Now, both B_2 and $\hat{\mathcal{B}}_3$ have $h^{i,0} = 0$ for $i > 0$ since they form the bases of CY manifolds, hence $\mathrm{ind}(X,\mathcal{O}_X) = 1$

in both cases, and so we have

$$\mathrm{B}_2: \quad \int_{B_2} \left(c_1(B_2)^2 + c_2(B_2)\right) = 12\,, \tag{4.69}$$

$$\hat{\mathcal{B}}_3: \quad \int_{\hat{\mathcal{B}}_3} c_1(\hat{\mathcal{B}}_3)c_2(\hat{\mathcal{B}}_3) = 24\,. \tag{4.70}$$

This establishes $\int_{\hat{\mathcal{B}}_3} \frac{1}{2}c_1(\hat{\mathcal{B}}_3)c_2(\hat{\mathcal{B}}_3) = \int_{B_2} \left(c_1(B_2)^2 + c_2(B_2)\right)$, which was the final equality that we needed. Hence we have established the equivalence of the two anomaly conditions. We note this shows that $\chi(\hat{Y}_4)$ is independent of the NS5-brane configuration, as we only used the fact that the E_8 singularities are geometrically non-Higgsable, dual to the fact the horizontal NS5-brane class is $-12K_{B_2}$.

Stability condition

Next we would like to match the flux stability conditions on the two sides of the duality. We write V for either of the heterotic bundles V_i, whose flux is identified with that on one of the E_8 surfaces in F-theory. We recall we have a sum of line bundles that are pullbacks,

$$V = \bigoplus_a L_a = \bigoplus_i \pi_H^*(N_a)\,. \tag{4.71}$$

As reviewed in Section 4.2, for preservation of supersymmetry we require that the slopes of all the line bundles vanish simultaneously,

$$0 \stackrel{!}{=} \int_{X_3} J^2 \wedge c_1(L_a) = \int_{X_3} J^2 \wedge \pi_H^*\left(c_1(N_a)\right) \quad \forall a\,. \tag{4.72}$$

We can rewrite this expression using Poincaré dual divisors and a knowledge of the triple intersection numbers from Section 4.2. We have

$$\begin{aligned} \int_{X_3} J^2 \wedge c_1(L_a) &= t^I t^J k_a^k D_I \cdot D_J \cdot D_k = t^I t^J k_a^k d_{IJk} \\ &= -(t^0)^2 \xi_k k_a^k + 2t^0 t^i k_a^k \mathfrak{g}_{ik} \\ &= 2t^0 \left(J_{B_2} - \tfrac{1}{2}t^0 K_{B_2}\right) \cdot \mathcal{C} \stackrel{!}{=} 0\,, \end{aligned} \tag{4.73}$$

where $J_{B_2} \equiv t^i \mathcal{C}_i$ and $\mathcal{C} \equiv c_1(N)$, and where we have recalled the intersection numbers from Section 4.2. We note that $t^0 \neq 0$ as it corresponds to the volume of the fiber, so the t^0 factor drops out of the condition. As we are working in the adiabatic limit of X_3, for which the volume of the elliptic fiber is small compared to volumes in the base, we can drop the second term and recover the usual D-term stability condition on a fluxed 7-brane

$$\int J \wedge F_a \stackrel{!}{=} 0\,, \tag{4.74}$$

where the F_a are the U(1) fluxes on the 7-brane corresponding in the duality to the heterotic U(1) fluxes of the line bundles L_a. One can see that this is the stability condition for a fluxed

7-brane from a local analysis, or from a global F-theory analysis where it corresponds to the condition $J \wedge G_4 = 0$. See for example Refs. [92–94] for discussions of this condition.

Matter multiplets

Next we would like to match the counts of matter multiplets charged under the E_8 gauge groups. We begin with the heterotic side. We have two vector bundles V_i, corresponding to the two E_8 factors, each given by a sum of line bundles that are pulled back from the base. We write $V = \bigoplus_a L_a = \bigoplus_i \pi_H^*(N_a)$ for either of these two bundles, as above. We are interested in the cohomologies of the L_a, as well as of tensor products and duals, since these determine the charged matter content. As the heterotic three-fold X_3 is elliptically fibered, we will use the Leray spectral sequence to determine these cohomologies. See e.g. Refs. [3, 37, 38] for details and examples of the application of this sequence in related contexts. We also discuss the Leray spectral sequence in more detail in Appendix C.

First we collect, from the general list in Appendix C.2, the direct image and higher direct image of the trivial bundle on the heterotic three-fold,

$$(\pi_H)_*\mathcal{O}_{X_3} = \mathcal{O}_{B_2}\,, \quad R^1(\pi_H)_*\mathcal{O}_{X_3} = K_{B_2}\,, \tag{4.75}$$

as well as the projection formulae $(\pi_H)_*(L_a) = (\pi_H)_*\mathcal{O}_{X_3}\otimes N_a$ and $R^1(\pi_H)_*(L_a) = R^1(\pi_H)_*\mathcal{O}_{X_3}\otimes N_a$. Next we recall, as discussed in Appendix C.1, that the Leray spectral sequence implies the results

$$H^0(L_a) = E_2^{0,0}\,, \quad H^3(L_a) = E_2^{2,1}\,, \tag{4.76}$$

$$0 \to E_2^{1,0} \to H^1(L_a) \to E_2^{0,1} \to E_2^{2,0} \to H^2(L_a) \to E_2^{1,1} \to 0\,, \tag{4.77}$$

where $E_2^{p,q} \equiv H^p(R^q(\pi_H)_*L_a)$ and where the sequence is exact. If for a given L_a one of $E_2^{0,1}$ or $E_2^{2,0}$ vanishes then the exact sequence splits. In fact we will show in a moment that $h^2(N_a) = 0$, so the exact sequence indeed always splits as the $E_2^{2,0}$ term is zero. Hence we have

$$\begin{aligned}
H^0(L_a) &= H^0(N_a)\,,\\
H^1(L_a) &= H^0(K_{B_2}\otimes N_a) \oplus H^1(N_a) = H^2(N_a^*)^* \oplus H^1(N_a)\,,\\
H^2(L_a) &= H^1(K_{B_2}\otimes N_a) \oplus H^2(N_a) = H^1(N_a^*)^* \oplus H^2(N_a)\,,\\
H^3(L_a) &= H^2(K_{B_2}\otimes N_a) = H^0(N_a^*)\,.
\end{aligned} \tag{4.78}$$

where we have also included the results after using Serre duality, which eliminates occurrences of K_{B_2}.

We are also interested in the cohomologies of tensor products and duals of the line bundles, since these enter in the counts of multiplets in various representations of the gauge group. We

note that the pullback commutes with taking duals or tensor products, so that the line bundles we need to consider will always be pullbacks, and hence the above analysis holds also in these cases. Hence quite generally, writing τ for a representation corresponding to a particular vector bundle $\tilde{V} = \pi_H^* \tilde{\mathcal{V}}$ built from taking tensor product and dual operations on V, we then have for the number n_τ of multiplets in this representation and the number n_{τ^*} in the conjugate representation,

$$\begin{aligned} n_\tau &= h^1(B_2, \tilde{\mathcal{V}}) + h^2(B_2, \tilde{\mathcal{V}}^*)\,, \\ n_{\tau^*} &= h^1(B_2, \tilde{\mathcal{V}}^*) + h^2(B_2, \tilde{\mathcal{V}})\,, \end{aligned} \tag{4.79}$$

which completes the computation of the numbers of charged multiplets.

Finally we also note the following results on vanishing cohomologies. From the supersymmetry conditions on the vector bundle V, it follows [19] for a sum of non-trivial line bundles that $h^0 = h^3 = 0$ for V and V^*. Since V is a line bundle sum, it follows that each line bundle in V must have $h^0 = h^3 = 0$. Hence it also follows that $h^0 = h^3 = 0$ for $\tilde{V}$ and $\tilde{V}^*$, since these are built from tensor products and duals of the line bundles. Additionally, it is then straightforward to see that $h^2(B_2, \tilde{\mathcal{V}}) = h^2(B_2, \tilde{\mathcal{V}}^*) = 0$ if $-K_{B_2}$ is effective (which is required for the existence of the elliptic fibration of X_3) as follows. We note the inclusions

$$\begin{aligned} H^2(B_2, \tilde{\mathcal{V}}\ ) &= H^0(B_2, \tilde{\mathcal{V}}^* \otimes K_{B_2})^* \subseteq H^0(B_2, \tilde{\mathcal{V}}^*)^* \\ H^2(B_2, \tilde{\mathcal{V}}^*) &= H^0(B_2, \tilde{\mathcal{V}}\ \otimes K_{B_2})^* \subseteq H^0(B_2, \tilde{\mathcal{V}}\ )^*\,, \end{aligned} \tag{4.80}$$

where in the equalities we have used Serre duality. Since $h^0(X_3, \tilde{V}) = 0$ and $h^0(B_2, \tilde{\mathcal{V}}) = h^0(X_3, \tilde{V})$, and similarly for $\tilde{V}^*$ and $\tilde{\mathcal{V}}^*$, we see from the inclusions that indeed $h^2(B_2, \tilde{\mathcal{V}}) = h^2(B_2, \tilde{\mathcal{V}}^*) = 0$. This result shows the exact sequence in the Leray spectral sequence always splits, as assumed above. It also reduces Equation (4.79) to the h^1 terms.

On the F-theory side, the proposed dual geometry contains two E_8 brane stacks, and it is the matter coming from flux on these brane stacks that we expect to match the above heterotic matter. We can consider each E_8 stack separately, so we will write S for either surface. The background flux is described by a vector bundle on this surface, and in the proposal in Section 4.2, this vector bundle is the same as appears on the base of the heterotic three-fold for the corresponding E_8 gauge group. The count of the charged multiplets for a given background flux on the surface has been computed in Ref. [48]. In particular the result is that the matter content in a representation τ corresponding to a vector bundle $\mathcal{T}$ is given by

$$H^0(S, \mathcal{T}^*)^* \oplus H^1(S, \mathcal{T}) \oplus H^2(S, \mathcal{T}^*)^*\,, \tag{4.81}$$

so the number n_τ of multiplets in the τ representation and the number n_{τ^*} of multiplets in the conjugate representation τ^* are given by

$$\begin{aligned} n_\tau &= h^0(S,\mathcal{T}^*) + h^1(S,\mathcal{T}) + h^2(S,\mathcal{T}^*)\,, \\ n_{\tau^*} &= h^0(S,\mathcal{T}) + h^1(S,\mathcal{T}^*) + h^2(S,\mathcal{T})\,. \end{aligned} \tag{4.82}$$

However, a non-zero $h^0(S,\mathcal{T})$ or $h^0(S,\mathcal{T}^*)$ would mean the F-theory compactification is inconsistent [47]. We note that these were also zero on the heterotic side. Rewriting the number of multiplets with this taken into account, we have

$$\begin{aligned} n_\tau &= h^1(S,\mathcal{T}) + h^2(S,\mathcal{T}^*)\,, \\ n_{\tau^*} &= h^1(S,\mathcal{T}^*) + h^2(S,\mathcal{T})\,. \end{aligned} \tag{4.83}$$

We see that this result precisely matches the heterotic side, so that we have established the matching of the two charged matter spectra. We also note that in Ref. [48] they find that $h^2(S,\mathcal{T}) = h^2(S,\mathcal{T}^*) = 0$ if both $-K_S$ is effective and $h^{2,0}(S) = 0$. Since S is diffeomorphic to the heterotic base B_2, both of these conditions hold since B_2 forms the base of a CY elliptic fibration. Hence these second cohomologies vanish for the S we consider, which matches what was found on the heterotic side.

Massless U(1)s

Finally we wish to match the count of extra massless U(1) vector bosons, which are a well-known possibility in line bundle sum models. For example, if a line bundle sum is used to break one of the E_8 gauge groups to a group containing SU(5), the commutant also necessarily contains four additional U(1) factors. These extra U(1) vector bosons tend to be massive by the Green-Schwarz mechanism, see e.g. Refs. [18,19]. We will count on both sides of the duality the number of the extra massless U(1) vector bosons. On the heterotic side, the mass matrix for the extra U(1) vector bosons in line bundle models is found to be at lowest order

$$M_{ab} = k_a^I G_{IJ} k_b^J\,, \tag{4.84}$$

where G is the Kähler metric, k_a^I are the integers specifying the line bundle sum as discussed in Section 4.2, and as also discussed there, in our models $k_a^0 = 0\ \forall a$, so that only k_a^i appears. Since G is invertible, the number of massless U(1) vector bosons is determined by the rank of k_a^i.

On the F-theory side, we recall the discussion from an M-theory perspective [94]. We write ω_α for two-forms pulled back from the base $\hat{\mathcal{B}}_3$ by the projection map of the elliptic fibration, and w_a, $a = 1,\ldots,\mathrm{rk}(E_8)$, for two-forms dual to the exceptional divisors in the blow-up of the

E_8 singularity, whose intersections give Cartan matrix factors C_{ab}. The G_4 flux is expanded in the w_a, which are the natural geometric objects,

$$G_4 = \tilde{F}^a \wedge \mathrm{w}_a \,, \tag{4.85}$$

where the $\tilde{F}^a$ are pullbacks of flux two-forms on the E_8 surface S. This corresponds to a choice of generators T_a of the adjoint representation of the Lie algebra such that $\mathrm{Tr}(T_a T_b) = C_{ab}$. The relevant Stückelberg mass term appears in a gauging of fields T_α, which are Kähler moduli of the base $\hat{\mathcal{B}}_3$,

$$\mathrm{D}T_\alpha = \mathrm{d}T_\alpha + iX_{\alpha a}\tilde{A}^a \,, \quad \text{where} \quad X_{\alpha i} := \tfrac{1}{2}\int_{\hat{Y}_4} \omega_\alpha \wedge \mathrm{w}_a \wedge G_4 \,, \tag{4.86}$$

and it follows straightforwardly that the Stückelberg mass term is

$$X_{\alpha a}\tilde{A}^a = -\frac{1}{2}C_{ab}\tilde{A}^a \int_S \omega_\alpha \wedge \tilde{F}^b \,. \tag{4.87}$$

The C_{ab} factor reflects the geometrically convenient basis choice in the Lie algebra. More generally we clearly have

$$-\frac{1}{2}\mathrm{Tr}\left(A\int_S \omega_\alpha \wedge F\right) \,. \tag{4.88}$$

We write $\{\omega_i\}$ for the subset of $\{\omega_\alpha\}$ that are pullbacks in $\hat{\mathcal{B}}_3$ from curves in S under the projection that collapses the $\mathbb{P}^1$. These survive in the above integral. Additionally as we have a line bundle sum on S, we can write $F = F^a k_a^i \omega_i$, where the k_a^i are identified in the duality with those of the heterotic line bundle sum. Then as well as factors of the intersection matrix $\mathfrak{g}_{ij} \equiv \int_S \omega_i \wedge \omega_j$ on S and factors of the moduli metric, which are both invertible, the mass matrix of U(1) vector bosons contains only occurrences of k_a^i. Hence the number of massless U(1) vector bosons is determined by the rank of (k_a^i) exactly as on the heterotic side.

Before turning to duality checks involving the NS5-brane/blow-up configuration, we make two final comments. First, there is an additional condition on the F-theory flux G_4 which we have not yet discussed. The flux G_4 is subject to the Freed-Witten quantisation condition [95],

$$G_4 + \frac{1}{2}c_2(\hat{Y}_4) \in H^4(\hat{Y}_4, \mathbb{Z}) \,. \tag{4.89}$$

In the F-theory models that we have constructed, G_4 is manifestly integrally quantised since the heterotic flux is integrally quantised, c.f. Equation (4.18). Hence we expect that $c_2(\hat{Y}_4)$ is always even. This is however difficult to fully verify, due to the difficulty in computing an integral basis for H^4. The fact that in our examples the Euler characteristic is divisible by 24 is a necessary check, since this is implied by evenness of $c_2(\hat{Y}_4)$ [95, 96]. Additionally, in the D3-brane charge cancellation condition, we know the number of D3-branes from the heterotic dual, and including

also the $\chi(\hat{Y}_4)/24$ contribution and the flux contribution from the E_8 branes this condition is satisfied, which seems to leave no room for additional G_4 flux. Finally, half-integrally quantised G_4 fluxes are localised on stacks of 7-branes [97], and in our situation the only 7-brane stacks are the E_8 brane stacks, whose flux seems to be matched with the heterotic line bundle flux. For further discussion of the Freed-Witten quantisation condition in F-theory see for example Refs. [97, 98].

Second, F-theory has an attractive mechanism [48,99] for breaking a GUT group to the gauge group of the Standard Model leaving the hypercharge massless. This requires the existence of a curve class in the GUT surface S that maps to a trivial curve class in the embedding of S into the base $\hat{\mathcal{B}}_3$. In our models, the GUT surfaces form the two sections of a $\mathbb{P}^1$ fibration. Curves in the GUT surfaces pull back to non-trivial divisors on $\hat{\mathcal{B}}_3$, whose intersection with the sections of the fibration return the original curves. Hence this F-theory mechanism is not possible in these models. This is expected, as it is well-known that this is not possible for models with a heterotic dual. See also Ref. [25] for more detail on the situation in heterotic string theory.

4.4.5 Duality checks concerning NS5-branes and blow-ups

In Section 4.4.4 we have performed checks of the duality between heterotic line bundle models and their proposed dual F-theory models, which did not depend on the precise NS5-brane configuration. We now turn to a match of multiplets whose number does depend on the precise configuration of NS5-branes. As explained in Sections 4.3.1 and 4.3.2, this corresponds to the choice of blow-ups in the F-theory base that resolve the $\tilde{E}_8$ singularities appearing where the E_8 stacks intersect the remaining D7-brane locus. We will write $\hat{Y}_4$ for the F-theory CY four-fold after all resolutions (both those that alter the base and those that do not), and $\hat{\mathcal{B}}_3$ for the blown-up base. On the heterotic side we have a CY three-fold X_3 with a base B_2.

Preliminaries

We first collect general expressions for the number of multiplets on each side, for a general NS5-brane configuration. We begin with the heterotic side, and we will ignore the vector multiplets of the $E_8 \times E_8$. There are $h^{1,1}(X_3) + h^{2,1}(X_3)$ chiral multiplets from the geometry and one from the heterotic dilaton. Second, we have the moduli from the NS5-branes, which have been counted in Ref. [100], and we briefly recall this count. For a single NS5-brane wrapping a genus g curve in the CY manifold, there is a single universal chiral multiplet and g vector multiplets. Additionally there are chiral multiplets from the deformation moduli.[28] We write $\mathcal{N}_5$ for the

[28]The number of deformation moduli in our cases will be rather clear, since we consider only vertical and

number of NS5-branes, and we write M_i for the i^{th} brane. We will also write $n_{\text{def.}}(M_i)$ for the number of (complex) deformation moduli of the i^{th} brane, and $g(M_i)$ for its genus. The number $n_{\text{ch.}}$ of chiral multiplets and the number $n_{\text{vec.}}$ of vector multiplets (excluding those from the $\text{E}_8 \times \text{E}_8$ sector) are then,

$$n_{\text{ch.}} = h^{1,1}(X_3) + h^{2,1}(X_3) + 1 + \mathcal{N}_5 + \sum_{M_i} n_{\text{def.}}(M_i)\,, \tag{4.90}$$

$$n_{\text{vec.}} = \sum_{M_i} g(M_i)\,. \tag{4.91}$$

Note that in our models we have chosen not to include vertical branes: as discussed in Section 4.4.1, the anomaly condition can be satisfied using only horizontal branes and line bundle flux.

On the F-theory side we have the following. We first note that in our models there is no G_4 flux away from the E_8 stacks, which could have lifted moduli. The number of massless neutral chiral multiplets $n_{\text{ch.}}$ and the rank of the resulting gauge group rk_V are then [101–103] (see also Refs. [94, 104] for a detailed discussion)

$$n_{\text{ch.}} = h^{3,1}(\hat{Y}_4) + h^{1,1}(\hat{\mathcal{B}}_3) + \left(h^{2,1}(\hat{Y}_4) - h^{2,1}(\hat{\mathcal{B}}_3)\right) + 3N_3\,, \tag{4.92}$$

$$\text{rk}_V = h^{1,1}(\hat{Y}_4) + h^{2,1}(\hat{\mathcal{B}}_3) - h^{1,1}(\hat{\mathcal{B}}_3) - 1 + N_3\,, \tag{4.93}$$

where N_3 is the number of D3-branes, which is zero in our models[29], corresponding to the choice to not include vertical NS5-branes. Additionally, we have not broken the two E_8 gauge symmetries by geometry, rather only by flux, so that in the rank computation we will find a contribution of 16 corresponding to these, which we have already discussed. The mass of the vector multiplets from these E_8 gauge groups are determined by the background G_4 flux pulled back from the brane, as reviewed in Section 4.4.4. We then have

$$n_{\text{vec.}} = h^{1,1}(\hat{Y}_4) + h^{2,1}(\hat{\mathcal{B}}_3) - h^{1,1}(\hat{\mathcal{B}}_3) - 1 - 16 \tag{4.94}$$

for the number of vector multiplets $n_{\text{vec.}}$ from the remaining sector.

Vector multiplet match

horizontal NS5-branes, rather than branes that are a combination. For a detailed discussion of the moduli space of general NS5-branes on elliptic CY three-folds see Ref. [89].

[29] Note however that the match between D3-branes and vertical NS5-branes is very simple. Each vertical NS5-brane contributes 1 to $\mathcal{N}_5$, and has 2 complex deformation parameters as it sits over a point in a two-fold base, giving 3 chiral multiplets. These branes wrap genus 1 curves, giving a single vector multiplet. These match the D3-brane contributions.

We now match the vector multiplet counts in general. First we note that $h^{1,1}(\hat{Y}_4) - h^{1,1}(\hat{\mathcal{B}}_3) - 1 - 16$ counts extra sections of the F-theory elliptic fibration, and these are not present in our F-theory models. Hence for the models we consider the matching condition for vector multiplets is

$$\sum_{M_i} g(M_i) \stackrel{?}{=} h^{2,1}(\hat{\mathcal{B}}_3)\,. \tag{4.95}$$

Before the blow-ups dual to horizontal NS5-branes, $\mathcal{B}_3 = B_2 \times \mathbb{P}^1$, so that $h^{2,1}(\mathcal{B}_3) = 0$ (using the Kunneth formula and that $h^{1,0}(B_2) = 0$ since otherwise $h^{1,0}(X_3) \neq 0$). In each blow-up, a curve C of genus g, diffeomorphic to the NS5-brane curve, is replaced by a $\mathbb{P}^1$ fiber bundle E over the curve, so by the additivity of the Euler characteristic,

$$\Delta\chi(\mathcal{B}_3) = \chi(E) - \chi(C) = 2(2-2g) - (2-2g) = 2 - 2g\,, \tag{4.96}$$

and noting that $\chi(\mathcal{B}_3) = 2 + 2(h^{1,1}(\mathcal{B}_3) - h^{2,1}(\mathcal{B}_3))$, which follows since $h^{1,0}(\mathcal{B}_3) = h^{2,0}(\mathcal{B}_3) = 0$ for Y_4 to be CY, this means $\Delta(h^{1,1}(\mathcal{B}_3) - h^{2,1}(\mathcal{B}_3)) = 1 - g$. Since C is irreducible we know $\Delta h^{1,1}(\mathcal{B}_3) = 1$, so we have shown that $\Delta h^{2,1}(\mathcal{B}_3) = g$. This proves the matching condition.

Chiral multiplet match

Next we look at matching the chiral multiplet counts. The required match is

$$h^{1,1}(X_3)+h^{2,1}(X_3)+1+\mathcal{N}_5+\sum_{M_i} n_{\text{def.}}(M_i) \stackrel{?}{=} h^{3,1}(\hat{Y}_4)+h^{1,1}(\hat{\mathcal{B}}_3)+\left(h^{2,1}(\hat{Y}_4) - h^{2,1}(\hat{\mathcal{B}}_3)\right)\,. \tag{4.97}$$

It will be useful for our purposes to reduce this equation to one involving fewer Hodge numbers. One uninterested in the derivation can skip directly to Equation (4.106). We first note that the heterotic CY three-fold X_3 is an elliptic fibration with a single section, from which we have

$$h^{1,1}(X_3) = h^{1,1}(B_2) + 1\,, \tag{4.98}$$

$$\chi(X_3) \equiv 2\left(h^{1,1}(X_3) - h^{2,1}(X_3)\right) = -60\int_{B_2} c_1(B_2)^2\,, \tag{4.99}$$

$$\Rightarrow \quad h^{2,1}(X_3) = h^{1,1}(B_2) + 1 + 30\int_{B_2} c_1(B_2)^2\,. \tag{4.100}$$

The expression for the Euler characteristic $\chi(X_3)$ of a smooth elliptic three-fold X_3 described by a Weierstrass equation is a simple consequence of adjunction. Furthermore

$$\int_{B_2} c_2(B_2) = h^{1,1}(B_2) + 2\,. \tag{4.101}$$

On the F-theory side, there is a relation between Hodge numbers of the CY four-fold [96], so

that the Euler characteristic can be written in terms of any three,

$$\begin{aligned} h^{2,2}(\hat{Y}_4) &= 44 + 4h^{1,1}(\hat{Y}_4) + 4h^{3,1}(\hat{Y}_4) - 2h^{2,1}(\hat{Y}_4)\,, \\ \chi(\hat{Y}_4) &= 4 + 2h^{1,1}(\hat{Y}_4) - 4h^{2,1}(\hat{Y}_4) + h^{2,2}(\hat{Y}_4) + 2h^{3,1}(\hat{Y}_4)\,, \\ \Rightarrow \quad \chi(\hat{Y}_4) &= 6\left(8 + h^{1,1}(\hat{Y}_4) - h^{2,1}(\hat{Y}_4) + h^{3,1}(\hat{Y}_4)\right)\,, \\ \Rightarrow \quad h^{3,1}(\hat{Y}_4) &= \frac{1}{6}\chi(\hat{Y}_4) - 8 - h^{1,1}(\hat{Y}_4) + h^{2,1}(\hat{Y}_4)\,, \\ \text{where} \quad \frac{1}{6}\chi(\hat{Y}_4) &= 48 + 40\int_{B_2} c_1(B_2)^2\,, \end{aligned} \tag{4.102}$$

in which the expression for $\chi(\hat{Y}_4)$ was given in the anomaly cancellation match in Section 4.4.4. We also recall from that discussion that

$$\int_{B_2}\left(c_1(B_2)^2 + c_2(B_2)\right) = 12 = \int_{\hat{\mathcal{B}}_3}\frac{1}{2}c_1(\hat{\mathcal{B}}_3)c_2(\hat{\mathcal{B}}_3)\,. \tag{4.103}$$

There is a single section of the F-theory elliptic fibration as noted in the vector multiplet match, and additionally from knowledge of the duality between F-theory base blow-ups and NS5-branes we have together

$$h^{1,1}(\hat{Y}_4) = h^{1,1}(\hat{\mathcal{B}}_3) + 1 + 16\,, \tag{4.104}$$

$$h^{1,1}(\hat{\mathcal{B}}_3) = h^{1,1}(B_2) + 1 + \mathcal{N}_5\,, \tag{4.105}$$

and we recall the relation in Equation (4.95). Using all of these expressions, it is straightforward to reduce the chiral multiplet match to

$$\sum_{M_i} n_{\text{def.}}(M_i) + \mathcal{N}_5 + \sum_{M_i} g(M_i) - 12c_1(B_2)^2 - 2h^{2,1}(\hat{Y}_4) \stackrel{?}{=} 0\,. \tag{4.106}$$

Subtlety in chiral multiplet match

This is clearly a more complicated match than in the case of vector multiplets. We will first show that it holds under a particular assumption, and then we will discuss the general case in Section 4.4.6 below. The assumption we impose is that

$$-K_{B_2}\cdot C \neq 0 \quad \forall C \quad \text{and} \quad h^{2,1}(\hat{Y}_4) = h^{2,1}(\hat{\mathcal{B}}_3)\,, \tag{4.107}$$

where C is any curve in the heterotic base B_2 wrapped by an NS5-brane. We will argue in Section 4.4.6 that the first condition is expected to enforce the second, so we will refer to this as a single assumption. We emphasise that there are many situations satisfying this. For example, this holds for any of the toric hypersurface cases with heterotic base $\mathbb{P}^1\times\mathbb{P}^1$ or $\mathbb{P}^2$, examples of which were shown in Figures 8 and 9. Using this assumption, the match is straightforward to show. From the first equation it follows that for a brane M_i wrapping a curve C,

$$n_{\text{def.}}(M_i) = -K_{B_2}\cdot C - 1 + g(C)\,, \tag{4.108}$$

where $g(C)$ is the genus of C. (We will prove this in a moment.) Additionally, the second equation allows us to write $h^{2,1}(\hat{Y}_4) = \sum_{M_i} g(M_i)$, as shown in the proof of Equation (4.95). Substituting these two expressions into the chiral multiplet match, we find that it is satisfied. Hence the match holds under the assumption above.

To derive the expression for $n_{\text{def.}}(M_i)$, let a horizontal NS5-brane wrap a curve C of genus g in the heterotic base B_2. As we will discuss below in Section 4.4.6, the condition $-K_{B_2} \cdot C \neq 0$ ensures that the NS5-brane can only be deformed within B_2. Hence the number of holomorphic deformations is counted by

$$h^0(C, N_{C/X_3}) = h^0(C, N_{C/B_2})\,, \tag{4.109}$$

where N_{C/X_3} and N_{C/B_2} are the normal bundles of C within X_3 and B_2, the latter being a line bundle. We can use the Riemann-Roch formula

$$h^0(C, N_{C/B_2}) - h^1(C, N_{C/B_2}) = c_1(N_{C/B_2}) + 1 - g\,, \tag{4.110}$$

to rewrite $h^0(C, N_{C/B_2})$, since as we now show, $h^1(C, N_{C/B_2}) = 0$. Note by Serre duality on C that

$$h^1(C, N_{C/B_2}) = h^0(C, N^*_{C/B_2} \otimes K_C)\,. \tag{4.111}$$

The bundle $N^*_{C/B_2} \otimes K_C$ has degree

$$\deg(N^*_{C/B_2} \otimes K_C) = -c_1(N_{C/B_2}) - c_1(T_C) = -c_1(T_{B_2}|_C) = K_{B_2} \cdot C\,, \tag{4.112}$$

and we can note that $K_{B_2} \cdot C \leq 0$ as B_2 is weak Fano, with the equality case ruled out by the assumption on C. Hence the degree is negative, giving $h^1(C, N_{C/B_2}) = 0$ from Equation (4.111). So the Riemann-Roch formula gives

$$h^0(C, N_{C/B_2}) = c_1(N_{C/B_2}) + 1 - g = -K_{B_2} \cdot C - 1 + g\,, \tag{4.113}$$

where we noted $c_1(N_{C/B_2}) = c_1(T_{B_2}|_C) - c_1(T_C) = -K_{B_2} \cdot C - \chi(C)$. This derivation completes the multiplet match above, under the specified assumption.

Examples

Before moving on to cases where the assumption in Equation (4.107) has been relaxed, we now give some examples that illustrate the matches of vector and chiral multiplets in cases obeying the assumption. We first consider the example in Figure 8, in which the F-theory four-fold is a toric hypersurface. Here the heterotic base is $B_2 = \mathbb{P}^1 \times \mathbb{P}^1$, and the NS5-branes/blow-ups are distributed equally between $u_1 = 0$ and $v_1 = 0$. For this choice of heterotic base space, we find the Hodge numbers

$$h^{1,1}(X_3) = 3\,, \quad h^{2,1}(X_3) = 243\,. \tag{4.114}$$

Additionally we have 48 NS5-branes wrapping $\mathbb{P}^1$s. As these branes wrap genus zero curves they do not give vector multiplets. Each however has a single complex deformation modulus, so that the branes contribute 96 chiral multiplets. Altogether this gives $n_{\text{ch.}} = 343$ chiral multiplets. On the F-theory side we find the following Hodge numbers,

$$\begin{aligned}
&\hat{\mathcal{B}}_3: \quad h^{1,1}(\hat{\mathcal{B}}_3) = 51\,, \quad h^{2,1}(\hat{\mathcal{B}}_3) = 0\,, \\
&\hat{Y}_4: \quad h^{1,1}(\hat{Y}_4) = 68\,, \quad h^{2,1}(\hat{Y}_4) = 0\,, \quad h^{3,1}(\hat{Y}_4) = 292\,, \quad h^{2,2}(\hat{Y}_4) = 1484\,, \\
&\text{with} \quad \chi(\hat{Y}_4) = 2208\,.
\end{aligned} \tag{4.115}$$

We see from the above expression for the multiplet count in F-theory that we have $n_{\text{ch.}} = 343$, as well as the E_8 vector multiplets, so that the multiplet content matches.

Next we illustrate the multiplet count for some models with more complicated NS5-brane configurations, whose F-theory dual geometries are described in general by complete intersections as described in Section 4.4.3. We take as an example the case of a heterotic base $\mathbb{P}^2$, where we keep some NS5-branes at the vanishing loci of toric coordinates, but the rest of the brane class will be in a single general genus g NS5-brane. For this choice of heterotic base, we have the Hodge numbers

$$h^{1,1}(X_3) = 2\,, \quad h^{2,1}(X_3) = 272\,. \tag{4.116}$$

The NS5-brane configuration was shown in Figure 10. The toric description of the F-theory geometry in this situation was given in Section 4.4.3. The complete intersection can be described by a nef partition, and hence the Hodge number computation is straightforward. In Table 4 we record on the two sides of the duality the number of chiral multiplets $n_{\text{ch.}}$, and the number of U(1) vector bosons $n_{\text{U(1)}}$ associated to this sector, in the case of a single NS5-brane wrapping a degree n curve in the heterotic base, for several choices of n. Since the heterotic base is $\mathbb{P}^2$, the genus of the Riemann surface wrapped by the brane is $g = \frac{1}{2}(n-1)(n-2)$.

4.4.6 Subtleties concerning NS5-branes not intersecting $-K_{B_2}$

Missing chiral multiplets

We have shown in Section 4.4.5 that the chiral multiplet match in Equation (4.106), between the heterotic and F-theory models, holds under the assumption that there are no branes wrapping curves C in the base B_2 that do not intersect the anti-canonical divisor, $-K_{B_2}$. However, in cases where this assumption does not hold, we have not given a proof of the match.

In fact, it turns out that the chiral multiplet match fails in general. That is, when we relax the assumption that $-K_{B_2} \cdot C \neq 0$ for all horizontal NS5-branes C, we find examples where

n	$\mathcal{N}_5$	$n_{\text{def.}}$	$h^{3,1}(\hat{Y}_4)$	$h^{2,1}(\hat{Y}_4)$	$h^{1,1}(\hat{Y}_4)$	$h^{1,1}(\hat{\mathcal{B}}_3)$	$h^{2,1}(\hat{\mathcal{B}}_3)$	$n_{\text{ch.}}$	$n_{\text{U(1)}}$
2	34+1	$34 \times 2 + 5$	346	0	54	37	0	383	0
3	33+1	$33 \times 2 + 9$	348	1	53	36	1	384	1
6	30+1	$30 \times 2 + 27$	360	10	50	33	10	393	10
9	27+1	$27 \times 2 + 54$	381	28	47	30	28	411	28

Table 4: *Multiplet matching in the case of $B_2 = \mathbb{P}^2$, when one NS5-brane wraps a degree n curve in B_2 and the other branes wrap $\mathbb{P}^1$s. In each case the class wrapped by NS5-branes is $\sigma(-12K_{B_2})$ as required by Equation (4.43). Note that $h^{1,1}(X_3) = 2$ and $h^{2,1}(X_3) = 272$. Here $n_{\text{U(1)}}$ is only the number of U(1) vector bosons associated to this sector – it does not include contributions from the* E_8 *sectors.*

there is an apparent chiral multiplet mismatch

$$n_{\text{ch.}}(\text{Het.}) \neq n_{\text{ch.}}(\text{F-th.})\,, \tag{4.117}$$

when $-K_{B_2} \cdot C = 0$ for some base curve C wrapped by a horizontal NS5-brane.

The simplest heterotic base in which the assumption $-K_{B_2} \cdot C \neq 0$ fails for some horizontal NS5-brane C is the Hirzebruch surface, $B_2 = \mathbb{F}_2$, when there is a non-zero number of NS5-branes wrapping the unique holomorphic curve of self-intersection -2. One finds in this case that the number of chiral multiplets predicted on the heterotic side is always larger by two than the predicted number on the F-theory side. We emphasise this difference is not proportional to the number of NS5-branes wrapping the (-2)-curve, rather it is a constant discrepancy. For example, in the notation of Figure 11, when 2 NS5-branes are wrapped on each of $u_2 = 0$, $u_3 = 0$, $u_4 = 0$, with 22 branes wrapping $u_1 = 0$, we find the following apparent mismatch of chiral multiplets,

$$\begin{aligned} h^{1,1}(X_3) + h^{2,1}(X_3) + 1 + \mathcal{N}_5 + \sum_{M_i} n_{\text{def.}}(M_i) &\stackrel{?}{=} h^{3,1}(\hat{Y}_4) + h^{1,1}(\hat{\mathcal{B}}_3) + \left(h^{2,1}(\hat{Y}_4) - h^{2,1}(\hat{\mathcal{B}}_3)\right) \\ 347 = 3 + 243 + 1 + 28 + 72 &\neq 313 + 31 + (1 - 0) = 345\,. \end{aligned} \tag{4.118}$$

This chiral multiplet mismatch is an interesting subtlety which requires explanation. We will now discuss in several stages the likely reasons behind it, using the above case of an $\mathbb{F}_2$ base as our example. First, we discuss how in these cases NS5-branes can move 'vertically' up the heterotic elliptic fiber. Second, we will determine precisely which moduli are the culprits in the multiplet mismatch. Finally, we argue for a likely cause of the mismatch.

Vertical deformations

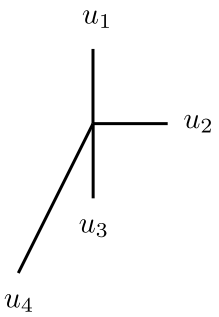

Figure 11: *The fan of the Hirzebruch surface* $\mathbb{F}_2$.

NS5-branes wrapping a curve C in the base B_2 that does not intersect the anti-canonical divisor are special. The reason is that the heterotic elliptic fibration is trivial over such a curve C: this follows as the discriminant locus is in the class $-K_{B_2}$, so does not intersect this curve C anywhere, and an elliptic surface S_C with no singular fibers is trivially fibered. Hence the brane sits in a subspace $S_C = T^2 \times C$. This fact is important because precisely these branes can move in the heterotic fiber direction, since any point in the T^2 can be specified holomorphically across the whole base region C. Summarising,

$$-K_{B_2} \cdot C = 0 \quad \Rightarrow \quad S_C = T^2 \times C \quad \Rightarrow \quad \text{'vertical' deformation possible}\,. \tag{4.119}$$

Such branes then have an additional single complex deformation modulus, in addition to any deformations within the base.[30]

As in the case of point-like NS5-branes in compactification to six dimensions, the fiber position of an NS5-brane is expected to be dual to a Ramond-Ramond modulus (in the IIB picture) on the F-theory side. In compactifications to four dimensions, the relevant moduli are counted by[31] [47, 94]

$$\text{No. of Ramond-Ramond moduli} \quad = \quad h^{2,1}(\hat{Y}_4) - h^{2,1}(\hat{\mathcal{B}}_3)\,. \tag{4.120}$$

This will be important for the discussion below. It is also why in Equation (4.107) we claimed the first condition is expected to imply the second.

Identifying the moduli

We now turn to identifying which heterotic chiral multiplets correspond to the 'extra' multiplets. In particular, we will use the example of a space with a Hirzebruch $\mathbb{F}_2$ base which we have

[30] We note that if C has genus zero, then by adjunction $C^2 = -2$ so while the brane can move in the fiber direction it is is rigid in B_2. However for higher genus, curves, $C^2 \geq 0$, so the brane can also be deformed in the base directions.

[31] This difference of Hodge numbers can also include Wilson line moduli on the D7-branes, arising from $(1,0)$-forms on the brane S. However these are not present in our cases, since S is diffeomorphic to B_2 and $b_1(B_2) = 0$.

discussed above. In this case there are two 'extra' chiral multiplets on the heterotic side. We now argue that specifically these are (i) one of the brane deformation moduli of the (-2)-branes in the fiber direction, and (ii) one of the complex structure deformations of the heterotic three-fold X_3. After establishing that these are the moduli involved in the apparent mismatch, we will discuss possible explanations.

We first discuss the brane deformation modulus. As discussed above, each vertical deformation modulus is expected to be dual to a Ramond-Ramond modulus, and in Equation (4.120) we recalled the F-theory count of the latter. However, when the heterotic base is $\mathbb{F}_2$ with a non-zero number of NS5-branes wrapping the (-2)-curve, the F-theory space is found to be missing an expected Ramond-Ramond modulus, that is

$$h^{2,1}(\hat{Y}_4) - h^{2,1}(\hat{\mathcal{B}}_3) = (\text{No. of branes on the } (-2)\text{-curve}) - 1\,. \tag{4.121}$$

We saw this already in the example given above: the final term on the right-hand side of Equation (4.118) gives 1 when from the heterotic NS5-brane content we would expect 2. Hence one of the moduli involved in the apparent mismatch is a modulus for the movement in the fiber direction of a horizontal NS5-brane wrapping a (-2)-curve.

Next we discuss the complex structure deformation. First we note that all even Hirzebruch surfaces differ only by complex structure [105]. In particular, a Hirzebruch surface $\mathbb{F}_n$ is a fiber product of $\mathbb{P}^1$ over $\mathbb{P}^1$, for which there are only two topologies. The $\mathbb{F}_n$ then fall into two classes: for even n the fiber product is trivial, while for odd n it is non-trivial. The remaining distinction is in complex structure: all $\mathbb{F}_{2n}$ are related by complex structure deformation, and similarly for $\mathbb{F}_{2n+1}$. The deformations change the set of effective curves.

In fact, $\mathbb{F}_2$ exists on a complex codimension one locus in the complex structure moduli space of $\mathbb{F}_0 = \mathbb{P}^1 \times \mathbb{P}^1$. This can be seen in a description of the deformation by an embedding. Consider the family of hypersurfaces S_t, in the ambient space $\mathcal{A} = \mathbb{P}^1 \times \mathbb{P}^2$,

$$S_t : \quad \{0 = x_0^2 y_1 - x_1^2 y_0 + t x_0 x_1 y_2\} \subset \mathcal{A}\,, \quad S_t \in \left[\begin{array}{c|c|c} \mathbb{P}^1 & 2 & [x_0, x_1] \\ \mathbb{P}^2 & 1 & [y_0, y_1, y_2] \end{array}\right]\,, \tag{4.122}$$

where $t \in \mathbb{C}$. It is not difficult to show [106] that this describes a $\mathbb{P}^1 \times \mathbb{P}^1$ for $t \neq 0$, while for $t = 0$ it describes an $\mathbb{F}_2$, and the family of hypersurfaces describes the complex structure deformation. The (-2)-curve in the $\mathbb{F}_2$ is given by $\{y_0 = y_1 = 0\} \subset S_0$.

The heterotic three-fold X_3 has an $\mathbb{F}_2$ base, so one available complex structure deformation of X_3 changes the base, leading to an elliptic fibration over a different base, $\mathbb{F}_0$. This deformation is also present in the F-theory four-fold $\hat{Y}_4$: this space is K3 fibered over $\mathbb{F}_2$, so one of the complex structure moduli corresponds to changing the base while preserving the K3 fibration. Or rather,

this is so until the base includes blow-ups over the (-2)-curve, corresponding to the presence of NS5-branes wrapping the (-2)-curve. In fact, one can check[32] that these blow-ups remove this deformation from $h^{3,1}(\hat{Y}_4)$,

$$\text{NS5-branes on } (-2)\text{-curve} \quad \Rightarrow \quad \text{F-theory deformation } \mathbb{F}_2 \to \mathbb{F}_0 \text{ lost from } h^{3,1}(\hat{Y}_4)\,. \quad (4.123)$$

Hence one of the heterotic moduli involved in the chiral multiplet mismatch is the analogous non-polynomial complex structure deformation of the heterotic space X_3, taking the base B_2 from $\mathbb{F}_2$ to $\mathbb{F}_0$. (Since on both sides this deformation concerns the space B_2, we expect these deformation moduli to be simply matched.)

Likely explanation for the mismatch

We have now identified which heterotic moduli contribute in the apparent overabundance of heterotic chiral multiplets in the example discussed around Equation (4.118): one is the complex structure deformation which takes the heterotic base from $\mathbb{F}_2$ to $\mathbb{F}_0$, and the other is a modulus for the vertical movement of a horizontal NS5-brane which wraps a (-2)-curve in the $\mathbb{F}_2$ base. The next question is the reason for the discrepancy. We will first discuss the complex structure modulus, which is most easily accounted for, and then we will turn to the more difficult case of the modulus for vertical movement of an NS5-brane.

We will now argue that the complex structure deformation of the heterotic space X_3 that takes the base B_2 from $\mathbb{F}_2$ to $\mathbb{F}_0$ is in fact massive, which will account for half of the discrepancy. This deformation takes the heterotic base from an $\mathbb{F}_2$ to an $\mathbb{F}_0$. The key point is that in this deformation, the (-2)-curve ceases to be holomorphic. This is clear since in $\mathbb{P}^1 \times \mathbb{P}^1$, the Mori cone is spanned by the hyperplane classes H_1 and H_2, and a (-2)-curve must be in a class $\pm(H_1 - H_2)$, which is not effective. If an NS5-brane wraps the (-2)-curve, then in the deformation its embedding could not remain holomorphic, and hence this deformation would break supersymmetry. We can hence conclude that when a brane wraps the (-2)-curve, as in the situation under discussion, the complex structure deformation taking $\mathbb{F}_2$ to $\mathbb{P}^1 \times \mathbb{P}^1$ is obstructed. Hence this modulus is massive.

The other extra heterotic chiral multiplet is more difficult to understand. In particular we now argue that, unlike in the previous case, it is not that this multiplet is secretly massive, but rather that an extra F-theory modulus is secretly massless, in particular in the stable degeneration limit, where our description is valid. This other heterotic chiral multiplet corresponds to the

[32]The deformation of the two-fold base of $\hat{Y}_4$ is seen in the toric description as a non-polynomial deformation. One can then check that indeed precisely one of these non-polynomial deformations is lost upon the blow-up.

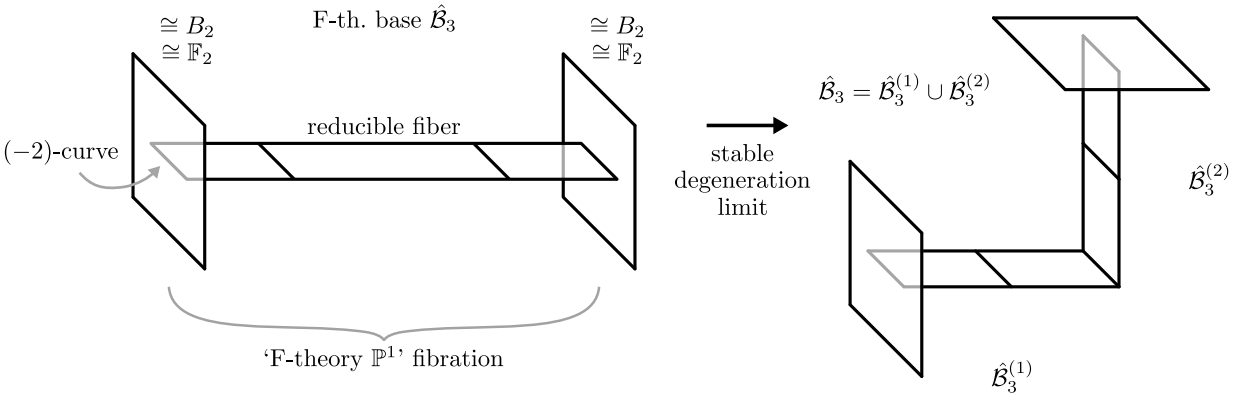

Figure 12: *Base $\hat{\mathcal{B}}_3$ of the F-theory four-fold $\hat{Y}_4$ in the stable degeneration limit, in the case where blow-ups have been performed over a (-2)-curve in the E_8 surfaces, which corresponds to NS5-branes wrapping the (-2)-curve in the heterotic base $B_2 = \mathbb{F}_2$. In the $\mathbb{P}^1$ fibration, only the reducible fibers over the (-2)-curve have been shown, for simplicity.*

deformation in the fiber direction of one of the horizontal NS5-branes wrapping a (-2)-curve in B_2, or rather some combination of all such deformations for all such NS5-brane. This appears to be a collective effect, rather than an effect for each brane, despite these branes being generically separated in the bulk. While this is reminiscent of the decoupling of a centre-of-mass mode, we do not believe it can be explained this way. In particular, we cannot mod out by isometries along the constant fiber over the (-2)-curve in B_2, as these cannot lift to isometries of X_3. Hence we expect the physical spectrum to depend on the 'distance' of the NS5-branes from the zero section and to contain states which are sensitive to the positions of the NS5-branes.

A possible explanation for the discrepancy is that the corresponding modulus in F-theory becomes massless in the stable degeneration limit. As discussed in Section 4.2.2, only in this limit do we have control over the various possible corrections to the simple supergravity theories that we have been primarily working with on both sides of the duality. If an F-theory modulus does become massless in this limit, then the discrepancy is resolved in the region of moduli space where our description is valid. Further, we may expect that the corresponding heterotic modulus is lifted by one of these corrections away from the stable degeneration limit.

We will now give a plausibility argument that indeed an F-theory modulus appears to become massless in the stable degeneration limit. First we consider the situation before we have taken the limit, and where on the heterotic side $N \geq 2$ NS5-branes wrap the (-2)-curve in the base $B_2 = \mathbb{F}_2$. In the F-theory dual, N blow-ups have been performed in the F-theory base $\hat{\mathcal{B}}_3$, over either of the (-2)-curves sitting in the two E_8 surfaces. This gives a reducible fiber of the $\mathbb{P}^1$ fibration, with $N+1$ $\mathbb{P}^1$ components, over each point on these (-2)-curves. These form $N+1$ exceptional divisors. This situation is depicted on the left of Figure 12. While the

divisors formed by the two 'end' components of the fiber (times the (-2)-curve) touch the E_8 surfaces and hence intersect the anti-canonical divisor $-K_{\hat{\mathcal{B}}_3}$, one can check that the other $N-1$ exceptional divisors do not. Hence the elliptic fibration of $\hat{Y}_4$ is trivial over these divisors in the base $\hat{\mathcal{B}}_3$. By taking the pullback to $\hat{Y}_4$ of the (1,1)-form corresponding to one of these exceptional divisors and wedging with a (1,0)- or (0,1)-form in the elliptic curve over the divisor, one obtains contributions to $h^{2,1}(\hat{Y}_4)$ and $h^{1,2}(\hat{Y}_4)$. These are the Ramond-Ramond moduli contributions. We can immediately see why this contribution to $h^{2,1}(\hat{Y}_4)$ does not match the number required to match the moduli of the NS5-branes, since we have introduced N NS5-branes but only $N-1$ Ramond-Ramond moduli.

In the stable degeneration limit, the F-theory base $\hat{\mathcal{B}}_3$ splits into two components, $\hat{\mathcal{B}}_3 = \hat{\mathcal{B}}_3^{(1)} \cup \hat{\mathcal{B}}_3^{(2)}$. The cohomology of the degenerated space can be computed from those of the two components by using the Clemens-Schmid exact sequence. (See Ref. [107] for more information on this exact sequence, and for example Ref. [43] for a description of its use in the stable degeneration limit of heterotic/F-theory duality.) A full computation is beyond our present scope; instead we confine ourselves to a plausibility argument for the existence of a single extra contribution to $h^{2,1}(\hat{Y}_4)$ in this limit. As the base has split into two components, exactly one of the N exceptional divisors over the (-2)-curve in the base $\hat{\mathcal{B}}_3$ is separated into two pieces in the degeneration. This situation is depicted on the right of Figure 12. Hence in the sum of cohomologies of $\hat{Y}_4^{(1)}$ or $\hat{Y}_4^{(2)}$, there exists an extra $(2,1)$-form constructed as above from the trivial elliptic fibration over the exceptional divisors being discussed. This brings the total number of such contributions to $h^{2,1}(\hat{Y}_4)$ up to N, matching those required for the corresponding NS5-brane moduli. We note that in the Clemens-Schmid exact sequence it is possible that this differential form will not contribute to $h^{2,1}(\hat{Y}_4)$ because of cohomological equivalences, and one would have to perform the full computation to check this.

This completes our discussion of the apparent chiral multiplet mismatch in Equation (4.118) for the example of a heterotic base $B_2 = \mathbb{F}_2$. We argued that one of the extra heterotic multiplets is actually massive. For the other, we were not able to find a source for the mass, however we have argued that it is plausible that an extra F-theory chiral multiplet becomes massless in the stable degeneration limit. We expect that all cases involving horizontal NS5-branes wrapping curves C with $-K_{B_2} \cdot C = 0$ can be treated in this way, not only the Hirzebruch $\mathbb{F}_2$ case used as an example here. We also emphasise that these cases are in some sense a higher order effect, with a large set of examples already within the remit of the proof in Section 4.4.5.

4.5 Coincident and intersecting NS5-/M5-branes

In Section 4.4 above, we have constructed global F-theory models dual to heterotic line bundle models. In this context we also discussed various configurations of horizontal NS5-branes. One can consider transitions between these configurations, passing through situations with intersecting branes. It is interesting to translate the various stages of these transitions into their dual descriptions as global F-theory models. This seems particularly tractable in the present context of heterotic line bundle models, since the F-theory geometries before transition are relatively simple. We also note that the effective four-dimensional theory of coincident or intersecting NS5-branes is not so well-understood. The F-theory duals provide another perspective on these theories and their various branches, so it may prove useful to present the details of these dual models.

We will first review what is known about the local geometry dual to coincident or intersecting horizontal NS5-branes, before considering their embedding into the global models we have discussed, where we will detail the correspondence between aspects of the horizontal NS5-brane configurations and the toric descriptions of the F-theory base. Finally we will make some comments on the effective field theories through the transitions. The theory on further compactification to three dimensions is most tractable, and we review the recent literature on such M-theory compactifications, connecting this to the brane transition picture.

Before turning to this discussion, we make three preliminary remarks. First, we assume that all horizontal NS5-branes are embedded by the unique section in the elliptic fibration of X_3, as discussed in Section 4.4.1. Second, we will not discuss the blow-ups of the remaining E_8 singularities, since these are away from the blow-ups dual to the horizontal NS5-branes, and hence do not play a role here. Third, we will simply say 'NS5-brane' when we mean horizontal NS5-brane, as we will not discuss vertical NS5-branes[33].

4.5.1 Branches in NS5-brane transitions

We first briefly discuss the situation in heterotic string theory, in particular possible sets of NS5-brane configurations connected by a transition. We consider a set of M5-branes at the same position in the 11d bulk, so that they sit in the same CY three-fold. This set of branes can have a complicated configuration, perhaps with point-like or curve-like intersections. We can imagine

[33] We recall the dual of a vertical NS5-brane is a D3-brane, so that the dual of a set of coincident vertical NS5-branes is a stack of D3-branes. One can also consider the intersection of a vertical and a horizontal NS5-brane, which is an interesting question, discussed in e.g. Ref. [45], but one that we do not attempt to discuss here. We hope to discuss this question in future work.

the collection of nearby possible configurations, some of which eliminate intersections. We will consider two particular situations for simplicity: (i) a configuration with a set of point-like intersections, and (ii) a configuration with a stack of completely coincident branes. In principle both can occur in the same configuration.

We first consider the collection of configurations around a transverse-intersection case. There exists an 11d 'resolution' branch, in which the M5-branes are separated in the 11d bulk, and often also a 'deformation' branch in which the equations describing the branes in the heterotic base B_2 are deformed to remove the intersection. These situations are shown schematically in an illustrative example in Figure 13. In this example the heterotic base is $B_2 = \mathbb{P}^1 \times \mathbb{P}^1$, and we have considered bringing together just two of the M5-branes, each of which wraps a $\mathbb{P}^1$ in the $\mathbb{P}^1 \times \mathbb{P}^1$. We note in passing that these branes cannot be made to coincide, so this does not form a possible configuration in a deformation of coincident branes.

We next consider the collection of configurations related to a stack of completely coincident branes. Again there is an 11d resolution branch, as well as a deformation branch. These possibilities are shown schematically in an illustrative example in Figure 14. In this example the heterotic base is $B_2 = \mathbb{P}^2$, and we have considered bringing together just three of the M5-branes, each of which wraps a $\mathbb{P}^1$ in the $\mathbb{P}^2$. In this example, shifting the branes in the CY manifold, giving a 'partial' deformation, leaves transverse-intersections, and there also exists a full deformation branch where there is a single connected brane.

There may be many interesting possibilities differing in some way from these examples. One such possibility is shown in Figure 15. Here shifting the branes in the CY manifold removes all intersections, giving a set of disconnected branes. However there exists no deformation to a connected smooth brane. We do not claim to be exhaustive by the possibilities we have discussed. We also note that, as seen in Figures 13 and 15, not all coincident cases and not all transverse-intersection cases occur in the collection of configurations connected to the other case. We see that when the two do occur in the same collection, as in Figure 14, it is possible to move between the 11d resolution and the deformation branch by passing through either one of the coincident or transverse-intersection configurations.

In addition to M5-branes that can be deformed only within the base B_2, there exist a special set of branes wrapping curves C in B_2 such that $-K_{B_2} \cdot C = 0$, which can also move in the heterotic fiber direction as discussed in Section 4.4.6. These fiber positions correspond on the F-theory side to Ramond-Ramond moduli (in the IIB picture), rather than to geometry as is the case for base positions. We will not treat this part of moduli space in this section, instead

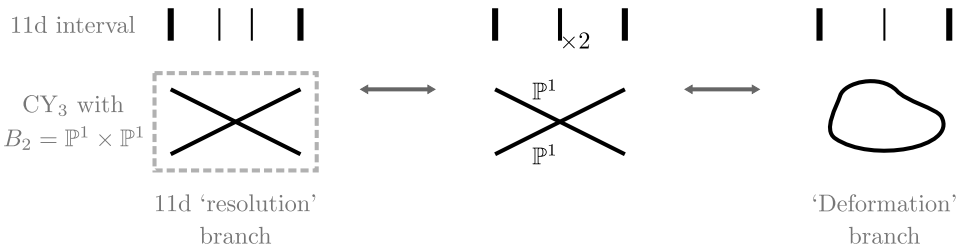

Figure 13: *Schematic depiction of transversely-intersecting M5-branes and the 'branches' that remove the intersection, as discussed in the main text. In this example, the heterotic base is* $B_2 = \mathbb{P}^1 \times \mathbb{P}^1$*, and two* $\mathbb{P}^1$ *M5-branes sit at for example* $u_1 = 0$ *and* $v_1 = 0$ *in* B_2*.*

restricting ourselves to deformations of M5-branes in the base B_2, and the corresponding F-theory geometry.

We note that upon restricting to base deformations alone, some intersecting or coincident brane situations involving curves C with $-K_{B_2} \cdot C = 0$ cannot be deformed to remove the intersection/coincidence. Recall that for supersymmetric branes the embedding is holomorphic, so only algebraic deformations preserve supersymmetry. In the Hirzebruch space $\mathbb{F}_2$ with weight system

$$\mathbb{F}_2 : \begin{array}{cccc} x & y & z & w \\ \hline 1 & 1 & 0 & 0 \\ 2 & 0 & 1 & 1 \end{array} , \tag{4.124}$$

the transverse-intersection given by $yw = 0$ cannot be deformed away: the general curve in this divisor class is $0 = y(az + bw)$ which preserves the intersection. Similarly the coincident brane situation given by $y^2 = 0$ has no deformations.

4.5.2 Review of local dual F-theory geometry

We now review the known local F-theory geometries dual to coincident or transversely-intersecting NS5-branes.

Coincident case

We first review the case of coincident NS5-branes. These are M5-branes in the Hořava-Witten picture wrapping the same curve in the base B_2 of the CY manifold X_3, and which are also at the same position in the 11d bulk. We consider the case of two coincident M5-branes, as the story with N branes is a straightforward generalisation. It is known [4, 45, 54, 63] that in the F-theory dual of this situation, a singular locus appears in the four-fold $\hat{Y}_4$: this locus consists of a complex surface in the four-fold $\hat{Y}_4$, which arises due to the appearance of a complex curve of singularities in the F-theory base $\hat{\mathcal{B}}_3$.

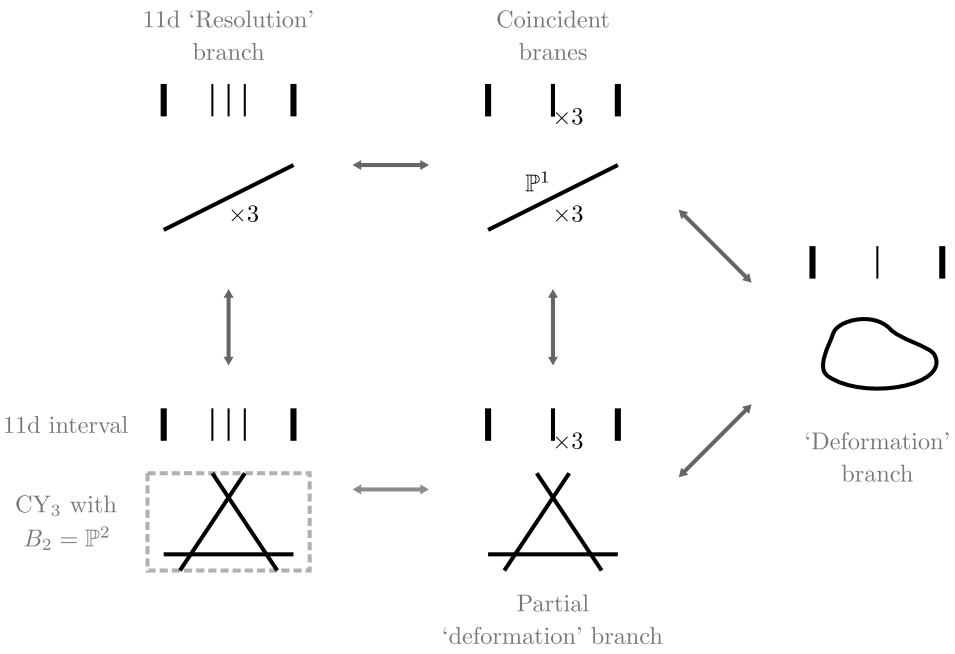

Figure 14: *Schematic depiction of coincident M5-branes and the 'branches' that remove the coincidence, as discussed in the main text. In this example, the heterotic base is* $B_2 = \mathbb{P}^2_u$*. In the coincident situation, three* $\mathbb{P}^1$ *M5-branes sit all at for example* $u_1 = 0$ *in* B_2*, while in the transverse-intersection case they are at for example* $u_1 = 0$*,* $u_2 = 0$*, and* $u_3 = 0$ *in* B_2*.*

The appearance of this curve of singularities in $\hat{\mathcal{B}}_3$ can be understood by bringing together branes with distinct positions in the 11d bulk. We recall that the blow-ups of the F-theory base correspond to the introduction of M5-branes as we pull instantons off the E_8 branes in the Hořava-Witten picture. Additionally, Kähler moduli associated to the blow-ups correspond to the positions in the 11d bulk of the M5-branes. As we bring two M5-branes together in the bulk, in the F-theory geometry we move to an edge of the Kähler cone[34], and a divisor collapses to zero volume. The curve of singularities in the base is the image of the base divisor under the blow-down, and corresponds to the coincident M5-branes. The situation before the blow-down is shown schematically in the middle of Figure 16a. Here all the exceptional divisors have finite size, and as the M5-branes are brought together the Kähler moduli are tuned so that one divisor shrinks to zero size. As a result a complex curve of A_1 singularities appears in the base, which corresponds to a complex surface of A_1 singularities in the four-fold. In the case of N coincident M5-branes, the singularity is A_{N-1}.

Often there will exist deformations of these singularities that are dual to deformations of the stack of NS5-branes in the heterotic base B_2 into a single connected NS5-brane. This branch

[34] Actually, in order to blow-down the divisor we will have to first flop the four-fold, passing into another Kähler cone on whose boundary the desired divisor can be blown-down. This is analogous to the discussion at the end of Section 4.3.2.

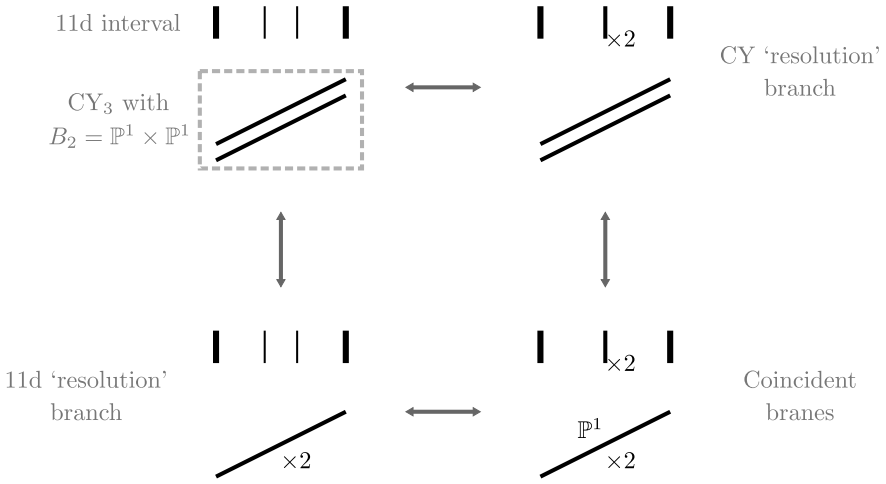

Figure 15: *Schematic depiction of coincident M5-branes and the 'branches' that remove the coincidence, as discussed in the main text. In this example, the heterotic base is* $B_2 = \mathbb{P}^1_u \times \mathbb{P}^1_v$. *In the coincident situation, two* $\mathbb{P}^1$ *M5-branes sit at for example* $u_1 = 0$ *in* B_2. *Deformation to a single smooth brane is impossible, with general deformations giving separated branes.*

is depicted schematically in the right of Figure 16a. The resulting structure of reducible fibers in this branch reflects the fact that we now have on the heterotic side a single brane, usually of higher genus, with some position in the 11d interval. As noted above in Section 4.5.1, in the M5-brane configuration it can happen that (i) base deformation results in multiple branes, or (ii) base deformation is not possible. The former case occurs in Figure 15; the dual F-theory deformation branch will simply shift the two exceptional divisors rather than combine them. In the latter case, there must not exist deformations of the singularity.

Transverse-intersection case

Next we review the F-theory dual of transversely-intersecting horizontal NS5-branes. These are M5-branes at the same position in the 11d bulk and wrapping transversely-intersecting curves in the base B_2 of the CY manifold X_3. We review the case of two transversely-intersecting M5-branes, with a single intersection point, as the story with N branes and/or multiple intersection points is a straightforward generalisation. As also discussed in Ref. [45], the F-theory dual of this situation contains conifold singularities in the base $\hat{\mathcal{B}}_3$, giving rise to complex curves of singularities in the four-fold $\hat{Y}_4$.

We can imagine reaching this situation by bringing together branes with distinct positions in the 11d bulk. This discussion is very analogous to that for coincident M5-branes above. However in this case, as the F-theory Kähler moduli are tuned to the edge of the Kähler cone, a curve in the base collapses to zero volume, rather than a divisor. This situation is shown schematically in the left and middle of Figure 16b. The result is a point-like A_1 singularity

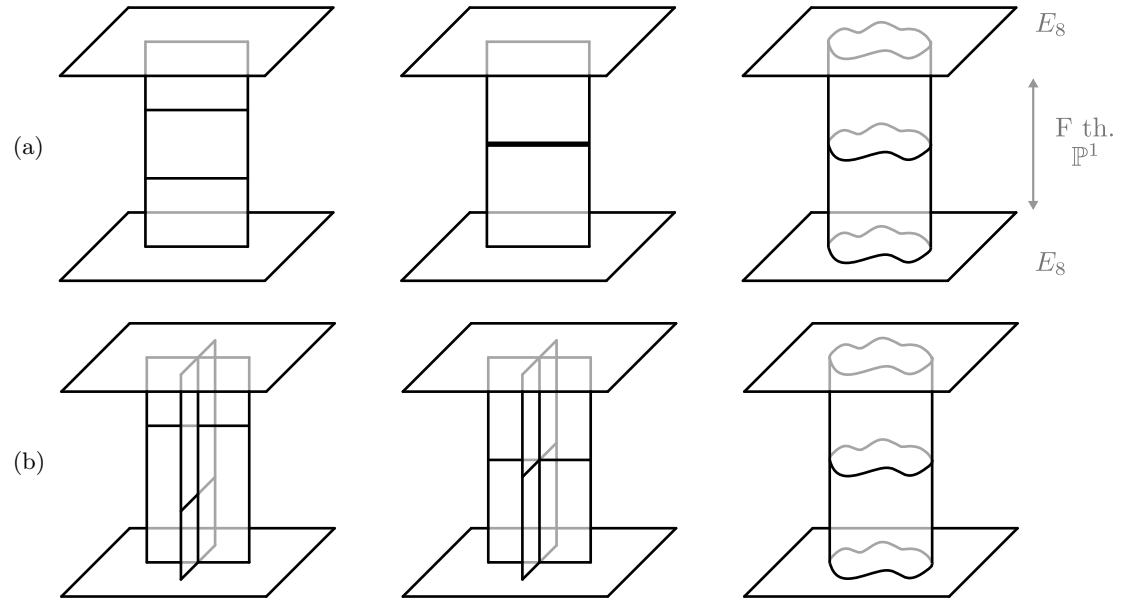

Figure 16: *A schematic depiction of the geometry in the base $\hat{\mathcal{B}}_3$ of the F-theory four-fold $\hat{Y}_4$, when in the dual geometry we pass through a situation with (a) coincident horizontal M5-branes and (b) transversely-intersecting horizontal M5-branes. In each case on the left is the resolved side, in the middle the singular situation, and on the right the deformed side. We have shown only those fibers that have multiple components; the other fibers remain $\mathbb{P}^1$s.*

in the base, giving a curve of A_1 singularities in the four-fold. In the case of N coincident M5-branes, the singularity is A_{N-1}. If there are multiple transverse-intersections then there are multiple conifold singularities.

As in the case of coincident branes, in the situation of transversely-intersecting branes there will often exist deformations of the singularity in the F-theory base $\hat{\mathcal{B}}_3$ that are dual to deformations of the NS5-branes in the heterotic base B_2 that give rise to a single connected NS5-brane. This branch is depicted schematically in the right of Figure 16b. Again the resulting structure of reducible fibers reflects the fact that we now have on the heterotic side a single brane. As noted above in Section 4.5.1, sometimes it is not possible to deform the branes in the base B_2 at all. In this case, the corresponding F-theory singularity must be non-deformable.

4.5.3 Global dual F-theory geometry

We now discuss how the local singular geometry dual to intersecting or coincident NS5-branes fits into the global F-theory models that we have constructed. The result will be a toric description of the F-theory four-folds dual to heterotic line bundle models with intersecting or coincident NS5-branes and the surrounding brane configurations. Note that we will mainly discuss the F-theory base rather than the four-fold itself, but the F-theory four-fold is constructed by taking an elliptic fibration, and hence the fan of the ambient space for the four-fold is implicitly specified

at each stage[35].

We first discuss the simplest global models, where the F-theory base is described by a toric fan. Here the four-fold is a toric hypersurface in a 5d toric ambient space, as opposed to a higher codimension complete intersection. Examples of these situations were shown in Figures 8 and 9. In the corresponding heterotic situation, there are a set of NS5-branes multiply wrapping $\mathbb{P}^1$s, and each brane has a distinct position in the bulk. We first discuss bringing two or more of these branes together by tuning their bulk positions. This may give rise to point-like or curve-like intersections between the branes. It will be simplest to first discuss the resolution branch and singular situation together, and then turn to the deformation branch.

Resolution branch

As reviewed in Section 4.5.2 above, transversely-intersecting NS5-branes are dual to point-like singularities in the F-theory base, while coincident NS5-branes are dual to curve-like singularities in the F-theory base. If the three-fold base is described away from the singular situation by a three-dimensional fan, then point-like singularities can arise when a 1d face is deleted in a 2d face, while curve-like singularities can arise when we blow down a ray. The resulting fan will describe the global singular F-theory geometry.

We consider as a first example the F-theory base shown on the right of Figure 9. In this example, the heterotic base B_2 is a $\mathbb{P}^2$, with all NS5-branes wrapping $\mathbb{P}^1$s at $u_3 = 0$. Correspondingly all blow-ups of $\hat{\mathcal{B}}_3$ are at $u_3 = 0$. The volumes of these exceptional divisors correspond to distances between M5-branes in the bulk. Hence we can think of the gaps between the blow-up rays ε_i as corresponding to the NS5-branes, and removing one of the blow-up rays ε_i joins two gaps reflecting the fact that two M5-branes have been brought together. This creates a curve of singularities at the intersection of the divisors ε_{i-1} and ε_{i+1}, where $\varepsilon_0 \equiv u_3$. An illustration of the triangulations before and after removal of a ray is shown in Figure 17. In general one can remove N internal blow-up rays to bring together $N+1$ NS5-branes, giving rise to an A_N singularity. We note that blowing down the rays at the top and bottom of the tower does not correspond to bringing NS5-branes together; rather this corresponds to putting NS5-branes back onto one of the E_8 branes at the ends of the 11d interval.

As a second example, consider the F-theory base shown in Figure 8. In this example the heterotic base B_2 is a $\mathbb{P}^1 \times \mathbb{P}^1$, and the NS5-branes sit in two stacks at $u_1 = 0$ and $v_1 = 0$. The gaps between the blow-up rays over u_1 and v_1 correspond to the NS5-branes at $u_1 = 0$ and

[35]Note when we discuss blowing down, this requires flops of the four-fold. After flopping but before blowing down the elliptic fibration is lost. (See the discussion in Section 4.3.2.)

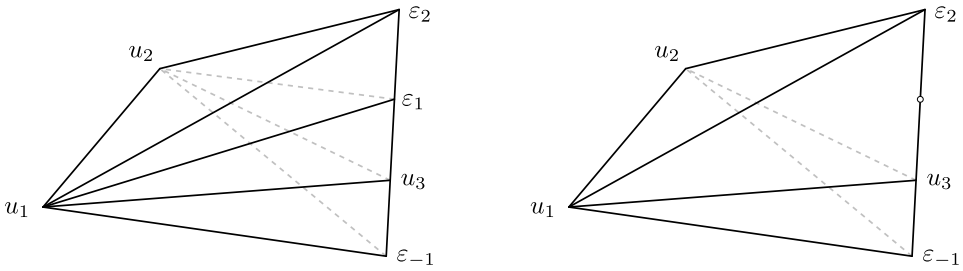

Figure 17: *Part of the triangulation of the ray system on the right of Figure 9 for the F-theory base $\hat{\mathcal{B}}_3$ when the heterotic base B_2 is a $\mathbb{P}^2$ with a particular NS5-brane configuration, in the situation before and after a removal of one of the blow-up rays. The result corresponds to a situation with two coincident NS5-branes, and gives rise to a curve of singularities.*

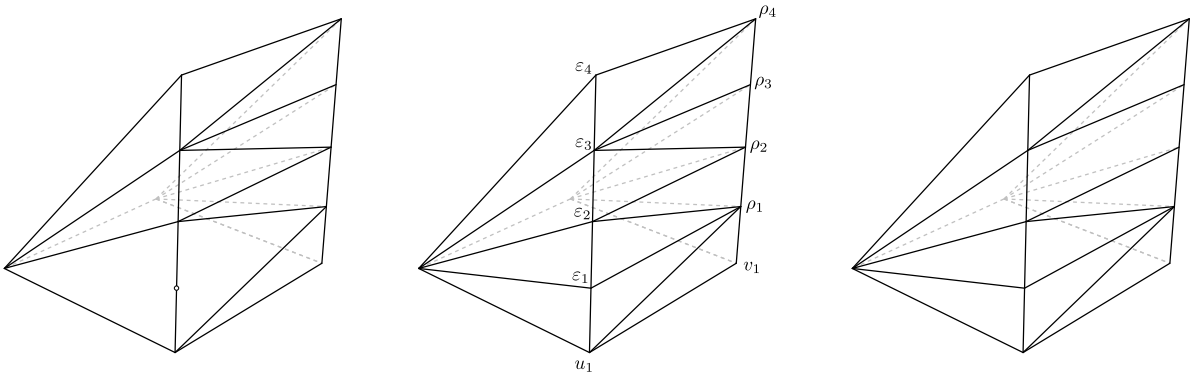

Figure 18: *Part of the triangulation of the ray system in Figure 8 for the F-theory base $\hat{\mathcal{B}}_3$ when the heterotic base B_2 is a $\mathbb{P}^1 \times \mathbb{P}^1$ with a particular NS5-brane configuration, in (centre) the non-singular situation, (left) after a removal of one of the blow-up rays to give coincident NS5-branes, and (right) after removing a 1d face to give transversely-intersecting NS5-branes.*

$v_1 = 0$ respectively. Removing a ray corresponds to bringing branes into coincidence, creating a curve of singularities in $\hat{\mathcal{B}}_3$. However there is also the possibility of transversely-intersecting branes, in contrast to the previous example. Thinking of the gaps between the blow-up rays as the M5-branes, we can bring a u_1 and a v_1 brane together in the bulk by removing a 1d face that separates a gap in one blow-up tower with a gap in the other. This creates a point-like singularity as expected from the dual picture. Figure 18 illustrates the triangulations after a ray has been removed and after a 1d face has been removed.

Choosing a different triangulation of the N-lattice polytope Δ^*, which translates to a different choice of fan for the base employing the same rays, corresponds to a different ordering of the M5-branes in the bulk. It is clear that only particular gaps in the two towers of blow-up rays can be connected to one another by removing a single 1d face. It is also clear that only particular rays can be removed while leaving a triangulation of the remaining polytope: for example, in the initial triangulation in Figure 18, we were able to blow down ε_1, but we could not have

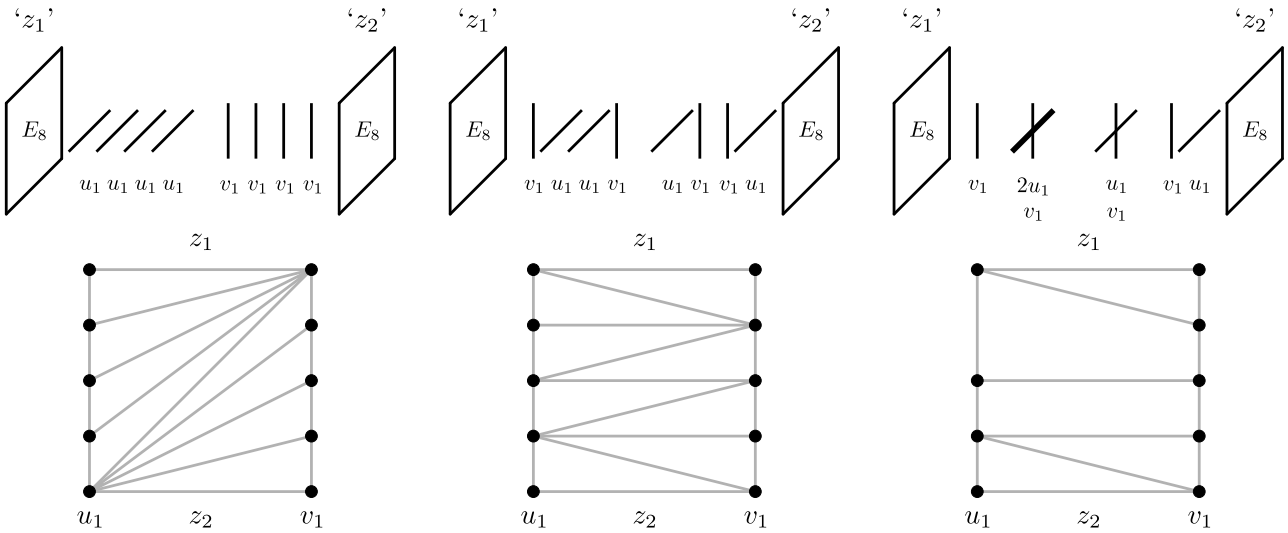

Figure 19: *Examples of the correspondence between the positions of the horizontal M5-branes in the bulk and triangulations of the '$u_1 - v_1$' face of the ray system in Figure 8 for the F-theory base $\hat{\mathcal{B}}_3$ when $B_2 = \mathbb{P}^1 \times \mathbb{P}^1$. In the example on the right, there are intersecting and coincident branes. Here we have included only 8 blow-ups rather than the full 24 for simplicity of the diagrams.*

blown-down for example ρ_1, as the result would not be a triangulation. Hence it is clear that the triangulation reflects the ordering of the M5-branes in the 11d interval, since it reflects which branes can be brought into contact with one another. Figure 19 shows some examples of the correspondence between orderings of M5-branes in the bulk and triangulations of the F-theory base space, for the example of a heterotic base $\mathbb{P}^1 \times \mathbb{P}^1$ with a particular blow-up pattern. For clarity we only show a subset of the branes, or equivalently only part of the triangulation. For any toric hypersurface example, there is a more complicated but analogous relation between triangulation and ordering of branes in the bulk.

Deformation branch

We have so far discussed singularities in the F-theory four-fold from the perspective of the resolution branch, as we collapse divisors and curves in $\hat{\mathcal{B}}_3$. We now discuss the deformation branch, in particular its toric description, which then will complete the picture of the global F-theory geometry dual to intersecting or coincident NS5-brane situations in heterotic line bundle models. We note the four-folds we have so far considered are toric hypersurfaces, which give the simplest global models from the perspective of toric geometry, and correspondingly are dual to particularly simple dual NS5-brane configurations. Once we have described the deformation branches of singularities in these cases, we have described the dual to complicated brane configurations anywhere in the 11d interval. One can then discuss singularities arising from bringing these branes together, and their deformation branches.

In the deformation branch, the singularity is removed by complex structure deformation, dual to deformations of the NS5-branes in the heterotic base B_2. We recall that if the N M5-branes, which are to be combined and deformed, are 'nearest' to an E_8 brane in the bulk, i.e. there are no branes between them and an end of the 11d interval, the deformation branch can be described torically as in Section 4.4.3. There we blew down n_i of the rays at the top of each i^{th} 'tower' of blow-up rays, over a ray u_i of B_2, before blowing up over a general curve in the curve class $\sum_i n_i[u_i]$ on $\{z_1 = 0\}$. On the heterotic side this corresponds to transforming the N branes back into small instantons on an E_8 brane, and then pulling out a single smooth M5-brane. This roundabout way of getting to the deformation branch misses the intermediate stage of coincident branes in the bulk, but must give the correct final description. More generally, if M5-branes have been brought together away from an E_8 brane, i.e. there are branes between them and the E_8 brane, then we could blow down also the rays corresponding to the intervening branes. We would then blow up first on the curve of the desired deformed brane, then sequentially on the curves of the branes that intervened between the brane stack and the E_8. To put this another way, since we have seen that changing the order of branes in the bulk corresponds to flops, we could also reach this situation by building the general brane configuration near an E_8 brane and then flopping until it is in the right position.

This is easier to visualise in compactification to six dimensions. We recall the toric bases in Figure 7. To describe the deformation branch when n of the point-like M5-branes come together in the bulk near an E_8 brane, we can blow down the top n rays over $u_1 = 0$ for example. We then extend the 2d fan of the base into 3d by adding an auxiliary ray $\vec{\xi}$, putting $\vec{u}_2$ at $-n$ in the new direction. We then add a blow-up ray at

$$\vec{\zeta} = \vec{\xi} + \vec{z}_1 \,. \tag{4.125}$$

(More precisely, at $\vec{\zeta} = \vec{\xi} + \vec{z}_1 + 2\vec{x} + 3\vec{y}$ in the 5d fan.) The two-fold base is then a hypersurface in a 3d ambient space, whose fan is shown schematically in the left of Figure 20. In this example we have only included one blow-up ray ε_1 for simplicity.

Clearly we may flop the triangulation of the $(\varepsilon_1, u_1, \xi, \zeta)$ face of the polytope. This corresponds to altering the ordering of M5-branes in the bulk, specifically bringing the 'deformed'[36] brane away from an E_8 brane, leaving an ε_1 brane in between. This is clear as in each triangulation, precisely one of ε_1 and ζ can be blown-down, reflecting which is nearest the E_8 brane.[37] The situation with multiple blow-up rays ε_i is an obvious generalisation. The situation

[36]The 'deformed' brane is a set of points, so that deformations are not very interesting in compactification to six dimensions.

[37]Of course, the singularity appearing during the flop should generically miss the hypersurface, intersecting it

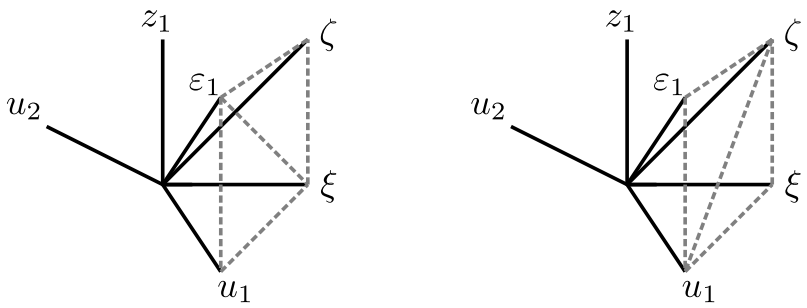

Figure 20: *Part of the triangulations giving the toric ambient space for the two-fold F-theory base in compactification to 6d for a situation in which we have included arbitrarily placed M5-branes through the blow-up ζ. In the triangulation on the left, the blow-up ζ is performed after ε_1, while on the right ζ is included first and then ε_1. The two situations are related by a flop, and correspond to different orderings of M5-branes in the 11d bulk.*

in compactification to four dimensions is clearly analogous, though more difficult to visualise. To include multiple arbitrary M5-branes will require going to higher codimension in the toric descriptions. The details of the fan associated with a choice of triangulation again reflect which of these branes can come into contact in the 11d bulk.

Finally we note one other global aspect of these singular transitions: the Euler characteristic is unchanged. This follows from the computation of the Euler characteristic in Section 4.4.4. This computation was independent of the precise NS5-brane configuration, and hence the Euler characteristic is unchanged under a singular transition dual to a transition between NS5-brane configurations. We note this means that after such a transition, there is no need to include extra G_4 flux to meet the anomaly condition. All of this is clear from the heterotic side as the overall class of NS5-branes remains unchanged.

4.5.4 Comments on effective theory through transition

In Section 4.4, we have described the field content in the various branches of a transition between NS5-brane configurations, but we have not attempted a description of the theory in the situation with coincident or transversely-intersecting branes. The coincident case is particularly interesting, and historically has been challenging to describe. We note that on the resolved side we have a gauge group $\mathrm{U}(1)^{g\cdot N}$, and on the deformed side a gauge group $\mathrm{U}(1)^{g_{\mathrm{def}}}$, where g and g_{def} are the genera of the branes in the stack and the deformed brane respectively. It is difficult to see how to understand in gauge field theory terms an enhancement to $\mathrm{SU}(N)$ at the coincident point. This is however not problematic since the intermediate theory is not expected

only when the hypersurface is tuned in a way that corresponds to the ε_1 and ζ branes being at the same position in the heterotic base.

to have a description in terms of a gauge theory. Instead, the four-dimensional theory will be a dimensional-reduction of a six-dimensional theory in which there will be tensionless strings arising from M2-branes stretching between two NS5-branes [68] or an NS5-brane and an E_8 brane [69, 70]. These strings are known as M- and E-strings, respectively.

It is beyond the scope of the present work to give a description of the four-dimensional theory obtained from compactifying F-theory on a four-fold with a curve of singularities in the base. Instead, we will confine ourselves to a study of the three-dimensional theory obtained from compactifying M-theory on the same four-fold. The advantage is that in the three-dimensional theory we have a bona fide gauge theory and avoid the subtleties coming with tensionless strings. This three-dimensional theory is then expected to lift to the four-dimensional theory. The three-dimensional resolution and deformation branches of M-theory on the smooth four-folds on either side of the singular transition have a straightforward description. Again, at the transition point, the M-theory four-fold develops a surface of singularities, whose field theory description is more difficult. However, this has been investigated recently in Ref. [108] and we can use their results to study the theory. The resulting correspondence may provide a useful perspective on the four-dimensional theories.

Lifting M-theory to F-theory

We first recall the field content of M-theory on a non-singular CY four-fold, and its lift to F-theory. This three-dimensional theory has $\mathcal{N} = 2$ supersymmetry, so there is a chiral multiplet and a vector multiplet, with all multiplets equivalent on shell, containing two real scalar fields and a Majorana spinor. The numbers of three-dimensional chiral multiplets $n_{\text{ch.}}$ and vector multiplets $n_{\text{vec.}}$ are

$$n_{\text{ch.}} = h^{2,1}(\hat{Y}_4) + h^{3,1}(\hat{Y}_4)\,, \quad n_{\text{vec.}} = h^{1,1}(\hat{Y}_4)\,. \tag{4.126}$$

When the four-fold is K3 fibered this theory is related by a 'lift' to the four-dimensional theory from F-theory, in which roughly the elliptic fibers are collapsed resulting in an effective extra

dimension after T-duality. In this lift the multiplets are mapped as follows [94],

$$h^{1,1}(\hat{Y}_4) \text{ 3d vector multiplets} \to \begin{cases} h^{1,1}(\hat{Y}_4) - h^{1,1}(\hat{\mathcal{B}}_3) - 1 \text{ 4d vector multiplets} \\ h^{1,1}(\hat{\mathcal{B}}_3) \text{ 4d chiral multiplets} \\ \text{metric of new non-compact direction} \end{cases}, \tag{4.127}$$

$$h^{2,1}(\hat{Y}_4) + h^{3,1}(\hat{Y}_4) \text{ 3d chiral multiplets} \to \begin{cases} h^{2,1}(\hat{\mathcal{B}}_3) \text{ 4d vector multiplets} \\ h^{2,1}(\hat{Y}_4) - h^{2,1}(\hat{\mathcal{B}}_3) \text{ 4d chiral multiplets} \\ h^{3,1}(\hat{Y}_4) \text{ 4d chiral multiplets} \end{cases}. \tag{4.128}$$

In the smooth resolution[38] or deformation branch of a singularity, these results give the lift of the three-dimensional matter content to four dimensions. We can note that the $h^{2,1}(\hat{\mathcal{B}}_3)$ four-dimensional vector multiplets correspond to three-dimensional chiral multiplets. It is these that correspond to the U(1) gauge symmetries from NS5-branes in the four-dimensional duality, c.f. Equation (4.95), hence the Abelian NS5-brane gauge groups and their possible enhancement corresponds in three dimensions to the chiral multiplet sector.

M-theory on a surface of singularities

We next review the three-dimensional theory resulting from compactification of M-theory on a four-fold $\hat{Y}_4$ with a complex surface $\mathcal{S}$ of A_{N-1} singularities, as developed in Ref. [108]. Following their notation we will write $q := h^{1,0}(\mathcal{S})$ and $p_g := h^{2,0}(\mathcal{S})$, which are respectively the irregularity and arithmetic genus of $\mathcal{S}$. In the singular situation, there is an SU(N) symmetry and the field content includes 1 vector multiplet and $q+p_g$ chiral multiplets, all in the adjoint. The singularity has a resolution branch and often also a deformation branch, which correspond respectively to the Coulomb and Higgs branches of the field theory. In the Coulomb branch, the non-zero vevs of scalars in the vector multiplets measure the Kähler moduli of the resolution, generically breaking SU(N) to U(1)$^{N-1}$. The gauge enhancement in three dimensions is straightforward, as a result of U(1) gauge symmetries being now associated to $h^{1,1}$ rather than $h^{2,1}$. In the Higgs branch the scalars of the chiral multiplets acquire vevs, measuring the complex structure deformations of the singularity, and breaking the gauge symmetry entirely.

[38] Note that resolution of the four-fold tends to destroy the elliptic fibration, so there is no obvious F-theory interpretation. However, this is related to an elliptic fibration by flops, which we can then perform. These leave multiplet counts unchanged: it is known that birationally equivalent smooth CY manifolds have identical Hodge numbers (see [109]). Hence F-theory multiplet counts can be performed before flopping.

The singularities that develop in our models are of a particular kind. They arise when we shrink some exceptional divisor(s) in the base $\hat{\mathcal{B}}_3$, whose volumes correspond in the duality to distances between M5-branes in the Hořava-Witten interval. This leaves a curve of singularities diffeomorphic to the curve $\mathcal{C}$ wrapped by the coincident heterotic NS5-branes. Hence the complex surface $\mathcal{S}$ of singularities in the four-fold is an elliptic surface with base curve $\mathcal{C}$. Note that this means $c_1(\mathcal{S})^2 = 0$, since the Poincaré dual of the first Chern class of an elliptic surface is proportional to the fiber class, and so also $12\chi_{\text{hol.}} = \chi$, where $\chi_{\text{hol.}}$ is the holomorphic Euler characteristic. The elliptic fibration of $\mathcal{S}$ is characterised by the number of singular fibers, equal to the Euler characteristic of $\mathcal{S}$. The Hodge diamond is one of two types, depending on whether the fibration is trivial (first case) or not (second case) (see e.g. Ref. [110])

$$\begin{array}{ccccc} & & 1 & & \\ & g+1 & & g+1 & \\ g & & 2g+2 & & g \\ & g+1 & & g+1 & \\ & & 1 & & \end{array} \quad , \qquad \begin{array}{ccccc} & & 1 & & \\ & g & & g & \\ p_g & & 10\chi_{\text{hol.}}+2g & & p_g \\ & g & & g & \\ & & 1 & & \end{array} \quad , \tag{4.129}$$

where in the second diamond $p_g = \chi_{\text{hol.}} + g - 1 = \frac{1}{12}\chi + g - 1$. The number of singular fibers is counted by the intersection $-12K_{\hat{\mathcal{B}}_3} \cdot \mathcal{C}$. Note $\hat{\mathcal{B}}_3$ has only orbifold singularities, so this intersection is well-defined. To compute this intersection, note there is by construction a projection collapsing the F-theory $\mathbb{P}^1$, that maps the singular $\hat{\mathcal{B}}_3$ to the smooth B_2 and under which the curve $\mathcal{C}$ is mapped one-to-one to a copy in B_2. The intersection, hence the number of singular fibers and also the Euler characteristic of $\mathcal{S}$, must then be counted by $-12K_{B_2} \cdot \mathcal{C}$ where here $\mathcal{C}$ is the image in B_2.

One can note that G_4 flux may lift massless directions, altering any massless multiplet counts. The offending flux may thread cycles involved in the transition. If there were no such flux on one side, one may be forced to include it on the other if the Euler characteristic changes, to preserve anomaly cancellation. In Ref. [108] a computation of the change in Euler characteristic in going from resolved to deformed side yields

$$\Delta\left(\chi(\hat{Y}_4)\right) = N(N-1)(N+1)K_{\mathcal{S}}^2\,. \tag{4.130}$$

We see that as $K_{\mathcal{S}}^2 = 0$ in the singular transitions we consider, the Euler characteristic is then predicted to be unchanged, as expected since we proved in Section 4.4.4 that the Euler characteristic is independent of the NS5-brane configuration.

Theory through the transition

In Ref. [108] the spectrum of the compactified M-theory is computed at each stage of the singular transition. However, their analysis is restricted to cases where $q = 0$, $p_g \geq 1$. This restriction is imposed to avoid non-perturbative corrections from M5-branes wrapping the shrinking divisors in the four-fold, which can contribute only if $p_g - q = 0$. The induced non-perturbative superpotential depends on the volume v of a shrinking divisor as e^{-v}, and hence blows up. We see from the above Hodge diamonds that the singular transitions we consider may not obey the particular restrictions imposed in Ref. [108], and in particular may have $p_g - q = 0$. In the latter case, this physical obstruction to the singular transition should appear dual to world-sheet instantons in the NS5-brane transition. We see from the above Hodge diamonds that the restriction $q = 0$, $p_g \geq 1$ implies that $g = 0$, so the matter spectra computations in Ref. [108] only apply when in the heterotic dual the NS5-branes multiply wrap a $\mathbb{P}^1$.

We now review the spectrum computations of Ref. [108], keeping in mind the above restrictions. At non-generic points in the Coulomb branch, vector multiplet scalar vevs coincide, corresponding to partial resolution of the singularity. If the i^{th} value occurs k_i times, the gauge symmetry at this point is

$$\mathrm{SU}(k_1) \times \ldots \mathrm{SU}(k_m) \times \mathrm{U}(1)^{m-1} \,, \tag{4.131}$$

where $\sum_{i=1}^{m} k_i = N$. At this point the Higgs branch has complex dimension

$$(p_g - 1) \sum_{i=1}^{m} (k_i^2 - 1) + p_g(m-1) \,, \tag{4.132}$$

corresponding to deformations of the remaining singularities. The expressions for generic points are the specialisations with $m = N$ and $k_i = 1$, $\forall i$. Additionally, one can note an alternative path from Coulomb to Higgs branch as follows. At generic points in the Coulomb branch there are $p_g(N-1)$ neutral chiral multiplets. Giving these vevs before sending the vector multiplet scalar vevs to zero results in a $\mathrm{U}(1)^{N-1}$ gauge symmetry, and leaves $(p_g - 1)N(N-1)$ charged chiral fields. The geometry then has curve-like singularities, and these can be deformed away by giving vevs to the charged fields, resulting in the full Higgs branch dimension.

Recalling the discussion above in Sections 4.5.2 and 4.5.3, it is clear how this M-theory geometry corresponds to dual NS5-brane configurations. The situation of an A_{N-1} singularity on $\mathcal{S}$ corresponds to a stack of N NS5-branes wrapping $\mathcal{C}$ in the heterotic base B_2. Resolution of the singularity (Coulomb branch) corresponds to moving M5-branes apart in the bulk, and deformation (Higgs branch) to deformation of the brane stack in the base of the CY manifold. The $N-1$ three-dimensional U(1) vector bosons on the Coulomb branch come from the four-dimensional chiral multiplets parametrising distances between M5-branes in the 11d bulk. The three-dimensional chiral fields parametrising the Higgs branch come from the four-dimensional

chiral multiplets parametrising brane configurations in the CY manifold. Partial resolution gives multiple stacks of branes, corresponding to the gauge group in Equation (4.131), and leaving available deformations of each stack, corresponding to the branch in Equation (4.132). Turning on vevs of the $p_g(N-1)$ neutral chiral multiplets at generic points in the Coulomb branch corresponds to moving the branes in the CY while at different 11d bulk positions. The alternate path between Coulomb and Higgs branch corresponds to first such a shift, followed by bringing the branes together in the bulk, and finally deforming the resulting transversely-intersecting configuration, as when following the lower path in the example of Figure 14, from resolution to deformation.

Since the four-dimensional field theories of the resolution and deformation branches are best-understood, the three-dimensional theory of the singular situation is of most interest. Given the above correspondence, the three-dimensional gauge enhancement at the brane stack appears to correspond to enhancement of four-dimensional chiral multiplets. This appears to be distinct from any gauge enhancement of four-dimensional vector multiplets, since those correspond to three-dimensional chiral multiplets. This is an interesting role reversal. We hope to investigate the lift to four dimensions further in future work.

4.6 Summary

We set out to describe F-theory duals of heterotic line bundle models in compactification to four dimensions. As we have argued, the spectral cover does not provide a useful description for these models, as all of the heterotic bundle information is in the spectral sheaf with the spectral sheet being trivial. The dual F-theory geometry correspondingly contains two E_8 singularities with G_4 flux on these loci that is naturally dual to the heterotic line bundles. The requirement of having a standard F-theory dual restricts the possible line bundle models, in particular they are necessarily non-chiral. These models furthermore require 'horizontal' NS5-branes wrapping curves in the base of the elliptic three-fold for anomaly cancellation. The remainder of the anomaly is cancelled by either line bundle flux or 'vertical' NS5-branes on the fiber.

The horizontal NS5-branes are dual to blow-ups in the base of the F-theory four-fold, and we treat this aspect of the duality in detail. We reviewed the local F-theory geometry dual to the inclusion of a horizontal NS5-brane, and described the global structure of F-theory four-folds dual to horizontal line bundle models with various choices of NS5-brane content. We studied situations for which the F-theory four-fold is described by a toric hypersurface, as well as more general situations, the case reflecting whether the NS5-branes wrap toric subspaces in the heterotic base.

We then verified various aspects of the duality for these models. We first treated the matches concerning the E_8 fluxes: matching of anomaly conditions and bundle stability conditions, and multiplets in the two E_8 sectors including massless U(1)s. We then examined the aspects related to NS5-brane configuration / F-theory base geometry: we gave the vector and chiral multiplet counts in this sector, and proved for a broad class of models that these matches hold quite generally. We also discussed an interesting subtlety: when NS5-branes wrap base curves that don't intersect the discriminant locus, the heterotic chiral multiplet count is naively larger than the F-theory count. We argued that the resolution has two parts: the first is that some heterotic moduli are actually massive, and the second is that some F-theory moduli may become massless only in the stable degeneration limit. For the latter, one may expect that the corresponding heterotic chiral multiplets are lifted away from the limit by corrections to the supergravity descriptions that are valid only in the stable degeneration limit.

Finally, having constructed F-theory duals of heterotic models with arbitrary NS5-brane content, we used these to explore the F-theory duals of coincident and intersecting NS5-branes. We found a satisfying picture of how the toric description of the F-theory base reflects the heterotic NS5-brane configuration: the ordering of these NS5-branes as M5-branes in the Hořava-Witten interval is neatly reflected in the triangulation of the toric polytope, and the coincidence or intersection of NS5-branes is reflected in an obvious removal of cones in the triangulation. In order to have a description of the transitions catalysed by coincident NS5-branes in terms of effective field theory, we have confined ourselves to a discussion of the three-dimensional theory resulting from compactification of M-theory on this singular four-fold.

5 Index Formulae for Line Bundle Cohomology on Complex Surfaces

In this chapter we derive closed-form index expressions for the cohomology dimensions of line bundles on del Pezzo and Hirzebruch surfaces. This also provides for all compact toric surfaces a simple algorithm to express any line bundle cohomology in terms of an index. For complex surfaces, these results explain the appearance of piecewise polynomial equations for cohomology and they are a first step towards understanding similar formulae recently obtained for CY three-folds. To derive our results we implement a form of Zariski decomposition and combine this procedure with vanishing theorems for nef bundles.

The work presented in this chapter is based on Ref. [15], and was completed in collaboration with Andrei Constantin, Rehan Deen, and Andre Lukas. We thank Fabian Ruehle and Damian

Rössler for useful discussions during preparation. We also note that Ref. [12] is a companion paper in which we have explored how techniques from machine learning can help to uncover the structure of line bundle cohomology. In particular we construct neural networks that are designed to learn the structures in cohomology dimensions that we uncover and describe in the present chapter.

5.1 Introduction

Cohomologies of line bundles are crucial for various types of string compactifications, for example in the context of heterotic and F-theory model building. Usually, these cohomologies are computed using algorithmic methods, based on Čech cohomology, spectral sequences and related mathematical tools. These methods can be computationally intense and they provide little insight into the origin and structure of the results. This makes a bottom-up approach to string model building difficult whenever line bundles are involved. Clearly, string theory would profit from more direct and systematic access to line bundle cohomology and in this chapter we report on some progress in this direction.

In Ref. [7] it was found that line bundle cohomology dimensions on (complete intersection) CY manifolds can be described by relatively simple formulae, which are piecewise polynomial.[39] More precisely, the Picard group of the manifold splits into a number of disjoint regions - which are frequently but not always cones - in each of which the cohomology dimensions are given by a cubic polynomial in the integers which label the line bundles. These results were obtained heuristically by looking at algorithmically computed cohomology data on a few complete intersection CY manifolds and smooth quotients thereof and by extracting analytic formulae from this data. The authors of Ref. [10] employed machine learning techniques to derive cohomology formulae for (hypersurfaces in) toric varieties. In a recent paper [11], these results were extended to a larger class of complete intersection manifolds with Picard number 2. The pattern conjectured from these results is that line bundle cohomology dimensions on manifolds with complex dimension n are piecewise polynomial, with polynomials of degree (at most) n. All this points to a yet to be fully discovered mathematical structure underlying line bundle cohomology.

In simple cases, it is possible to prove these results by spectral sequence chasing but this becomes tedious for more complicated manifolds. It is fair to say that the origin of these formulae for CY three-folds is currently not well-understood and that there is no simple and systematic method for their derivation. In fact, CY three-folds are fairly complicated objects and may not

[39] The first non-trivial instance of a line bundle cohomology formula appeared in the earlier work [8,9], in which generic hypersurfaces of type (2,2,2,2) in a product of four complex projective spaces were studied.

provide the best setting to uncover the structure underlying line bundle cohomology.

In the present work, we, therefore, explore these issues in the simpler setting of complex surfaces. A line bundle $L \to S$ over a complex surface S has three cohomology dimensions $h^q(S, L)$, where $q = 0, 1, 2$, but knowledge of one of these for all line bundles implies the other two via Serre duality and the index theorem. For this reason, we will focus our study on the zeroth cohomology dimension, $h^0(S, L)$. Following standard notation, the line bundle associated to a divisor (class) $D \subset S$ is denoted by $\mathcal{O}_S(D)$ and frequently we introduce a basis D_i of divisor (classes), so that $D = \sum_i k_i D_i$, with $k_i \in \mathbb{Z}$. Having fixed such a basis, we also occasionally write the corresponding line bundle as $\mathcal{O}_S(\mathbf{k}) := \mathcal{O}_S(D)$, where $\mathbf{k} = (k_i)$ is an integer vector.

As a first step, we proceed in much the same way as has been done for CY three-folds. We produce cohomology data from algorithmic methods and extract analytic formulae for the zeroth cohomology dimension by "eyeballing". The examples we will be studying in this context are the Hirzebruch and del Pezzo surfaces. The results turn out to be analogous to the ones obtained for CY three-folds: the dimensions $h^0(S, \mathcal{O}_S(\mathbf{k}))$ are described by equations which are piecewise quadratic in the integers k_i. This provides further evidence that piecewise polynomial formulae for line bundle cohomology dimensions are a general feature which is neither limited to the CY case nor to three complex dimensions.

However, for surfaces we are able to go further. For both Hirzebruch and del Pezzo surfaces we are able to express the piecewise quadratic formulae in terms of basis-independent, intrinsic objects, specifically the generators of the effective and nef cones, the irreducible negative self-intersection divisors and the intersection form on S. This re-writing naturally corresponds to a specific map $D \to \tilde{D}$ for effective divisors which we provide explicitly and which leaves the zeroth cohomology dimension unchanged, that is, $h^0(S, \mathcal{O}_S(D)) = h^0(S, \mathcal{O}_S(\tilde{D}))$. We further observe that for all Hirzebruch and del Pezzo surfaces the line bundle $\mathcal{O}_S(\tilde{D})$ satisfies $h^q(S, \mathcal{O}_S(\tilde{D})) = 0$ for $q = 1, 2$. Combining these statements implies that the cohomology of $\mathcal{O}_S(D)$ can be computed in terms of the index of the shifted divisor $\tilde{D}$ as

$$h^0(S, \mathcal{O}_S(D)) = h^0(S, \mathcal{O}_S(\tilde{D})) = \mathrm{ind}(\mathcal{O}_S(\tilde{D}))\,. \tag{5.1}$$

At this stage, the result (5.1) for Hirzebruch and del Pezzo surfaces together with the map $D \to \tilde{D}$ is still empirical, that is, inferred from a finite set of cohomology data.

Based on these empirical results, we write down a general form of the map $D \to \tilde{D}$ which applies to all smooth compact complex projective surfaces and we prove that it preserves the zeroth cohomology dimensions, that is, $h^0(S, \mathcal{O}_S(\tilde{D})) = h^0(S, \mathcal{O}_S(D))$. Moreover, it follows that iterating the map $D \to \tilde{D}$ leads, after a finite number of steps, to a divisor $\underline{\tilde{D}}$ in the nef cone.

This map can then be seen to correspond to a particular instance of a map in the mathematics literature, known as Zariski decomposition [111]. Provided there is a vanishing theorem which asserts that $h^q(S, \mathcal{O}_S(\underline{\tilde{D}})) = 0$ for $q = 1, 2$, it follows that

$$h^0(S, \mathcal{O}_S(D)) = h^0(S, \mathcal{O}_S(\underline{\tilde{D}})) = \mathrm{ind}(\mathcal{O}_S(\underline{\tilde{D}}))\,. \tag{5.2}$$

For such cases, which we show include Hirzebruch and del Pezzo surfaces as well as all compact toric surfaces we have, therefore, a mathematical proof for the existence of index formulae for h^0 and a practical way of deriving them. These formulae are quasi-topological in nature: the quantity $\mathrm{ind}(\mathcal{O}_S(\underline{\tilde{D}}))$ is purely topological, while the map $D \to \tilde{D}$ depends in general on the complex structure.

For Hirzebruch and del Pezzo surfaces we prove that a single application of the map $D \to \tilde{D}$ already projects into the nef cone and that a suitable vanishing theorem is available in either case. This leads to a mathematical proof for the empirical formula (5.1).

We will presently provide a summary of our main results. Subsequently, the plan for the remainder of the chapter is as follows. In the next section, we explain how cohomology formulae can be extracted from cohomology data, computed by algorithmic methods, focusing on Hirzebruch and del Pezzo surfaces. In a first instance, we extract piecewise quadratic formulae from the data which are subsequently refined to index formulae. The reader less interested in this "empirical" aspect of the work can skip to Section 5.3 which contains our main mathematical statements. Section 5.4 illustrates these mathematical results in the context of simple examples. We conclude in Section 5.5.

Summary of results

We outline below the way in which the index formulae can be applied to specific surfaces. For a smooth compact complex projective surface S we first require knowledge of the effective (Mori) cone[40], $\mathcal{M}(S)$. In practice this amounts to providing the set of Mori cone generators $\hat{\mathcal{M}}(S)$ or the set of generators $\hat{\mathcal{N}}(S)$ of the nef cone $\mathcal{N}(S)$, which is dual to the Mori cone. We also need to know the intersection form $(D, D') \to D \cdot D'$ on S. For all divisors not in the Mori cone, that is $D \notin \mathcal{M}(S)$, we have $h^0(S, \mathcal{O}_S(D)) = 0$. On the other hand, all divisors $D \in \mathcal{M}(S)$ have strictly positive zeroth cohomology dimension. For such effective divisors we utilise the map $D \to \tilde{D}$ by

$$\tilde{D} = D - \sum_{C \in \mathcal{I}} \theta(-D \cdot C)\, \mathrm{ceil}\left(\frac{D \cdot C}{C^2}\right) C\,, \tag{5.3}$$

[40]For the examples discussed in this chapter the Mori and the effective cones coincide, though there exist surfaces for which this is not the case, see e.g. Example 1.5.1 in Ref. [112].

where the sum runs over the set $\mathcal{I}$ of all irreducible curves with negative self-intersection. The Heaviside function θ ensures that only curves C with $D \cdot C < 0$ contribute to the sum and ceil is the ceiling function. Hence, to write down this map explicitly, we need to know the irreducible, negative self-intersection curves on the surface S - information that can be obtained for many cases of interest.

The key statement about the map (5.3) is that it leaves the zeroth cohomology dimension unchanged, that is, $h^0(S, \mathcal{O}_S(\tilde{D})) = h^0(S, \mathcal{O}_S(D))$. Since the nef cone $\mathcal{N}(S)$ is the cone of divisors D which intersect all algebraic curves non-negatively, it is clear that repeated application of the map (5.3) eventually leads to a divisor $\underline{\tilde{D}}$ in the nef cone. Such a decomposition goes by the name of a 'Zariski decomposition'. If there is a vanishing theorem, typically Kodaira vanishing or one of its refinements, which asserts that $h^q(S, \mathcal{O}_S(\underline{\tilde{D}})) = 0$ for $q = 1, 2$ then the zeroth cohomology can be written as an index, using Eq. (5.2). It turns out that this is the case for many surfaces of interest, including Hirzebruch surfaces, del Pezzo surfaces, and compact toric surfaces, and, hence, index formulae for the zeroth cohomology dimensions exist for all these cases. The relevant vanishing theorems will be reviewed in the main text.

Let us first summarise how this general result applies to Hirzebruch surfaces $\mathbb{F}_n$. The Picard lattice of any Hirzebruch surface is two-dimensional and we can introduce a basis (D_1, D_2) of divisor classes, such that the intersection form is defined by $D_1^2 = -n$, $D_1 \cdot D_2 = 1$ and $D_2^2 = 0$ (see Appendix E.1 for details). Then, the Mori cone is generated by D_1 and D_2. This means effective divisors are of the form $D = k_1 D_1 + k_2 D_2$ with non-negative k_i and all other divisors with at least one k_i negative have vanishing zeroth cohomology. The unique irreducible class with negative self-intersection is $C = D_1$. Inserting all this into the map (5.3) shows that $\tilde{D}$ is always in the nef cone. Theorem 5.53 guarantees the necessary vanishing, so that Eq. (5.1) can be applied. Combining these results we obtain the index formula

$$h^0\left(\mathbb{F}_n, \mathcal{O}_{\mathbb{F}_n}(D)\right) = \mathrm{ind}\left(D - \theta(-D \cdot C)\,\mathrm{ceil}\left(\frac{D \cdot C}{C^2}\right) C\right), \tag{5.4}$$

for the zeroth cohomology dimension of effective divisors D on Hirzebruch surfaces. The explicit formula for the index of line bundles on Hirzebruch surfaces is provided in Eq. (5.12).

Let us now summarise the analogous results for del Pezzo surfaces. Del Pezzo surfaces (other than $\mathbb{P}^1 \times \mathbb{P}^1$ which is trivial in our context) are blow-ups of the projective plane $\mathbb{P}^2$ in n generic points, where $n = 0, 1, \ldots, 8$, and they are denoted by dP_n. The rank of their Picard lattice is $n+1$ and a standard basis of divisor classes consists of the hyperplane class l of $\mathbb{P}^2$ and the classes e_i of the exceptional divisors associated to the blow-ups, where $i = 1, \ldots, n$. The intersection

form is fixed by the relations $l^2 = 1$, $l \cdot e_i = 0$ and $e_i \cdot e_j = -\delta_{ij}$. The list of generators of the Mori and nef cones is too long to be listed here, at least for the larger values of n, but has been explicitly provided in Appendix E.2. The irreducible negative self-intersection classes C are precisely the Mori cone generators, which have self-intersection $C^2 = -1$. It can be shown that a single application of the map (5.3) projects into the nef cone and Corollary 5.58 provides the appropriate vanishing statement so that Eq. (5.1) holds. This leads to the index formula

$$h^0\left(\mathrm{dP}_n, \mathcal{O}_{\mathrm{dP}_n}(D)\right) = \mathrm{ind}\left(D + \sum_{C \in \hat{\mathcal{M}}} \theta(-D \cdot C)\,(D \cdot C) C\right), \tag{5.5}$$

for the zeroth cohomology dimension of effective divisors D on del Pezzo surfaces, where $\hat{\mathcal{M}} = \hat{\mathcal{M}}(\mathrm{dP}_n)$ are the generators of the Mori cone.

5.2 From data to index formulae

The mathematical results presented in this chapter have been motivated following a somewhat unorthodox method which might be described as experimental algebraic geometry. The starting point is line bundle cohomology data on various surfaces, produced by algorithmic methods. From this data, we first read off simple piecewise quadratic formulae for cohomology dimensions. These formulae are then put through a process of gradual refinement until they are expressed in terms of intrinsic geometric objects of the underlying surface. In this form, the equations are very suggestive and lead to conjectures for line bundle cohomology on smooth compact complex projective surfaces which we state and derive in the next section. The main purpose of the present section is to describe this "experimental" approach, focusing on our two main classes of examples, the Hirzebruch and del Pezzo surfaces. This may be of interest to anyone wishing to pursue a similar procedure, for example for a different class of manifolds. The reader mainly interested in the general mathematical results for surfaces can safely skip this section and move on to Section 5.3.

5.2.1 Outline of approach

We have already mentioned Refs. [7,11], where piecewise cubic formulae for line bundle cohomology dimensions on certain CY three-folds have been obtained, starting with cohomology data computed by algorithmic methods. These results suggest that line bundle cohomology dimensions on surfaces, S, can be described by formulae which are piecewise quadratic in the integers k_i which label the line bundles. This expectation, which we will confirm for our examples, as well as for larger classes of surfaces, is the starting point of our discussion. We will then gradually

refine the piecewise quadratic equations in k_i and attempt to re-write them in terms of intrinsic geometric objects, in our quest to uncover the mathematical origin of these equations.

Let us first recall that line bundles $L = \mathcal{O}_S(D) \to S$ on surfaces have three cohomology dimensions, $h^q(S, L)$, where $q = 0, 1, 2$. However, Serre duality and the index theorem provide two relations

$$h^2(S, L) = h^0(S, L^* \otimes K_S)\,, \quad h^1(S, L) = h^0(S, L) + h^2(S, L) - \mathrm{ind}(S, L)\,, \tag{5.6}$$

between those three quantities. Here, K_S is the canonical bundle[41] of the surface S and the index, $\mathrm{ind}(S, L)$, of the line bundle can be easily computed from the Riemann-Roch formula as

$$\mathrm{ind}(S, \mathcal{O}_S(D)) = \mathrm{ind}(S, \mathcal{O}_S) + \frac{1}{2} D \cdot (D - K_S)\,, \quad \mathrm{ind}(S, \mathcal{O}_S) = \frac{1}{12}(K_S^2 + \chi(S))\,, \tag{5.7}$$

where $\chi(S)$ is the Euler characteristic. Written in terms of the line bundle integers k_i the index is a quadratic polynomial. The upshot of this discussion is that knowledge of all zeroth cohomology dimensions $h^0(S, L)$ for all line bundles L determines all other cohomology dimensions. Moreover, piecewise quadratic formulae for h^0 directly translate into piecewise quadratic formulae for h^1 and h^2 via the above relations. For this reason, we will focus on the zeroth cohomology dimension in the following.

The basic steps of our approach are as follows.

- For the complex surface S, we generate cohomology data, $(\mathbf{k}, h^0(S, \mathcal{O}_S(\mathbf{k})))$, for a range of integer vectors $\mathbf{k}$, typically taken from a box with $|k_i| \leq k_{\max}$, computed using suitable algorithmic methods.

- From this data, we extract conjectures for piecewise quadratic formulae for $h^0(S, \mathcal{O}_S(\mathbf{k}))$ as a function of $\mathbf{k}$. Typically this is done by first identifying the regions in the Picard lattice for which the behaviour is quadratic. The experience from CY three-folds suggests that these regions are frequently - but not always - cones. For each such region, we then fit a quadratic polynomial in $\mathbf{k}$ to the data. In a companion paper [12] we explain how this process can be facilitated by methods from machine learning.

- Next, we attempt to re-write the piecewise quadratic formulae in k_i in a basis-independent way, using intrinsic geometric objects of the underlying surface. For the surfaces we treat, one finds that the relevant objects are the effective (Mori) cone $\mathcal{M}(S)$ and its list

[41] We will freely write the same symbol K_S for the canonical divisor. It will be clear from context which is in use.

of generators $\hat{\mathcal{M}}(S)$, the nef cone $\mathcal{N}(S)$ and its list of generators $\hat{\mathcal{N}}(S)$, the irreducible negative self-intersection curves and the intersection form $(D, D') \to D \cdot D'$ on S.

- Finally, we would like to bring the formula into a compact, manageable form. This is particularly relevant for surfaces with high Picard number, where the number of regions in the Picard lattice and, hence, the number of case distinctions required can be large. It turns out that such a compact form can indeed be found using the formula for the index. In this final form, our empirical results are quite suggestive and point to more general mathematical statements which we formulate and prove in Section 5.3.

The above programme will be carried out for two main classes of surfaces, the Hirzebruch and del Pezzo surfaces, and we now briefly review their basic properties.

5.2.2 Basic properties of Hirzebruch surfaces

The Hirzebruch surfaces $\mathbb{F}_n$ are indexed by a non-negative integer n. They correspond to different fibrations of a $\mathbb{P}^1$ fiber over a $\mathbb{P}^1$ base, with n characterising the twisting. Their non-zero Hodge numbers are $h^{0,0}(\mathbb{F}_n) = h^{2,2}(\mathbb{F}_n) = 1$ and $h^{1,1}(\mathbb{F}_n) = 2$ and, hence, the Picard number is two for any n. The Picard lattice is spanned by the classes of the two projective lines that form the fiber bundle. There exist toric and complete intersection representations of the Hirzebruch surfaces, and details of these have been relegated to Appendix E.1. Here, we focus on a few basic properties, relevant to our discussion, which can, for example, be deduced from the toric description. We write D_1 for the divisor[42] corresponding to the $\mathbb{P}^1$ base of the fiber bundle, and D_2 for the divisor corresponding to the $\mathbb{P}^1$ fiber. Then, the intersection form of $\mathbb{F}_n$ is determined by

$$D_1^2 = -n\,, \quad D_1 \cdot D_2 = 1\,, \quad D_2^2 = 0\,. \tag{5.8}$$

Divisors on $\mathbb{F}_n$ can be written as linear combinations $D = k_1 D_1 + k_2 D_2$ with $k_1, k_2 \in \mathbb{Z}$ and line bundles $\mathcal{O}_{\mathbb{F}_n}(\mathbf{k}) = \mathcal{O}_{\mathbb{F}_n}(k_1 D_1 + k_2 D_2)$ are parametrised by two-dimensional integer vectors $\mathbf{k} = (k_1, k_2)$.

The two divisors D_1 and D_2 also correspond to the generators of the Mori cone $\mathcal{M}(\mathbb{F}_n)$, that is,

$$\hat{\mathcal{M}}(\mathbb{F}_n) = \{D_1, D_2\}\,. \tag{5.9}$$

This means effective divisors are of the form $D = k_1 D_1 + k_2 D_2$ with $k_1, k_2 \in \mathbb{Z}_{\geq 0}$. In addition,

[42] For most of the chapter, the term "divisor" is used as a short-hand for "divisor class". Whenever the distinction between divisor and divisor class becomes relevant we will state this explicitly.

from the above intersection form, the dual nef cone has generators

$$\hat{\mathcal{N}}(\mathbb{F}_n) = \{D_2, D_1 + nD_2\}\,. \tag{5.10}$$

The anti-canonical divisor $-K_{\mathbb{F}_n}$ of the Hirzebruch surface $\mathbb{F}_n$ is given by

$$-K_{\mathbb{F}_n} = 2D_1 + (n+2)D_2\,. \tag{5.11}$$

Inserting into the Riemann-Roch formula (5.7) an arbitrary divisor $D = k_1 D_1 + k_2 D_2$, the above expression for the anti-canonical divisor and the result $\mathrm{ind}(\mathbb{F}_n, \mathcal{O}_{\mathbb{F}_n}) = 1$ (which follows from the second equation (5.7) with $K^2_{\mathbb{F}_n} = 8$ and $\chi(\mathbb{F}_n) = 4$) gives

$$\mathrm{ind}(\mathbb{F}_n, \mathcal{O}_{\mathbb{F}_n}(D)) = 1 + \frac{1}{2}D\cdot(D - K_{\mathbb{F}_n}) = 1 + k_1 + k_2 + k_1k_2 - \frac{1}{2}nk_1 - \frac{1}{2}nk_1^2\,. \tag{5.12}$$

There are several algorithmic methods to compute line bundle cohomology on Hirzebruch surfaces.

- Using the toric realisation of the Hirzebruch surfaces (see Appendix E.1), the dimension of the zeroth cohomology, which is all we require for our discussion, can be computed from the weight system.
- Hirzebruch surfaces can also be constructed as complete intersections in products of projective spaces (see Appendix E.1) and the techniques described in Refs. [22,113–116], based on the Bott-Borel-Weil formalism and spectral sequences, can be applied.
- Finally, again using the toric realisation, we can use the methods to calculate line bundle cohomology on toric spaces developed in Refs. [30,117,118].

5.2.3 Basic properties of del Pezzo surfaces

A del Pezzo surface is isomorphic to either $\mathbb{P}^1 \times \mathbb{P}^1$ or to a blow-up of the complex projective plane $\mathbb{P}^2$ in $n \in \{0, 1, \ldots, 8\}$ generic points. The cases of $\mathbb{P}^1 \times \mathbb{P}^1$ and $\mathbb{P}^2$ are trivial for our purposes since the result directly follows from Bott's formula for line bundle cohomology on projective spaces. For this reason we focus on del Pezzo surfaces which correspond to a blow-up of $\mathbb{P}^2$ in $n \in \{1, \ldots, 8\}$ generic points, and we denote these surfaces by dP_n.

Del Pezzo surfaces dP_n can be realised as complete intersections in products of projective spaces and, for $n = 1, 2, 3$, as toric spaces. Details of this are provided in Appendix E.2. Here, we merely collect the information essential to our discussion.

The non-zero Hodge numbers of del Pezzo surfaces are $h^{0,0}(\mathrm{dP}_n) = h^{2,2}(\mathrm{dP}_n) = 1$ and $h^{1,1}(\mathrm{dP}_n) = n + 1$, so the rank of the Picard lattice is $n + 1$. A basis for the Picard lattice

is given by $(l, e_1, \ldots, e_n)$, where l is the hyperplane class of $\mathbb{P}^2$ and e_i, where $i = 1, \ldots, n$, are the exceptional classes, related to the blow-ups. Relative to this basis, the intersection form is defined by the relations

$$l^2 = 1\,, \quad l \cdot e_i = 0\,, \quad e_i \cdot e_j = -\delta_{ij}\,. \tag{5.13}$$

A general divisor is written as

$$D = k_0 l + \sum_{i=1}^{n} k_i e_i\,. \tag{5.14}$$

with $k_0, k_i \in \mathbb{Z}$ and, hence, line bundles $\mathcal{O}_{\mathrm{dP}_n}(\mathbf{k}) = \mathcal{O}_{\mathrm{dP}_n}(k_0 l + k_1 e_1 + \cdots + k_n e_n)$ are labelled by $(n+1)$-dimensional integer vectors $\mathbf{k} = (k_0, k_1, \ldots, k_n)$. For another divisor D' with components $\mathbf{k}' = (k_0', k_1', \ldots, k_n')$ the intersection form can also be written as

$$D \cdot D' = \mathbf{k}^T G\, \mathbf{k} =: \langle \mathbf{k}, \mathbf{k}' \rangle\,, \quad G = \mathrm{diag}(1, -1, \ldots, -1)\,. \tag{5.15}$$

The lists of Mori and nef cone generators are denoted by $\hat{\mathcal{M}} = \hat{\mathcal{M}}(\mathrm{dP}_n)$ and $\hat{\mathcal{N}} = \hat{\mathcal{N}}(\mathrm{dP}_n)$ respectively, and they are thought of as containing the actual divisors or their coordinates vectors relative to the basis $(l, e_1, \ldots, e_n)$, depending on context. In the latter form, they are explicitly provided in Appendix E.2.

The anti-canonical class of dP_n is given by

$$-K_{\mathrm{dP}_n} = 3l - \sum_{i=1}^{n} e_i\,. \tag{5.16}$$

Inserting into the Riemann-Roch formula a general divisor (5.14), the above expression for the anti-canonical class and the result $\mathrm{ind}(\mathrm{dP}_n, \mathcal{O}_{\mathrm{dP}_n}) = 1$ (which follows from the second Eq. (5.7) with $K^2_{\mathrm{dP}_n} = 9 - n$ and $\chi(\mathrm{dP}_n) = 3 + n$) gives

$$\mathrm{ind}(\mathrm{dP}_n, \mathcal{O}_{\mathrm{dP}_n}(D)) = 1 + \frac{1}{2} D \cdot (D - K_{\mathrm{dP}_n}) = 1 + \frac{1}{2} k_0(k_0 + 3) + \frac{1}{2} \sum_{i=1}^{n} k_i(1 - k_i)\,. \tag{5.17}$$

As for Hirzebruch surfaces, there are several algorithmic methods available to calculate line bundle cohomology on del Pezzo surfaces.

- For the del Pezzo surfaces dP_n, with $n = 1, 2, 3$ which have a toric realisation (see Appendix E.2), we can compute h^0 either from the toric weight system or via the methods for line bundle cohomology on toric spaces from Refs. [30, 117, 118].

- All del Pezzo surfaces have a realisation as complete intersections in products of projective spaces (see Appendix E.2), so the methods of Refs. [22, 113–116] can be applied.

- It was noticed in Appendix B of Ref. [119] that line bundle cohomology on del Pezzo surfaces can be computed by counting certain polynomials on $\mathbb{P}^2$ and we use a computational implementation of this method.

There is one further result which relates line bundle cohomology of del Pezzo surfaces dP_n for different n which will be helpful in the following. The cohomology dimension of a divisor D on dP_{n+1} with no component along the exceptional class e_{n+1} is the same as the cohomology dimension of D seen as a divisor on dP_n, that is,

$$h^0(\mathrm{dP}_{n+1}, \mathcal{O}_{\mathrm{dP}_{n+1}}(D)) = h^0(\mathrm{dP}_n, \mathcal{O}_{\mathrm{dP}_n}(D)) \quad \text{for} \quad D = k_0 l + \sum_{i=1}^{n} k_i e_i \,. \tag{5.18}$$

This can be shown, for example, by thinking about blowing-down one exceptional divisor or by using the relation between del Pezzo cohomology and polynomials on $\mathbb{P}^2$ from Ref. [119].

5.2.4 Warm up: line bundle cohomology on Hirzebruch surfaces

The complexity of our task clearly increases with the Picard number of the surface. Hirzebruch surfaces, which all have Picard number two, therefore provide a simple setting for an initial exploration. In particular, it is possible to plot cohomology data and identify the regions in the Picard lattice by "eyeballing". Once the regions are known, the quadratic polynomials can be fixed by a simple fit to a number of points in each region. This results in a piecewise quadratic formula which represents the first step on our path from data to general mathematical statements. Of course this piecewise quadratic formula should then be checked against all available cohomology data.

We recall that line bundles on Hirzebruch surfaces $\mathbb{F}_n$ are labelled by a two-dimensional integer vector $\mathbf{k} = (k_1, k_2)$, relative to the divisor basis introduced in Section 5.2.2. In Figure 21 we plot the zeroth cohomology dimension, $h^0(\mathbb{F}_n, \mathcal{O}_{\mathbb{F}_n}(\mathbf{k}))$, as a function of (k_1, k_2), for the first three Hirzebruch surfaces $\mathbb{F}_0$, $\mathbb{F}_1$ and $\mathbb{F}_2$. For a better visualisation, we have joined the discrete data points into a surface. We recall from Section 5.2.2 that the cone of effective divisors, that is, the region where $h^0(\mathbb{F}_n, \mathcal{O}_{\mathbb{F}_n}(\mathbf{k})) > 0$, is characterised by $k_1 \geq 0$ and $k_2 \geq 0$. This is consistent with the plots in Figure 21 which indicate a non-zero cohomology precisely in the positive quadrant.

What is the structure in the positive quadrant? The obvious feature in the plots for $\mathbb{F}_1$ and $\mathbb{F}_2$ in Figure 21 is the presence of two regions which we expect require two different quadratic polynomials. In fact, it can be checked that this structure persists for all Hirzebruch surfaces with $n \geq 1$ and that the two regions are separated by the hyperplane through the origin, described by the equation

$$k_2 = n k_1 \,. \tag{5.19}$$

Now that we have identified the regions we can attempt polynomial fits. The region $k_2 \geq n k_1$ corresponds to the easy case. Here, the relevant polynomial for all Hirzebruch surfaces is simply

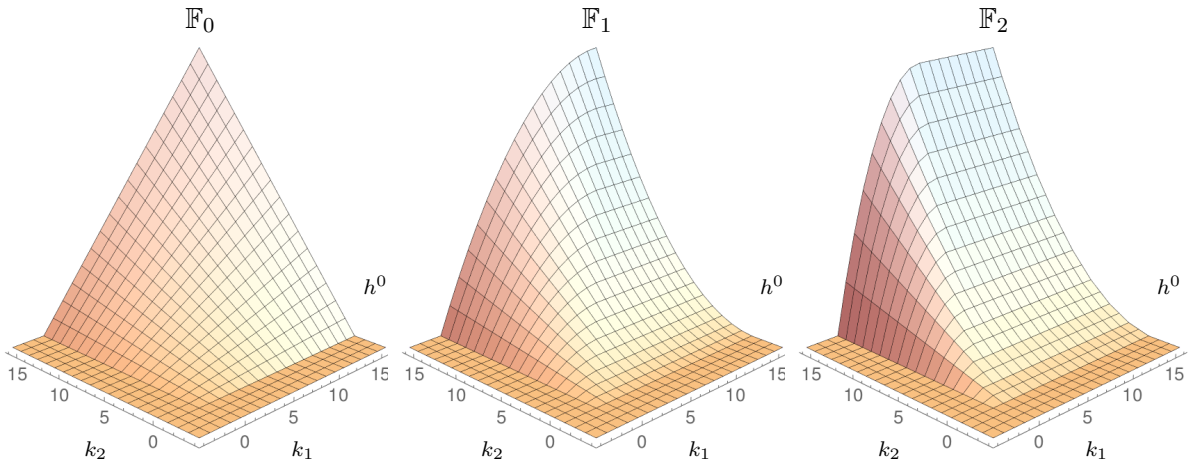

Figure 21: *Zeroth cohomology* $h^0(\mathbb{F}_n, \mathcal{O}_{\mathbb{F}_n}(k_1 D_1 + k_2 D_2))$ *as a function of* (k_1, k_2) *for the Hirzebruch surfaces* $\mathbb{F}_0$, $\mathbb{F}_1$, $\mathbb{F}_2$. *For clarity, we have joined the discrete data points into a surface.*

the index, given in Eq. (5.12). The other region, where $k_2 < nk_1$ and which exists for all Hirzebruch surfaces with $n \geq 1$, is more problematic. A polynomial fit to the data in this region succeeds for $\mathbb{F}_1$ but it fails for $\mathbb{F}_2$ and all higher Hirzebruch surfaces. The problem becomes apparent when we plot the cohomology data for $\mathbb{F}_3$, $\mathbb{F}_4$, and $\mathbb{F}_5$ as we have done in Figure 22. The cohomology values in the region $k_2 < nk_1$ show a mod n structure which can of course not

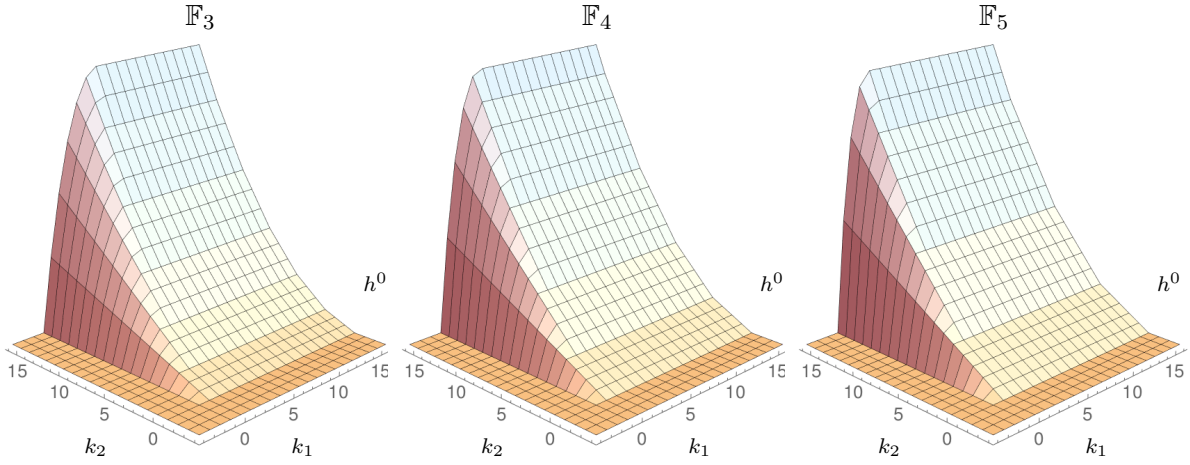

Figure 22: *Zeroth cohomology* $h^0(\mathbb{F}_n, \mathcal{O}_{\mathbb{F}_n}(k_1 D_1 + k_2 D_2))$ *on a region of the Picard lattice for the Hirzebruch surfaces* $\mathbb{F}_3$, $\mathbb{F}_4$, $\mathbb{F}_5$. *This function is lattice-valued; we have joined the lattice data points into a surface for clarity.*

be captured by a single quadratic polynomial. A similar structure has been observed in some of the examples studied in Ref. [10]. However, it is not too difficult to account for this mod n

behaviour by including a ceiling function. This leads to the following conjecture

$$h^0\left(\mathbb{F}_n, \mathcal{O}_{\mathbb{F}_n}(\mathbf{k})\right) = \begin{cases} \text{ind}(\mathcal{O}_{\mathbb{F}_n}(\mathbf{k})) & \text{if } k_1, k_2 \geq 0 \text{ and } k_2 \geq nk_1 \quad \text{(Region 1)} \\ \frac{1}{2}(1-c_2)(2+2k_2+nc_2) & \text{if } k_1, k_2 \geq 0 \text{ and } k_2 < nk_1 \quad \text{(Region 2)} \\ 0 & \text{otherwise} \quad \text{(Region 3)} \end{cases}$$

$$\text{where } c_2 = \text{ceil}\left(\tfrac{-k_2}{n}\right) \tag{5.20}$$

for the zeroth cohomology dimension on any Hirzebruch surface $\mathbb{F}_n$. The explicit expression for the index can be found in Eq. (5.12). This result lends further support to the conjecture that line bundle cohomology on complex surfaces is described by equations which are (basically) piecewise quadratic. However, the appearance of the ceiling function which accounts for the mod n behaviour is new and, as we will see, points to an important feature of the more general formula we are seeking.

This completes the first two parts of our programme. The remaining tasks are, firstly, to write Eq. (5.20) in a basis-independent way and, secondly, to find a compact form, in terms of natural geometric objects. The current example of the Hirzebruch surfaces is simple enough to carry out both steps at once.

Consider first the boundary between Region 1 and Region 2. A quick glance at the intersection rules (5.8) shows that, for $D = k_1 D_1 + k_2 D_2$, we have $D \cdot D_1 = -nk_1 + k_2$. Hence, these two regions can be characterised by saying that D needs to be in the effective cone, while, in addition, we require that $D \cdot D_1 \geq 0$ for Region 1 and $D \cdot D_1 < 0$ for Region 2. Finally, Region 3 is characterised by saying that D is not in the effective cone. Since we can think of $D_1 = C$ as the unique irreducible divisor with negative self-intersection, this provides a natural basis-independent formulation of the regions.

What about the polynomial expressions in those regions? In Region 1, the cohomology is already described by an intrinsic geometrical object, the index, but it is not immediately obvious how to proceed in Region 2. A useful observation is that the cohomology dimension in Region 2 does not depend on k_1. This means that a projection exists: one can relate a cohomology result in Region 2 to one in Region 1 by a lattice projection along the negative k_1 direction. Since cohomology dimensions in Region 1 are described by the index we conclude that the same must be true for Region 2, however, the argument of the index is now a different, projected divisor.

It turns out that the required lattice projection is

$$D \to \tilde{D} = D - \text{ceil}\left(\frac{k_2 - nk_1}{-n}\right) D_1 = D - \text{ceil}\left(\frac{D \cdot C}{-n}\right) C\,, \tag{5.21}$$

with $C = D_1$. Note that the expression on the right-hand-side is written entirely in terms of natural geometric objects of the Hirzebruch surface. With this projection, we can re-write the cohomology Eq. (5.20) as

$$h^0\left(\mathbb{F}_n, \mathcal{O}_{\mathbb{F}_n}(D)\right) = \begin{cases} \text{ind}\left(D - \theta\left(-D \cdot C\right) \text{ceil}\left(\dfrac{-D \cdot C}{-n}\right) C\right) & \text{if } D \in \mathcal{M}(\mathbb{F}_n) \\ 0 & \text{if } D \notin \mathcal{M}(\mathbb{F}_n) \end{cases} \tag{5.22}$$

where $C = D_1$ is the unique irreducible divisor with negative self-intersection and θ is the Heaviside step function, defined by $\theta(x) = 1$ for $x > 0$ and $\theta(x) = 0$ otherwise.

The above result, albeit in a very suggestive mathematical form, is still a conjecture since it has been extracted from a finite amount of cohomology data. In fact, Hirzebruch surfaces are sufficiently simple so that a direct proof can be found, for example from the weight system of the associated toric diagrams. We will not pursue this explicitly since we will also find these results as a special case of the derivations in Section 5.3.

5.2.5 Regions and polynomials for del Pezzo surfaces

We would now like to repeat the process from data to a concise mathematical formula for the case of del Pezzo surfaces. This is of course considerably more complicated, given that Picard numbers reach up to nine. In fact, writing down piecewise polynomial formulae explicitly becomes impractical for higher Picard numbers as the number of regions and, hence, case distinctions required, increases considerably. This is of course one of the reasons we are seeking concise mathematical formulae for cohomology dimensions.

We will tackle the problem of finding concise formulae in the next two sub-sections, but presently we would like to explain how to extract piecewise polynomial formulae from data. In practice we begin with the lower del Pezzo surfaces, dP_n, and gradually increase n. Eq. (5.18) tell us that the structure found for dP_n is preserved as we move on to dP_{n+1}. This means that at each stage we have some partial information available from the del Pezzo surfaces with lower n. For example, when determining some hyperplane boundaries, we already know some entries in their normal vectors.

The first step is to find the region boundaries and regions. Once this has been accomplished it is easy to find the quadratic polynomial in each region by a simple fit to the data. For the cases dP_1 and dP_2 we can proceed as for the Hirzebruch surfaces, that is, by simply reading the boundaries off from a plot. Even for higher Picard numbers it is possible to proceed by "eyeballing"

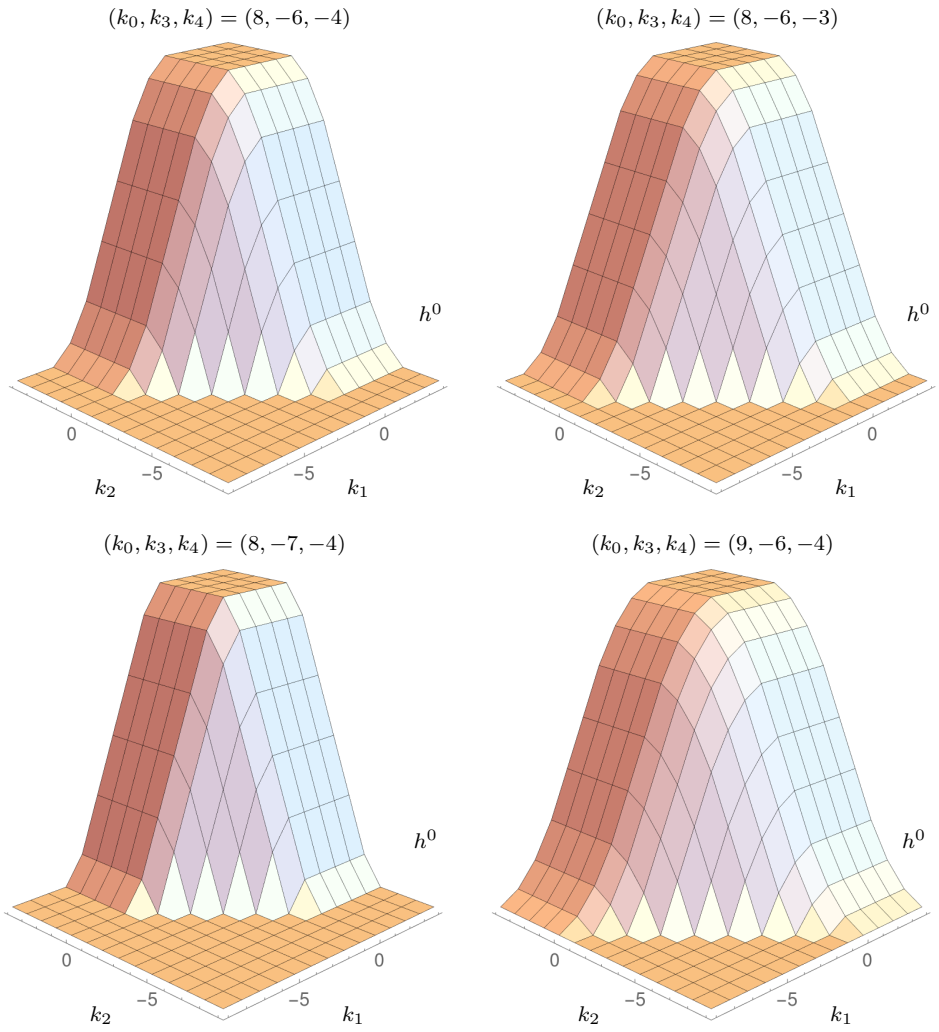

Figure 23: *Zeroth cohomology* $h^0(\mathrm{dP}_4, \mathcal{O}_{\mathrm{dP}_4}(k_0 l + k_1 e_1 + \ldots + k_4 e_4))$ *as a function of* (k_1, k_2) *in the range* $k_1, k_2 = -9, \ldots, 4$*, for four sets of fixed values for* (k_0, k_3, k_4)*. The lattice data points have been joined into surfaces for clarity.*

if we focus on two-dimensional slices in the Picard lattice and combine the information from various such slices. We recall that line bundles on dP_n are labelled by an $(n+1)$-dimensional integer vector $\mathbf{k} = (k_0, k_1, \ldots, k_n)$, with the associated divisor given in Eq. (5.14).

Let us illustrate the process of finding the region boundaries for the example dP_4. The Picard number of this space is five, so a two-dimensional slice misses the behaviour of a boundary in the remaining three directions. We begin with slices in the (k_1, k_2) plane, taken for various fixed choices of the remaining coefficients (k_0, k_3, k_4). In Figure 23 we have plotted four such two-dimensional slices through the Picard lattice of dP_4 which show several region boundaries. As an example, we focus on the diagonal boundary which separates the regions of zero and non-zero cohomology.

The dependence on k_1 and k_2 is immediately clear: this boundary must be of the form $k_1 + k_2 + \ldots = 0$. To find the dependence on the remaining k_i, we compare slices. Take as a

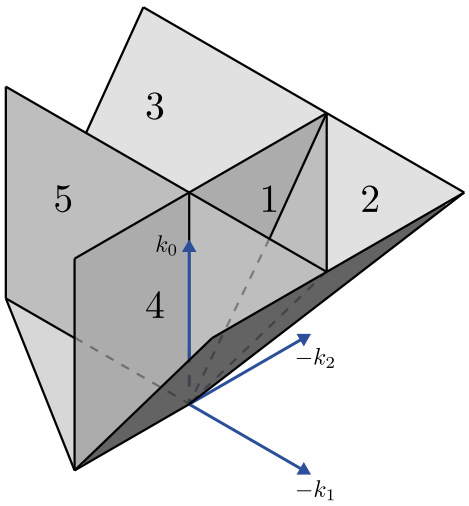

Figure 24: *Depiction of the Picard lattice of the del Pezzo surface* dP_2*. We do not draw the lattice points to avoid clutter. The five numbered cones are regions where different non-zero polynomials describe the zeroth cohomology; together they make up the Mori cone.*

starting point the slice with $(k_0, k_3, k_4) = (8, -6, -4)$ (upper left plot). When we increase k_4 (upper right plot), the boundary advances by one unit and when k_3 decreases by one (lower left plot), the boundary recedes by one unit. Finally, when we instead increase k_0 (lower right plot), the boundary advances by two units. Hence the equation of this boundary is

$$2k_0 + k_1 + k_2 + k_3 + k_4 = 0\,. \tag{5.23}$$

As one would expect, four slices were sufficient to determine this boundary. The other boundaries visible in Figure 23 can be determined in the same way. The polynomials can then be obtained by a fit to the data in each region. The formulae obtained in this way are of course still conjectures, extracted from a finite amount of cohomology data.

As already mentioned, the piecewise polynomial formulae for dP_n become quite complicated for larger n and have too many case distinctions to be reproduced here. However, it is possible to discuss dP_2 in a concise way and we do this now for illustration. The Picard number of this surface is three and line bundles are labelled by a three-dimensional integer vector $\mathbf{k} = (k_0, k_1, k_2)$. Figure 24 is a plot of the regions that correspond to distinct polynomials. All region boundaries in this case are hyperplanes through the origin, so the regions themselves are cones with their bases at the origin. Evidently, there are five distinct non-zero regions as numbered in

the diagram, and they are described by the following sets of inequalities.

$$\begin{array}{lccccccc}
\text{Region 1:} & -k_1 \geq 0 & -k_2 \geq 0 & k_0+k_1+k_2 \geq 0 & & & & \\
\text{Region 2:} & & & k_0+k_1+k_2 < 0 & k_0+k_1 \geq 0 & k_0+k_2 \geq 0 & & \\
\text{Region 3:} & -k_1 < 0 & -k_2 \geq 0 & & & k_0+k_2 \geq 0 & & \\
\text{Region 4:} & -k_1 \geq 0 & -k_2 < 0 & & & k_0+k_2 \geq 0 & & \\
\text{Region 5:} & -k_1 < 0 & -k_2 < 0 & & & & k_0 \geq 0 &
\end{array} \tag{5.24}$$

Note that Region 1 is the nef cone and that the union of the five regions is the Mori cone. The polynomials that describe the zeroth cohomology dimension in each of these five regions are as follows.

$$h^0(\mathrm{dP}_2, \mathcal{O}_{\mathrm{dP}_2}(\mathbf{k})) = \begin{cases} 1+\frac{3}{2}k_0+\frac{1}{2}k_0^2+\frac{1}{2}k_1-\frac{1}{2}k_1^2+\frac{1}{2}k_2-\frac{1}{2}k_2^2 & \text{in Region 1} \\ 1+2k_0+k_0^2+k_1+k_0k_1+k_2+k_0k_2+k_1k_2 & \text{in Region 2} \\ 1+\frac{3}{2}k_0+\frac{1}{2}k_0^2+\frac{1}{2}k_2-\frac{1}{2}k_2^2 & \text{in Region 3} \\ 1+\frac{3}{2}k_0+\frac{1}{2}k_0^2+\frac{1}{2}k_1-\frac{1}{2}k_1^2 & \text{in Region 4} \\ 1+\frac{3}{2}k_0+\frac{1}{2}k_0^2 & \text{in Region 5}\,. \end{cases} \tag{5.25}$$

The main features of this formula - regions which are cones with bases at the origin and cohomology dimensions described by a quadric in each region - persist for all del Pezzo surfaces. Writing down the analogous formulae for dP_n with $n > 2$ becomes impractical as the number of regions increases very quickly with n. For this reason, we will now extract a more concise formula which works for all del Pezzo surfaces.

There is a more sophisticated way to extract regions and polynomials from data by using methods from machine learning. This is discussed in detail in a companion paper [12].

5.2.6 A compact formula for del Pezzo surfaces

The first step towards extracting a concise formula which works for all del Pezzo surfaces is to understand the structure of the hyperplanes which separate the regions. Each such hyperplane is determined by a normal vector $\mathbf{v}$ such that the boundary is described by the equation $\langle \mathbf{v}, \mathbf{k} \rangle = \mathbf{v}^T G\, \mathbf{k} = 0$, where G is the intersection matrix in Eq. (5.15). For dP_2 these normal vectors can be read off from the inequalitites in the first three columns of (5.24), while the last three columns correspond to the boundaries of the Mori cone. Repeating the exercise for dP_3 we find

the following lists of normal vectors.

$$\begin{aligned}
&\mathrm{dP}_2: \quad \mathbf{v} \in \{(0,1,0)\,,\,(0,0,1)\,,\,(1,-1,-1)\} \\
&\mathrm{dP}_3: \quad \mathbf{v} \in \{(0,1,0,0)\,,\,(0,0,1,0)\,,\,(0,0,0,1)\,,\,(1,-1,-1,0)\,,\,(1,-1,0,-1)\,,\,(1,0,-1,-1)\}
\end{aligned} \tag{5.26}$$

For dP_4, the normal vectors have the same structure as for dP_3 but with the other obvious permutations included. The same is true for dP_5, except, additionally, the new vector $\mathbf{v} = (2,-1,-1,-1,-1,-1)$ appears.

The reader familiar with the properties of del Pezzo surfaces will immediately recognise the above divisors as the generators of the Mori cone or, equivalently, as the exceptional divisors with self-intersection -1. We conclude that the bounding hyperplanes for the various regions are described by the Mori cone generators and, it turns out, this holds for all dP_n with $n = 1,\ldots,8$. We denote the set of Mori and nef cone generators for dP_n by $\hat{\mathcal{M}}$ and $\hat{\mathcal{N}}$, respectively, and their elements are explicitly listed in Appendix E.2.

Our next task is to find the quadratic polynomials that describe the cohomology in the various regions of the Picard lattice. To this end, it is instructive to look at the difference between two polynomials P and $\tilde{P}$ in neighbouring regions, separated by a boundary hyperplane with normal vector $\mathbf{v}$. By inspecting examples, it turns out that the change is always of the form

$$P - \tilde{P} = \frac{1}{2} q(q+1)\,, \tag{5.27}$$

where q is a linear expression in the k_i with integer coefficients. In fact these integer coefficients follow a pattern too. If the region with polynomial P is characterised by $\langle \mathbf{k}, \mathbf{v}\rangle \geq 0$ and the one with polynomial $\tilde{P}$ by $\langle \mathbf{k}, \mathbf{v}\rangle < 0$, where $\mathbf{v} \in \hat{\mathcal{M}}$, then we have

$$P - \tilde{P} = \frac{1}{2}\langle \mathbf{k}, \mathbf{v}\rangle(\langle \mathbf{k}, \mathbf{v}\rangle + 1)\,. \tag{5.28}$$

The above term on the right-hand side appears when we cross a boundary with normal vector $\mathbf{v}$ into a region with $\langle \mathbf{k}, \mathbf{v}\rangle < 0$. It is therefore natural to start in the "simplest" region where $\langle \mathbf{k}, \mathbf{v}\rangle \geq 0$ for all $\mathbf{v} \in \hat{\mathcal{M}}$. This region is of course precisely the nef cone $\mathcal{N}(\mathrm{dP}_n)$, the dual of the Mori cone, where the zeroth cohomology dimension is given by the index. Hence, for the divisor $D = k_0 l + k_1 e_1 + \cdots + k_n e_n$, we have the following formula

$$h^0\left(\mathrm{dP}_n, \mathcal{O}_{\mathrm{dP}_n}(\mathbf{k})\right) = \begin{cases} \mathrm{ind}(\mathcal{O}_{\mathrm{dP}_n}(\mathbf{k})) + \dfrac{1}{2}\displaystyle\sum_{\mathbf{v}\in\hat{\mathcal{M}}} \theta\left(-\langle \mathbf{k}, \mathbf{v}\rangle\right)\langle \mathbf{k}, \mathbf{n}\rangle(\langle \mathbf{k}, \mathbf{n}\rangle + 1) & \text{if } \begin{cases} \langle \mathbf{k}, \mathbf{w}\rangle \geq 0 \\ \forall\, \mathbf{w} \in \hat{\mathcal{N}} \end{cases} \\ 0 & \text{otherwise} \end{cases} \tag{5.29}$$

for the zeroth cohomology dimensions, where we recall that $\langle \mathbf{k}, \mathbf{v} \rangle = \mathbf{k}^T G \mathbf{v}$ is the intersection form in our standard basis, as defined in Eq. (5.15). Further, $\hat{\mathcal{M}}$ and $\hat{\mathcal{N}}$ are the sets of Mori and nef cone generators which are explicitly provided in Appendix E.2.

As for the earlier formula (5.25) for dP_2, this result has been extracted from data and is, hence, still at the level of a conjecture. However, we have validated Eq. (5.29) for all dP_n by comparing with data in a box with $|k_i| \leq k_{\max} \simeq 20$.

It is easy to convert Eq. (5.29) into the basis-independent form

$$h^0(\mathrm{dP}_n, \mathcal{O}_{\mathrm{dP}_n}(D)) = \begin{cases} \mathrm{ind}(D) + \frac{1}{2} \sum_{C \in \hat{\mathcal{M}}} \theta\left(-D \cdot C\right) \left(D \cdot C\right) \left(D \cdot C + 1\right) & \text{if } D \in \mathcal{M}(\mathrm{dP}_n) \\ 0 & \text{otherwise} \end{cases} . \tag{5.30}$$

Even though this is already quite concise there is an even better way of writing this formula which suggests a natural origin of the additional terms in the above sum. We will now derive this alternative form.

5.2.7 An index formula for del Pezzo surfaces

Our guiding principle for a re-formulation of Eq. (5.30) is the hope that the entire right-hand side can be written as an index, similar to what we have found for Hirzebruch surfaces. In this context, a key observation is that each additional term $\frac{1}{2}\left(D \cdot C\right)\left(D \cdot C + 1\right)$ in Eq. (5.30) can be written as a difference between two indices. Specifically, we have

$$\begin{aligned} \mathrm{ind}\left(D + (D \cdot C)C\right) &= 1 + \frac{1}{2}\left(D + (D \cdot C)C\right) \cdot \left(D + (D \cdot C)C - K_{\mathrm{dP}_n}\right) \\ &= \mathrm{ind}\left(D\right) + \frac{1}{2}(D \cdot C)\left[2(D \cdot C) + (D \cdot C)C^2 - (C \cdot K_{\mathrm{dP}_n})\right] \\ &= \mathrm{ind}\left(D\right) + (D \cdot C)\left[(D \cdot C) + 1\right] , \end{aligned} \tag{5.31}$$

where the first equality follows from the Riemann-Roch theorem (5.7). In the third step we have used the fact that C is an exceptional curve, that is a curve with genus $g = 1$ and self-intersection $C^2 = -1$, which implies that $C \cdot K_{\mathrm{dP}_n} = 1$. The last statement follows immediately from the adjunction formula

$$g = \frac{1}{2}(K_S \cdot C + C \cdot C) + 1 \tag{5.32}$$

for the genus g of a curve $C \subset S$ on a surface S.

The above result shows that every term in the sum in Eq. (5.30) can be written as an index. Is this perhaps the case for the entire sum? A natural guess for how a single index might capture the entire expression in Eq. (5.30) is

$$\mathrm{ind}\left(D + \sum_{C \in \hat{\mathcal{M}}} \theta\left(-D \cdot C\right) \left(D \cdot C\right) C\right) \stackrel{?}{=} \mathrm{ind}(D) + \frac{1}{2} \sum_{C \in \hat{\mathcal{M}}} \theta\left(-D \cdot C\right) \left(D \cdot C\right) \left(D \cdot C + 1\right) . \tag{5.33}$$

Is this correct? Working out the left-hand side of Eq. (5.33) by using Eq. (5.31), one finds

$$\text{ind}\left(D+\sum_{C\in\hat{\mathcal{M}}_D}(D\cdot C)C\right)=\text{ind}(D)+\frac{1}{2}\sum_{C\in\hat{\mathcal{M}}_D}(D\cdot C)\left[2(D\cdot C)+\sum_{C'\in\hat{\mathcal{M}}_D}(D\cdot C')(C\cdot C')+1\right], \tag{5.34}$$

where we have introduced the set $\hat{\mathcal{M}}_D=\{C\in\hat{\mathcal{M}}\,|\,C\cdot D<0\}$ for ease of notation. Unfortunately, the right-hand sides of Eqs. (5.33) and (5.34) are not quite the same. However, if any two distinct exceptional divisors $C,C'\in\hat{\mathcal{M}}_D$ satisfy $C\cdot C'=0$ we have a perfect match. A quick look at the exceptional divisors in Appendix E.2 shows that not all distinct pairs have a vanishing intersection. But this is also too strong a requirement - all we need is that any two distinct exceptional divisors C and C' with $D\cdot C<0$ and $D\cdot C'<0$ for a given effective divisor D do not intersect. Remarkably, this weaker statement turns out to be true as shown in the following theorem.

Theorem 5.35. *Let C and C' be distinct generators of the Mori cone of dP_n such that $C\cdot C'\neq 0$. If $D\cdot C\leq 0$ and $D\cdot C'<0$ then D is not in the cone of effective divisors.*

Proof. Assume, for contradiction, that D is in the cone of effective divisors. Denote the generators of the effective cone by C_i and set $C_1=C$ and $C_2=C'$ for convenience. Then we can write $D=\sum_i\alpha_iC_i$, where all $\alpha_i\geq 0$. It follows that

$$0\geq D\cdot C_1=-\alpha_1+\alpha_2(C_1\cdot C_2)+\sum_{i>2}\alpha_i(C_1\cdot C_i)\geq-\alpha_1+\alpha_2\,,$$

and, hence, that $\alpha_1\geq\alpha_2$. An analogous calculation using $0>D\cdot C_2$ leads to $\alpha_2>\alpha_1$ which is a contradiction. Hence, D is not effective. □

Therefore, two distinct exceptional divisors $C,C'\in\hat{\mathcal{M}}_D$ do indeed satisfy $C\cdot C'=0$ and using this fact (together with $C^2=-1$) on the right-hand side of Eq. (5.34) shows that Eq. (5.33) is indeed correct. This allows us to write our cohomology formula in its final form as

$$h^0\left(\text{dP}_n,\mathcal{O}_{\text{dP}_n}(D)\right)=\begin{cases}\text{ind}\left(D+\sum_{C\in\hat{\mathcal{M}}}\theta\left(-D\cdot C\right)(D\cdot C)C\right) & \text{if } D\in\mathcal{M}(\text{dP}_n)\\ 0 & \text{otherwise}\end{cases}. \tag{5.36}$$

We recall that $\hat{\mathcal{M}}$ is the list of Mori cone generators for dP_n, given in Appendix E.2. At this stage, the above formula is still a conjecture, since it is ultimately based on analysing cohomology data. Nevertheless it is quite remarkable in a number of ways. First of all, it allows for a practical computation of the zeroth cohomology dimensions even for the del Pezzo surfaces with larger Picard numbers. For a given divisor D it is easy to identify the Mori cone generators C with

a negative intersection, $D \cdot C < 0$, which enter the sum in Eq. (5.36). This is quite unlike the piecewise quadratic formulae, such as Eq. (5.25), considered earlier which become quickly unmanageable as the Picard number increases.

Secondly, it is surprising that the zeroth cohomology dimension of an effective divisor D can be written as the index,

$$h^0\left(\mathrm{dP}_n, \mathcal{O}_{\mathrm{dP}_n}(D)\right) = \mathrm{ind}(\tilde{D})\,, \tag{5.37}$$

of a different, shifted divisor

$$\tilde{D} = D + \sum_{C \in \hat{\mathcal{M}}} \theta\left(-D \cdot C\right)\left(D \cdot C\right) C\,. \tag{5.38}$$

This is in line with what we have found for Hirzebruch surfaces in Eq. (5.22). We will see that these results are part of a more general mathematical story in the next section, which implies the above index formula for del Pezzo surfaces as well as the earlier one for Hirzebruch surfaces.

5.3 Theorems for general surfaces

In the previous section, we have studied line bundle cohomology on Hirzebruch and del Pezzo surfaces, starting from algorithmically computed data. After several steps of re-writing our empirical formulae we have arrived at a remarkable result. The dimension of the zeroth cohomology can be written as an index,

$$h^0\big(S, \mathcal{O}_S(D)\big) = \mathrm{ind}\big(\tilde{D}\big)\,, \tag{5.39}$$

of a shifted divisor $\tilde{D}$. For Hirzebruch surfaces this shifted divisor has been defined in Eq. (5.21) and the analogous result for del Pezzo surfaces is given in Eq. (5.38).

The main purpose of this section is to develop the mathematics underlying Eq. (5.39) in as much generality as possible and to find proofs for the Hirzebruch and del Pezzo index formulae. It turns out that the argument naturally proceeds in two steps. The first step, discussed in the following subsection, is to introduce a certain divisor shift which can be shown to leave the zeroth cohomology dimension unchanged. The second step is taken in Section (5.3.2) where we combine the divisor shift with certain vanishing theorems. As we will see, this will lead to index formulae for certain classes of surfaces, including Hirzebruch and del Pezzo surfaces. For general mathematical background see, for example, Refs. [120, 121].

5.3.1 Cohomology-preserving shifts

For both Hirzebruch and del Pezzo surfaces we have seen that a certain divisor shift plays a crucial role in writing down an index formula. Moreover, the equations (5.21) and (5.38) for

these shifts have a similar structure which suggests there exists a generalisation to all complex surfaces. The following theorem defines this general shift and asserts that it leaves the dimension of the zeroth cohomology unchanged.

Theorem 5.40. *Let D be an effective divisor on a smooth compact complex projective surface S, with associated line bundle $\mathcal{O}_S(D)$. Let $\mathcal{I}$ be the set of irreducible negative self-intersection divisors. Then the following map on the Picard lattice,*

$$D \to \tilde{D} = D - \sum_{C \in \mathcal{I}} \theta(-D \cdot C)\, \mathrm{ceil}\left(\frac{D \cdot C}{C^2}\right) C\,, \tag{5.41}$$

preserves the zeroth cohomology,

$$h^0\big(S, \mathcal{O}_S(\tilde{D})\big) = h^0\big(S, \mathcal{O}_S(D)\big)\,. \tag{5.42}$$

While it can happen that there are infinitely many irreducible negative self-intersection divisors, only finitely many can have a negative intersection with a given divisor D. This means only finitely many terms appear in the sum in Eq. (5.41). Note that once the intersection form and the negative self-intersection divisors on S are known it is straightforward to evaluate Eq. (5.41) explicitly. We will sometimes refer to Eq. (5.41) as the "master formula" for cohomology.

Let us first give an intuitive explanation of this theorem and then a slightly more rigorous proof. In this paragraph and the next two, the term "divisor" will refer to an actual divisor, rather than to a divisor class as in the rest of the chapter. First recall that in the context of the divisor line bundle correspondence the projectivisation of the zeroth cohomology $H^0(S, \mathcal{O}_S(D))$ can be identified with the linear system, $|D|$, of the associated divisor. The linear system $|D|$ of a divisor consists of all effective divisors equivalent to D and we can, loosely, think of it as the deformations of D. The dimension of the linear system and, hence, the dimension of the zeroth cohomology remains unchanged if we remove from D a piece without deformations, that is, a rigid piece.

How can a rigid piece in a divisor D be detected? A rigid divisor C has negative self-intersection, $C^2 < 0$. If such a rigid divisor C is contained in D it gives a negative contribution to the intersection number $D \cdot C$. Of course this negative contribution might be overwhelmed by other positive ones but if it so happens that $D \cdot C < 0$ we can conclude that D contains the rigid divisor C. This is the detection method for rigid divisors underlying Theorem 5.40, as the step function in Eq. (5.41) indicates. In fact, the value of the ceiling function in Eq. (5.41) gives the multiple of C contained in D. Eq. (5.41) removes the multiples of all rigid divisors in

D which can be detected in this manner and, hence, the dimension of the zeroth cohomology remains unchanged.

A slightly more rigorous proof is as follows. On a surface any effective divisor D can be expanded as

$$D = \sum_a \beta_a D_a \,, \tag{5.43}$$

where D_a are pairwise distinct irreducible divisors and $\beta_a \geq 0$. If we assume that there is a negative intersection $D \cdot D_i < 0$ for some irreducible divisor, $i \in \{a\}$, then we have

$$0 > D \cdot D_i = \sum_a \beta_a D_a \cdot D_i = \beta_i D_i^2 + (\text{non-negative terms}) \geq \beta_i D_i^2 \,, \tag{5.44}$$

since distinct irreducible divisors have non-negative intersections. This implies the bound

$$\beta_i \geq \text{ceil}\left(\frac{-D \cdot D_i}{-D_i^2}\right) . \tag{5.45}$$

Since the bound (5.45) depends on intersection products only, it must apply to any element of $|D|$, since every element in the complete linear system $|D|$ is linearly equivalent. Hence every element in the complete linear system must contain this piece, and hence does not contribute to the dimension count of $|D|$. Repeating for any other irreducible divisors that negatively intersect D, we see that we can remove the following divisor from D while preserving the dimension of $|D|$,

$$F = \sum_{i:\, D\cdot D_i<0} \text{ceil}\left(\frac{-D_i \cdot D}{-D_i^2}\right) D_i$$

That is,

$$\dim|D| = \dim|D - F| \,, \tag{5.46}$$

or, equivalently,

$$h^0(S, \mathcal{O}(D)) = h^0(S, \mathcal{O}(D - F)) \,. \tag{5.47}$$

It is important to note that iterating the map (5.41) is not necessarily trivial. The rigid pieces which can be detected in the divisor $\tilde{D}$, obtained after applying the map to D once, might well be different from the ones detected in D. Hence, we should apply the map (5.41) multiple times until the result stabilises. We denote the divisor which results from this process by $\underline{\tilde{D}}$ and this divisor has the following property.

Corollary 5.48. *Write $\underline{\tilde{D}}$ for the divisor that is the result of iterating the map $D \to \tilde{D}$ defined by Eq. (5.41), until stabilisation after a finite number of steps. Then $\underline{\tilde{D}}$ is a nef divisor such that $h^0\big(S, \mathcal{O}(D)\big) = h^0\big(S, \mathcal{O}(\underline{\tilde{D}})\big)$.*

It is clear from Theorem 5.40 that $\underline{\tilde{D}}$ has the same zeroth cohomology dimension as D but why is $\underline{\tilde{D}}$ a nef divisor? Recall that, by definition, a divisor $\mathcal{D}$ is nef if there are no irreducible, negative self-intersection divisors C with $\mathcal{D}\cdot C < 0$. By construction, the divisor $\underline{\tilde{D}}$ has precisely this property. This iteration of the map $D \to \tilde{D}$ can be seen to be a particular implementation of Zariski decomposition [111].

For the purpose of computing cohomology, Theorem 5.40 and its corollary can be helpful if the cohomology dimension of the new divisor $\underline{\tilde{D}}$ is easier to determine than that of D. This can happen if a suitable vanishing theorem applies to the nef divisors $\underline{\tilde{D}}$ and this is what we will discuss in the next sub-section.

5.3.2 Combination with vanishing theorems

In the previous sub-section we have seen that the problem of computing the zeroth cohomology dimensions over the full Picard lattice reduces to computing these cohomologies in the nef cone. Frequently, there is a vanishing theorem which asserts that higher cohomologies vanish for nef divisors $\mathcal{D}$. In this case, the zeroth cohomology for such divisors can be computed from the index, that is, if

$$h^q(S, \mathcal{O}_S(\mathcal{D})) = 0 \text{ for } q = 1, 2 \quad \Rightarrow \quad h^0(S, \mathcal{O}_S(\mathcal{D})) = \text{ind}(\mathcal{D})\,. \tag{5.49}$$

Hence, we have the following simple corollary.

Corollary 5.50. *If a vanishing theorem on a smooth compact complex projective surface S establishes that higher cohomologies vanish in the nef cone, then any effective divisor D satisfies $h^0\big(S, \mathcal{O}(D)\big) = \text{ind}\big(S, \mathcal{O}(\underline{\tilde{D}})\big)$, where $\underline{\tilde{D}}$ is the divisor obtained from D by iterating the map (5.41).*

Which known vanishing theorems might be used to establish the required vanishing property in the nef cone? The prototypical example of a vanishing theorem for higher cohomologies is the Kodaira vanishing theorem and a particularly powerful generalisation of this theorem is the Kawamata-Viehweg vanishing theorem.

Theorem 5.51 (Kawamata-Viehweg vanishing theorem for surfaces)**.** *Let S be a smooth complex projective surface, and let D be a nef and big*[43] *divisor on S. Then*

$$h^q\left(S, \mathcal{O}_S(K_S + D)\right) = 0 \quad \text{for } q > 0\,. \tag{5.52}$$

[43] A nef divisor is big if and only if its self-intersection is strictly positive.

When a space is toric, there is the stronger Demazure vanishing theorem.

Theorem 5.53 (Demazure vanishing theorem for surfaces)**.** *Let S be a toric surface whose fan has convex support, and let D be a nef divisor. Then*

$$h^q\left(S, \mathcal{O}_S(D)\right) = 0 \quad \text{for } q > 0\,. \tag{5.54}$$

For which spaces do these theorems guarantee that higher cohomologies vanish in the nef cone? The Demazure vanishing theorem holds for the entire nef cone and applies to toric varieties whose fans have convex support. In fact, the fan has convex support for any compact toric surface - see for example Ref. [84] - so we have the following corollary.

Corollary 5.55. *Let S be a compact toric surface, and let D be an effective divisor. Then*

$$h^0\big(S, \mathcal{O}(D)\big) = \mathrm{ind}(\underline{\tilde{D}})\,, \tag{5.56}$$

where the divisor $\underline{\tilde{D}}$ is obtained from D by iterating the map (5.41).

Clearly, this covers a large and important set of surfaces, including all Hirzebruch surfaces, as well as their blow-ups, the del Pezzo surfaces dP_n for $n = 1, 2, 3$, and their blow-ups and the toric surfaces that correspond to the 16 reflexive polytopes. What we have shown is that index formulae for the zeroth cohomology dimension exist for all these cases. Since all these toric surfaces frequently appear in compactification these results are of direct relevance for string theory.

The Kawamata-Viehweg vanishing theorem applies to a very general class of surfaces S, but it guarantees vanishing in a region that is not precisely the nef cone. Specifically, it asserts vanishing of the higher cohomologies of a divisor D if $D - K_S$ is nef and big. It applies to divisors in the intersection of the nef and big cones, shifted by the anti-canonical divisor $-K_S$. This is of partial use, since this region has some overlap with the nef cone and, hence, leads to index formulae for some but not all effective divisors. Sometimes this overlap covers almost all of the nef cone and this can be shown to happen for Hirzebruch surfaces.

However, for surfaces with a nef and big anti-canonical bundle $-K_S$ the Kawamata-Viehweg vanishing theorem can be applied to all nef divisors D. To see this, first note that both D and $-K_S$ being nef immediately impies that $D - K_S$ is nef. To show that $D - K_S$ is big we consider its self-intersection

$$(D - K_S)^2 = D^2 + 2D \cdot (-K_S) + (-K_S)^2\,. \tag{5.57}$$

Since $-K_S$ is nef and D is effective, the first two terms on the right-hand-side are ≥ 0. Additionally since $-K_S$ is big, $(-K_S)^2 > 0$, so that $(D - K_S)^2 > 0$ and, hence, $D - K_S$ is big. This leads to the following corollary.

Corollary 5.58. *Let S be a smooth compact complex projective surface with nef and big anti-canonical divisor, $-K_S$, and let D be an effective divisor. Then*

$$h^0\big(S, \mathcal{O}(D)\big) = \mathrm{ind}(\underline{\tilde{D}})\,, \tag{5.59}$$

where the divisor $\underline{\tilde{D}}$ is obtained from D by iterating the map (5.41).

A quick glance at Eq. (5.16) shows that the anti-canonical divisor for dP_n is nef and big. Hence Corollary 5.58 applies to all del Pezzo surfaces dP_n, where $n = 0, 1, \ldots, 8$, and guarantees the existence of an index formula.

We have now seen that index formulae exist for many types of surfaces. However, the divisor in the argument of the index is obtained by iterating the master formula (5.41) and is, hence, fairly complicated in general. In practice, this corresponds to an algorithm for computing the cohomology dimension rather than explicit formula. However, there are surfaces where a single application of the master formula (5.41) already maps into the nef cone. In such cases, we have a simple index formula for the cohomology dimension as stated in the following corollary.

Corollary 5.60. *Let S be a smooth compact complex projective surface on which a vanishing theorem guarantees that higher cohomologies vanish in the nef cone. If additionally, for any effective divisor D the divisor $\tilde{D}$ defined in Eq. (5.41) is in the nef cone, then we have*

$$h^0\left(S, \mathcal{O}_S(D)\right) = \mathrm{ind}\left(D - \sum_{C\in\mathcal{I}} \theta(-D\cdot C)\,\mathrm{ceil}\left(\frac{D\cdot C}{C^2}\right) C\right), \tag{5.61}$$

where $\mathcal{I}$ is the set of irreducible negative self-intersection divisors.

We have already established for both Hirzebruch and del Pezzo surfaces dP_n that higher cohomologies vanish in the nef cone. Now we show that the second condition in Corollary 5.60 is also satisfied, that is, the master formula (5.41) maps into the nef cone for both classes of surfaces.

This is quite easy to see for Hirzebruch surfaces $\mathbb{F}_n$ since there exists only one irreducible negative self-intersection divisor $C = D_1$ with $C^2 = -n$. The master formula removes as many copies of C from D as are detected by the intersection number $D\cdot C$. So, even if $D\cdot C < 0$ we have

$$\tilde{D}\cdot C = D\cdot C - \mathrm{ceil}\left(\frac{D\cdot C}{C^2}\right) C^2 \geq 0\,. \tag{5.62}$$

This means applying the master formula once more to $\tilde{D}$ leaves the divisor unchanged. Hence, from Corollary 5.60, we have the following index formula for the Hirzebruch surfaces.

Corollary 5.63. *Let D be any effective divisor on the Hirzebruch surface $\mathbb{F}_n$. Then*

$$h^0\left(\mathbb{F}_n, \mathcal{O}_{\mathbb{F}_n}(D)\right) = \mathrm{ind}\left(D - \theta(-D\cdot C)\,\mathrm{ceil}\left(\frac{D\cdot C}{C^2}\right) C\right), \tag{5.64}$$

where C is the unique irreducible negative self-intersection divisor, for which $C^2 = -n$.

This proves the index formula for Hirzebruch surfaces, conjectured from cohomology data in Eq. (5.22).

For del Pezzo surfaces dP_n we can also show that the map (5.41) stabilises after the first step and, hence, that the divisor $\tilde{D}$ is in the nef cone. However, the proof is slightly more difficult than for Hirzebruch surfaces due to the presence of multiple irreducible divisors with negative self-intersection. We proceed in steps.

Lemma 5.65. *Let D be an effective divisor on a smooth complex projective surface, and write $\{D_i\}$ for the finite collection of irreducible divisors D_i with $D \cdot D_i < 0$. Then $D_i \cdot D_{j\neq i} < \max(-D_i^2, -D_j^2)$.*

Proof. Let D_i and D_j be as above and write the curve decomposition of D

$$D = \beta_i D_i + \beta_j D_j + D_{\text{eff.}} \,, \tag{5.66}$$

where $D_{\text{eff.}}$ is an effective divisor and the integers $\beta_i, \beta_j \geq 0$. Then

$$\begin{aligned} 0 > D \cdot D_i &= \beta_i(D_i^2) + \beta_j(D_i \cdot D_j) + (\text{non-negative terms}) \,, \\ 0 > D \cdot D_j &= \beta_i(D_i \cdot D_j) + \beta_j(D_j^2) + (\text{non-negative terms}) \,. \end{aligned} \tag{5.67}$$

Hence

$$\begin{aligned} 0 > \beta_i(D_i^2) + \beta_j(D_i \cdot D_j) \quad &\Rightarrow \quad \beta_i > \left(\frac{D_i \cdot D_j}{-D_i^2}\right)\beta_j \,, \\ 0 > \beta_i(D_i \cdot D_j) + \beta_j(D_j^2) \quad &\Rightarrow \quad \beta_j > \left(\frac{D_i \cdot D_j}{-D_j^2}\right)\beta_i \,. \end{aligned} \tag{5.68}$$

But these are inconsistent unless at least one of the bracketed factors is less than one, which proves the theorem. □

Corollary 5.69. *Under the same conditions as the lemma, if there are no irreducible divisors with self-intersection < -1, then $D_i \cdot D_j = -\delta_{ij}$.*

Proof. This is immediate. □

Theorem 5.70. *On smooth projective surfaces containing no negative curves with self-intersection < -1 the map $D \to \tilde{D} \to \tilde{\tilde{D}} \to \ldots$ applied to an effective divisor stabilises after at most one application.*

Proof. As D is effective, write its curve decomposition as

$$D = \sum_i \beta_i D_i + \sum_\alpha \beta_\alpha D_\alpha + \sum_\mu \beta_\mu D_\mu \,, \tag{5.71}$$

where i, α, μ index, respectively, the irreducible divisors such that $D \cdot D_i < 0$, those such that $D_\alpha^2 < 0$ but $D \cdot D_\alpha \geq 0$, and the remainder. As usual, denote by $\tilde{D}$ the single shift of D,

$$\tilde{D} = D + \sum_i (D_i \cdot D)\, D_i \,. \tag{5.72}$$

To show that $\tilde{D}$ is nef, first note that $\tilde{D} \cdot D_\mu \geq 0$. Furthermore, note that

$$\tilde{D} \cdot D_j = D \cdot D_i + \sum_i (D_i \cdot D)\,(D_i \cdot D_j) = 0 \tag{5.73}$$

by Corollary 5.69. It remains only to show that $\tilde{D} \cdot D_\alpha \geq 0$. Collect the terms proportional to D_i in $\tilde{D}$

$$\begin{aligned} \tilde{D} &= \sum_i (\beta_i + D_i \cdot D)\, D_i + \sum_\alpha \beta_\alpha D_\alpha + \sum_\mu \beta_\mu D_\mu \\ &= \sum_i \left(\sum_\alpha \beta_\alpha (D_i \cdot D_\alpha) + \sum_\mu \beta_\mu (D_i \cdot D_\mu) \right) D_i + \sum_\alpha \beta_\alpha D_\alpha + \sum_\mu \beta_\mu D_\mu \,, \end{aligned} \tag{5.74}$$

where we have used again the relation $D_i \cdot D_j = -\delta_{ij}$. The only negative contribution in $\tilde{D} \cdot D_\alpha$ is $\beta_\alpha D_\alpha^2 = -\beta_\alpha$. Now, if $D_i \cdot D_\alpha = 0$ for all i, then $\tilde{D} \cdot D_\alpha = D \cdot D_\alpha \geq 0$ from the definition of $\tilde{D}$. So assume there is at least one i such that $D_i \cdot D_\alpha > 0$. But then from the above expression for $\tilde{D}$ it follows that

$$\tilde{D} \cdot D_\alpha = \beta_\alpha (D_i \cdot D_\alpha)^2 - \beta_\alpha + \text{ non-negative terms } \geq 0 \,. \tag{5.75}$$

Hence $\tilde{D}$ is in the nef cone. □

It is a well-known statement that the irreducible negative self-intersections divisors C of dP_n satisfy $C^2 = -1$, so the above theorem applies to del Pezzo surfaces. Together with Corollary 5.60 this leads to the following index formula for del Pezzo surfaces dP_n.

Corollary 5.76. *Let dP_n be the del Pezzo surface constructed by blowing up n generic points of the complex projective plane $\mathbb{P}^2$, where $n \in \{0, 1, \ldots, 8\}$, and let D be any effective divisor. Then*

$$h^0\left(\mathrm{dP}_n, \mathcal{O}_{\mathrm{dP}_n}(D)\right) = \mathrm{ind}\left(D + \sum_{C \in \mathcal{I}} \theta(-D \cdot C)\,(D \cdot C) C \right), \tag{5.77}$$

where $\mathcal{I}$ is the set of irreducible negative self-intersection divisors.

This proves the result we have conjectured in Eq. (5.36). Note that the ceiling function present in the master formula (5.41) disappears for del Pezzo surfaces since $C^2 = -1$ for all irreducible, negative self-intersection curves C.

5.4 Example applications

In Section 5.2 we have described the path from cohomology data to index formulae in some detail and in the previous section we have provided proofs for these index formulae. Here, we would like to take the mathematical results of the previous section for granted and illustrate how to derive cohomology formulae for specific surfaces from these general results. The examples we discuss are the Hirzebruch surface $\mathbb{F}_2$ and the del Pezzo surface dP_2.

5.4.1 The Hirzebruch surface $\mathbb{F}_2$

Much of the relevant information for Hirzebruch surfaces has already been summarised in Section 5.2.2. However, all Hirzebruch surfaces $\mathbb{F}_n$ are toric and therefore provide a good illustration for how to extract the relevant information from toric data. We will briefly discuss how to do this, based on the information provided in Appendix E.1.

First recall the following basic facts from toric geometry. The Picard lattice of a toric surface is spanned by integer combinations of the toric divisors, which correspond to rays of the toric diagram. Equivalence relations between toric divisors follow from the weight system and choosing representatives for the equivalence classes leads to a basis for the Picard lattice. For $\mathbb{F}_2$ we choose a basis (D_1, D_2) of the Picard lattice as explained in Appendix E.1 and in line with our conventions in Section 5.2.2. A general divisor is written as $D = k_1 D_1 + k_2 D_2$, so is labelled by a two-dimensional integer vector $\mathbf{k} = (k_1, k_2)$, and the Mori cone, $\mathcal{M}(\mathbb{F}_2)$, consists of all divisors with $k_1 \geq 0$ and $k_2 \geq 0$. The intersections between toric divisors are easily extracted: distinct toric divisors intersect if they correspond to neighbouring rays in the diagram, and self-intersections are determined by equivalence relations between toric divisors. From Appendix E.1, this leads to the $\mathbb{F}_2$ intersection rules

$$D_1^2 = -2\,, \quad D_1 \cdot D_2 = 1\,, \quad D_2^2 = 0\,, \tag{5.78}$$

in line with Eq. (5.8). From Eq. (5.10), the generators of the nef cone $\mathcal{N}(\mathbb{F}_2)$ are given by

$$\hat{\mathcal{N}}(\mathbb{F}_2) = \{D_2, D_1 + 2D_2\}\,. \tag{5.79}$$

It is straightforward to verify that the irreducible negative self-intersection divisors are precisely the toric divisors with negative self-intersection. For Hirzebruch surfaces there is precisely one such divisor, namely $C = D_1$. This is all the information we need to evaluate the index formula (5.60).

We refer to the region of non-effective divisors as Region 3, so

$$D \text{ not effective} \quad \Leftrightarrow \quad k_1 < 0 \text{ or } k_2 < 0 \quad (\text{Region 3})\,. \tag{5.80}$$

Obviously, in this region we have $h^0(\mathbb{F}_2, \mathcal{O}_{\mathbb{F}_2}(\mathbf{k})) = 0$. The Mori cone splits into precisely two regions, since there is only one irreducible negative self-intersection divisor. These two regions are given by

$$D \text{ effective and } D \cdot C \geq 0 \quad \Leftrightarrow \quad k_1 \geq 0,\, k_2 \geq 0,\, -2k_1 + k_2 \geq 0 \quad \text{(Region 1)} \tag{5.81}$$

$$D \text{ effective and } D \cdot C < 0 \quad \Leftrightarrow \quad k_1 \geq 0,\, k_2 \geq 0,\, -2k_1 + k_2 < 0 \quad \text{(Region 2)}\,. \tag{5.82}$$

Region 1 is the nef cone. The master formula (5.41) in this region is simply the identity map and, hence, the zeroth cohomology dimension is given by the index. In Region 2, the master formula specialises to

$$\tilde{D} = D - \text{ceil}\left(\frac{D \cdot C}{C^2}\right) C = \left(k_1 - \text{ceil}\left(\frac{nk_1 - k_2}{n}\right)\right) D_1 + k_2 D_2\,. \tag{5.83}$$

and the zeroth cohomology of D is given by the index of this shifted divisor $\tilde{D}$. As illustrated in Figure 25, Eq. (5.83) corresponds to a shift from Region 2 into the nef cone (Region 1). Combining this information with the explicit expression (5.12) for the index then leads to the

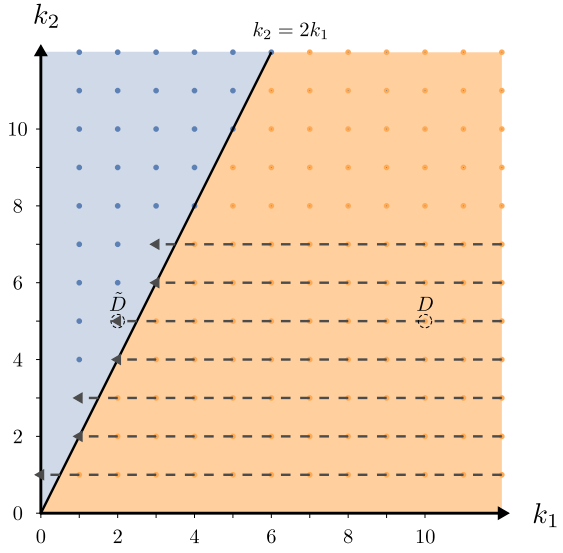

Figure 25: *The Picard lattice of the Hirzebruch surface $\mathbb{F}_2$. The positive quadrant is the Mori cone - outside of it the zeroth cohomology vanishes. The nef cone is the blue area. We show the shifts $D \to \tilde{D}$ that map into the nef cone. Note every point on a dotted line maps to the same final divisor.*

formula

$$h^0\left(\mathbb{F}_n, \mathcal{O}_{\mathbb{F}_n}(\mathbf{k})\right) = \begin{cases} \text{ind}(\mathcal{O}_{\mathbb{F}_2}(\mathbf{k})) & \text{(Region 1)} \\ \text{ind}(\mathcal{O}_{\mathbb{F}_2}(\mathbf{k})) + \frac{1}{2}nc - \frac{1}{2}nc^2 - ck_2 + nck_1 - c & \text{(Region 2)} \\ 0 & \text{(Region 3)} \end{cases} \tag{5.84}$$

$$c = \text{ceil}\left(\frac{nk_1 - k_2}{n}\right)\,.$$

This formula is consistent with the earlier one, Eq. (5.20), which we have extracted from cohomology data.

5.4.2 The del Pezzo surface dP_2

On del Pezzo surfaces dP_n, the Mori cone, irreducible negative self-intersection divisors, and the intersection form are well-known and we have collected these in Section 5.2.3 and in Appendix E.2. Let us recall what these look like for the case of dP_2. The rank of the dP_2 Picard lattice is three and a basis of divisors is given by

$$D_0 = l\,, \quad D_1 = e_1\,, \quad D_2 = e_2\,, \tag{5.85}$$

where l is the hyperplane class of the underlying complex projective plane $\mathbb{P}^2$, and e_1 and e_2 are the exceptional classes of the two blow-ups. The intersection form is fixed by the relations

$$l^2 = 1\,, \quad l \cdot e_i = 0\,, \quad e_i \cdot e_j = -\delta_{ij}\,. \tag{5.86}$$

A general divisor is written as $D = k_0 D_0 + k_1 D_1 + k_2 D_2$ and is, hence, labelled by a three-dimensional integer vector $\mathbf{k} = (k_0, k_1, k_2)$. The Mori and nef cone generators are

$$\hat{\mathcal{M}}(\mathrm{dP}_2) = \{C_1 = e_1,\, C_2 = e_2,\, C_3 = l - e_1 - e_2\} \tag{5.87}$$

$$\hat{\mathcal{N}}(\mathrm{dP}_2) = \{N_1 = l - e_1,\, N_2 = l - e_2,\, N_3 = l\} \tag{5.88}$$

The irreducible negative self-intersection divisors are the exceptional curves which are precisely the Mori cone generators, $C \in \hat{\mathcal{M}}(\mathrm{dP}_2)$. More explicitly, the Mori cone is characterised by the equations

$$\left.\begin{array}{l} D \cdot N_1 \geq 0 \\ D \cdot N_2 \geq 0 \\ D \cdot N_3 \geq 0 \end{array}\right\} \quad \Leftrightarrow \quad \left\{\begin{array}{l} k_0 + k_1 \geq 0 \\ k_0 + k_2 \geq 0 \\ k_0 \geq 0 \end{array}\right. \tag{5.89}$$

and line bundles $\mathcal{O}_{\mathrm{dP}_2}(\mathbf{k})$ outside this cone have vanishing zeroth cohomology.

As for Hirzebruch surfaces, the master formula (5.41) maps into the nef cone, without the need for iteration, and, from Corollary 5.76, the resulting index formula for effective divisors D is

$$h^0\left(\mathrm{dP}_n, \mathcal{O}_{\mathrm{dP}_n}(D)\right) = \mathrm{ind}\left(D + \sum_{i=1}^{3} \theta(-D \cdot C_i)\,(D \cdot C_i) C_i\right). \tag{5.90}$$

The regions within the Mori cone are separated off from one another by hyperplanes which can be read off from the arguments of the three theta functions in Eq. (5.90). These hyperplanes

are

$$\left.\begin{aligned} D\cdot C_1 &= 0\\ D\cdot C_2 &= 0\\ D\cdot C_3 &= 0 \end{aligned}\right\} \quad\Leftrightarrow\quad \left\{\begin{aligned} k_1 &= 0\\ k_2 &= 0\\ k_0+k_1+k_2 &= 0 \end{aligned}\right. \tag{5.91}$$

In principle, these three hyperplanes define eight regions but only the following five intersect the Mori cone.

$$(D\cdot C_1, D\cdot C_2, D\cdot C_3)\left\{\begin{array}{l} (\geq,\geq,\geq)\\ (\geq,\geq,<)\\ (<,\geq,\geq)\\ (\geq,<,\geq)\\ (<,<,\geq) \end{array}\right\} 0 \quad\begin{array}{l} \text{(Region 1)}\\ \text{(Region 2)}\\ \text{(Region 3)}\\ \text{(Region 4)}\\ \text{(Region 5)} \end{array} \tag{5.92}$$

Inserting the C_i into the master formula (5.41), we find the explicit expression for the divisor shifts from those five regions into the nef cone (Region 1).

$$\tilde{D} = \left\{\begin{array}{l} D\\ D+(D\cdot C_3)C_3\\ D+(D\cdot C_1)C_1\\ D+(D\cdot C_2)C_2\\ D+\sum_{i=1}^{2}(D\cdot C_i)C_i \end{array}\right\} \leftrightarrow \left\{\begin{array}{l} (k_0,k_1,k_2)\\ (2k_0+k_1+k_2,-k_0-k_2,-k_0-k_1)\\ (k_0,0,k_2)\\ (k_0,k_1,0)\\ (k_0,0,0) \end{array}\right\} \begin{array}{l} \text{(Region 1)}\\ \text{(Region 2)}\\ \text{(Region 3)}\\ \text{(Region 4)}\\ \text{(Region 5)} \end{array} \tag{5.93}$$

Here, the second bracket lists the coordinate vectors of the shifted divisors $\tilde{D}$ relative to the basis (l, e_1, e_2). The five regions together with the coordinate shifts are indicated in Figure 26. The number of terms required for each shift equals the number of hyperplanes which have to be crossed to reach the nef cone. Also note that the shifts map precisely to the boundaries of the nef cone. Inserting these divisor shifts into the expression (5.17) for the index finally gives the desired piecewise quadratic formula for the zeroth cohomology dimension.

$$h^0\left(\mathrm{dP}_2, \mathcal{O}_{\mathrm{dP}_2}(\mathbf{k})\right) = \begin{cases} 1+\frac{3}{2}k_0+\frac{1}{2}k_0^2+\frac{1}{2}k_1-\frac{1}{2}k_1^2+\frac{1}{2}k_2-\frac{1}{2}k_2^2 & \text{(Region 1)}\\ 1+2k_0+k_0^2+k_1+k_0k_1+k_2+k_0k_2+k_1k_2 & \text{(Region 2)}\\ 1+\frac{3}{2}k_0+\frac{1}{2}k_0^2+\frac{1}{2}k_2-\frac{1}{2}k_2^2 & \text{(Region 3)}\\ 1+\frac{3}{2}k_0+\frac{1}{2}k_0^2+\frac{1}{2}k_1-\frac{1}{2}k_1^2 & \text{(Region 4)}\\ 1+\frac{3}{2}k_0+\frac{1}{2}k_0^2 & \text{(Region 5)} \end{cases} . \tag{5.94}$$

This is consistent with our earlier empirical result (5.25) which was extracted from cohomology data.

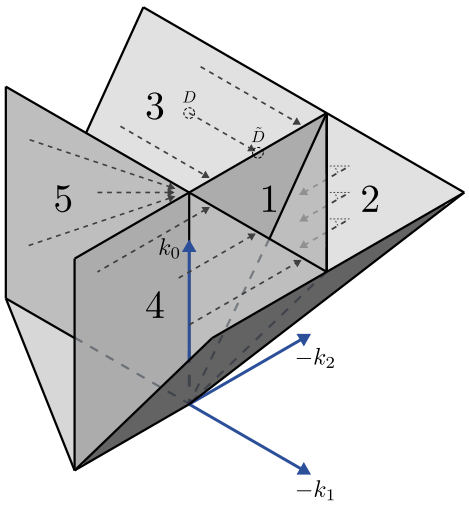

Figure 26: *The Picard lattice of the del Pezzo surface* dP_2*. We do not draw the lattice points to avoid clutter. The five numbered cones are the regions defined in Eq.* (5.92) *which, together, make up the Mori cone. Region 1 is the nef cone. In each region a different quadratic polynomial describes the zeroth cohomology. The arrows indicate the divisor shifts* (5.93) *into the nef cone.*

5.5 Summary

In this chapter, we have analysed line bundle cohomology on complex surfaces, focusing on the examples of Hirzebruch and del Pezzo surfaces. Starting from algorithmically computed cohomology data, we have shown how to conjecture piecewise quadratic formulae for the zeroth cohomology dimension on these manifolds. Through a process of gradual re-writing, we have brought these equations into a suggestive form where the cohomology dimension is expressed in terms of an index.

Based on these examples, we conjectured and proved topological index formulae. We discussed how a certain shift $D \to \tilde{D}$ of effective divisors, explicitly defined in Eq. (5.41), leaves the zeroth cohomology dimension unchanged, so that $h^0(S, \mathcal{O}_S(D)) = h^0(S, \mathcal{O}_S(\tilde{D}))$. Repeated application of this shift results in a Zariski decomposition, ending up with a divisor $\underline{\tilde{D}}$ that in the nef cone and, provided a suitable vanishing theorem exists, the zeroth cohomology dimension can, remarkably, be written in terms of the index as

$$h^0(S, \mathcal{O}_S(D)) = \mathrm{ind}(\mathcal{O}_S(\underline{\tilde{D}}))\,. \tag{5.95}$$

It turns out that a suitable vanishing theorem exists for many classes of surfaces, including Hirzebruch and del Pezzo surfaces as well as compact toric surfaces. Moreover, for Hirzebruch and del Pezzo surfaces, the nef cone is already reached after a single shift, as given in Eqs. (5.21) and (5.38), and this explains the explicit index formulae for these manifolds.

6 Summary and outlook

Goals and approach

The work in this thesis was undertaken with the long-term goal of furthering understanding of aspects of string phenomenology, specifically in heterotic string theory and F-theory.

Broadly, one goal is to lay the groundwork that allows one to transfer advantages of the F-theory description via heterotic/F-theory duality to heterotic model building, as well as the converse, in order to gain further understanding and computational control. Our approach here is to construct and analyse explicit pairs of dual models, where one side features an aspect whose dual we would like to understand. A second broad goal, which is complementary, is to develop technical tools in other areas relevant for heterotic or F-theory model building, where heterotic/F-theory duality does not provide assistance.

We focused in particular on heterotic line bundle models and their F-theory duals. The first reason to do this is that line bundle models offer one of the most powerful frameworks for constructing phenomenologically interesting models, so it is directly desirable to understand them further via their F-theory dual description. The second reason to focus on the F-theory duals of line bundle models is that they provide a very well-controlled environment in which to study the dual description of features common to all heterotic models.

Summary of methods and results

In Chapter 3 we have studied heterotic line bundle models which simultaneously have (1) phenomenological interest and (2) the potential for F-theory duals. First, we described what this class of models looks like. We described the conditions that result from the two above requirements, on the elliptic fibration, its base, and the line bundle sum. One particularly important condition was that the elliptically fibered CY three-fold should have two sections, in order for there to exist a freely-acting involution, and we studied these fibrations in detail. We also described constraints on possible base spaces, and we constructed several examples, and constructed the required involutions explicitly. Second, we constructed the tools required to analyse the line bundle models on these spaces, including the calculation of line bundle cohomology on elliptic fibrations with two sections.

Finally, we constructed a large class of example models. This was important (1) to check for any characteristic or atypical features compared with line bundle models in general, and (2) to provide a database in which one can attempt to answer specific questions. We found several hundred models whose spectra and gauge symmetries are consistent with those of the

(supersymmetric) Standard Model. A surprising feature of these models is the presence of vector-like states, suggesting that line bundle models with potential F-theory duals may be somewhat atypical, compared for example to earlier constructions with complete intersections.

In Chapter 4 we turned to the F-theory duals of heterotic line bundle models. Since the standard approach of spectral covers is not appropriate, we first conjectured the F-theory duals of heterotic line bundle models. These dual models are a new class in heterotic/F-theory duality, being constructed with a method essentially perpendicular to the standard approach. We then verified the conjecture by matching many properties: gauge groups, spectra, supersymmetry conditions, and anomaly conditions, and we also treated in detail some interesting subtleties not captured by standard lore.

We also took the opportunity to study in detail the F-theory dual of NS5-branes. These are a crucial feature of heterotic models, including line bundle models, and historically have been little-utilised in model building. We focused on this aspect because line bundle models provide an excellent background in which to study NS5-branes, since they are well-controlled. In particular, we constructed and analysed global heterotic/F-theory dual models with various NS5-brane configurations, and discovered many pleasing correspondences between brane properties and the toric representation of the F-theory geometry. This was also true when we studied the duality between heterotic brane transitions and F-theory geometric transitions. This F-theory dual picture provides a new angle to gain understanding and control of NS5-branes of heterotic model building.

In Chapter 5, we turned to the problem of developing a deeper understanding of line bundle cohomologies. The determination of cohomologies is currently computationally intensive, and is for the most part a 'black box'. If one had compact formulae underlying cohomologies, this would (1) save a significant amount of time and computational power, and (2) be a significant advance towards allowing for bottom-up model building. This is a question where heterotic/F-theory duality does not provide assistance, and we instead developed new methods and tools.

In particular we have constructed and explained methods and results for line bundle cohomology on complex surfaces. We determined explicit formulae for cohomology on all del Pezzo surfaces and all Hirzebruch surfaces, and gave an algorithm to determine formulae for any compact toric surface, in both cases using an implementation of Zariski decomposition. We also showcased methods to compute formulae for any space, treating in explicit detail the example of the del Pezzo spaces, and we have expounded specialised machine learning methods expounded in a companion paper [12]. This work represents an important step towards understanding more

complicated spaces, and since surfaces are the bases for elliptic three-folds, it is possible to lift their cohomology to give formulae also on many CY three-folds.

Outlook

The work in Chapters 3 and 4 laid some of the groundwork for various important questions to be addressed. However there is more to do to complete the programme. Let us mention two of the most important aspects. First, further work needs to be done to determine if chiral models have F-theory duals. An important observation is that chiral heterotic line bundle models require flux in the fiber direction. Since heterotic/F-theory duality has not yet been extended to this case, currently it is not understood how to map chiral heterotic models into F-theory. We note that, in addition to being important to map chiral line bundle models, this is an important question in its own right. In fact, since line bundle constructions provide global models that are well-understood and well-controlled, this provides a fruitful background in which to study this question. Second, it remains to work out the full duality for models with Wilson lines. Crucially, one needs to understand first the F-theory duals of heterotic models where the elliptic fibration has multiple sections. Additionally, one must then also understand the F-theory dual of a map exchanging those sections, in order to dualise the quotient map that introduces the Wilson lines. In fact, recently there has been progress in this direction [122, 123]. As in the previous case, line bundle models in fact offer a useful arena in which to address this question.

With the groundwork already completed in Chapters 3 and 4, there are various questions now within reach. Let us mention two interesting directions to pursue, both related to NS5-branes. The first direction is to further the understanding of coincident NS5-branes. F-theory models with surfaces of singularities in the base provide an alternative description of the four-dimensional theory arising from coincident heterotic NS5-branes, and it would be very interesting to use F-theory to elucidate the physics of such configurations. If understanding could be transferred to heterotic models, this would be a new and useful addition to the set of heterotic model building tools. The second question is the heterotic perspective on fractional D3-branes. In Chapter 4 we did not discuss intersections of horizontal and vertical NS5-branes. While coincident horizontal NS5-branes correspond to singularities in the F-theory base, vertical branes correspond to D3-branes. Intersections between these sectors hence give a heterotic (or F-theory) description of D3-branes at singularities in Type IIB string theory, which is a very interesting and important feature in IIB constructions. Investigation of this aspect may reveal new tools for model building in heterotic string theory, and is accessible in the global models we have constructed.

Our work on line bundle cohomologies in Chapter 5 enables various exciting future directions. In the context of complex surfaces there are two main questions. First, it is desirable to better understand the interplay between the divisor shift and the required vanishing theorem. Can we identify further classes of surfaces for which index formulae can be derived in this way? Second, we know that higher cohomology dimensions can be expressed in terms of the zeroth cohomology, using Serre duality and the index theorem. But it is not clear if higher cohomologies can also be written in terms of a single index formula, similar to Eq. (5.60).

There are also immediate applications to string theory. Note first that our cohomology formulae can be lifted in various ways to results on Calabi-Yau three-folds. One obvious example is in using these complex surfaces as bases for elliptically fibered Calabi-Yaus. On three-folds where we gain an analytic understanding of line bundle cohomology, there are various clear applications. One obvious direction is jumping loci. We have already noted the quasi-topological nature of the cohomology formulae: the quantity $\text{ind}(\mathcal{O}_S(\underline{\tilde{D}}))$ is purely topological, while the map $D \to \tilde{D}$ depends in general on the complex structure. The complex structure dependence of the map $D \to \tilde{D}$ may greatly facilitate the study of jumping loci for cohomology (see Ref. [124] for a discussion of jumping loci in complex structure moduli stabilisation; in string model building jumping loci frequently enter the construction of Higgs fields).

Looking further ahead, what is the situation for general three-folds or complex manifolds of even higher dimension? Complex surfaces are special in that curves and divisors have the same dimension, so the results of this paper cannot be straightforwardly extended to higher-dimensional cases. On the other hand, Refs. [7, 11] show that piecewise cubic formulae for line bundle cohomology dimensions can be written down for Calabi-Yau three-folds. This strongly suggests an underlying mathematical structure, although its nature and formulation is not known at present. These questions are currently under investigation.

A Elliptic fibrations and half-shifts

In this appendix we review the required mathematics for elliptically fibered CY three-folds with a freely-acting involution and two sections. Much of the material is not new but can be found in various places in the literature [26, 27].

A.1 The group law on elliptic curves and half-shifts

An elliptic curve E can be described by the polynomial equation,

$$zy^2 = x^3 + fxz^2 + gz^3\,, \tag{A.1}$$

where x, y, z are homogeneous coordinates on $\mathbb{P}^2$ and f, g are complex constants. This does indeed describe a smooth curve as long as the discriminant, defined by

$$\Delta = 4f^3 + 27g^2 \tag{A.2}$$

is non-vanishing.

If we denote the nowhere vanishing $(1,0)$-form on E by Ω and introduce a basis of one-cycles A, B with $A \cdot B = 1$ on E the periods can be defined by

$$\begin{aligned} \tau_A &= \int_A \Omega \,, \\ \tau_B &= \int_B \Omega \,. \end{aligned} \tag{A.3}$$

For a suitable normalisation of Ω we have $\tau_B = 1$. The other period, $\tau = \tau_A$, is called the modular parameter of the torus. We can introduce the lattice $\Lambda \subset \mathbb{C}$ generated by 1 and τ and the Jacobian $\mathbb{C}/\Lambda$ of the elliptic curve. Then, the Abel-Jacobi map $E \to \mathbb{C}/\Lambda$ is defined by

$$p \mapsto \int_\gamma \Omega \,, \tag{A.4}$$

where γ is a path linking p with a given point $p_0 \in E$ (conveniently taken as $p_0 = [x : y : z] = [0 : 1 : 0]$). From now on we work in the patch of $\mathbb{P}^2$ where we can set $z = 1$. In this patch, the inverse of the Abel-Jacobi map can be expressed in terms of the Weierstrass $\wp$-function as

$$w \to (x, y) = (\wp(w), \tfrac{1}{2}\wp'(w)) \,, \tag{A.5}$$

where $w \in \mathbb{C}/\Lambda$ [125].

Via this inverse map, the obvious addition of points in $\mathbb{C}/\Lambda$ can be translated into an addition law on the elliptic curve E. Specifically, if we consider three points $w_1, w_2, w_3 \in \mathbb{C}/\Lambda$ with $w_3 = w_1 + w_2$, and introduce the corresponding points $(x_i, y_i) = (\wp(w_i), \frac{1}{2}\wp'(w_i))$, where $i = 1, 2, 3$, on the elliptic curve, the addition law on E takes the form

$$x_3 = -x_1 - x_2 + \left(\frac{y_1 - y_2}{x_1 - x_2}\right)^2 \,, \tag{A.6}$$

$$y_3 = -\left(\frac{y_1 - y_2}{x_1 - x_2}\right)^3 + \frac{x_1 y_1 - x_2 y_2 + 2(x_2 y_1 - x_1 y_2)}{x_1 - x_2} \,. \tag{A.7}$$

For fixed (x_2, y_2), this defines a map from (x_1, y_1) to (x_3, y_3) which, provided the discriminant is non-zero, is an automorphism of the elliptic curve.

Since we are interested in constructing involutions of elliptic CY three-folds it is natural to start with involutions on elliptic curves. In the Jacobian description, $\mathbb{C}/\Lambda$, obvious involutions are half-shifts of the form $w \to w + \omega_i$, with the three possible choices $\omega_1 = \frac{1}{2}$, $\omega_2 = \frac{\tau}{2}$ or $\omega_3 = \frac{1}{2} + \frac{\tau}{2}$ for the shift. Note that these half-shifts are clearly freely-acting and, due to the

quotient by the lattice Λ, they do indeed square to the identity. Via the map (A.5), the half-shift points $\omega_i \in \mathbb{C}/\Lambda$ can be translated to certain points (x, y) of the elliptic curve E. It turns out that $\wp'(\omega_i) = 0$ and, hence, that the resulting points are of the form $(x, y) = (e_i, 0) \in E$, where $e_i := \wp(\omega_i)$. Since the y-coordinates of these three points vanish the x-coordinates e_i must be zeros of the right-hand side of the Weierstrass equation (A.1).

To be specific, we focus on the first half-shift by ω_1 with corresponding half-shift point $(x, y) = (\alpha, 0)$, where $\alpha := e_1$. Since α must be a zero of the right-hand side of Eq. (A.1), the Weierstrass equation (for $z = 1$) factorises as

$$y^2 = (x - \alpha)(x^2 + \alpha x + \beta)\,, \tag{A.8}$$

where β is another complex number. Comparison with the standard form (A.1) of the Weierstrass equation shows that $f = \beta - \alpha^2$ and $g = -\alpha\beta$. The discriminant (A.2) factorises as well and can be written as

$$\Delta = \Delta_1 \Delta_2^2\,, \qquad \Delta_1 = 4\beta - \alpha^2\,, \qquad \Delta_2 = 2\alpha^2 + \beta\,. \tag{A.9}$$

In terms of shifted coordinates, defined as $X := x - \alpha$, $Y := y$, the above Weierstrass equation takes the form

$$Y^2 = X(X^2 + 3\alpha X + \Delta_2)\,. \tag{A.10}$$

Setting $x_2 = \alpha$, $y_2 = 0$, $x_1 = x$, $y_1 = y$, $x_3 = x'$ and $y_3 = y'$ in Eqs. (A.6), (A.7) we can translate the half-shift $w \to w + \omega_1$ on the Jacobian into a map on the elliptic curve which we denote by ι_E. In the affine (x, y) coordinates this map reads explicitly

$$x' = -x - \alpha + \left(\frac{y}{x - \alpha}\right)^2\,, \tag{A.11}$$

$$y' = -\left(\frac{y}{x - \alpha}\right)^3 + y\left(\frac{x + 2\alpha}{x - \alpha}\right)\,. \tag{A.12}$$

In terms of the shifted X, Y coordinates and their primed counterparts, these transformations can be re-written as

$$X' = \frac{1}{X^2}\left(Y^2 - X^2\,(X + 3\alpha)\right)\,, \qquad Y' = -\frac{YX'}{X}\,. \tag{A.13}$$

Finally, using the Weierstrass equation (A.10) to replace Y^2 in the equation for X', the map ι_E can be cast into the simple form

$$\iota_E : \quad X \to X' = \frac{\Delta_2}{X}\,, \quad Y \to Y' = -\frac{\Delta_2 Y}{X^2}\,. \tag{A.14}$$

Clearly, since the half-shift $w \to w + \omega_1$ is freely-acting on the Jacobian, the action of ι_E is also free, as long as the elliptic curve is smooth. For later purposes, we note that, in the smooth case,

ι_E maps the point $[x:y:z]=[\alpha:0:1]$ into the point $[x:y:z]=[0:1:0]$ or, equivalently,

$$\iota_E([0:1:0])=[\alpha:0:1]\,. \tag{A.15}$$

To see this we have to convert the two points into affine coordinates on the patch where $z=1$. The point $[\alpha:0:1]\in\mathbb{P}^2$ then corresponds to $(x,y)=(\alpha,0)$ while the point $[0:1:0]\in\mathbb{P}^2$ is mapped to infinity, $x,y\to\infty$, with $y^2=x^3$. By taking limits carefully, it can indeed be shown that (A.14) exchanges these two affine points.

Let us discuss what happens when the elliptic curve becomes singular, that is, when $\Delta_1=0$ or $\Delta_2=0$. If $\Delta_2=0$, the Weierstrass equation (A.8) acquires a double root at $x=\alpha$ (that is, the second factor on the right-hand side of Eq. (A.8) develops a root at α). In this case, the transformation (A.14) clearly degenerates badly as all points (X,Y) are mapped to the origin $(X',Y')=(0,0)$. As we will explain, in the context of elliptic fibrations, such fibers will be blown-up and the degeneracy of the transformation will be removed in this way.

If $\Delta_1=0$, the Weierstrass equation (A.8) develops a double root at $x=-\alpha/2$, solely from the second factor on the right-hand side. In this case, $\Delta_2=\frac{9}{4}\alpha^2$, so that the points $(X,Y)=(\frac{3}{2}\alpha,0)$ and $(X,Y)=(-\frac{3}{2}\alpha,0)$ are fixed. The second of these points is indeed on the elliptic curve E, as can be verified by inserting into Eq. (A.10), and, hence, ι_E is not fixed point free if $\Delta_1=0$.

A.2 Elliptically fibered CY three-folds with involutions

We would now like to apply the discussion of the previous section to the construction of elliptically fibered CY three-folds, X, with an involution ι_X. The idea is to construct ι_X by combining the above half-shift ι_E on the elliptic fibers with a suitable involution ι_B on the base B of the fibration.

We start with an elliptically fibered CY three-fold X with two-fold base B, projection $\pi: X\to B$ and section $\sigma: B\to X$. Each elliptic fiber $E_b=\pi^{-1}(b)$ over $b\in B$ is described by a Weierstrass equation

$$zy^2=x^3+fxz^2+gz^3\,, \tag{A.16}$$

where x,y,z are now sections $x\in\Gamma(K_B^{-2})$, $y\in\Gamma(K_B^{-3})$, $z\in\Gamma(\mathcal{O}_B)$ and f, g are sections $f\in\Gamma(K_B^{-4})$, $g\in\Gamma(K_B^{-6})$, with K_B the canonical bundle of the base. Then, the section σ is located at the point $[x:y:z]=[0:1:0]$ in each fiber.

We would now like to consider a situation where a half-shift ι_E acts on every (smooth) elliptic fiber as in Eq. (A.14). From the previous sub-section we know that this leads to a factorisation of the Weierstrass equation, namely

$$zy^2=(x-\alpha z)(x^2+\alpha xz+\beta z^2)\,, \tag{A.17}$$

where α and β should now be seen as sections of K_B^{-2} and K_B^{-4}, respectively. This relates to the standard Weierstrass form (A.16) via

$$f = \beta - \alpha^2 \,, \quad g = -\alpha\beta \,. \tag{A.18}$$

As we have seen before, the discriminant factors as

$$\Delta = \Delta_1 \Delta_2^2 \,, \qquad \Delta_1 = 4\beta - \alpha^2 \,, \qquad \Delta_2 = 2\alpha^2 + \beta \,. \tag{A.19}$$

As a consequence, the discriminant locus on the base B consists of the two components $\{b \in B \,|\, \Delta_1(b) = 0\}$ and $\{b \in B \,|\, \Delta_2(b) = 0\}$.

The half-shift on the fibers leads to a second section, $\zeta := \iota_E \circ \sigma$ which, in view of Eq. (A.15), is located at $[x : y : z] = [\alpha : 0 : 1]$. We are, therefore, considering elliptically fibered CY three-folds with two sections, which are explicitly given by

$$\sigma(b) = (b, [0 : 1 : 0]) \,, \qquad \zeta(b) = (b, [\alpha : 0 : 1]) \,. \tag{A.20}$$

Note that the second section ζ does indeed take values on the elliptic curve (A.17), due to the factorisation of the equation. Hence, the factorisation with holomorphic sections α and β is crucial for the existence of a second section.

We should now discuss the singular fibers which arise over the discriminant locus and the fate of the involution ι_E over these fibers. We begin with the component of the discriminant locus defined by $\Delta_2 = 0$. As can be seen from Eq. (A.10), the three-fold has an A_1 singularity at $X = Y = 0$ over this locus which needs to be resolved in order to arrive at a smooth CY three-fold.

A convenient technique to find crepant resolutions of such singularities is to first promote Δ_2 to a coordinate of the ambient space, which then has to satisfy the equation

$$\Delta_2 = 2\alpha^2 + \beta \,. \tag{A.21}$$

The blow-up is realised by introducing the new coordinates $\hat{X}$, $\hat{Y}$, $\hat{\Delta}_2$ and ξ, excising the locus $\{\hat{X} = \hat{Y} = \hat{\Delta}_2\}$ and modding out by a $\mathbb{C}^*$ action with weights

$\hat{X}$	$\hat{Y}$	$\hat{\Delta}_2$	ξ
1	1	1	-1

(A.22)

These new coordinates relate to the old ones as

$$X = \hat{X}\xi \,, \quad Y = \hat{Y}\xi \,, \quad \Delta_2 = \hat{\Delta}_2 \xi \,. \tag{A.23}$$

After the proper transform, the Weierstrass equation (A.10) and Eq. (A.21), turn into

$$\hat{Y}^2 = \hat{X}\left(\hat{X}^2\xi + 3\alpha\hat{X} + \hat{\Delta}_2\right) \,, \quad \hat{\Delta}_2\xi = 2\alpha^2 + \beta \,, \tag{A.24}$$

which describe a smooth CY three-fold. Note that due to the special form of Eq. (A.10), the proper transform removes two powers of ξ, so that the blow-up is crepant. The previously singular fibers over $\Delta_2 = 0$ have now been replaced by two irreducible components, $\hat{\Delta}_2 = 0$ and $\xi = 0$, both of which are $\mathbb{P}^1$s. These two $\mathbb{P}^1$'s are explicitly given by

$$\hat{Y}^2 = \hat{X}^2\left(\hat{X}\xi + 3\alpha\right) \quad \text{for } \hat{\Delta}_2 = 0 \,, \tag{A.25}$$

$$\hat{Y}^2 = \hat{X}\left(3\alpha\hat{X} + \hat{\Delta}_2\right) \quad \text{for } \xi = 0 \,, \tag{A.26}$$

and they evidently touch in the two points

$$\frac{\hat{Y}}{\hat{X}} = \pm\sqrt{3\alpha} \,. \tag{A.27}$$

What remains to be discussed is the action of the half-shift (A.14) on the blown-up space. First note that as long as $\Delta_2 \neq 0$, we can set $\xi = 1$ and our equations return to the ones before the blow-up, so that our earlier discussion applies. This means that the action of ι_E remains free for fibers which are away from the discriminant locus and that it has fixed points on fibers over $\Delta_1 = 0$.

In order to discuss the situation for fibers over the locus $\Delta_2 = 0$, we first need to properly define the half-shift in terms of the new coordinates $\hat{X}$, $\hat{Y}$, $\hat{\Delta}_2$ and ξ. Of course, we wish to preserve the action of the map on $X = \xi\hat{X}$ and $Y = \xi\hat{Y}$, which should still be given by Eq. (A.14). Translating these equations into the new coordinates implies

$$\xi'\hat{X}' \stackrel{!}{=} \frac{\Delta_2}{X} = \frac{\hat{\Delta}_2}{\hat{X}} \,, \qquad \xi'\hat{Y}' \stackrel{!}{=} -\frac{\Delta_2 Y}{X^2} = -\frac{\hat{\Delta}_2\hat{Y}}{\hat{X}^2} \,. \tag{A.28}$$

We also know that, away from the discriminant locus, the half-shift exchanges the two sections and that, for the reducible fibers over the locus $\Delta_2 = 0$, each $\mathbb{P}^1$ component is met by one of the sections. Since the two $\mathbb{P}^1$'s are given by $\hat{\Delta}_2 = 0$ and $\xi = 0$, respectively, this suggests that ι_E should exchange the coordinates $\hat{\Delta}_2$ and ξ. Hence the appropriate generalisation of the half-shift involution to the blown-up space is

$$\iota_E : \begin{pmatrix} \hat{X} \\ \hat{Y} \\ \hat{\Delta}_2 \\ \hat{\xi} \end{pmatrix} \longrightarrow \begin{pmatrix} \frac{1}{\hat{X}} \\ -\frac{\hat{Y}}{\hat{X}^2} \\ \hat{\xi} \\ \hat{\Delta}_2 \end{pmatrix} \,. \tag{A.29}$$

This transformation respects Eq. (A.28) and it exchanges the two $\mathbb{P}^1$'s, defined by $\hat{\Delta}_2 = 0$ and $\xi = 0$, in the reducible fibers.

What about the fixed points for this refined version of the involution ι_E? By construction, Eq. (A.29) reduces to the previous action for all fibers away from the locus $\Delta_2 = 0$. Hence, it is fixed point free on fibers away from the discriminant locus and it has fixed points on fibers over the locus $\Delta_1 = 0$ (certainly as long as $\Delta_2 \neq 0$). For fibers over the locus $\Delta_2 = 0$, the map (A.29) exchanges the two fiber components $\xi = 0$ and $\hat{\Delta}_2 = 0$. These two $\mathbb{P}^1$ components touch in the two points (A.27) which are also swapped by the map (A.29). Hence, as long as these two points are different the action of ι_E on fibers over the locus $\Delta_2 = 0$ is fixed point free. The two points coincide precisely when $\Delta_2 = \Delta_1 = 0$ and the resulting fixed point is what we expect on fibers over the locus $\Delta_1 = 0$. In summary, the involution ι_E, as defined by Eq. (A.29), is fixed point free over all fibers with $\Delta_1 \neq 0$ and it has fix points over fibers with $\Delta_1 = 0$.

It remains to discuss the two sections σ and ζ for the blown-up version of the CY three-fold. The zero section σ is specified by mapping a point in the base to the point

$$\hat{X} \to \infty\,, \quad \hat{Y} \to \infty\,, \quad \hat{\Delta}_2 = 2\alpha^2 + \beta\,, \quad \hat{\xi} = 1\,, \tag{A.30}$$

where $\hat{X}$ and $\hat{Y}$ are taken to infinity such that $\hat{Y}^2 = \hat{X}^3\hat{\xi}$ is satisfied along the path. (This is required for the first equation in (A.24) to be satisfied in the limit.) The second section, ζ, maps a point in the base to

$$\hat{X} \to 0\,, \ \hat{Y} \to 0\,, \ \hat{\Delta}_2 = 1\,, \ \hat{\xi} = 2\alpha^2 + \beta\,, \tag{A.31}$$

where $\hat{X}$ and $\hat{Y}$ are taken to zero such that $\hat{Y}^2 = \hat{X}\hat{\Delta}_2$ is satisfied along the path. (This is required for the first equation in (A.24) to be satisfied in the limit.) It is straightforward to check that the involution (A.29) swaps the two section points (A.30) and (A.31) and, hence, swaps the two sections σ and ζ.

A.3 Alternative realisation of elliptic CY three-folds with half-shifts

There exists another presentation of elliptic CY three-folds with a second section at the two-torsion point which uses a different embedding of the elliptic fiber. Embedding the elliptic fiber in the Hirzebruch surface $\mathbb{F}_2$ (which can also be found as a blow-up of $\mathbb{P}^2_{112}$), an elliptic fibration with two sections has the realisation

$$x_1^2 = x_2^2(x_3^4 + b_2 x_3^2 x_4^2 + b_3 x_3 x_4^3 + b_4 x_4^4)\,. \tag{A.32}$$

Here, the x_i are the homogeneous coordinates of a toric variety with weight system

$$\begin{array}{cccc} x_1 & x_2 & x_3 & x_4 \\ \hline 1 & 1 & 0 & 0 \\ 2 & 0 & 1 & 1 \end{array} \tag{A.33}$$

and Stanley-Reisner ideal generated by $\{x_1, x_2\}, \{x_3, x_4\}$. Note that we may always find this form by appropriately redefining the coordinates x_1 and x_3 of a general hypersurface in $\mathbb{F}_2$. In order for a fibration with the above elliptic curve to form a CY space, the b_i must be sections of the line bundles $-K_B^{\otimes i}$.

The two sections of such a model are located at $x_4 = x_1 \pm x_2 x_3^2 = 0$. Choosing one of the two as the zero section, the other section is located at the two-torsion point if we set $b_3 \equiv 0$. The involution corresponding to the half-shift is then simply given by

$$(x_1, x_2, x_3, x_4) \to (-x_1, x_2, x_3, -x_4) \tag{A.34}$$

and the discriminant becomes the same as (A.19), when using the replacements $b_2 = -6i\alpha$ and $b_4 = \Delta_1 = 4\beta - \alpha^2$. This action is free as long as $b_4 = \Delta_1 \neq 0$.

In contrast to the realisation via a specialised Weierstrass model, no further blow-ups are required in order to find a smooth CY three-fold X. Furthermore, for a toric base space B, this presentation allows a description of X as a toric hypersurface as follows. Let us denote the rays of the fan of the toric base B by $\mathbf{w}_i \in \mathbb{Z}^2$. If the convex hull of the vectors

$$\begin{pmatrix} 1 \\ 0 \\ \mathbf{0} \end{pmatrix}, \begin{pmatrix} -1 \\ 0 \\ \mathbf{0} \end{pmatrix}, \begin{pmatrix} 0 \\ -1 \\ \mathbf{0} \end{pmatrix}, \begin{pmatrix} 2 \\ 1 \\ \mathbf{0} \end{pmatrix}, \begin{pmatrix} 2 \\ 1 \\ \mathbf{w}_i \end{pmatrix}, \tag{A.35}$$

forms a reflexive polytope Δ°, we can realise (A.32) as a generic toric hypersurface which sits in a fibration of $\mathbb{F}_2$ over B. For the base spaces we consider, which are toric weak Fano two-folds, this condition is always met. In order to find candidate free involutions, we may then restrict to cases where $b_3 = 0$. In this form, our examples should also be found using the algorithm of Ref. [126].

A further upshot of this alternative realisation is that it allows for an easy alternative method to compute line bundle cohomologies. Instead of exploiting the elliptic fibration, as described in Appendix C, we may simply compute cohomologies on the toric ambient four-fold, using the code cohomCalg [30, 31], and then apply the Koszul sequence to find the cohomologies on X. We have used this alternative method to check our results for line bundle cohomology.

A.4 Intersection theory and Mori and Kähler cones

Intersection theory on CY three-folds with involutions

The main purpose of this section is to introduce a suitable integral basis of curve and divisor classes on the CY three-fold X in terms of a basis of curve classes on the base B and to study the resulting intersection properties.

We begin by introducing the required objects on the base B. These consist of a basis, $\{\mathcal{C}^i\}$, where $i, j, \ldots = 1, \ldots, h^{1,1}(B)$, of curve classes, its dual basis $\{\mathcal{C}_i\}$ such that

$$\mathcal{C}^i \cdot \mathcal{C}_j = \delta^i_j \,, \tag{A.36}$$

and the various intersection numbers

$$g_{ij} = \mathcal{C}_i \cdot \mathcal{C}_j \,, \quad g^{ij} = \mathcal{C}^i \cdot \mathcal{C}^j \,, \quad \lambda_i = K_B \cdot \mathcal{C}_i \,, \quad \lambda = \lambda^i \lambda_i \,, \tag{A.37}$$

where K_B is the canonical bundle of B. Note that g^{ij} is the inverse of g_{ij} and that these two metrics can be used to raise and lower indices. In particular, we have $\lambda^i = g^{ij}\lambda_j$.

Next, we should construct a basis of curve classes on the CY three-fold X which can be done by "lifting" the above curve classes $\mathcal{C}^i$ on the base, using the sections σ or ζ. There are two further curve classes on X which cannot be obtained in this way, namely the class of the generic fiber and the new class introduced by the blow-up. We denote the class of the generic fiber by F and the new class, represented by the $\xi = 0$ component of the reducible fibers, by N. The other component, defined by $\hat{\Delta}_2 = 0$, of the reducible fibers then has the class $F - N$. It turns out that, for a general curve class, $\mathcal{C}$, on the base we have the relation [26]

$$\zeta(\mathcal{C}) = \sigma(\mathcal{C}) + (\mathcal{C} \cdot c_1(B))[F - 2N] \,. \tag{A.38}$$

This means that the lifts of a base curve by the two sections are linearly related and that we can focus on one of the sections for the purpose of constructing a basis of curve classes on X. With this in mind we introduce a basis $\{C^I\}$, where $I = (0, \hat{0}, i)$ and $i = 1, \ldots, h^{1,1}(B)$, of curve classes on X by setting

$$C^0 = F - N \,, \quad C^{\hat{0}} = N \,, \quad C^i = \sigma(\mathcal{C}^i) - \lambda^i (F - N) \,. \tag{A.39}$$

(The last term in the definition of C^i has been included for later convenience.) Then, an arbitrary second homology class in $H_2(X, \mathbb{Z})$ can then be written as $C = n_I C^I$, where $n_I \in \mathbb{Z}$.

To obtain an integral basis of divisor classes on X, we proceed as follows. We can find divisors of X by lifting curves of the base using the inverse projection map, π^{-1}, of the fibration. There are only two further divisor classes, the images $\sigma(B)$ and $\zeta(B)$ of the base, which cannot

be obtained in this way. Hence, we introduce the basis $\{D_I\}$, where $I = (0, \hat{0}, i)$ and $i = 1, \ldots, h^{1,1}(B)$, by

$$D_0 = \sigma(B) \ , \quad D_{\hat{0}} = \zeta(B) \ , \quad D_i = \pi^{-1}(\mathcal{C}_i) \ . \tag{A.40}$$

As Table 5 shows, this basis is dual to the above basis of curve classes, that is

$$D_I \cdot C^J = \delta_I^J \ . \tag{A.41}$$

We also require the intersections of two divisors which are summarised in Table 6. Combining

	$D_0 = \sigma(B)$	$D_{\hat{0}} = \zeta(B)$	$\pi^{-1}(\mathcal{C}')$
$C^0 = F - N$	1	0	0
$C^{\hat{0}} = N$	0	1	0
$\sigma(\mathcal{C})$	$\mathcal{C} \cdot K_B$	0	$\mathcal{C} \cdot \mathcal{C}'$
$\zeta(\mathcal{C})$	0	$\mathcal{C} \cdot K_B$	$\mathcal{C} \cdot \mathcal{C}'$

Table 5: *Intersection properties of curve classes and divisor classes. Here, $\mathcal{C}$ and $\mathcal{C}'$ are two curve classes on the base.*

	$D_0 = \sigma(B)$	$D_{\hat{0}} = \zeta(B)$	$\pi^{-1}(\mathcal{C}')$
$D_0 = \sigma(B)$	$\sigma(K_B)$	0	$\sigma(\mathcal{C}')$
$D_{\hat{0}} = \zeta(B)$	0	$\zeta(K_B)$	$\zeta(\mathcal{C}')$
$\pi^{-1}(\mathcal{C})$	$\sigma(\mathcal{C})$	$\zeta(\mathcal{C})$	$(\mathcal{C} \cdot \mathcal{C}')F$

Table 6: *Intersection properties of two divisor classes. Here, $\mathcal{C}$ and $\mathcal{C}'$ are two curve classes on the base.*

the information from Table 5 and Table 6, we can work out the triple intersection numbers

$$d_{IJK} := D_I \cdot D_J \cdot D_K \ , \tag{A.42}$$

which are explicitly given by

$$d_{000} = d_{\hat{0}\hat{0}\hat{0}} = \lambda \ , \quad d_{00i} = d_{\hat{0}\hat{0}i} = \lambda_i \ , \quad d_{0ij} = d_{\hat{0}ij} = g_{ij} \ , \tag{A.43}$$

with all other components fixed by symmetry or else vanishing.

Finally, it can be shown [26, 27] that on an elliptically fibered CY X with two sections, the second Chern class $c_2(X)$ and the Euler number $\chi(X)$ can be expressed in terms of properties

of the base as

$$\begin{aligned} c_2(X) &= 12\sigma(c_1(B)) + (c_2(B) + 11c_1(B)^2)(F-N) + (c_2(B) - c_1(B)^2)N \qquad \text{(A.44)} \\ &= (c_2(B) - \lambda)(C^0 + C^{\hat{0}}) - 12\lambda_i C^i \,, \qquad \text{(A.45)} \\ \chi(X) &= -36 \int_B c_1(B)^2 = -36\lambda \,. \qquad \text{(A.46)} \end{aligned}$$

Mori cone and Kähler cone

For the purpose of checking the heterotic anomaly condition we need to know the Mori cone of the CY three-fold, after the blow-up. As we will see, the Mori cone $\mathcal{M}_X$ of X can be expressed in terms of the Mori cone $\mathcal{M}_B$ of the base.

First we note that for two effective curve classes $\mathcal{C}, \mathcal{C}' \in \mathcal{M}_B$ in the base, the curve class

$$C = m(F-N) + nN + \sigma(\mathcal{C}) + \zeta(\mathcal{C}') \,, \qquad \text{(A.47)}$$

where $n, m \in \mathbb{Z}^{\geq 0}$, must be in the Mori cone of X. We would now like to argue that all effective curve classes on X are, in fact, obtained in this way.

It is sufficient to show that all irreducible effective classes can be represented in the form (A.47) (since an extremal ray of the cone of effective classes is an irreducible effective class). We write a general class $\hat{C} \in H_2(X, \mathbb{Z})$ as,

$$\hat{C} = \sigma(\mathcal{C}) + \hat{m}(F-N) + \hat{n}N \,, \qquad \text{(A.48)}$$

with $\mathcal{C}$ an element of $H_2(B, \mathbb{Z})$ and $\hat{m}, \hat{n} \in \mathbb{Z}$. (Note that, by virtue of the relation (A.38), we do not need to include a term $\zeta(\mathcal{C}')$ in this expression.) Let us now require that $\hat{C}$ is effective and irreducible. Effectiveness means that the projection of $\hat{C}$ onto the base, which is simply $\mathcal{C}$, is an effective class on the base. Irreducibility of $\hat{C}$ implies, in particular, that a curve in this class intersects non-negatively any effective divisor in which it is not contained, or more precisely whenever the generic element of the curve class does not sit inside the generic element of the divisor class. If $\hat{C}$ is not contained in $\sigma(B)$ or $\zeta(B)$, then exploiting this fact leads to the conditions

$$0 \leq \sigma(B) \cdot \hat{C} = \hat{m} + K_B \cdot \mathcal{C} \,, \qquad 0 \leq \zeta(B) \cdot C = \hat{n} \,. \qquad \text{(A.49)}$$

We have seen that the curve $\mathcal{C}$ is effective and, for the base spaces we consider, we have $-K_B \cdot \mathcal{C} \geq 0$ for all effective curves. Hence, we conclude that $\hat{m} \geq 0$ and $\hat{n} \geq 0$. In conclusion, if the effective (and irreducible) class $\hat{C}$ is not contained in $\sigma(B)$ or $\zeta(B)$ then it is of the form (A.47). Now suppose $\hat{C}$ is contained in $\sigma(B)$. Then it follows that $\hat{C} = \sigma(\mathcal{C})$ and, since $\mathcal{C}$ is effective on the base, this is already of the form (A.47). A similar argument applies if $\hat{C}$ is contained in $\zeta(B)$.

In this case, $\hat{C} = \zeta(\mathcal{C}')$ with an effective $\mathcal{C}'$, which is again of the form (A.47). In summary, the Mori cone of the elliptically fibered CY three-fold X consists of classes of the form (A.47) and can, hence, be written as

$$\mathcal{M}_X = \left\{ m(F-N) + nN + \sigma(\mathcal{C}) + \zeta(\mathcal{C}') \,|\, m,n \in \mathbb{Z}^{\geq 0} \;,\;\; \mathcal{C},\mathcal{C}' \in \mathcal{M}_B \right\} \;, \tag{A.50}$$

where $\mathcal{M}_B$ is the Mori cone of the base B.

In the context of line bundle model building, we will need to check if the slope of line bundles vanishes somewhere in the Kähler cone, $\mathcal{K}_X$, of the CY three-fold X and, hence, we need an explicit description of $\mathcal{K}_X$. For the manifolds in question the Kähler cone is the dual of the Mori cone (see for example Theorem 1.4.9 in [112]). Writing a general Kähler form as $J = t^I D_I$, where $\mathbf{t} = (t^I)$ are the Kähler moduli relative to a basis $\{D_I\}$ of divisor classes, and writing a general curve class as $n_I C^I$ relative to a dual basis $\{C^I\}$ (which satisfies $C_I \cdot D^J = \delta_I^J$), the Kähler cone can be expressed as

$$\mathcal{K}_X \cong \{\mathbf{t} \,|\, \mathbf{t}\cdot\mathbf{n} \geq 0 \text{ for all } n_I C^I \in \mathcal{M}_X\} \;, \tag{A.51}$$

and can, hence, be obtained from the Mori cone of X.

B Base spaces suitable for involution

So far, we have expressed all relevant properties of elliptically fibered CY three-folds with two sections in terms of corresponding properties of the base. In this appendix, we will focus on the six suitable toric base spaces which we have identified. More specifically, from the 61,359 possible toric two-folds classified in Ref. [28] only the 16 cases identified in Refs. [28,29] lead to generically smooth elliptic fibrations in Weierstrass form. These are the 16 reflexive polytopes, which we depict in Figure 27

From those 16 two-folds we have found involutions with at most fixed points (and which can be realised linearly on the homogeneous coordinates) on precisely the aforementioned six spaces. These spaces are denoted by $B = F_2, F_4, F_7, F_9, F_{13}, F_{15}$ and their associated polygons are shown in Figure 1 in the main text.

Our main goal is to list all required properties for these six base spaces B. This includes simple topological properties such as the canonical bundle $K_B = -c_1(B)$, the second Chern class $c_2(B)$ and the Hodge number $h^{1,1}(B)$. Further, we provide an integral basis $\{\mathcal{C}^i\}$ of curve classes, where $i,j,\ldots = 1,\ldots,h^{1,1}(B)$, as well as a corresponding dual basis $\{\mathcal{C}_i\}$ which satisfies

$$\mathcal{C}^i \cdot \mathcal{C}_j = \delta^i_j \;. \tag{B.1}$$

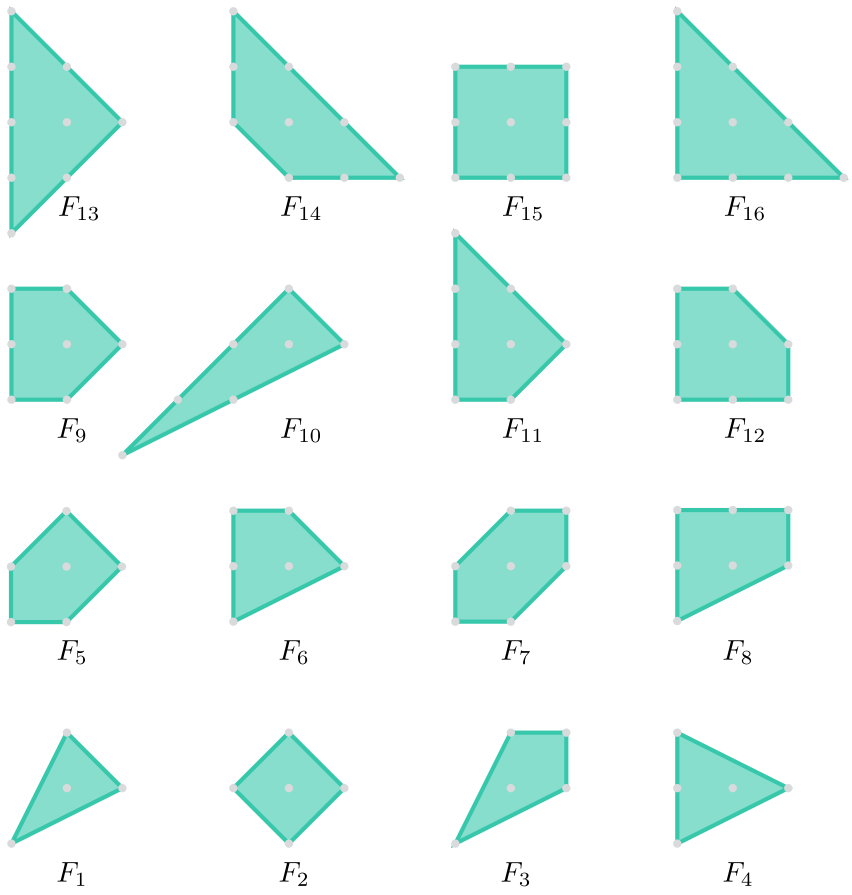

Figure 27: *The 16 reflexive polytopes. This is a reproduction of Figure 2 of Ref. [40], and the notation F_i follows their naming convention. Some simple isomorphisms are $F_1 \cong \mathbb{P}^2$, $F_2 \cong \mathbb{P}^1 \times \mathbb{P}^1$, $F_3 \cong \mathrm{dP}_1 \cong \mathbb{F}_1$, $F_4 \cong \mathbb{F}_2$, $F_5 \cong \mathrm{dP}_2$, and $F_7 \cong \mathrm{dP}_3$, where dP_n and $\mathbb{F}_n$ are the del Pezzo and Hirzebruch surfaces.*

We also explain how this basis relates to the divisors $[x_i]$, associated to the curves defined by $x_i = 0$, where x_i are the coordinates assigned to the edges of the polygons in Figure 1. For this basis, we provide the intersection numbers

$$g_{ij} := \mathcal{C}_i \cdot \mathcal{C}_j \ , \quad \lambda_i := K_B \cdot \mathcal{C}_i \ , \quad \lambda := K_B^2 = c_1(B)^2 = \lambda^i \lambda_i \ , \tag{B.2}$$

and we note that the intersection matrix $g^{ij} := \mathcal{C}^i \cdot \mathcal{C}^j$ is the inverse of g_{ij}. The metric g_{ij} and its inverse g^{ij} can be used to lower and raise indices so that, for example, $\lambda^i = g^{ij}\lambda_j$. We will also provide a set of generators of the Mori cone $\mathcal{M}_B$.

We note that for any of these bases B these properties can be read off from the corresponding polytope in Figure 1. First note that for any vector $\vec{v}$ in the plane of the polytope there is a linear relation between divisors,

$$\sum_{i=1}^{n} \left(\vec{x_i}^T \vec{v} \right) [x_i] = 0 \, , \tag{B.3}$$

where n is the number of external points on the polygon, and where $\vec{x_i}$ is the vector of the point on the edge of the polytope. Note that there are two independent such relations, and

hence $h^{1,1}(B) = n - 2$. To compute intersection numbers, first note that two $[x_i]$ corresponding to adjacent points have mutual intersection number 1. Self-intersections $[x_i] \cdot [x_i]$ can then be computed by combining this fact with the linear relations between divisors. Additionally we can read off the Chern classes,

$$c_1(B) = -K_B = \sum_{i=1}^{n} [x_i] \ , \quad c_2(B) = n \ . \tag{B.4}$$

Finally, the Mori cone is generated by the collection of the $[x_i]$.

We have searched for involutions which can be linearly realised on the homegeneous coordinates and which have at most fixed points. We will explicitly specify the action of these involution ι_B on the homogeneous coordinates. In addition, we also provide the matrix I_B which describes the action of ι_B on the curve classes in line with the relation

$$\iota_B(\mathcal{C}_j) = I^i_{Bj} \mathcal{C}_i \ . \tag{B.5}$$

Finally, we indicate the most general form of curve classes $\mathcal{C} = k^i \mathcal{C}_i$ which are invariant under ι_B as a list of constraints on the integers k^i and the resulting dimension, $h^{1,1}_{\text{inv}}(B)$, of the sub-space of invariant classes.

As for the resulting CY three-folds over these base spaces B, recall from Eqs. (3.23), (3.25) and (3.18) that we can express the second Chern class $c_2(X)$, the Euler characteristic $\chi(X)$ and the Mori cone $\mathcal{M}_X$ in terms of properties of the base B. We also recall that the Kähler cone of the three-fold X is obtained as the dual cone to the Mori cone. Concretely this means one can obtain the inequalities constraining the Kähler moduli by dotting the vector (t^I) of Kähler moduli into each of the Mori cone generators (seeing the latter as vectors relative to the basis $\mathcal{C}^I$). Finally, by noting that $h^{1,1}(X) = h^{1,1}(B) + 2$ we can also obtain the Hodge numbers of the three-fold. Using these results, we will list explicitly, for each base space B, the properties of the associated elliptically fibered CY three-fold X with two sections over that base.

Base $B = F_2 = \mathbb{P}^1 \times \mathbb{P}^1$

Our first and simplest base space is $B = F_2 = \mathbb{P}^1 \times \mathbb{P}^1$ with the basic topological characteristics

$$K_B = -c_1(B) = -2(l_1 + l_2) \ , \quad c_2(B) = 4 \ , \quad h^{1,1}(B) = 2 \ . \tag{B.6}$$

Here, l_1 and l_2 are the divisor classes which correspond to one of the $\mathbb{P}^1$ factors times a point in the other. (These are the pullbacks of the two $\mathbb{P}^1$ hyperplane classes to the product space.) In terms of the coordinates indicated in Figure 1, they can also be written as $l_1 = [x_1]$ and $l_2 = [x_2]$.

The intersections of l_1 and l_2 are clearly given by $l_1 \cdot l_1 = l_2 \cdot l_2 = 0$ and $l_1 \cdot l_2 = 1$ and, hence, we can introduce a basis of curve classes and its dual by

$$(\mathcal{C}^i) = (l_1, l_2) \ , \quad (\mathcal{C}_i) = (l_2, l_1) \ . \tag{B.7}$$

The relevant intersection numbers are then given by

$$(g_{ij}) = \begin{pmatrix} 0 & 1 \\ 1 & 0 \end{pmatrix} \ , \quad (\lambda_i) = (-2, -2) \ , \quad \lambda = 8 \ . \tag{B.8}$$

The Mori cone can be written as

$$\mathcal{M}_B = \langle l_1, l_2 \rangle \ , \tag{B.9}$$

where the angle brackets are used to denote the list of generators. With the homogenous coordinates (x_1, x_2, x_3, x_4) as in Figure 1 (where (x_1, x_3) correspond to one $\mathbb{P}^1$ factor and (x_2, x_4) to the other), the action of the involution takes the form

$$\iota_B(x_1, x_2, x_3, x_4) = (x_1, x_2, -x_3, -x_4) \ . \tag{B.10}$$

Both curve classes l_1 and l_2 are invariant under ι_B so that $I_B = \mathbb{1}_2$. Consequently, every curve class on B is ι_B invariant and we have $h^{1,1}_{\text{inv}}(B) = 2$.

The resulting properties of the CY three-fold X over this base are

$$h^{1,1}(X) = 4 \ , \quad h^{2,1}(X) = 148 \ , \quad \chi(X) = -288 \ , \quad c_2(X) = -4(C^0 + C^{\hat{0}}) + 24(C^1 + C^2) \ , \tag{B.11}$$

$$\mathcal{M}_X = \langle C^{\hat{0}}, C^0, -2C^0 + C^1, -2C^0 + C^2, C^1 - 2C^{\hat{0}}, C^2 - 2C^{\hat{0}} \rangle \ . \tag{B.12}$$

Base $B = F_4 = \mathbb{F}_2$

This base has the basic properties

$$K_B = -c_1(B) = -2[x_2] \ , \quad c_2(B) = 4 \ , \quad h^{1,1}(B) = 2 \ . \tag{B.13}$$

In terms of the coordinates in Figure 1, we can introduce a basis of curve classes by $\mathcal{C}^1 = [x_2]$ and $\mathcal{C}^2 = [x_3]$ with dual basis $\mathcal{C}_1 = [x_3]$ and $\mathcal{C}_2 = [x_2 - 2x_3]$. The corresponding intersection numbers are

$$(g_{ij}) = \begin{pmatrix} 0 & 1 \\ 1 & -2 \end{pmatrix} \ , \quad (\lambda_i) = (-2, 0) \ , \quad \lambda = 8 \ , \tag{B.14}$$

and the Mori cone is given by

$$\mathcal{M}_B = \langle [x_2], [x_3], [x_2 - 2x_3] \rangle \ . \tag{B.15}$$

For the action of the involution ι_B on the homogeneous coordinates we have

$$\iota_B(x_1, x_2, x_3, x_4) = (x_1, x_2, -x_3, -x_4) \,. \tag{B.16}$$

The resulting transformation on the curve classes is trivial so that $I_B = \mathbb{1}_2$. Consequently, every curve class on B is ι_B invariant and, hence, $h^{1,1}_{\text{inv}}(B) = 2$.

For the associated CY three-fold this leads to

$$h^{1,1}(X) = 4 \,, \quad h^{2,1}(X) = 148 \,, \quad \chi(X) = -288 \,, \quad c_2(X) = -4(C^0 + C^{\hat{0}}) + 24C^1 \,, \tag{B.17}$$

$$\mathcal{M}_X = \langle C^{\hat{0}}, C^0, C^1, -2C^0 + C^2, C^2 - 2C^{\hat{0}} \rangle \,. \tag{B.18}$$

Base $B = F_7 = \text{dP}_3$

This space corresponds to the del Pezzo surface dP_3 which can be seen as $\mathbb{P}^2$ blown-up in three distinct points. Its basic topological properties are

$$K_B = -c_1(B) = -3l + e_1 + e_2 + e_3 \,, \quad c_2(B) = 6 \,, \quad h^{1,1}(B) = 4 \,. \tag{B.19}$$

Here, l is the hyperplace class and e_a, where $a = 1, 2, 3$, are the classes of the three blow-ups. In terms of the coordinates in Figure 1, these classes can also be expressed as

$$l = [x_4] + [x_5] + [x_6] \,, \quad e_1 = [x_6] \,, \quad e_2 = [x_2] \,, \quad e_3 = [x_4] \,. \tag{B.20}$$

The intersections are given by

$$l \cdot l = 1 \,, \quad l \cdot e_a = 0 \,, \quad e_a \cdot e_b = -\delta_{ab} \,, \tag{B.21}$$

so that a suitable choice for the basis of curve classes and its dual is given by

$$(\mathcal{C}^i) = (l, e_a) \,, \quad (\mathcal{C}_i) = (l, -e_a) \,. \tag{B.22}$$

In terms of this basis choice the intersection numbers read

$$(g_{ij}) = \begin{pmatrix} 1 & 0 \\ 0 & -\mathbf{1}_3 \end{pmatrix} \,, \quad (\lambda_i) = (-3, 1, 1, 1) \,, \quad \lambda = 6 \,. \tag{B.23}$$

The Mori cone is generated by

$$\mathcal{M}_B = \langle e_1, e_2, e_3, l - e_1 - e_2, l - e_1 - e_3, l - e_2 - e_3 \rangle \,. \tag{B.24}$$

The action of ι_B on the homogeneous coordinates

$$\iota_B(x_1, x_2, x_3, x_4, x_5, x_6) = (x_4, x_5, x_6, x_1, x_2, x_3) \,, \tag{B.25}$$

leads to the action on the curve classes specified by

$$I_B = \begin{pmatrix} 2 & -1 & -1 & -1 \\ 1 & 0 & -1 & -1 \\ 1 & -1 & 0 & -1 \\ 1 & -1 & -1 & 0 \end{pmatrix} . \tag{B.26}$$

The most general ι_B invariant curve class $k^i\mathcal{C}_i$ is then characterised by the constraint

$$k^1 = k^2 + k^3 + k^4 , \tag{B.27}$$

so that $h^{1,1}_{\text{inv}}(B) = 3$.

The associated CY three-fold has the properites

$$h^{1,1}(X) = 6 , \quad h^{2,1}(X) = 114 , \quad \chi(X) = -216 , \quad c_2(X) = 12(3C^1 - C^2 - C^3 - C^4) , \tag{B.28}$$

$$\begin{aligned} \mathcal{M}_X \;=\; & \langle C^{\hat{0}}, C^0, -C^0 + C^2, -C^0 + C^3, -C^0 + C^4, -C^0 + C^1 - C^2 - C^3, \\ & -C^0 + C^1 - C^2 - C^4, -C^0 + C^1 - C^3 - C^4, C^2 - C^{\hat{0}}, C^3 - C^{\hat{0}}, C^4 - C^{\hat{0}}, \\ & C^1 - C^2 - C^3 - C^{\hat{0}}, C^1 - C^2 - C^4 - C^{\hat{0}}, C^1 - C^3 - C^4 - C^{\hat{0}} \rangle . \end{aligned} \tag{B.29}$$

Base $B = F_9$

The basic properties of this space are given by

$$K_B = -c_1(B) = -[x_2] - 2[x_3] - [x_4] , \quad c_2(B) = 6 , \quad h^{1,1}(B) = 4 , \tag{B.30}$$

where $x_1, \ldots, x_6$ are the homogeneous coordinates as indicated in Figure 1. The standard basis of curve classes and its dual can be introduced as

$$\mathcal{C}^1 = [x_2] , \quad \mathcal{C}^2 = [x_3] , \quad \mathcal{C}^3 = [x_4] , \quad \mathcal{C}^4 = [x_5] \tag{B.31}$$

$$\mathcal{C}_1 = [x_4 + x_5 - x_2] , \quad \mathcal{C}_2 = [x_4 + x_5] \tag{B.32}$$

$$\mathcal{C}_3 = [x_2 + x_3 - x_4 - x_5] , \quad \mathcal{C}_4 = [x_2 + x_3 - x_4 - 2x_5] . \tag{B.33}$$

This leads to the intersections

$$(g_{ij}) = \begin{pmatrix} -1 & 0 & 1 & 1 \\ 0 & 0 & 1 & 1 \\ 1 & 1 & -1 & -1 \\ 1 & 1 & -1 & -2 \end{pmatrix} , \quad (\lambda_i) = (-1, -2, -1, 0) , \quad \lambda = 6 . \tag{B.34}$$

The Mori cone is generated by

$$\mathcal{M}_B = \langle [x_2], [x_3], [x_4], [x_5], [x_4 + x_5 - x_2], [x_2 + x_3 - x_4 - 2x_5] \rangle \ . \tag{B.35}$$

With the involution ι_B given by

$$\iota_B(x_1, x_2, x_3, x_4, x_5, x_6) = (x_5, x_4, x_3, x_2, x_1, -x_6) \tag{B.36}$$

the action on the curve classes is specified by

$$I_B = \begin{pmatrix} 0 & 0 & 1 & 0 \\ 0 & 1 & 0 & 0 \\ 1 & 0 & 0 & 0 \\ -1 & 0 & 1 & 1 \end{pmatrix} , \tag{B.37}$$

leading to ι_B invariant classes $k^i \mathcal{C}_i$ characterised by

$$k^1 = k^3 \ . \tag{B.38}$$

This implies $h^{1,1}_{\text{inv}}(B) = 3$.

For the associated CY three-fold we find

$$h^{1,1}(X) = 6 \ , \quad h^{2,1}(X) = 114 \ , \quad \chi(X) = -216 \ , \quad c_2(X) = 12(C^1 + 2C^2 + C^3) \ , \tag{B.39}$$

$$\begin{aligned} \mathcal{M}_X \ = \ & \langle C^{\hat{0}}, C^0, -C^0 - C^1 + C^3 + C^4, -C^0 + C^1, -C^0 + C^3, -C^0 + C^4, \\ & C^1 + C^2 - C^3 - 2C^4, -C^1 + C^3 + C^4 - C^{\hat{0}}, C^1 - C^{\hat{0}}, C^3 - C^{\hat{0}}, C^4 - C^{\hat{0}} \rangle \end{aligned} \tag{B.40}$$

Base $B = F_{13}$

The basic topological characteristics of this space are

$$K_B = -c_1(B) = -[x_3] - 2[x_4] - [x_5] \ , \quad c_2(B) = 8 \ , \quad h^{1,1}(B) = 6 \ . \tag{B.41}$$

and, in terms of the coordinates in Figure 1, a suitable basis of curves is defined by

$$\mathcal{C}^i = [x_{i+1}] \ , \quad i = 1, \ldots, 6 \ . \tag{B.42}$$

From the intersection numbers

$$(g_{ij}) = \begin{pmatrix} -2 & -1 & 0 & 1 & 2 & 1 \\ -1 & -1 & 0 & 1 & 2 & 1 \\ 0 & 0 & 0 & 1 & 2 & 1 \\ 1 & 1 & 1 & -1 & -2 & -1 \\ 2 & 2 & 2 & -2 & -6 & -3 \\ 1 & 1 & 1 & -1 & -3 & -2 \end{pmatrix} , \quad (\lambda_i) = (0, -1, -2, -1, 0, 0) \ , \quad \lambda = 4 \ , \tag{B.43}$$

we can infer the form of the dual basis in terms of classes $[x_i]$ by using the relation $\mathcal{C}_i = g_{ij}\mathcal{C}^j$. The Mori cone of this space is generated by

$$\mathcal{M}_B = \langle [x_2], \ldots, [x_7], [x_2 + x_3 + x_4 - x_5 - 3x_6 - 2x_7], [-2x_2 - x_3 + x_5 + 2x_6 + x_7] \rangle \ . \quad \text{(B.44)}$$

The involution acts on the homogeneous coordinates as

$$\iota_B(x_1, x_2, x_3, x_4, x_5, x_6, x_7, x_8) = (x_7, x_6, x_5, x_4, x_3, x_2, x_1, -x_8) \ , \quad \text{(B.45)}$$

leading to an action on the curves classes specified by

$$I_B = \begin{pmatrix} 0 & 0 & 0 & 0 & 1 & 0 \\ 0 & 0 & 0 & 1 & 0 & 0 \\ 0 & 0 & 1 & 0 & 0 & 0 \\ 0 & 1 & 0 & 0 & 0 & 0 \\ 1 & 0 & 0 & 0 & 0 & 0 \\ -2 & -1 & 0 & 1 & 2 & 1 \end{pmatrix} . \quad \text{(B.46)}$$

This means that ι_B invariant classes $k^i\mathcal{C}_i$ are characterised by

$$k^1 = k^5 \ , \quad k^2 = k^4 \ , \quad \text{(B.47)}$$

so that $h^{1,1}_{\text{inv}}(B) = 4$.

The associated CY three-fold has the following properties

$$h^{1,1}(X) = 8 \ , \quad h^{2,1}(X) = 80 \ , \quad \chi(X) = -144 \ , \quad \text{(B.48)}$$

$$c_2(X) = 4(C^0 + C^{\hat{0}}) + 12(C^2 + 2C^3 + C^4) \ , \quad \text{(B.49)}$$

$$\begin{aligned} \mathcal{M}_X \ = \ & \langle C^{\hat{0}}, C^0, -2C^1 - C^2 + C^4 + 2C^5 + C^6, -C^0 + C^1, C^2, C^4, -C^0 + C^5, \\ & C^6, C^1 + C^2 + C^3 - C^4 - 3C^5 - 2C^6, C^1 - C^{\hat{0}}, C^5 - C^{\hat{0}} \rangle \ . \end{aligned} \quad \text{(B.50)}$$

Base $B = F_{15}$

The basic topological characteristics of this space are

$$K_B = -c_1(B) = -[x_3] - 2[x_4] - 2[x_5] - 2[x_6] - [x_7] \ , \quad c_2(B) = 8 \ , \quad h^{1,1}(B) = 6 \ . \quad \text{(B.51)}$$

A suitable choice for the basis of curve classes is given by

$$\mathcal{C}^i = [x_{i+1}] \ , \quad i = 2, \ldots, 7 \ , \quad \text{(B.52)}$$

and the dual basis can be inferred from $\mathcal{C}_i = g_{ij}\mathcal{C}^j$ using the intersection numbers

$$(g_{ij}) = \begin{pmatrix} -2 & -1 & 0 & 1 & 2 & 1 \\ -1 & -1 & 0 & 1 & 2 & 1 \\ 0 & 0 & 0 & 1 & 2 & 1 \\ 1 & 1 & 1 & 0 & 0 & 0 \\ 2 & 2 & 2 & 0 & -2 & -1 \\ 1 & 1 & 1 & 0 & -1 & -1 \end{pmatrix} , \quad (\lambda_i) = (0, -1, -2, -2, -2, -1) , \quad \lambda = 4 . \tag{B.53}$$

The Mori cone is generated by

$$\mathcal{M}_B = \langle [x_2], \ldots, [x_7], [x_2 + x_3 + x_4 - x_6 - x_7], [-2x_2 - x_3 + x_5 + 2x_6 + x_7] \rangle . \tag{B.54}$$

For the involution, we find there are two inequivalent choices, which we refer to as cases (a) and (b). Their actions on the homogeneous coordinates are given by

$$\iota_B^{(a)}(x_1, \ldots, x_8) = (x_5, x_6, x_7, x_8, x_1, x_2, x_3, x_4) \tag{B.55}$$

$$\iota_B^{(b)}(x_1, \ldots, x_8) = (x_7, x_6, x_5, x_4, x_3, x_2, x_1, -x_8) \tag{B.56}$$

with corresponding actions

$$I_B^{(a)} = \begin{pmatrix} 0 & 0 & 0 & 0 & 1 & 0 \\ 0 & 0 & 0 & 0 & 0 & 1 \\ 1 & 1 & 1 & 0 & -1 & -1 \\ -2 & -1 & 0 & 1 & 2 & 1 \\ 1 & 0 & 0 & 0 & 0 & 0 \\ 0 & 1 & 0 & 0 & 0 & 0 \end{pmatrix} , \quad I_B^{(b)} = \begin{pmatrix} 0 & 0 & 1 & 0 & 0 & 0 \\ 0 & 1 & 0 & 0 & 0 & 0 \\ 1 & 0 & 0 & 0 & 0 & 0 \\ -2 & -1 & 0 & 1 & 2 & 1 \\ 1 & 1 & 1 & 0 & -1 & -1 \\ 0 & 0 & 0 & 0 & 0 & 1 \end{pmatrix} , \tag{B.57}$$

on the curve classes. The ι_B invariant curve classes $k^i\mathcal{C}_i$ are characterised by

$$\begin{array}{llllll} k^1 = k^5 & k^2 = k^6 & & \text{case (a)} \\ k^1 = k^3 & k^2 = k^6 + 2k^5 - 2k^3 & & \text{case (b)} \end{array} , \tag{B.58}$$

which means that $h^{1,1}_{\text{inv}}(B) = 4$ in either case.

For the associated CY three-fold we find

$$h^{1,1}(X) = 8 , \quad h^{2,1}(X) = 80 , \quad \chi(X) = -144 , \tag{B.59}$$

$$c_2(X) = 4(C^0 + C^{\hat{0}}) + 12(C^2 + 2C^3 + 2C^4 + 2C^5 + C^6) , \tag{B.60}$$

$$\begin{aligned} \mathcal{M}_X = \langle & C^{\hat{0}}, C^0, -C^0 + C^1 + C^2 + C^3 - C^5 - C^6, -2C^1 - C^2 + C^4 + 2C^5 + C^6, \\ & -C^0 + C^1, C^2, -C^0 + C^3, C^4, -C^0 + C^5, C^6, C^1 + C^2 + C^3 - C^5 - C^6 - C^{\hat{0}}, \\ & C^1 - C^{\hat{0}}, C^3 - C^{\hat{0}}, C^5 - C^{\hat{0}} \rangle . \end{aligned} \tag{B.61}$$

C Line bundle cohomology on elliptically fibered CYs with two sections

In this section we collect useful information on line bundles on elliptically fibered CY manifolds, in particular on how to calculate their cohomology. The material of this appendix can also be found in the literature [3, 37, 38] and we collect and summarise all the properties relevant to heterotic line bundle model building.

C.1 Premilinaries

Basic properties of line bundles

First we recall some basic facts about line bundles. We consider CY three-folds X with a basis $\{D_I\}$ of divisor classes and a dual basis $\{C^I\}$ of curve classes (such that $D_I \cdot C^J = \delta_I^J$) and denote the triple intersection numbers by $d_{IJK} = D_I \cdot D_J \cdot D_K$. A general Kähler form is written as $J = t^I D_I$, where t^I are the Kähler moduli relative to the chosen basis of divisor classes.

The line bundle L on X associated to the divisor $D = k^I D_I$ is denoted by $L = \mathcal{O}_X(D)$ or sometimes, when it is clear which divisor basis is being referred to, simply by $L = \mathcal{O}_X(\mathbf{k})$. The first Chern class of this line bundle is given by

$$c_1(L) = D = k^I D_I \ . \tag{C.1}$$

For the Chern character one finds

$$\begin{aligned} \mathrm{ch}_1(L) &= c_1(L) = k^I D_I \ , & \text{(C.2)} \\ \mathrm{ch}_2(L) &= \frac{1}{2} c_1(L)^2 = \frac{1}{2} d_{IJK} k^I k^J C^K \ , & \text{(C.3)} \\ \mathrm{ch}_3(L) &= \frac{1}{6} c_1(L)^3 = \frac{1}{6} d_{IJK} k^I k^J k^K \ . & \text{(C.4)} \end{aligned}$$

The Todd class of a CY three-fold is given by $\mathrm{Td}(X) = 1 + c_2(X)/12$, where $c_2(X) = c_{2I}(X) C^I$ is its second Chern class. Then, using the index theorem $\mathrm{ind}(L) = \mathrm{ch}(L)\mathrm{Td}(X)$, the index of a line bundle can be written as

$$\mathrm{ind}(L) = \mathrm{ch}_3(L) + \frac{1}{12} c_1(L) c_2(X) = \frac{1}{6} d_{IJK} k^I k^J k^K + \frac{1}{12} k^I c_{2I}(X) \ . \tag{C.5}$$

Another quantity we will require is the slope of the line bundle L, defined by

$$\mu_X(L) := \int_X J \wedge J \wedge c_1(L) = d_{IJK} t^I t^J k^K \ . \tag{C.6}$$

These above results for single line bundles can be easily generalised to line bundle sums

$$V = \bigoplus_{a=1}^{r} L_a \quad \text{where} \quad L_a = \mathcal{O}_X(\mathbf{k}_a) \ , \tag{C.7}$$

with rank $r = \mathrm{rk}(V)$. The first Chern class for such a line bundle sum is

$$c_1(V) = \left(\sum_{a=1}^{n} k_a^I\right) D_I \,. \tag{C.8}$$

We will normally be interested in line bundle sums V with $c_1(V) = 0$ and in this case the second Chern class and the index of V are given by

$$c_2(V) = -\frac{1}{2} d_{IJK} \left(\sum_a k_a^I k_a^J\right) C^K \,, \quad \mathrm{ind}(V) = \frac{1}{6} d_{IJK} \sum_a k_a^I k_a^J k_a^K \,. \tag{C.9}$$

General theorems and methods

We first collect a number of mathematical results which will enter the calculation of line bundle cohomology.

We will make use of the **Serre duality** theorem. Let X be a compact complex n-dimensional manifold with canonical bundle K_X, and let $V \to X$ be a vector bundle with dual bundle V^*. Then, Serre duality states that

$$H^q(X, V) \cong H^{n-q}(X, K_X \otimes V^*) \,. \tag{C.10}$$

In particular, for a CY three-fold, the canonical bundle K_X is trivial, so that $H^q(X, V) \cong H^{3-q}(X, V^*)$.

In order to exploit the fibration structure of the CY three-folds we will require **(higher) direct images**. Let X be an elliptically fibered CY three-fold, with base B and projection map $\pi : X \to B$. Given a short exact sequence of vector bundles, $V_i \to X$, one can ask if such a sequence implies the existence of a short exact sequence for the direct images (or push-forwards), $\pi_* V_i$, which are bundles on the base B. This question finds a general answer in the language of derived functors and higher direct images, as follows. Suppose we have the short exact sequence of bundles

$$0 \to V_1 \to V_2 \to V_3 \to 0 \,. \tag{C.11}$$

The direct image functor π_* is left exact, so applying it to the above sequence leads to the exact sequence

$$0 \to \pi_* V_1 \to \pi_* V_2 \to \pi_* V_3 \,. \tag{C.12}$$

How can this sequence be continued on the right, so as to keep it exact? The answer is (see, for example, Chapter III, Theorem 1.1A of Ref. [120])

$$\begin{aligned} 0 \quad &\to \quad \pi_* V_1 \to \pi_* V_2 \to \pi_* V_3 && \text{(C.13)} \\ &\to \quad R^1\pi_* V_1 \to R^1\pi_* V_2 \to R^1\pi_* V_3 && \text{(C.14)} \\ &\to \quad R^2\pi_* V_1 \to R^2\pi_* V_2 \to R^2\pi_* V_3 && \text{(C.15)} \\ &\to \quad \ldots \,, && \text{(C.16)} \end{aligned}$$

where $R^q\pi_*$ are called the 'right derived functors' of the direct image functor, and $R^q\pi_*V_i$ are called the 'higher direct images' of the bundles V_i. It can be shown (see, for example, Chapter III, Proposition 8.1 of [120]) that the higher direct image $R^q\pi_*V$ $(q \geq 1)$ is the sheaf associated to the pre-sheaf

$$U \mapsto H^q\left(\pi^{-1}(U), V|_{f^{-1}(U)}\right) . \tag{C.17}$$

There are two very useful identities for higher direct images that will be helpful below. The first of these identities is the **projection formula**,

$$R^q\pi_*(\pi^*\mathcal{L} \otimes V) = \mathcal{L} \otimes R^q\pi_*V , \tag{C.18}$$

where $\mathcal{L}$ is a bundle on the base B and V a bundle on the total space (see, for example, Chapter III.8 in Ref. [120]). The second identity, referred to as **relative duality**, is given by (see, for example, Chapter III.12 in Ref. [127])

$$R^1\pi_*V = (\pi_*V^*)^* \otimes K_B . \tag{C.19}$$

This result is frequently applied in the context of spectral cover bundles, as for example in Ref. [3].

Finally, we will make extensive use of the **Leray spectral sequence** (see, for example, Chapter 5 of Ref. [128]). This sequence relates cohomologies of bundles on the total space X to cohomologies of bundles on the base B. For our purposes the following will suffice. For a bundle V, write $H^p \equiv H^p(X, V)$ and define $E_2^{p,q} \equiv H^p(B, R^q\pi_*V)$. From the Leray spectral sequence one can show the existence of the exact sequence

$$0 \to E_2^{1,0} \to H^1 \to E_2^{0,1} \to E_2^{2,0} \to \mathrm{Ker}\left(H^2 \to E_2^{0,2}\right) \to E_2^{1,1} \to E_2^{3,0} . \tag{C.20}$$

In our case, $E_2^{3,0}$ is a third cohomology on the two-dimensional base B and, hence, vanishes. Similarly, $E_2^{0,2}$ vanishes, since it involves $R^2\pi_*V$, and this is associated to second cohomologies on the one-dimensional fiber. As a result we have $\mathrm{Ker}\left(H^2 \to E_2^{0,2}\right) = H^2$ and the above exact sequence becomes

$$0 \to E_2^{1,0} \to H^1 \to E_2^{0,1} \to E_2^{2,0} \to H^2 \to E_2^{1,1} \to 0 . \tag{C.21}$$

If this sequence splits (as it will in all cases we are interested in) it determines H^1 and H^2 in terms of cohomology on the base B. The other two cohomologies can also be expressed in terms of cohomology on the base, via the relations $H^0 = E_2^{0,0}$ and $H^3 = E_2^{2,1}$.

C.2 Computing the cohomologies

Line bundle cohomology on the base

For most of the base spaces considered in this chapter, no analytic expressions for line bundle cohomology are available, and we use the code cohomCalg [30, 31] to compute cohomologies on the base. However the cohomology of line bundles on del Pezzo surfaces has been computed, in Appendix B of Ref. [119]. Since one of the base spaces we consider is a del Pezzo surface, we briefly present these results[44] for reference. Consider a del Pezzo surface dP_r with $r \leq 8$, given by a $\mathbb{P}^2$ blown-up at r distinct points p_a, where $a = 1, \ldots, r$, with hyperplane class l and exceptional divisors $e_a = \rho^{-1}(p_a)$ and the blow-down map ρ. A line bundle on dP_r can then be written as

$$\mathcal{L} = \mathcal{O}_{\mathrm{dP}_r}\left(nl + \sum_a b_a e_a - \sum_a c_a e_a\right) , \tag{C.22}$$

where $n \in \mathbb{Z}$ and $b_a, c_a \in \mathbb{Z}^{\geq 0}$. For $n \geq -2$, the cohomology of the line bundle $\mathcal{L}$ is given by

$$h^q(B,\mathcal{L}) = \begin{cases} A_{\sum c_a p_a}(n) & \text{for } q = 0 \\ A_{\sum c_a p_a}(n) - \binom{n+2}{2} + \sum_a \binom{b_a}{2} + \sum_a \binom{c_a+1}{2} & \text{for } q = 1 \\ 0 & \text{for } q = 2 \end{cases} , \tag{C.23}$$

while the cohomology for $n < -2$ can be obtained by Serre duality, $h^q(B,\mathcal{L}) = h^{2-q}(B, \mathcal{L}^* \otimes K_{\mathrm{dP}_r})$, using the expression

$$K_B = \mathcal{O}_{\mathrm{dP}_r}\left(-3l + \sum_a e_a\right) \tag{C.24}$$

for the canonical bundle. Here $A_{\sum c_a p_a}(n)$ is the dimension of the space of homogeneous polynomials of degree n on $\mathbb{P}^2$ that have order c_a zeroes at the points p_a.

Line bundle cohomology for elliptic fibrations with a single section

As a preparation, we first consider line bundle cohomology on an elliptically fibered CY threefold X over base B, with projection $\pi : X \to B$ and a single section $\sigma : B \to X$. To make some formulae easier to read, in this subsection and the next we will sometimes abuse notation and write σ for the image of the section $\sigma(B)$, and similarly ζ for $\zeta(B)$, and it should be clear from context which one is meant. Let $V \to X$ be a vector bundle over X and, as before, we write $H^p = H^p(X,V)$ and $E_2^{p,q} \equiv H^p(B, R^q\pi_* V)$. From above we know that the Leray spectral sequence implies the exact sequence

$$0 \to E_2^{1,0} \to H^1 \to E_2^{0,1} \to E_2^{2,0} \to H^2 \to E_2^{1,1} \to 0 , \tag{C.25}$$

[44] Note however that the expression of their final result, equation (286), contains a typo: in h^1, the term $A_{\sum c_j p_j}(a)$ should appear with a plus rather than a minus.

and, in addition, the results $H^0 = E_2^{0,0}$ and $H^3 = E_2^{2,1}$. A line bundle L on X can be written as

$$L \equiv \mathcal{O}_X(n\sigma) \otimes \pi^*\mathcal{L}\,, \tag{C.26}$$

where $\mathcal{L}$ is a line bundle on B and n is an integer. Using the projection formula, $R^q\pi_*(V \otimes \pi^*\mathcal{L}) = R^q\pi_* V \otimes \mathcal{L}$, we can write the exact sequence explicitly as

$$\begin{aligned} 0 \;\to\; & H^1(B, \pi_*\mathcal{O}_X(n\sigma) \otimes \mathcal{L}) \to H^1(X, L) \to H^0(B, R^1\pi_*\mathcal{O}_X(n\sigma) \otimes \mathcal{L}) \\ \to\; & H^2(B, \pi_*\mathcal{O}_X(n\sigma) \otimes \mathcal{L}) \to H^2(Z, L) \to H^1(B, R^1\pi_*\mathcal{O}_X(n\sigma) \otimes \mathcal{L}) \to 0\,. \end{aligned} \tag{C.27}$$

To work this out further we require the (higher) direct images of the line bundles $\mathcal{O}_X(n\sigma)$. These have been worked out in Appendix C of Ref. [37] and the result is

$$\pi_*\mathcal{O}_X(n\sigma) = \begin{cases} 0 & \text{for } n < 0 \\ \mathcal{O}_B & \text{for } n = 0, 1 \\ \mathcal{O}_B \oplus K_B^2 \oplus K_B^3 \ldots \oplus K_B^n & \text{for } n \geq 2 \end{cases}, \tag{C.28}$$

$$R^1\pi_*\mathcal{O}_X(n\sigma) = \begin{cases} 0 & \text{for } n > 0 \\ K_B & \text{for } n = -1, 0 \\ K_B^1 \oplus K_B^{-1} \oplus K_B^{-2} \oplus \ldots \oplus K_B^{1-n} & \text{for } n \leq -2 \end{cases}. \tag{C.29}$$

From these results, we should distinguish the following cases.

- $\underline{n > 0}$: We have $R^1\pi_* L = 0$, and so,

$$H^3 = 0\,, \text{ and } H^p = E_2^{p,0} \text{ for } p = 0, 1, 2\,. \tag{C.30}$$

- $\underline{n < 0}$: We have $\pi_* L = 0$, and so,

$$H^0 = 0\,, \text{ and } H^p = E_2^{p-1,1} \text{ for } p = 1, 2, 3\,. \tag{C.31}$$

- $\underline{n = 0}$: We have $\pi_* L = \mathcal{L}$ and $R^1\pi_* L = K_B \otimes \mathcal{L}$, and so,

$$H^0 = E_2^{0,0}\,,\; H^3 = E_2^{2,1}\,. \tag{C.32}$$

  In this case, the other two cohomologies, H^1 and H^2 can only be obtained by elementary methods if the sequence (C.27) splits, that is, if $E_2^{0,1} = 0$ or $E_2^{2,0} = 0$. Fortunately, this turns out to be always the case for the base spaces we consider.

Line bundle cohomology for elliptic fibrations with two sections

As we have seen, elliptically fibered CY three-folds X with two sections, $\sigma : B \to X$ and $\zeta : B \to X$, have to be blown-up and, as a result, contain a further curve and divisor class, relative to the single section case. The most general line bundle $L \to X$ can now be written as

$$L = \mathcal{O}_X(m\sigma) \otimes \mathcal{O}_X(n\zeta) \otimes \pi^*\mathcal{L} \,, \tag{C.33}$$

where $m, n \in \mathbb{Z}$ and $\mathcal{L} \to B$ is a line bundle on the base. In fact, for our model building purposes we only require line bundles in a sub-class which consists of line bundles of the form

$$L = \mathcal{O}_X(n\Sigma) \otimes \pi^*\mathcal{L} \,, \tag{C.34}$$

where $n \in \mathbb{Z}$ and $\Sigma = \sigma(B) + \zeta(B)$.

In order to compute the cohomology of such line bundles, we follow Appendix A of Ref. [38]. Note that the subsequent derivation only holds if $H^1(B, K_B^{-n}) = 0$ for all $n \geq 0$, a condition which is satisfied for toric weak Fano base spaces B and, hence, for all base spaces considered in this chapter. That this condition holds for toric weak Fano bases can be seen as follows (for more information see for example Ref. [84]). The toric Kawamata-Viehweg theorem states that on a compact toric variety B, if D is a nef and big divisor then

$$H^p(B, K_B \otimes \mathcal{O}_B(D)) = 0 \quad \text{for all } p > 0 \,. \tag{C.35}$$

If B is weak Fano, then K_B^{-1} is of the form $\mathcal{O}_B(D)$ where D is nef and big, and from this it follows that this is true also of K_B^{-n} for $n > 1$. Hence for weak Fano bases B, using K_B^{-n-1} in the theorem we have that $H^1(B, K_B^{-n}) = 0$ for $n \geq 0$.

We begin by recalling relative duality which states that

$$R^1\pi_* L = (\pi_* L^*)^* \otimes K_B \,. \tag{C.36}$$

In particular, this implies that $R^1\pi_*\mathcal{O}_X(n\Sigma) = 0$ for $n > 0$. Now consider the short exact sequence,

$$0 \to \mathcal{O}_X(-\zeta) \to \mathcal{O}_X \to \mathcal{O}_\zeta \to 0 \,, \tag{C.37}$$

and tensor this sequence with $\mathcal{O}_X(\Sigma)$ to obtain

$$0 \to \mathcal{O}_X(\sigma) \to \mathcal{O}_X(\Sigma) \to \mathcal{O}_X(\Sigma) \otimes \mathcal{O}_\zeta \to 0 \,. \tag{C.38}$$

Now we consider the associated long exact sequence of higher direct images, but, since $R^1\pi_*\mathcal{O}_X(\sigma) = 0$, this leads to the short exact sequence

$$0 \to \mathcal{O}_B \to \pi_*\mathcal{O}_X(\Sigma) \to K_B \to 0 \,, \tag{C.39}$$

for the direct images. Here, we have used that $\pi_*\mathcal{O}_X(\sigma) = \mathcal{O}_B$ and $\pi_*(\mathcal{O}_X(\Sigma)\otimes\mathcal{O}_\zeta) = K_B$. The space of extensions defined by the sequence (C.39) is isomorphic to $H^1(B, K_B^*)$ and, from our assumption about the base space B, this cohomology vanishes. As a result, the sequence (C.39) splits and we have

$$\pi_*\mathcal{O}_X(\Sigma) = \mathcal{O}_B \oplus K_B \ . \tag{C.40}$$

Starting from this result, we will now prove by induction that

$$\pi_*\mathcal{O}_X(n\Sigma) = \mathcal{O}_B \oplus K_B \oplus \left(K_B^{\otimes 2} \oplus K_B^{\otimes 3} \oplus \ldots \oplus K_B^{\otimes n}\right)^{\oplus 2} \quad \text{for all } n > 1 \ . \tag{C.41}$$

The starting point for the proof is the short exact sequence

$$0 \to \mathcal{O}_X((n-1)\Sigma) \to \mathcal{O}_X(n\Sigma) \to \mathcal{O}_X(n\Sigma)\otimes\mathcal{O}_X|_\Sigma \to 0 \ , \tag{C.42}$$

along with the relation $\mathcal{O}_X(n\Sigma)\otimes\mathcal{O}_X|_\Sigma = \mathcal{O}_X(n\Sigma)|_\Sigma$. Since $R^1\pi_*\mathcal{O}_X(m\Sigma) = 0$ for all $m > 0$, we have $R^1\pi_*\mathcal{O}_X((n-1)\Sigma) = 0$ for $n > 1$, so that the associated long exact sequence of higher direct images truncates to the short exact sequence

$$0 \to \pi_*\mathcal{O}_X((n-1)\Sigma) \to \pi_*\mathcal{O}_X(n\Sigma) \to \pi_*\mathcal{O}_X(n\Sigma)|_\Sigma \to 0 \ . \tag{C.43}$$

We note that $\pi_*\mathcal{O}_X(n\Sigma)|_\Sigma = K_B^n \oplus K_B^n$. Recall that we are working with a base B for which $H^1(B, K_B^{-m}) = 0$ for all $m \geq 0$. Then, by the induction hypothesis for $\pi_*\mathcal{O}_X((n-1)\Sigma)$, we see that this exact sequence splits, and that the result (C.41) follows. An expression for $R^1\pi_*\mathcal{O}_X(n\sigma)$ can then be obtained from relative duality.

In summary, the results for the direct images and higher direct images of the line bundles $\mathcal{O}_X(n\Sigma)$ for all $n \in \mathbb{Z}$, where $\Sigma \equiv \sigma(B) + \zeta(B)$, are:

$$\pi_*\mathcal{O}_X(n\Sigma) = \begin{cases} 0 & \text{for } n < 0 \\ \mathcal{O}_B & \text{for } n = 0 \\ \mathcal{O}_B \oplus K_B & \text{for } n = 1 \\ \mathcal{O}_B \oplus K_B \oplus \left(K_B^{\otimes 2} \oplus K_B^{\otimes 3} \oplus \ldots \oplus K_B^{\otimes n}\right)^{\oplus 2} & \text{for } n \geq 2 \end{cases} , \tag{C.44}$$

$$R^1\pi_*\mathcal{O}_X(n\Sigma) = \begin{cases} 0 & \text{for } n > 0 \\ K_B & \text{for } n = 0 \\ \mathcal{O}_B \oplus K_B & \text{for } n = -1 \\ \mathcal{O}_B \oplus K_B \oplus \left(K_B^{\otimes(-1)} \oplus K_B^{\otimes(-2)} \oplus \ldots \oplus K_B^{\otimes(-n+1)}\right)^{\oplus 2} & \text{for } n \leq -2 \end{cases} . \tag{C.45}$$

Deriving the cohomology for line bundles L of the form (C.34) then proceeds in complete analogy with the single section case discussed in the previous sub-section. All we have to do is replace

σ by Σ and, instead of using the results for the (higher) direct images of $\mathcal{O}_X(n\sigma)$, we use the above results for $\mathcal{O}_X(n\Sigma)$.

D Explicit blow-ups

D.1 Explicit blow-ups in 6d case

In this appendix we explicitly perform the blow-ups discussed in Section 4.3.3, for the example in the left of Figure 7, verifying that this toric procedure indeed removes any singularities worse than E_8. We recall the setup. We are interested in global F-theory models dual to six-dimensional heterotic line bundle models. In this case there are E_8 singularities at the two poles of the F-theory $\mathbb{P}^1$, and hence the intersection of the remaining brane locus with these E_8 singularities produces even more severe singularities, specifically with vanishing orders $(f, g, \Delta) \sim (4, 6, 12)$, which we call $\tilde{\mathrm{E}}_8$ singularities. The locus of these intersections has class $-12K_{\mathcal{B}_2}$, and these singularities require blow-ups in the F-theory base. We proposed that a possible F-theory three-fold after these blow-ups is the fibration over the base given in the leftmost diagram of Figure 7. However it is not immediately obvious that this is so, since we may expect that torically we do not have enough freedom to blow up over all the intersection points. We see that if we want to use toric blow-ups to resolve the $\tilde{\mathrm{E}}_8$ singularities we must collect these singularities together in single points on each E_8 stack, then perform repeated blow-ups over this point. We do this explicitly below, showing the result is a crepant resolution of these two singularities, leaving in the end only the two E_8 singularities.

We write z_i for the homogeneous coordinates of the F-theory $\mathbb{P}^1$, and u_i for the homogeneous coordinates of the heterotic base, which forms the other $\mathbb{P}^1$ of the F-theory base $\mathcal{B}_2$. After tuning E_8 singularities at $z_1 = 0$ and $z_2 = 0$ we have for the Weierstrass model the expressions

$$f = z_1^4 z_2^4 f_4\,, \quad g = z_1^5 z_2^5 \left(z_1^2 g_7 + z_1 z_2 g_6 + z_2^2 g_5\right)\,, \quad \Delta = z_1^{10} z_2^{10} \Delta_r\,, \tag{D.1}$$

$$\Delta_r = 4 z_1^2 z_2^2 f_4^3 + 27 \left(z_1^2 g_7 + z_1 z_2 g_6 + z_2^2 g_5\right)^2\,. \tag{D.2}$$

Now we tune such that all the intersections of $\{\Delta_r = 0\}$ with $\{z_1 = 0\}$ are at $u_1 = 0$, and all the intersections with $\{z_2 = 0\}$ are at $u_1 = 0$ too. These intersections are clearly governed by g_7 and g_5, so we are restricting to the case

$$f = z_1^4 z_2^4 f_4\,, \quad g = z_1^5 z_2^5 \left(\alpha z_1^2 u_1^{12} + z_1 z_2 g_6 + \beta z_2^2 u_1^{12}\right)\,, \tag{D.3}$$

where α and β are arbitrary non-zero constants, and f_4 and g_6 remain arbitrary polynomials in $\{u_1, u_2\}$. We now blow up at $\{z_1 = 0, u_1 = 0, x = 0, y = 0\}$, adding a new coordinate ε_1,

and taking the appropriate proper transform, giving a crepant resolution. We put hats on the resulting coordinates to indicate they are the coordinates after resolution. We then have the identifications

$$z_1 = \hat{z}_1\varepsilon_1\,, \quad u_1 = \hat{u}_1\varepsilon_1\,, \quad x = \hat{x}\varepsilon_1^2\,, \quad y = \hat{y}\varepsilon_1^3\,, \tag{D.4}$$

$$\hat{f} = \varepsilon_1^{-4} f = \hat{z}_1^4\hat{z}_2^4 f_4\,, \quad \hat{g} = \varepsilon_1^{-6} g = \hat{z}_1^5\hat{z}_2^5\left(\alpha\hat{z}_1^2\hat{u}_1^{12}\cdot\varepsilon_1^{13} + \hat{z}_1\hat{z}_2 g_6 + \beta\hat{z}_2^2\hat{u}_1^{12}\cdot\varepsilon_1^{11}\right)\,. \tag{D.5}$$

We can now perform another similar blow-up, this time at $\{z_1 = 0, \varepsilon_1 = 0, x = 0, y = 0\}$. We will continue to write a single hat on a coordinate to indicate it is the coordinate after the blow-up. Then we have the following,

$$z_1 = \hat{z}_1\varepsilon_1\varepsilon_2^2\,, \quad z_1 = \hat{z}_1\varepsilon_1\varepsilon_2\,, \quad x = \hat{x}\varepsilon_1^2\varepsilon_2^4\,, \quad y = \hat{y}\varepsilon_1^3\varepsilon_2^6\,, \tag{D.6}$$

$$\hat{f} = \varepsilon_2^{-4}\varepsilon_1^{-4} f = \hat{z}_1^4\hat{z}_2^4 f_4\,, \quad \hat{g} = \varepsilon_2^{-6}\varepsilon_1^{-6} g = \hat{z}_1^5\hat{z}_2^5\left(\alpha\hat{z}_1^2\hat{u}_1^{12}\cdot\varepsilon_1^{13}\varepsilon_2^{14} + \hat{z}_1\hat{z}_2 g_6 + \beta\hat{z}_2^2\hat{u}_1^{12}\cdot\varepsilon_1^{11}\varepsilon_2^{10}\right)\,. \tag{D.7}$$

We continue in this way until we have blown-up all the way to ε_{12}. It is straightforward to see that we will then have the following expressions,

$$z_1 = \hat{z}_1 L_\varepsilon\,, \quad u_1 = \hat{u}_1 C_\varepsilon\,, \quad x = \hat{x}L_\varepsilon^2\,, \quad y = \hat{y}L_\varepsilon^3\,, \tag{D.8}$$

$$\hat{f} = C_\varepsilon^{-4} f = \hat{z}_1^4\hat{z}_2^4 f_4\,, \quad \hat{g} = C_\varepsilon^{-6} g = \hat{z}_1^5\hat{z}_2^5\left(\alpha\hat{z}_1^2\hat{u}_1^{12}\cdot L_\varepsilon C_\varepsilon^{12} + \hat{z}_1\hat{z}_2 g_6 + \beta\hat{z}_2^2\hat{u}_1^{12}\cdot L_\varepsilon^{-1}C_\varepsilon^{12}\right)\,. \tag{D.9}$$

where $L_\varepsilon = \varepsilon_1\varepsilon_2^2\varepsilon_3^3\ldots\varepsilon_{12}^{12}$ and $C_\varepsilon = \varepsilon_1\ldots\varepsilon_{12}$. We see that in the term with a β coefficient, there are no powers of ε_{12}. Hence we cannot perform any more of these blow-ups, as we would not be able to divide ε_{13}^6 out of g. It is also clear that in order to be able to perform the 12 blow-ups, we did need all 12 of the points of intersection of $z_1 = 0$ with $\Delta_r = 0$ to sit on top of one another, since if g_5 had a lower power of $\hat{u}_1$ we would have run out of powers of ε factors earlier.

We can now perform the blow-ups on the other E_8 brane. Analogously to above, we start with the point $\{z_2 = 0, u_1 = 0, x = 0, y = 0\}$, and perform successive blow-ups, with new coordinates $\varepsilon_{-1}, \varepsilon_{-2}, \ldots$. Clearly after this process is complete we will have the following expressions,

$$z_1 = \hat{z}_1 L_{\varepsilon_+}\,, \quad z_2 = \hat{z}_2 L_{\varepsilon_-}\,, \quad u_1 = \hat{u}_1 C_{\varepsilon_+} C_{\varepsilon_-}\,, \quad x = \hat{x}L_{\varepsilon_+}^2 L_{\varepsilon_-}^2\,, \quad y = \hat{y}L_{\varepsilon_+}^3 L_{\varepsilon_-}^3\,, \tag{D.10}$$

$$\hat{f} = C_{\varepsilon_+}^{-4}C_{\varepsilon_-}^{-4} f = \hat{z}_1^4\hat{z}_2^4 f_4\,, \quad \hat{g} = C_{\varepsilon_+}^{-6}C_{\varepsilon_-}^{-6} g = \hat{z}_1^5\hat{z}_2^5\left(\alpha\hat{z}_1^2\hat{u}_1^{12}\cdot A + \hat{z}_1\hat{z}_2 g_6 + \beta\hat{z}_2^2\hat{u}_1^{12}\cdot B\right)\,, \tag{D.11}$$

where

$$A = L_{\varepsilon_+}L_{\varepsilon_-}^{-1}C_{\varepsilon_+}^{12}C_{\varepsilon_-}^{12}\,, \quad B = L_{\varepsilon_+}^{-1}L_{\varepsilon_-}C_{\varepsilon_+}^{12}C_{\varepsilon_-}^{12}\,, \tag{D.12}$$

in which

$$L_{\varepsilon_\pm} = \varepsilon_{\pm 1}\varepsilon_{\pm 2}^2\ldots\varepsilon_{\pm 12}^{12}\,, \quad C_{\varepsilon_\pm} = \varepsilon_{\pm 1}\ldots\varepsilon_{\pm 12}\,. \tag{D.13}$$

These are the expressions in the final situation, after all blow-ups have been performed. The hypersurface is determined by the standard Weierstrass equation in the new coordinates,

$$\hat{y}^2 = \hat{x}^3 + \hat{f}\hat{x}\hat{w}^4 + \hat{g}\hat{w}^6 \,. \tag{D.14}$$

It is clear that we still have two E_8 singularities, which now sit at $\hat{z}_1 = 0$ and $\hat{z}_2 = 0$ (and it is straightforward to check from the ray diagram that $\hat{z}_1 = 0$ and $\hat{z}_2 = 0$ remain $\mathbb{P}^1$s in the three-fold base). It is also clear that the E_8 singularities are geometrically non-Higgsable, by the following argument. The weight system has a row

$\hat{y}$	$\hat{x}$	$\hat{w}$	$\hat{z}_1$	$\hat{z}_2$	$\hat{u}_1$	$\hat{u}_2$	ε_1	$\ldots$	ε_{11}	ε_{12}	ε_{-1}	$\ldots$	ε_{-12}
42	28	0	0	12	0	1	0	$\ldots$	0	1	0	$\ldots$	0

. (D.15)

It is easy to check that each term in g has degree 84 under this scaling. We see we could not have a term with 8 or more powers of $\hat{z}_2$ in g, as it would overshoot the degree for the scaling above. Since we also know every term in g contains a factor $\hat{z}_1^a \hat{z}_2^b$ with $a + b = 12$, we see that we cannot have a term with fewer than 5 powers of $\hat{z}_1$. Analogously we cannot have a term with fewer than 5 powers of $\hat{z}_2$, and hence we have that $g \propto \hat{z}_1^5 \hat{z}_2^5$. We can also make the analogous statement for f, so that $f \propto \hat{z}_1^4 \hat{z}_2^4$. Hence we always have that $\Delta \propto \hat{z}_1^{10} \hat{z}_2^{10}$, so the E_8 singularities are geometrically non-Higgsable. It is also clear that we have removed all intersections of the remaining brane locus with the E_8 stacks, as follows. At $\hat{z}_1 = 0$ we have

$$\Delta_r|_{\hat{z}_1=0} = 27(\beta \hat{z}_2^2 \hat{u}_1^{12} B)^2 \,. \tag{D.16}$$

This expression involves only $\hat{z}_2$, $\hat{u}_1$, and the $\varepsilon_{-i}, \varepsilon_i$. From the fan it is clear that of these only ε_{12} is allowed to vanish when $\hat{z}_1 = 0$. However this is precisely the coordinate that does not appear in B. Hence we have that $\Delta_r|_{\hat{z}_1=0} \neq 0$. Clearly we can make an analogous statement for the $\hat{z}_2 = 0$ surface. Hence the remaining brane locus does not intersect either of the E_8 singularities. Finally we also note that for a generic f_4 and g_6 there should be no other singularities.

D.2 Explicit blow-ups in 4d case

In this appendix, analogously to the six-dimensional case in Appendix D.1, we show in an example that toric blow-ups are sufficient to remove all singularities worse than E_8 in the F-theory four-fold dual to a four-dimensional heterotic line bundle model. This example was discussed above in Section 4.4.2, and the result upon performing all toric blow-ups will be the F-theory base fan shown in Figure 8.

In this example, the heterotic base is $B_2 = \mathbb{P}^1 \times \mathbb{P}^1$, where the two $\mathbb{P}^1$s have coordinates u_i

and v_i respectively. Additionally we specialise to a particular tuning[45] of the functions in the Weierstrass equation,

$$g_7 = \alpha u_1^{12} v_1^{12}\,, \quad g_5 = \beta u_1^{12} v_1^{12}\,. \tag{D.17}$$

We then proceed to blow up multiple times over $u_1 = 0$ and $v_1 = 0$ in each of the two $z_{1,2} = 0$ surfaces, each time blowing up on a previous exceptional divisor, and each time taking the proper transform to describe the crepant resolution. This is exactly analogous to the procedure in Appendix D.1, so we do not repeat it. Altogether we will blow up 12 times over each of the four severely-singular loci. After all these blow-ups and proper transforms, it is straightforward to see that we end up with the following expressions for the Weierstrass model,

$$\hat{f} = \hat{z}_1^4 \hat{z}_2^4 f_4\,, \quad \hat{g} = \hat{z}_1^5 \hat{z}_2^5 \left(\alpha \hat{z}_1^2 \hat{u}_1^{12} \hat{v}_1^{12} \cdot A + \hat{z}_1 \hat{z}_2 g_6 + \beta \hat{z}_2^2 \hat{u}_1^{12} \hat{v}_1^{12} \cdot B\right)\,. \tag{D.18}$$

where

$$A = \prod_{i=1}^{12} (\varepsilon_{-i}\rho_{-i})^{12-i} (\varepsilon_i \rho_i)^{12+i}\,, \quad B = \prod_{i=1}^{12} (\varepsilon_{-i}\rho_{-i})^{12+i} (\varepsilon_i \rho_i)^{12-i}\,, \tag{D.19}$$

again analogously to the six-dimensional case.

We can also verify that each of $\hat{z}_1 = 0$ and $\hat{z}_2 = 0$, intersected with the section, are $\mathbb{P}^1 \times \mathbb{P}^1$s, so they are diffeomorphic to the heterotic base. Let us focus on the $\hat{z}_1 = 0$ case. We know that none of the following coordinates can vanish, $\{\varepsilon_{-i}, \rho_{-i}, \varepsilon_1, \ldots, \varepsilon_{11}, \rho_1, \ldots, \rho_{11}, u_1, v_1, z_2\}$, so we can set them to 1 using scaling relations. Noting that

$$\vec{v}_2 + \vec{\rho}_{12} + 12\vec{\hat{z}}_2 = 0 \quad \text{and} \quad \vec{u}_2 + \vec{\varepsilon}_{12} + 12\vec{\hat{z}}_2 = 0\,, \tag{D.20}$$

we see that can rework the weight system to look as follows.

$\hat{u}_1$	$\hat{u}_2$	$\hat{v}_1$	$\hat{v}_2$	ε_{12}	ρ_{12}
1	1	0	0	0	0
0	0	1	1	0	0
0	1	0	0	1	0
0	0	0	1	0	1

(D.21)

We can then use the first two rows to set $\hat{u}_1 = \hat{v}_1 = 1$, giving the weight system for a $\mathbb{P}^1 \times \mathbb{P}^1$,

$\hat{u_2}$	$\hat{v}_2$	ε_{12}	ρ_{12}
1	0	1	0
0	1	0	1

(D.22)

[45] While we are here treating an example case with a particular B_2 and a particular tuning of g_7 and g_5, it will be clear that the computations apply also to an arbitrary B_2 and to different choices of tuning allowing toric blow-ups.

Clearly we can make the same computation for $\hat{z}_2 = 0$. We can also ask whether the remaining brane locus $\Delta_r = 0$ intersects either of the E_8 stacks at $\hat{z}_1 = 0$ and $\hat{z}_2 = 0$. This computation is exactly analogous to the six-dimensional computation in Appendix D.1. At $\hat{z}_1 = 0$ we have

$$\Delta_r|_{z_1=0} = 27(\beta \hat{z}_2^2 \hat{u}_1^{12} \hat{v}_1^{12} B)^2 \,. \tag{D.23}$$

This expression involves only $\hat{z}_2$, $\hat{u}_1$, $\hat{v}_1$ and the $\varepsilon_{-i}, \varepsilon_i, \rho_{-i}, \rho_i$. From the fan it is clear that of these only ε_{12} and ρ_{12} are allowed to vanish when $\hat{z}_1 = 0$. However these are precisely the coordinates that do not appear in B, and hence we have that $\Delta_r|_{z_1=0} \neq 0$. Clearly we can make an analogous statement for the $\hat{z}_2 = 0$ surface. So we see that the remaining brane locus does not intersect either of the E_8s. We can also ask whether the E_8 singularities at $\hat{z}_1 = 0$ and $\hat{z}_2 = 0$ are now geometrically non-Higgsable. The result is that indeed they are, and one can verify this with an exactly analogous computation as we used in the case of compactification to six dimensions in Appendix D.1. Additionally, for a generic f_4 and g_6, there should be no other singularities.

E Surfaces

E.1 Hirzebruch surfaces

The Hirzebruch surfaces are complex manifolds which correspond to the various ways of fibering $\mathbb{P}^1$ over another $\mathbb{P}^1$ base. They are denoted by $\mathbb{F}_n$ and are indexed by an integer $n \geq 0$ that corresponds to the number of times the fiber $\mathbb{P}^1$ 'twists' as one moves along the base[46]. The Hirzebruch surfaces with small n are isomorphic to other well-known spaces. Specifically, we have $\mathbb{F}_0 \cong \mathbb{P}^1 \times \mathbb{P}^1$ and $\mathbb{F}_1 \cong \mathrm{dP}_1$ where dP_1 is the del Pezzo surface obtained by blowing up $\mathbb{P}^2$ at a single point. Hirzebruch surfaces can be constructed using toric geometry or complete intersections in products of projective spaces and we discuss these two possibilities in turn.

Toric representations

The toric diagram for $\mathbb{F}_n$ together with its weight system is shown in Figure 28. The weight system, that is, the set of charges of the toric coordinates $z_1, \ldots, z_4$ under the two toric scalings, follows from linear equivalences of the toric rays.

[46] Up to real diffeomorphisms there are only two ways to fiber a sphere over a sphere. However up to complex diffeomorphisms there are infinitely many. The even Hirzebruch surfaces, $\mathbb{F}_{2n}$, are isomorphic as real manifolds to the trivial fiber bundle, while the odd cases, $\mathbb{F}_{2n+1}$, are isomorphic as real manifolds to the unique non-trivial fiber bundle.

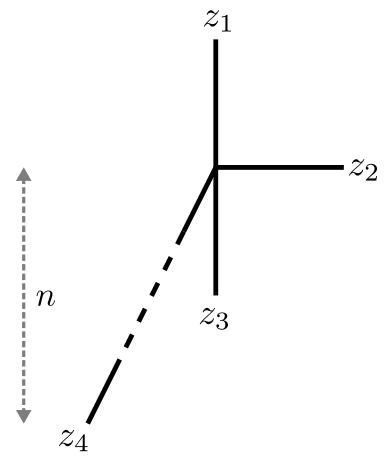

Weight system:

z_1	z_2	z_3	z_4
1	0	1	0
n	1	0	1

,

Figure 28: *Toric diagram and derived weight system for the Hirzebruch surface $\mathbb{F}_n$. All distances in the toric ray diagram are 1 except the vertical value of z_4 which is $-n$.*

The weight system implies the following divisor equivalences,

$$[z_2] = [z_4]\,, \quad [z_1] = [z_3] + n[z_4]\,. \tag{E.1}$$

As a basis of the Picard lattice, we can choose the two divisors $D_1 = [z_3]$ and $D_2 = [z_4]$. The anti-canonical divisor $-K_{\mathbb{F}_n}$ is simply the sum of all toric divisors, and so in this basis it is given by

$$-K_{\mathbb{F}_n} = 2D_1 + (n+2)D_2\,. \tag{E.2}$$

The intersection form can also be read off from the toric diagram: distinct toric divisors intersect once if they correspond to neighbouring rays and do not intersect otherwise, and self-intersections follow from divisor equivalences. The leads to the intersections

$$D_1^2 = -n\,, \quad D_1 \cdot D_2 = 1\,, \quad D_2^2 = 0\,. \tag{E.3}$$

The Mori cone is given by the non-negative linear combinations of the toric divisors and, hence, the Mori cone generators are $\hat{\mathcal{M}}(\mathbb{F}_n) = \{D_1, D_2\}$. From this, the generators of the dual nef cone can be determined as $\hat{\mathcal{N}}(\mathbb{F}_n) = \{D_2, D_1 + nD_2\}$.

Complete intersection representations

The Hirzebruch surfaces also have complete intersection representations. A complete intersection can be specified by a configuration matrix, where the entries in the first column are the projective spaces whose product forms the ambient space, and each further column specifies the multi-degree of one of the defining equations. The Hirzebruch surface $\mathbb{F}_n$ can be represented as a hypersurface in $\mathbb{P}^1 \times \mathbb{P}^2$, defined by the zero locus of a polynomial with bi-degree $(n, 1)$. Hence,

the corresponding configuration matrix is[47]

$$\mathbb{F}_n \in \left[\begin{array}{c|c} \mathbb{P}^1 & n \\ \mathbb{P}^2 & 1 \end{array}\right] . \tag{E.4}$$

E.2 Del Pezzo surfaces

Del Pezzo surfaces are defined to be smooth compact complex projective surfaces with ample anti-canonical bundle; these are the two-dimensional Fano varieties. A del Pezzo surface is either isomorphic to the product of complex projective lines $\mathbb{P}^1 \times \mathbb{P}^1$ or it is isomorphic to the blow-up of the complex projective plane $\mathbb{P}^2$ at up to eight points in general position. Conversely, any blow-up of $\mathbb{P}^2$ at eight points in general position is a del Pezzo surface. The condition that the points are in general position is equivalent to ampleness of the anti-canonical divisor class of the resulting space [129, Théorème 1].

The subset of the del Pezzo surfaces that are of primary interest in this chapter are those constructed by blowing up the complex projective plane $\mathbb{P}^2$ at n points in general position, where $n = 0, \ldots, 8$. We denote these surfaces by dP_n throughout[48]. Below we will collect relevant information about the surfaces dP_n; note that the analogous properties for $\mathbb{P}^1 \times \mathbb{P}^1$ would be trivial. In particular, after recalling some basic methods to construct del Pezzo surfaces, we will list the generators of the Mori and nef cones, which we use in the main text.

Picard lattice and anti-canonical divisor

There is a natural choice for a basis of the dP_n Picard lattice which consists of the hyperplane class l of the underlying projective plane $\mathbb{P}^2$ and the exceptional divisor class e_i, where $i = 1, \ldots, n$, which correspond to the blow-ups. Relative to the basis $l, e_1, \ldots, e_n)$, the intersection form is fixed by the relations

$$l^2 = 1\,, \quad l \cdot e_i = 0\,, \quad e_i \cdot e_j = -\delta_{ij}\,. \tag{E.5}$$

The anti-canonical divisor is given by

$$-K_{\mathrm{dP}_n} = 3l - \sum_{i=1}^{n} e_i\,. \tag{E.6}$$

[47] A $\in$ symbol is used since the configuration matrix represents the full set of possible choices of polynomials. While generic polynomials will describe the desired space, some choices will, for example, not be smooth.

[48] Sometimes the del Pezzo surfaces are numbered by their degree. The degree d of a del Pezzo surface, which is defined to be the self-intersection number of the anti-canonical divisor class, is at least 1 and at most 9. For a del Pezzo surface isomorphic to the blow-up of $\mathbb{P}^2$ at n points in general position, the degree is $d = 9 - n$. When the del Pezzo surface is isomorphic to $\mathbb{P}^1 \times \mathbb{P}^1$ the degree is $d = 8$.

Toric representations

There are toric representations for a subset of the del Pezzo surfaces, namely for the spaces isomorphic to $\mathbb{P}^1 \times \mathbb{P}^1$ and the spaces isomorphic to dP_n, where $n = 0, \ldots, 3$. In Figure 29 we recall the toric ray diagrams and the associated weight systems for the three non-trivial cases dP_1, dP_2, and dP_3. The weight system, that is, the set of charges of the toric coordinates under the toric scalings, follows from linear equivalences of the toric rays. We also note the following

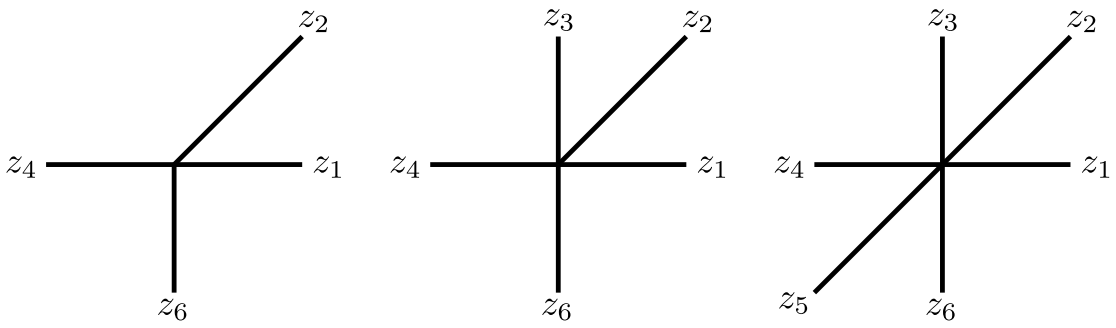

Toric dP_1 diagram, with weight system:

z_1	z_2	z_4	z_6
0	1	1	1
1	0	1	0

Toric dP_2 diagram, with weight system:

z_1	z_2	z_3	z_4	z_6
0	1	0	1	1
1	0	0	1	0
0	0	1	0	1

Toric dP_3 diagram, with weight system:

z_1	z_2	z_3	z_4	z_5	z_6
0	1	0	1	0	1
1	0	0	1	0	0
0	0	1	0	0	1
0	1	0	0	1	0

Figure 29: *Toric diagrams and weight systems for* dP_1, dP_2, *and* dP_3, *which are the blow-ups of the projective plane* $\mathbb{P}^2$ *at respectively 1, 2, and 3 points in general position.*

relations between the toric divisors and the basis $(l, e_1, \ldots, e_n)$.

$$\begin{aligned}
\mathrm{dP}_1: &\quad [z_1] = e_1\,, \quad [z_2] = l - e_1\,, && [z_4] = l\,, && [z_6] = l - e_1\,,\\
\mathrm{dP}_2: &\quad [z_1] = e_1\,, \quad [z_2] = l - e_1 - e_2\,, \quad [z_3] = e_2\,, \quad [z_4] = l - e_2\,, && [z_6] = l - e_1\,,\\
\mathrm{dP}_3: &\quad [z_1] = e_1\,, \quad [z_2] = l - e_1 - e_2\,, \quad [z_3] = e_2\,, \quad [z_4] = l - e_2 - e_3\,, \quad [z_5] = e_3\,, \quad [z_6] = l - e_1 - e_3\,.
\end{aligned}$$

Complete intersection representations

Del Pezzo surfaces can also be represented as complete intersections in products of projective spaces. Below we list a set of possible configuration matrices, where the entries in the first column specify the projective spaces whose product forms the ambient space, and each other

column specifies the multi-degree of one of the defining equations.

$$\mathrm{dP}_1 \in \left[\begin{array}{c|c} \mathbb{P}^2 & 1 \\ \mathbb{P}^1 & 1 \end{array}\right] \quad \mathrm{dP}_2 \in \left[\begin{array}{c|cc} \mathbb{P}^2 & 1 & 1 \\ \mathbb{P}^1 & 1 & 0 \\ \mathbb{P}^1 & 0 & 1 \end{array}\right] \quad \mathrm{dP}_3 \in \left[\begin{array}{c|c} \mathbb{P}^1 & 1 \\ \mathbb{P}^1 & 1 \\ \mathbb{P}^1 & 1 \end{array}\right] \quad \mathrm{dP}_4 \in \left[\begin{array}{c|c} \mathbb{P}^2 & 2 \\ \mathbb{P}^1 & 1 \end{array}\right]$$
$$\mathrm{dP}_5 \in \left[\begin{array}{c|cc} \mathbb{P}^4 & 2 & 2 \end{array}\right] \quad \mathrm{dP}_6 \in \left[\begin{array}{c|c} \mathbb{P}^3 & 3 \end{array}\right] \quad \mathrm{dP}_7 \in \left[\begin{array}{c|c} \mathbb{P}^2 & 2 \\ \mathbb{P}^1 & 2 \end{array}\right] \quad \mathrm{dP}_8 \in \left[\begin{array}{c|c} \mathbb{P}^2 & 3 \\ \mathbb{P}^1 & 1 \end{array}\right]. \tag{E.7}$$

These representations are simple but they are not all favourable, that is, not every divisor class descends from one on the ambient space. This is easy to see since for example in the dP_8 case which has Picard number nine but only two divisors classes descend from the ambient space. It is possible to write down a favourable complete intersection representation in each case by sacrificing simplicity. In fact, the complete intersection[49]

$$\mathrm{dP}_n \in \left[\begin{array}{c|ccccc} \mathbb{P}^1 & 1 & 0 & \cdots & 0 & 0 \\ \mathbb{P}^1 & 0 & 1 & \cdots & 0 & 0 \\ \vdots & \vdots & \vdots & \ddots & \vdots & \vdots \\ \mathbb{P}^1 & 0 & 0 & \cdots & 1 & 0 \\ \mathbb{P}^1 & 0 & 0 & \cdots & 0 & 1 \\ \mathbb{P}^2 & 1 & 1 & \cdots & 1 & 1 \end{array}\right], \tag{E.8}$$

where the top right block is an $n \times n$ identity matrix, provides a favourable realisation of all del Pezzo surfaces dP_n.

Mori and nef cone generators

Finally, we list the Mori and nef cone generators for dP_n which are required in the main text.

The generators of the Mori cone of dP_n are the exceptional curves[50], and the generators of the dual nef cone can be found by standard algorithms for dual cones. For compactness of notation we will write the generators as vectors with respect to the standard basis $(l, e_1, \ldots, e_n)$, that is, we write a divisor $D = k_0 l + k_1 e_1 + \cdots + k_n e_n$ as a vector $(k_0, k_1, \ldots, k_n)$. Since the blow-ups are at general position, the classes e_i are on equal footing, and so the generator lists are invariant under their exchange. We, therefore, only list the generators subject to the ordering

[49]This representation reflects the fact that a blow-up of $\mathbb{P}^2$ can be implemented by introducing a $\mathbb{P}^1$ into the ambient space and providing a linear equation that allows 'movement along' the $\mathbb{P}^1$ only over the blow-up point.

[50]The two spaces dP_0 and dP_1 are exceptions: in these cases one has to include the hyperplane class l which is not exceptional as a generator of the Mori cone. From dP_2 onwards l is not needed as a generator since $l - e_i - e_j$ are exceptional curves.

$k_1 \geq k_2 \geq \cdots \geq k_n$, keeping in mind that the other generators are obtained by permuting $k_1, \ldots, k_n$. We also note that it is sufficient to list the generators for dP_8. The generators for dP_n with $n < 8$ can be obtained from the dP_8 ones by extracting the vectors with zero entries in the last $8 - n$ positions and then removing those entries.

It turns out that the number of ordered generators for the Mori and nef cones for dP_8 is 7 and 50 respectively and, after including the permutations, these numbers increase to 240 and 19440, respectively. The list of dP_8 Mori cone generators is

$$\begin{aligned} -\hat{\mathcal{M}}(\mathrm{dP}_8) = \{ & (0,-1,0,0,0,0,0,0,0), \quad (-1,1,1,0,0,0,0,0,0), \quad (-2,1,1,1,1,1,0,0,0), \\ & (-3,2,1,1,1,1,1,1,0) \quad (-4,2,2,2,1,1,1,1,1), \quad (-5,2,2,2,2,2,2,1,1), \\ & (-6,3,2,2,2,2,2,2,2), \quad \ldots \quad \}. \end{aligned} \tag{E.9}$$

The dP_8 nef cone generators are

$$\begin{aligned} -\hat{\mathcal{N}}(\mathrm{dP}_8) = \{ & (-1,1,0,0,0,0,0,0,0), \quad (-1,0,0,0,0,0,0,0,0), \quad (-2,1,1,1,1,0,0,0,0), \\ & (-2,1,1,1,0,0,0,0,0), \quad (-3,2,1,1,1,1,1,0,0), \quad (-3,2,1,1,1,1,0,0,0), \\ & (-4,3,1,1,1,1,1,1,1), \quad (-4,3,1,1,1,1,1,1,0), \quad (-4,2,2,2,1,1,1,1,0), \\ & (-4,2,2,2,1,1,1,0,0), \quad (-5,3,2,2,2,1,1,1,1), \quad (-5,3,2,2,2,1,1,1,0), \\ & (-5,2,2,2,2,2,2,1,0), \quad (-5,2,2,2,2,2,2,0,0), \quad (-6,4,2,2,2,2,1,1,1), \\ & (-6,3,3,3,2,1,1,1,1), \quad (-6,3,3,2,2,2,2,1,1), \quad (-6,3,3,2,2,2,2,1,0), \\ & (-7,4,3,3,2,2,2,1,1), \quad (-7,4,3,2,2,2,2,2,2), \quad (-7,3,3,3,3,2,2,2,1), \\ & (-7,3,3,3,3,2,2,2,0), \quad (-8,5,3,3,2,2,2,2,2), \quad (-8,4,4,3,3,2,2,2,1), \\ & (-8,4,3,3,3,3,3,1,1), \quad (-8,4,3,3,3,3,2,2,2), \quad (-8,3,3,3,3,3,3,3,1), \\ & (-8,3,3,3,3,3,3,3,0), \quad (-9,5,4,3,3,3,2,2,2), \quad (-9,4,4,4,4,2,2,2,2), \\ & (-9,4,4,4,3,3,3,2,1), \quad (-9,4,4,3,3,3,3,3,2), \quad (-10,6,3,3,3,3,3,3,3), \\ & (-10,5,5,3,3,3,3,3,2), \quad (-10,5,4,4,4,3,3,2,2), \quad (-10,4,4,4,4,4,3,3,1), \\ & (-10,4,4,4,4,3,3,3,3), \quad (-11,6,4,4,4,3,3,3,3), \quad (-11,5,5,4,4,4,3,3,2), \\ & (-11,4,4,4,4,4,4,4,3), \quad (-12,6,5,4,4,4,4,3,3), \quad (-12,5,5,5,5,4,3,3,3), \\ & (-12,5,5,5,4,4,4,4,2), \quad (-13,6,6,4,4,4,4,4,4), \quad (-13,6,5,5,5,4,4,4,3), \\ & (-14,6,6,5,5,5,4,4,4), \quad (-14,6,5,5,5,5,5,5,3), \quad (-15,6,6,6,5,5,5,5,4), \\ & (-16,6,6,6,6,6,5,5,5), \quad (-17,6,6,6,6,6,6,6,6), \quad \ldots \quad \}. \end{aligned} \tag{E.10}$$

For either list, the dots indicate the vectors obtained from the ones listed by permuting the last eight entries.

F Alternative proof of divisor shifts

In this appendix we sketch an alternative proof for Theorem 5.40 to the one based on linear systems of divisors, which uses ideas that may be more familiar for some readers.

We start with a smooth compact complex projective surface S and a divisor $D \subset S$ with associated line bundle $\mathcal{O}_S(D)$. Further, we have an irreducible curve $C \subset S$ which intersects D negatively, so $D \cdot C < 0$. (This implies that $C^2 < 0$.) Then we have the short exact Koszul sequence

$$0 \to \mathcal{O}_S(D - C) \to \mathcal{O}_S(D) \to \mathcal{O}_S(D)|_C \to 0 \tag{F.1}$$

for the restriction $\mathcal{O}_S(D)|_C$ of the line bundle $\mathcal{O}_S(D)$ to the curve C. The degree of this restricted line bundle is negative since $\deg \mathcal{O}_S(D)|_C = D \cdot C < 0$. It is well-known that negative degree line bundles on curves have a vanishing zeroth cohomology (see, for example, Ref. [121]), that is, $H^0(C, \mathcal{O}_S(D)|_C) = 0$. This vanishing, together with the long exact sequence associated to the Koszul sequence (F.1), immediately implies that

$$h^0(S, \mathcal{O}_S(D - C)) = h^0(S, \mathcal{O}_S(D))\,. \tag{F.2}$$

This means taking away from the divisor D an irreducible curve C which intersects D negatively does not change the dimension of the zeroth cohomology. Hence, we have

Lemma F.1. *Let S be a smooth compact complex projective surface, $D \subset S$ an effective divisor and $C \subset S$ an irreducible curve with $D \cdot C < 0$. Then we have*

$$h^0(S, \mathcal{O}_S(D - C)) = h^0(S, \mathcal{O}_S(D))\,. \tag{F.3}$$

This completes the first step of the argument.

Next, we would like to iterate this process and work out how many times C can be subtracted from D without changing the zeroth cohomology dimension. Define the sequence of divisors $D_k = D - kC$, for $k \geq 0$. From the above argument, the two divisors D_k and D_{k+1} have the same zeroth cohomology dimension if $D_k \cdot C < 0$. This condition immediately translates into

$$k < \frac{D \cdot C}{C^2} \tag{F.4}$$

This means we have the following

Lemma F.2. *Let S be a smooth compact complex projective surface, $D \subset S$ an effective divisor and $C \subset S$ an irreducible curve with $D \cdot C < 0$. Define the divisors $D_k := D - k\,C$, where $k = 0, 1, \ldots, n$ and*

$$n = \text{ceil}\left(\frac{D \cdot C}{C^2}\right)\,. \tag{F.5}$$

Then, $h^0(S, \mathcal{O}_S(D_k)) = h^0(S, \mathcal{O}_S(D))$ *for all* $k = 0, 1, \ldots n$. *(Here,* ceil *is the ceiling function.)*

In particular, this lemma implies that the divisor

$$D_n = D - \text{ceil}\left(\frac{D \cdot C}{C^2}\right) C\,, \tag{F.6}$$

obtained by taking away the largest possible multiple of C, leads to the same zeroth cohomology dimension as D.

The next step is to apply Lemma F.2 repeatedly, starting with the effective divisor $D \subset S$ and a number of irreducible curves C_i with $D \cdot C_i < 0$, where $i = 1, \ldots, N$. This leads to

Lemma F.3. *Let* S *be a smooth compact complex projective surface,* $D \subset S$ *an effective divisor and* $C_i \subset S$ *irreducible (pairwise different) curves with* $D \cdot C_i < 0$, *where* $i = 1, \ldots, N$. *Define the divisors* $D_{(i)}$, *where* $i = 0, 1, \ldots, N$, *recursively by* $D_{(0)} = D$ *and* $D_{(i)} = D_{(i-1)} - k_i C_i$, *where* $k_i \in \{0, 1, \ldots, m_i\}$ *but otherwise arbitrary and*

$$m_i = \text{ceil}\left(\frac{D_{(i-1)} \cdot C_i}{C_i^2}\right)\,. \tag{F.7}$$

Then $h^0(S, \mathcal{O}_S(D_{(i)})) = h^0(S, \mathcal{O}_S(D))$ *for all* $i = 0, 1, \ldots, N$.

Proof. We proceed by induction on i and first note that the statement is clearly true for $i = 0$, since $D_{(0)} = D$. Suppose the statement is true for all $j = 0, 1, \ldots, i-1$. From $D_{(i-1)} = D - \sum_{j=1}^{i-1} k_j C_j$ it follows that

$$D_{(i-1)} \cdot C_i = D \cdot C_i - \sum_{j=1}^{i-1} k_j\, C_j \cdot C_i\,. \tag{F.8}$$

The first term on the right-hand side is negative by assumption and the second term is less equal than zero, since $C_j \cdot C_i \geq 0$ and $k_j \geq 0$. It follows that $D_{(i-1)} \cdot C_i < 0$ and we can, hence, apply Lemma F.2 with $D = D_{(i-1)}$ and $C = C_i$. This implies that $h^0(S, \mathcal{O}_S(D_{(i)})) = h^0(S, \mathcal{O}_S(D_{(i-1)})) = h^0(S, \mathcal{O}_S(D))$. □

In particular, the sequence $D_{(i)}$ of divisors defined by $D_{(0)} = D$ and $D_{(i)} = D_{(i-1)} - m_i C_i$, with m_i given in Eq. (F.7), where the largest possible multiple of the C_i is subtracted at each step, satisfies $h^0(S, \mathcal{O}_S(D_{(i)})) = h^0(S, \mathcal{O}_S(D))$ for all $i = 0, 1, \ldots, N$.

For our application in the main text, we require a statement slightly weaker than Lemma F.3 which is not recursive in nature. To this end, we consider

Lemma F.4. *Let* S *be a smooth compact complex projective surface,* $D \subset S$ *an effective divisor and* $C_i \subset S$ *irreducible (pairwise different) curves with* $D \cdot C_i < 0$, *where* $i = 1, \ldots, N$. *Define the divisors* $D_{(i)}$, *where* $i = 0, 1, \ldots, N$, *recursively by* $D_{(0)} = D$ *and* $D_{(i)} = D_{(i-1)} - n_i C_i$, *where*

$$n_i = \text{ceil}\left(\frac{D \cdot C_i}{C_i^2}\right)\,. \tag{F.9}$$

Then $h^0(S, \mathcal{O}_S(D_{(i)})) = h^0(S, \mathcal{O}_S(D))$ *for all* $i = 0, 1, \ldots, N$.

Proof. The recursive definition implies that $D_{(i-1)} = D - \sum_{j=1}^{i-1} n_i C_i$, so that

$$D_{(i-1)} \cdot C_i = D \cdot C_i - \sum_{j=1}^{i-1} n_j \, C_j \cdot C_i \,. \tag{F.10}$$

This equation shows that $n_i \leq m_i$ with n_i and m_i defined in Eqs. (F.9) and (F.7), respectively. Hence, Lemma F.3 implies the desired result. □

In particular, the last lemma shows that the divisor

$$\tilde{D} := D - \sum_{C_i \text{ irr.}} \theta(-D \cdot C_i) \, \text{ceil}\left(\frac{D \cdot C_i}{C_i^2}\right) C_i \tag{F.11}$$

satisfies $h^0(S, \mathcal{O}_S(\tilde{D})) = h^0(S, \mathcal{O}_S(D))$. (Here, θ is the Heaviside function which has been included in the sum in order to ensure that only irreducible curves C_i with $D \cdot C_i < 0$ contribute.) This is precisely the statement we wanted to prove.

Bibliography

[1] J. Polchinski, *Dirichlet Branes and Ramond-Ramond charges*, *Phys. Rev. Lett.* **75** (1995) 4724–4727, [hep-th/9510017].

[2] S. B. Giddings, S. Kachru and J. Polchinski, *Hierarchies from fluxes in string compactifications*, *Phys. Rev.* **D66** (2002) 106006, [hep-th/0105097].

[3] R. Friedman, J. Morgan and E. Witten, *Vector bundles and F theory*, *Commun. Math. Phys.* **187** (1997) 679–743, [hep-th/9701162].

[4] D. R. Morrison and C. Vafa, *Compactifications of F theory on Calabi-Yau threefolds. 2.*, *Nucl. Phys.* **B476** (1996) 437–469, [hep-th/9603161].

[5] B. Andreas and G. Curio, *Three-branes and five-branes in N=1 dual string pairs*, *Phys. Lett.* **B417** (1998) 41–44, [hep-th/9706093].

[6] B. Andreas and G. Curio, *Horizontal and vertical five-branes in heterotic / F theory duality*, *JHEP* **01** (2000) 013, [hep-th/9912025].

[7] A. Constantin and A. Lukas, *Formulae for Line Bundle Cohomology on Calabi-Yau Threefolds*, 1808.09992.

[8] A. Constantin, *Heterotic String Models on Smooth Calabi-Yau Threefolds*. PhD thesis, Oxford U., 2018. 1808.09993.

[9] E. I. Buchbinder, A. Constantin and A. Lukas, *The Moduli Space of Heterotic Line Bundle Models: a Case Study for the Tetra-Quadric*, *JHEP* **03** (2014) 025, [1311.1941].

[10] D. Klaewer and L. Schlechter, *Machine Learning Line Bundle Cohomologies of Hypersurfaces in Toric Varieties*, *Phys. Lett.* **B789** (2019) 438–443, [1809.02547].

[11] M. Larfors and R. Schneider, *Line bundle cohomologies on CICYs with Picard number two*, 1906.00392.

[12] C. R. Brodie, A. Constantin, R. Deen and A. Lukas, *Machine Learning Line Bundle Cohomology*, 1906.08730.

[13] A. P. Braun, C. R. Brodie and A. Lukas, *Heterotic Line Bundle Models on Elliptically Fibered Calabi-Yau Three-folds*, 1706.07688.

[14] A. P. Braun, C. R. Brodie, A. Lukas and F. Ruehle, *NS5-Branes and Line Bundles in Heterotic/F-Theory Duality*, *Phys. Rev.* **D98** (2018) 126004, [1803.06190].

[15] C. R. Brodie, A. Constantin, R. Deen and A. Lukas, *Index Formulae for Line Bundle Cohomology on Complex Surfaces*, 1906.08769.

[16] K. Uhlenbeck and S.-T. Yau, *On the Existence of Hermitian-Yang-Mills Connections in Stable Vector Bundles*, *Comm. Pure App. Math.* **39** (1986) .

[17] S. K. Donaldson, *Anti Self-Dual Yang-Mills Connections Over Complex Algebraic Surfaces and Stable Vector Bundles*, *Proc. Lond. Math. Soc.* **50** (1985) 1–26.

[18] S. Groot Nibbelink, J. Held, F. Ruehle, M. Trapletti and P. K. S. Vaudrevange, *Heterotic Z(6-II) MSSM Orbifolds in Blowup*, *JHEP* **03** (2009) 005, [0901.3059].

[19] L. B. Anderson, J. Gray, A. Lukas and E. Palti, *Heterotic Line Bundle Standard Models*, *JHEP* **06** (2012) 113, [1202.1757].

[20] V. Braun, Y.-H. He, B. A. Ovrut and T. Pantev, *A Heterotic standard model*, *Phys. Lett.* **B618** (2005) 252–258, [hep-th/0501070].

[21] V. Bouchard and R. Donagi, *An SU(5) heterotic standard model*, *Phys. Lett.* **B633** (2006) 783–791, [hep-th/0512149].

[22] L. B. Anderson, J. Gray, Y.-H. He and A. Lukas, *Exploring Positive Monad Bundles And A New Heterotic Standard Model*, *JHEP* **02** (2010) 054, [0911.1569].

[23] V. Braun, P. Candelas, R. Davies and R. Donagi, *The MSSM Spectrum from (0,2)-Deformations of the Heterotic Standard Embedding*, *JHEP* **05** (2012) 127, [1112.1097].

[24] L. B. Anderson, J. Gray, A. Lukas and E. Palti, *Two Hundred Heterotic Standard Models on Smooth Calabi-Yau Threefolds*, *Phys. Rev.* **D84** (2011) 106005, [1106.4804].

[25] L. B. Anderson, A. Constantin, S.-J. Lee and A. Lukas, *Hypercharge Flux in Heterotic Compactifications*, *Phys. Rev.* **D91** (2015) 046008, [1411.0034].

[26] R. Donagi, B. A. Ovrut, T. Pantev and D. Waldram, *Standard models from heterotic M theory*, *Adv. Theor. Math. Phys.* **5** (2002) 93–137, [hep-th/9912208].

[27] B. Andreas, G. Curio and A. Klemm, *Towards the Standard Model spectrum from elliptic Calabi-Yau*, *Int. J. Mod. Phys.* **A19** (2004) 1987, [hep-th/9903052].

[28] D. R. Morrison and W. Taylor, *Toric bases for 6D F-theory models*, *Fortsch. Phys.* **60** (2012) 1187–1216, [1204.0283].

[29] J. Halverson and W. Taylor, $\mathbb{P}^1$*-bundle bases and the prevalence of non-Higgsable structure in 4D F-theory models*, *JHEP* **09** (2015) 086, [1506.03204].

[30] R. Blumenhagen, B. Jurke, T. Rahn and H. Roschy, *Cohomology of Line Bundles: A Computational Algorithm*, *J. Math. Phys.* **51** (2010) 103525, [1003.5217].

[31] "cohomcalg package." Download link. High-performance line bundle cohomology computation based on [30].
http://wwwth.mppmu.mpg.de/members/blumenha/cohomcalg/, 2010.

[32] L. B. Anderson, A. Constantin, J. Gray, A. Lukas and E. Palti, *A Comprehensive Scan for Heterotic SU(5) GUT models*, *JHEP* **01** (2014) 047, [1307.4787].

[33] D. R. Morrison and D. S. Park, *F-Theory and the Mordell-Weil Group of Elliptically-Fibered Calabi-Yau Threefolds*, *JHEP* **10** (2012) 128, [1208.2695].

[34] T. W. Grimm and T. Weigand, *On Abelian Gauge Symmetries and Proton Decay in Global F-theory GUTs*, *Phys. Rev.* **D82** (2010) 086009, [1006.0226].

[35] C. Mayrhofer, E. Palti and T. Weigand, *U(1) symmetries in F-theory GUTs with multiple sections*, *JHEP* **03** (2013) 098, [1211.6742].

[36] S. Kobayashi, *Differential Geometry of Vector Bundles*. Princeton University Press, 1986.

[37] R. Donagi, Y.-H. He, B. A. Ovrut and R. Reinbacher, *The Particle spectrum of heterotic compactifications*, *JHEP* **12** (2004) 054, [hep-th/0405014].

[38] B. Andreas and G. Curio, *Extension Bundles and the Standard Model*, *JHEP* **07** (2007) 053, [hep-th/0703210].

[39] Y.-H. He, R.-K. Seong and S.-T. Yau, *Calabi–Yau Volumes and Reflexive Polytopes*, *Commun. Math. Phys.* **361** (2018) 155–204, [1704.03462].

[40] V. Braun, T. W. Grimm and J. Keitel, *Geometric Engineering in Toric F-Theory and GUTs with U(1) Gauge Factors*, *JHEP* **12** (2013) 069, [1306.0577].

[41] Download bundle data for physically promising models from http://www-thphys.physics.ox.ac.uk/projects/CalabiYau/HeteroticBundles/index.html.

[42] P. S. Aspinwall and D. R. Morrison, *Point-like instantons on K3 orbifolds*, *Nucl. Phys.* **B503** (1997) 533–564, [hep-th/9705104].

[43] P. S. Aspinwall, *Aspects of the hypermultiplet moduli space in string duality*, *JHEP* **04** (1998) 019, [hep-th/9802194].

[44] P. S. Aspinwall and R. Y. Donagi, *The Heterotic string, the tangent bundle, and derived categories*, *Adv. Theor. Math. Phys.* **2** (1998) 1041–1074, [hep-th/9806094].

[45] D.-E. Diaconescu and G. Rajesh, *Geometrical aspects of five-branes in heterotic / F theory duality in four-dimensions*, *JHEP* **06** (1999) 002, [hep-th/9903104].

[46] J. de Boer, R. Dijkgraaf, K. Hori, A. Keurentjes, J. Morgan, D. R. Morrison et al., *Triples, fluxes, and strings*, *Adv. Theor. Math. Phys.* **4** (2002) 995–1186, [hep-th/0103170].

[47] R. Donagi and M. Wijnholt, *Model Building with F-Theory*, *Adv. Theor. Math. Phys.* **15** (2011) 1237–1317, [0802.2969].

[48] C. Beasley, J. J. Heckman and C. Vafa, *GUTs and Exceptional Branes in F-theory - I*, *JHEP* **01** (2009) 058, [0802.3391].

[49] V. Kumar, D. R. Morrison and W. Taylor, *Mapping 6D $N = 1$ supergravities to F-theory*, *JHEP* **02** (2010) 099, [0911.3393].

[50] V. Kumar, D. R. Morrison and W. Taylor, *Global aspects of the space of 6D $N = 1$ supergravities*, *JHEP* **11** (2010) 118, [1008.1062].

[51] C. Lüdeling and F. Ruehle, *F-theory duals of singular heterotic K3 models*, *Phys. Rev.* **D91** (2015) 026010, [1405.2928].

[52] A. P. Braun and S. Schafer-Nameki, *Compact, Singular G2-Holonomy Manifolds and M/Heterotic/F-Theory Duality*, 1708.07215.

[53] C. Vafa, *Evidence for F theory*, *Nucl. Phys.* **B469** (1996) 403–418, [hep-th/9602022].

[54] D. R. Morrison and C. Vafa, *Compactifications of F theory on Calabi-Yau threefolds. 1*, *Nucl. Phys.* **B473** (1996) 74–92, [hep-th/9602114].

[55] M. Blaszczyk, S. Groot Nibbelink, O. Loukas and F. Ruehle, *Calabi-Yau compactifications of non-supersymmetric heterotic string theory*, *JHEP* **10** (2015) 166, [1507.06147].

[56] S. Groot Nibbelink, O. Loukas and F. Ruehle, *(MS)SM-like models on smooth Calabi-Yau manifolds from all three heterotic string theories*, *Fortsch. Phys.* **63** (2015) 609–632, [1507.07559].

[57] S. Groot Nibbelin and F. Ruehle, *Line bundle embeddings for heterotic theories*, *JHEP* **04** (2016) 186, [1601.00676].

[58] P. Horava and E. Witten, *Heterotic and type I string dynamics from eleven-dimensions*, *Nucl. Phys.* **B460** (1996) 506–524, [hep-th/9510209].

[59] P. Horava and E. Witten, *Eleven-dimensional supergravity on a manifold with boundary*, *Nucl. Phys.* **B475** (1996) 94–114, [hep-th/9603142].

[60] A. Lukas, B. A. Ovrut and D. Waldram, *On the four-dimensional effective action of strongly coupled heterotic string theory*, *Nucl. Phys.* **B532** (1998) 43–82, [hep-th/9710208].

[61] A. Lukas, B. A. Ovrut, K. S. Stelle and D. Waldram, *The Universe as a domain wall*, *Phys. Rev.* **D59** (1999) 086001, [hep-th/9803235].

[62] R. Friedman, J. W. Morgan and E. Witten, *Vector bundles over elliptic fibrations*, alg-geom/9709029.

[63] G. Rajesh, *Toric geometry and F theory / heterotic duality in four-dimensions*, *JHEP* **12** (1998) 018, [hep-th/9811240].

[64] P. Berglund and P. Mayr, *Heterotic string / F theory duality from mirror symmetry*, *Adv. Theor. Math. Phys.* **2** (1999) 1307–1372, [hep-th/9811217].

[65] J. J. Heckman, D. R. Morrison and C. Vafa, *On the Classification of 6D SCFTs and Generalized ADE Orbifolds*, *JHEP* **05** (2014) 028, [1312.5746].

[66] M. Del Zotto, J. J. Heckman, A. Tomasiello and C. Vafa, *6d Conformal Matter*, *JHEP* **02** (2015) 054, [1407.6359].

[67] J. J. Heckman, D. R. Morrison, T. Rudelius and C. Vafa, *Atomic Classification of 6D SCFTs*, *Fortsch. Phys.* **63** (2015) 468–530, [1502.05405].

[68] A. Strominger, *Open p-branes*, *Phys. Lett.* **B383** (1996) 44–47, [hep-th/9512059].

[69] O. J. Ganor and A. Hanany, *Small E(8) instantons and tensionless noncritical strings*, *Nucl. Phys.* **B474** (1996) 122–140, [hep-th/9602120].

[70] M. Bershadsky and A. Johansen, *Colliding singularities in F theory and phase transitions*, *Nucl. Phys.* **B489** (1997) 122–138, [hep-th/9610111].

[71] S. Sethi, C. Vafa and E. Witten, *Constraints on low dimensional string compactifications*, *Nucl. Phys.* **B480** (1996) 213–224, [hep-th/9606122].

[72] A. P. Braun, F. Fucito and J. F. Morales, *U-folds as K3 fibrations*, *JHEP* **10** (2013) 154, [1308.0553].

[73] I. García-Etxebarria, D. Lust, S. Massai and C. Mayrhofer, *Ubiquity of non-geometry in heterotic compactifications*, *JHEP* **03** (2017) 046, [1611.10291].

[74] L. B. Anderson and W. Taylor, *Geometric constraints in dual F-theory and heterotic string compactifications*, *JHEP* **08** (2014) 025, [1405.2074].

[75] N. Seiberg and E. Witten, *Comments on string dynamics in six-dimensions*, *Nucl. Phys.* **B471** (1996) 121–134, [hep-th/9603003].

[76] E. Witten, *Phase transitions in M theory and F theory*, *Nucl. Phys.* **B471** (1996) 195–216, [hep-th/9603150].

[77] E. Witten, *Physical interpretation of certain strong coupling singularities*, *Mod. Phys. Lett.* **A11** (1996) 2649–2654, [hep-th/9609159].

[78] S.-J. Rey, *Heterotic M(atrix) strings and their interactions*, *Nucl. Phys.* **B502** (1997) 170–190, [hep-th/9704158].

[79] J. A. Minahan, D. Nemeschansky and N. P. Warner, *Investigating the BPS spectrum of noncritical E(n) strings*, *Nucl. Phys.* **B508** (1997) 64–106, [hep-th/9705237].

[80] J. A. Minahan, D. Nemeschansky, C. Vafa and N. P. Warner, *E strings and N=4 topological Yang-Mills theories*, *Nucl. Phys.* **B527** (1998) 581–623, [hep-th/9802168].

[81] K.-S. Choi and S.-J. Rey, *E(lementary) Strings in Six-Dimensional Heterotic F-Theory*, *JHEP* **09** (2017) 092, [1706.05353].

[82] A. P. Braun and T. Watari, *Heterotic-Type IIA Duality and Degenerations of K3 Surfaces*, *JHEP* **08** (2016) 034, [1604.06437].

[83] W. Fulton, *Introduction to Toric Varieties*. Annals of Mathematics Studies. Princeton University Press, 1993.

[84] D. Cox, J. Little and H. Schenck, *Toric Varieties*. Graduate Studies in Mathematics. American Mathematical Soc., 2011.

[85] H. Skarke, *String dualities and toric geometry: An Introduction*, *Chaos Solitons Fractals* **10** (1999) 543, [hep-th/9806059].

[86] J. Knapp and M. Kreuzer, *Toric Methods in F-theory Model Building*, *Adv. High Energy Phys.* **2011** (2011) 513436, [1103.3358].

[87] W. Buchmüller, M. Dierigl, P. K. Oehlmann and F. Ruehle, *The Toric SO(10) F-Theory Landscape*, *JHEP* **12** (2017) 035, [1709.06609].

[88] V. V. Batyrev, *Dual polyhedra and mirror symmetry for Calabi-Yau hypersurfaces in toric varieties*, *J. Alg. Geom.* **3** (1994) 493–545, [alg-geom/9310003].

[89] R. Donagi, B. A. Ovrut and D. Waldram, *Moduli spaces of five-branes on elliptic Calabi-Yau threefolds*, *JHEP* **11** (1999) 030, [hep-th/9904054].

[90] V. V. Batyrev and L. A. Borisov, *On Calabi-Yau complete intersections in toric varieties*, alg-geom/9412017.

[91] M. Esole, P. Jefferson and M. J. Kang, *Euler Characteristics of Crepant Resolutions of Weierstrass Models*, 1703.00905.

[92] M. Cvetic, T. W. Grimm and D. Klevers, *Anomaly Cancellation And Abelian Gauge Symmetries In F-theory*, *JHEP* **02** (2013) 101, [1210.6034].

[93] T. W. Grimm, M. Kerstan, E. Palti and T. Weigand, *Massive Abelian Gauge Symmetries and Fluxes in F-theory*, *JHEP* **12** (2011) 004, [1107.3842].

[94] T. W. Grimm, *The N=1 effective action of F-theory compactifications*, *Nucl. Phys.* **B845** (2011) 48–92, [1008.4133].

[95] E. Witten, *On flux quantization in M theory and the effective action*, *J. Geom. Phys.* **22** (1997) 1–13, [hep-th/9609122].

[96] A. Klemm, B. Lian, S. S. Roan and S.-T. Yau, *Calabi-Yau fourfolds for M theory and F theory compactifications*, *Nucl. Phys.* **B518** (1998) 515–574, [hep-th/9701023].

[97] A. Collinucci and R. Savelli, *On Flux Quantization in F-Theory*, *JHEP* **02** (2012) 015, [1011.6388].

[98] A. Collinucci and R. Savelli, *On Flux Quantization in F-Theory II: Unitary and Symplectic Gauge Groups*, *JHEP* **08** (2012) 094, [1203.4542].

[99] R. Donagi and M. Wijnholt, *Breaking GUT Groups in F-Theory*, *Adv. Theor. Math. Phys.* **15** (2011) 1523–1603, [0808.2223].

[100] A. Lukas, B. A. Ovrut and D. Waldram, *Nonstandard embedding and five-branes in heterotic M theory*, *Phys. Rev.* **D59** (1999) 106005, [hep-th/9808101].

[101] K. Mohri, *F theory vacua in four-dimensions and toric threefolds*, *Int. J. Mod. Phys.* **A14** (1999) 845–874, [hep-th/9701147].

[102] B. Andreas, G. Curio and D. Lust, *N=1 dual string pairs and their massless spectra*, *Nucl. Phys.* **B507** (1997) 175–196, [hep-th/9705174].

[103] G. Curio and D. Lust, *A Class of N=1 dual string pairs and its modular superpotential*, *Int. J. Mod. Phys.* **A12** (1997) 5847–5866, [hep-th/9703007].

[104] T. W. Grimm and W. Taylor, *Structure in 6D and 4D N=1 supergravity theories from F-theory*, *JHEP* **10** (2012) 105, [1204.3092].

[105] F. Hirzebruch, *Über eine Klasse von einfach-zusammenhängenden komplexen Mannigfaltigkeiten*, *Mathematische Annalen* **124** (1951/52) 77–86.

[106] W. Barth, K. Hulek, C. Peters and A. van de Ven, *Compact Complex Surfaces*. Ergebnisse der Mathematik und ihrer Grenzgebiete. 3. Folge / A Series of Modern Surveys in Mathematics. Springer Berlin Heidelberg, 2015.

[107] D. R. Morrison, *The Clemens-Schmid Exact Sequence and Applications*, pp. 101–120. Princeton University Press, 1984.

[108] H. Jockers, S. Katz, D. R. Morrison and M. R. Plesser, *SU(N) Transitions in M-Theory on Calabi–Yau Fourfolds and Background Fluxes*, *Commun. Math. Phys.* **351** (2017) 837–871, [1602.07693].

[109] C.-L. Wang, *On the topology of birational minimal models*, *J. Differential Geom.* **50** (1998) 129–146, [9804050].

[110] M. Schütt and T. Shioda, *Elliptic Surfaces*, 0907.0298.

[111] O. Zariski, *The theorem of riemann-roch for high multiples of an effective divisor on an algebraic surface*, *Annals of Mathematics* **76** (1962) 560–615.

[112] R. Lazarsfeld, *Positivity in algebraic geometry*. Springer, Berlin, 2004.

[113] L. B. Anderson, Y.-H. He and A. Lukas, *Heterotic Compactification, An Algorithmic Approach*, *JHEP* **07** (2007) 049, [hep-th/0702210].

[114] J. Gray, Y.-H. He, A. Ilderton and A. Lukas, *A New Method for Finding Vacua in String Phenomenology*, *JHEP* **07** (2007) 023, [hep-th/0703249].

[115] L. B. Anderson, Y.-H. He and A. Lukas, *Monad Bundles in Heterotic String Compactifications*, *JHEP* **07** (2008) 104, [0805.2875].

[116] Y.-H. He, S.-J. Lee and A. Lukas, *Heterotic Models from Vector Bundles on Toric Calabi-Yau Manifolds*, *JHEP* **05** (2010) 071, [0911.0865].

[117] T. Rahn and H. Roschy, *Cohomology of Line Bundles: Proof of the Algorithm*, *J. Math. Phys.* **51** (2010) 103520, [1006.2392].

[118] S.-Y. Jow, *Cohomology of toric line bundles via simplicial Alexander duality*, *Journal of Mathematical Physics* **52** (Mar, 2011) 033506–033506, [1006.0780].

[119] R. Blumenhagen, V. Braun, T. W. Grimm and T. Weigand, *GUTs in Type IIB Orientifold Compactifications*, *Nucl. Phys.* **B815** (2009) 1–94, [0811.2936].

[120] R. Hartshorne, *Algebraic geometry*. Springer Science+Business Media, Inc, New York, 2010.

[121] P. Griffiths and J. Harris, *Principles of Algebraic Geometry*. Wiley Classics Library. Wiley, 2014.

[122] H. Clemens and S. Raby, *Heterotic/F-theory Duality and Narasimhan-Seshadri Equivalence*, 1906.07238.

[123] H. Clemens and S. Raby, *Heterotic-**F**-theory Duality with Wilson Line Symmetry-breaking*, 1908.01913.

[124] L. B. Anderson, J. Gray, A. Lukas and B. Ovrut, *The Atiyah Class and Complex Structure Stabilization in Heterotic Calabi-Yau Compactifications*, *JHEP* **10** (2011) 032, [1107.5076].

[125] S. Lang, *Complex Analysis*. Springer, New York, 4 ed., 1999.

[126] A. Braun, A. Lukas and C. Sun, *Discrete Symmetries of Calabi-Yau Hypersurfaces in Toric Four-Folds*, 1704.07812.

[127] W. Barth, *Compact Complex Surfaces*. Springer, Berlin New York, 2004.

[128] C. Weibel, *An introduction to homological algebra*. Cambridge University Press, Cambridge England New York, 1994.

[129] M. Demazure, *Surfaces de Del Pezzo: II - Éclater n points dans* $\mathbb{P}^2$, *Séminaire sur les singularités des surfaces* (1976-1977) 1–13.